2020 IBDP Final Static Geological Model Development and Dynamic Modelling

---

Wade Zaluski P.Geo.
Si-Yong Lee, Ph.D.

This work was performed for Archer Daniels Midland Company (ADM) and the Illinois State Geological Survey (ISGS) through the Illinois Basin – Decatur Project. The ISGS is funded for this project by the U.S. Department of Energy through the National Energy Technology Laboratory (contract number DE-FC26-05NT42588).

July 18, 2021

Any interpretation, research, analysis, data, results, estimates, or recommendation furnished with the services or otherwise communicated by Schlumberger to the customer at any time in connection with the services are opinions based on inferences from measurements, empirical relationships and/or assumptions, which inferences, empirical relationships and/or assumptions are not infallible, and with respect to which professionals in the industry may differ. Accordingly, Schlumberger cannot and does not warrant the accuracy, correctness or completeness of any such interpretation, research, analysis, data, results, estimates or recommendation. Customer acknowledges that it is accepting the services "as is", that Schlumberger makes no representation or warranty, express or implied, of any kind or description in respect thereto. Specifically, customer acknowledges that Schlumberger does not warrant that any interpretation, research, analysis, data, results, estimates, or recommendation is fit for a particular purpose, including but not limited to compliance with any government request or regulatory requirement. Customer further acknowledges that such services are delivered with the explicit understanding and agreement that any action taken based on the services received shall be at its own risk and responsibility and no claim shall be made against Schlumberger as a consequence thereof.

© 2021 Schlumberger. All rights reserved.
An asterisk is used throughout this document to denote a mark of Schlumberger.

Other company, product, and service names are the properties of their respective owners.

Table of Contents

Table of Figures

Table of Tables

List of Acronyms

ADM: Archer Daniels Midland Company
AI: Acoustic impedance
VSP: Baseline Vertical Seismic Profile
BHP: bottomhole pressure
CO_2: Carbon dioxide
DOE: Department of Energy
DFN: discreet fracture model
EPA: Environmental Protection Agency
FEM: Finite element model
FMI: Fullbore formation microimager logs
GRFS: Gaussian random function simulation
CCS1: IBDP Carbon Capture and Storage Well #1
GM1: IBDP Geophysical Monitoring Well #1
VW1: IBDP Verification Well #1
CCS2: ICCS Carbon Capture and Storage Well #1
GM2: ICCS Geophysical Monitoring Well #2
VW2: ICCS Verification Well #2
IBDP: Illinois Basin – Decatur Project
ICCS: Illinois Industrial Carbon Capture and Storage
ISGS: Illinois State Geological Survey
MD: Measured Depth
MGSC: Midwest Geological Sequestration Consortium
NRM: Non-rigid matching
PNL: Pulsed neutron capture logging
RST: Reservoir saturation tool
SIS: Sequential Indicator Simulation
TPD: Tonnes/day
TVD: True vertical depth
PIGN: Well log effective porosity
WB: Westbay

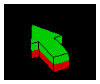 North Arrow for 3D figures

1 Executive Summary

The Midwest Geological Sequestration Consortium (MGSC) is one of seven US Department of Energy (DOE) Regional Carbon Sequestration Partnerships and is administered through DOE's National Energy Technology Laboratory. The MGSC's Illinois Basin – Decatur Project (IBDP) is a DOE-funded project led by the Illinois State Geological Survey (ISGS) at the University of Illinois. Archer Daniels Midland Company (ADM), Schlumberger, Projeo Corporation, and other subcontractors partnered with the ISGS. In November 2014, the IBDP reached its goal of injecting one million tonnes of CO_2 into a 55-ft (16.7m). section at the bottom of the Mt. Simon Sandstone at a depth of 7,000 ft (2,134m). A second project at the site, Illinois Industrial Carbon Capture and Storage (ICCS), is led by ADM and expands the site's CO_2 injection and storage capability to that of a commercial-scale operation with the ability to capture, inject, and store over one million tonnes per year. During the project (2008-2021), in collaboration with the ISGS, Schlumberger was provided a sub-award to complete and regularly update geological and CO_2 injection simulation models. Duriing the project, Schlumberger worked in collaboration with the ISGS to characterize the IBDP site for CCS.

The geomodel was significantly improved with the inclusion of the reprocessed 2011 baseline seismic survey (2019 Seismic Reprocessing Volume), this model version enhanced the structural interpretation of the subsurface faults and horizons. A petrophysical analysis was redone in 2020 to represent the facies, porosity, and permeability of the formations more consistently with geologic interpretations. Because relatively less permeable sandstones can act as vertical barriers (baffles) to CO_2 migration, a facies model was stochastically generated for sand (reservoir) and baffle (non-reservoir) facies. In addition, a discreet fracture model (DFN) within the Precambrian developed by the ISGS improved the permeabilities of the fractured Precambrian rocks. This updated geomodel was used as the primary input for reservoir simulations of carbon dioxide (CO_2) migration in the Mt. Simon Formation. Dynamic modeling of reservoir simulations was completed primarily with the multiwell and multilevel bottomhole pressure (BHP) data. Parameters used for history matching included facies, porosity, lateral and vertical permeabilities of reservoir rock, cross-fault transmissibility based on fault orientation, and well connection transmissibility factors of the IBDP injection well (CCS1) and the ICCS injection well (CCS2). With the significant geomodel updates, a substantial improvement in history matching was achieved. Overall, history matching to multiwell and multilevel downhole pressure data showed a good match except for the CCS1 response to CCS2 injection; however, history matching to less-frequent data (time-lapse saturation logs, spinner survey, and time-lapse seismic data) are not in strong agreement. History matching efforts with each of the dynamic data types provided valuable insights into the architecture of the reservoir and confining units that could not be captured through the static characterization process. Additional data after CCS2 injection showed the significant effect of geologic heterogeneity (preferential pathway/channel and/or low-permeability baffles) between wells. The major observations from this history matching work are:

- The iterative process of modeling and simulation has successfully incorporated and integrated new observed data to refine, improve, and honor the complex geologic features at the site.
- Simulation results show that injected CO_2 is confined within the Mt. Simon injection zones and there exists no leakage (pathway) of CO_2.
- According to observed bottom hole pressure (BHP) responses, injectivity of the CCS1 and CCS2 deteriorates over time possibly due to the salt precipitation, scaling, or solids buildup in the perforation and injection intervals. Continuous monitoring of CCS2 injectivity and additional spinner surveys are recommended to evaluate the temporal evolution of well performance.
- Different BHP responses at CCS1 and IBDP deep monitoring well Zone 1 (VW1_Z1) due to CCS2 injection suggest the presence of strong spatial heterogeneity that is not captured in the model.
- Compared to the pulsed neutron capture loggings (PNLs), the simulated first arrival time of CO_2 at VW1 indicates that CO_2 migrates much faster than originally expected through a preferential pathway.
- Injection into a multi-interval reservoir involves more complexity in terms of understanding the injection behavior. There are inconsistencies in the interpretation from the spinner survey at CCS1 and CO_2 saturation logs at VW1, which were not fully recreated in the history matching work. There also exist inconsistencies in the spinner surveys at CCS2 which would be better understood through additional spinner surveys and continuous monitoring.

2 Introduction

2.1 Project Overview

The Illinois Basin – Decatur Project (IBDP) is led by the Midwest Geological Sequestration Consortium (MGSC), a federally funded regional partnership through the U. S. Department of Energy's National Energy Technology Laboratory (DOE). The IBDP is a carbon capture and storage (CCS) demonstration pilot for CO_2 injection into a deep saline reservoir and is a collaboration led by the Illinois State Geological Survey (ISGS) at the University of Illinois, along with the Archer Daniels Midland Company (ADM), Schlumberger, Projeo Corporation, Trimeric Corporation, and other subcontractors. The IBDP site is located on ADM property in Decatur, IL. Injection began in November 2011 and continued at a rate of approximately one thousand tonnes per day for three years. In November 2014, IBDP reached its goal of injecting one million tonnes of CO_2 over a 3-year period into a 55-ft (16.7m) interval at the bottom of the Mt. Simon Sandstone. This is one of the first projects in the seven DOE Regional Carbon Sequestration Partnerships to do so at this scale.

A second CCS project on the ADM property called the Illinois Industrial Carbon Capture and Storage (ICCS) started injecting in April 2017 and has injected 1,716,754 tonnes of CO_2 into the Mt. Simon Formation (as of March 2020). The main objective of both projects is to validate the necessary technology to safely store a large volume of CO_2 in a saline reservoir and monitor its location in the subsurface.

2.2 Modeling and Simulation Background in the Context of the IBDP Project

All CCS projects need to demonstrate to the regulators and to the public that any injected CO_2 will be safely contained within the subsurface. In the United States, the Environmental Protection Agency (EPA) oversees and approves CCS injection wells under the Underground Injection Control (UIC) regulations. The EPA has a specific category for CO_2 injection wells called Class VI. These regulations ensure that injection well operations are safe and will not contaminate underground sources of drinking water. To demonstrate CO_2 containment for IBDP, a team of geologists, geophysicists, and reservoir engineers developed and updated geological models of the subsurface and simulations of CO_2 injection.

As the IBDP geological model was developed, available data from wells, seismic and monitoring was integrated with the geological understanding of the Illinois Basin provide by the ISGS. This model is a digital representation of the structural and petrophysical (porosity, permeability, and facies) properties of the subsurface. The reservoir engineers then used this geological model and simulated CO_2 injection down the wells to illustrate the expected vertical and horizontal extent of the CO_2 migration. During the life of this project (Site Pre-Selection Feasibility, Pre-Injection, Injection), the development of these models and simulations was an iterative process which started from basic concepts with sparse data sets (2008) to becoming sophisticated models with abundant data sets (2020) (Table 1). During the project, periodic reports were prepared to document the current findings, this report summarizes the final geomodeling and reservoir simulation work that was completed in 2020.

Table 1. Modeling and Simulation High Level Summary

Project Phase	Year	Phase Description
Site Pre-Selection Feasibility	2008-2010	In the earliest stages of the project, sparse public well data were used to create a sub-regional scale geomodel of the Illinois Basin under the ADM plant in Decatur. This model was used to determine if a CCS project was feasible here.
Pre-Injection	2010-2011	A 3D seismic survey, the drilling of an injection well and monitoring well was used to greatly enhance the accuracy of the model and simulations with site-specific data. The reservoir simulation results showed that the risk of vertical leakage and extensive horizonal plume migration from a CCS project here would be low. These results were accepted by the EPA when they reviewed the EPA Class VI permit application. The EPA granted the IBDP Project permission to inject CO_2.
Injection	2011-2014: IBDP 2017-Present: ICCS	During injection, monitoring data was collected (well logs, reservoir pressure, fluid sampling, microseismic, seismic reprocessing, time-lapse seismic etc.). These data provided insight as to the geological heterogeneity and CO_2 migration path that could not be seen before injection. Both static and dynamic models were updated when new data became available; the modeling accuracy evolved accordingly. These results were used to show the EPA that the CO_2 is contained and behaving in safe and predictable ways.

During the IBDP/ICCS projects (2008-2020), several generations of modeling improvements have been made; therefore, the modeling results have evolved in accuracy as new data became available. The key elements and historic model development are as follows:

- Prior to drilling any wells, publicly available well logs within 60 miles were used to create a sub-regional scale geomodel. In the 2008 preliminary model, a layer cake model was developed where homogeneity was assumed in porosity and permeability.
- After drilling the first wells, the porosity and permeability were computed from well logs.
- The 2011 model incorporated 3D seismic survey performed in 2010 to provide structural features to the geomodel.
- The 2013 model includes the updates according to the extended 3D seismic survey in 2011. Starting from 2013 model, structural features such as faults were inferred from microseismic data.
- In the 2016 model update, the 2015 seismic survey was completed to be a time lapse survey for IBDP injection and as a baseline survey for ICCS injection with a 0.41-mile extension to the north.
- For the 2018 model updates, low porosity and low permeability baffle facies were introduced into the model to achieve more reliable history matching results. 3D architecture of baffle facies provided a local flow barrier and/or preferential pathway. In addition, history matching to the CO_2 plume outline from the time-lapse seismic anomalies, a hypothetical flow barrier having geometric characteristics consistent with the time-lapse anomaly was introduced after review of the 2011 survey through seismic attribute and inversion analysis.
- For the 2020 Final model, the baseline 3D seismic survey was reprocessed in 2019 to provide much higher resolution for more precise interpretation of horizons and faults in the 2020 final model. Combined with reprocessed petrophysical well logs, the 3D seismic inversion was used to develop a much more detailed static geological model. The permeabilities of the Precambrian rocks were also updated according to the fracture permeabilities and porosity obtained from a discreet fracture model analysis.

2.3 Purpose of this Report

This report is intended to summarize the combined work for the IBDP and the ICCS Project for geomodeling and reservoir simulation work that was finalized in 2020. This work will be used to finalize site characterization and monitoring efforts. The Petrel* E&P software platform is a key component for site characterization throughout the IBDP geological modeling. The 9.7-mile × 9.3-mile geomodel is a structural and petrophysical (porosity and permeability) representation of the Eau Claire Shale (confining unit), the Mt. Simon Sandstone (reservoir), and underlying formations. Well data, three-dimensional (3D) seismic data, and 3D seismic inversion products were used to develop the geomodel. This geomodel is the primary input for reservoir simulations of CO_2 migration in the Mt. Simon Sandstone. In this report, emphasis is on the 2020 seismic update with a concise review of the development history. The report focuses on data, the process used to develop the geomodel, reservoir simulations, the challenges encountered, and the solutions applied.

3 Site Location and Geology

3.1 Site Location

There are two projects, the IBDP and the ICCS, with a total of six wells, located on the ADM property in Decatur, Illinois (Figure 1). The wells are listed in Table 2. A site map is shown in Figure 2.

Figure 1. IBDP Project location in Decatur Illinois. Illinois Basin in Blue.

Table 2. Well list

Well Name	Well Function	Project	Used in Property Modelling	Year of operation
CCS1	CO_2 injection well (injected 1.0 million tonnes)	IBDP	Yes	Nov 2011
VW1	Monitoring well #1	IBDP	Yes	Nov 2011
GM1	IBDP vertical seismic profile (VSP)	IBDP	No	Nov 2011
	IBDP microseismic monitoring		Yes	
CCS2	ICCS CO_2 injection well (injecting 1 million tonnes per year)	ICCS	Yes	April 2017
VW2	Monitoring well #2	ICCS	Yes	April 2017
GM2	ICCS geophysical monitoring	ICCS	No	2012

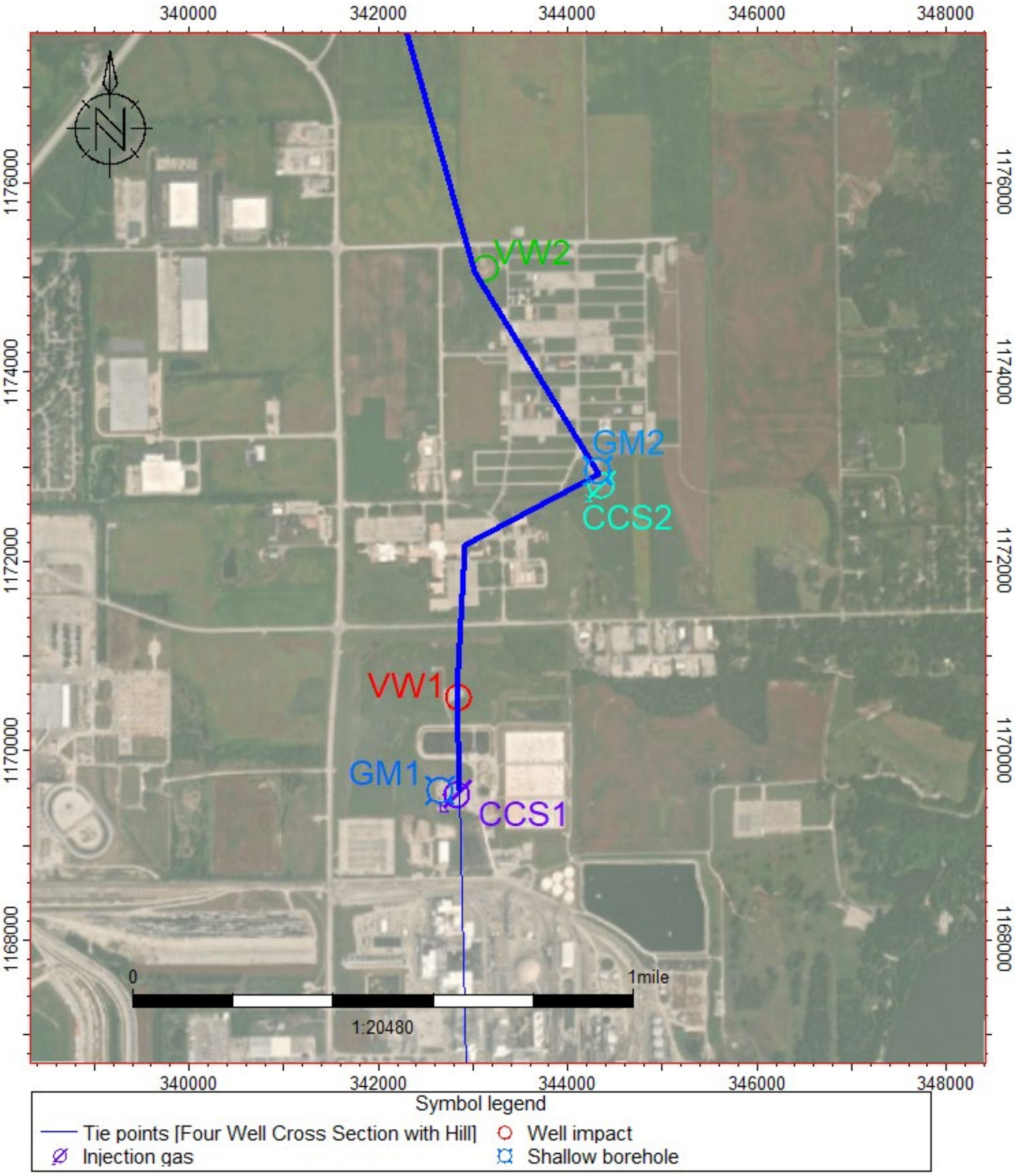

Figure 2. ADM site map showing the location of all six wells.

3.2 Geology

For both the IBDP and ICCS projects, the CO_2 injection reservoir are the sandstones of the Lower Mt. Simon Formation within the Illinois Basin. A stratigraphic column specific to the IBDP/ICCS is shown in Figure 3. The Lower Mt. Simon is ideal for CO_2 injection because the formation has porosity up to 27% and permeability up to >1,000 mD (Freiburg J. T., 2014). Figure 4 displays the petrophysical results (Section 4.4) of the Mt Simon Formation. The facies of the Lower Mt. Simon are a mixture of several depositional environments that include subaqueous coast, subaerial coast, lagoon, river, plain, and eolian plain (Freiburg J. T., 2016). The Lower Mt. Simon is divided into three subunits (B, A-Upper, A-Lower).

STRATIGRAPHIC COLUMN OF THE ILLINOIS BASIN

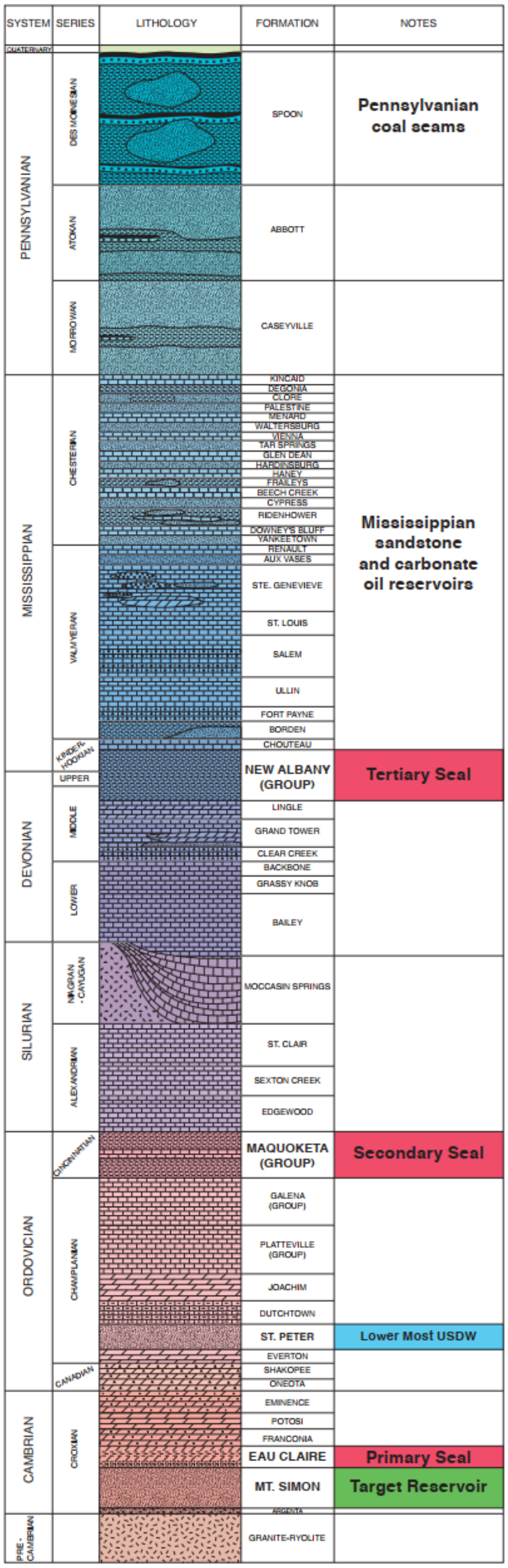

Figure 3. Stratigraphic Column for the Illinois Basin (ISGS, 2011)

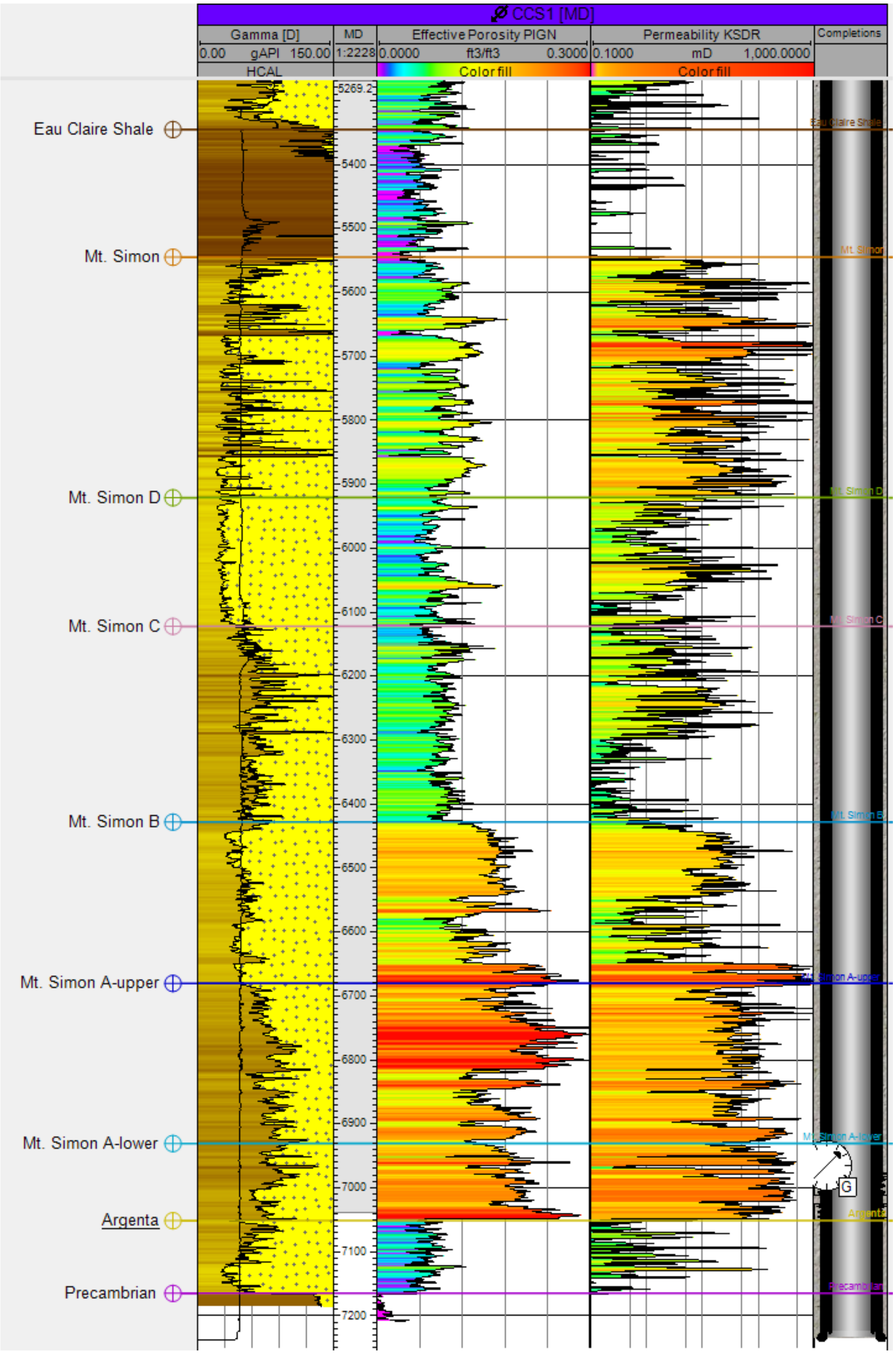

Figure 4. Petrophysics at CCS1. gamma ray, porosity, and permeability.

3.3 Geomodel and CO_2 Simulation Development History

The modeling and simulation started in 2008 and has come a long way since the first layer cake stratigraphy modeling was completed. Over the years, the model and CO_2 injection simulations were updated periodically when new well data, new seismic or monitoring data became available (Table 3). These periodic updates resulted in improved accuracy of the geomodels and CO_2 plume simulations. These updates were completed by various geologists, geophysicists, and reservoir engineers. The geological model was finalized in 2020 with the integration of repossessed baseline 3D seismic (2019 Seismic Reprocessing Volume) and reprocessed petrophysics. The most recent final update was in 2020 with the inclusion of reservoir simulation history matching, which used the reprocessed seismic.

Table 3. Model development history

	Structure/Stratigraphy/ Discrete Features		Hydrodynamic Properties	Reference
2008 Preliminary	• Layer cake stratigraphy defined by well tops from analog well 60 miles away. • No discrete features.	• Uniform zonal porosity and permeability. • Assigned using logs from analog well 60 miles away.	• Site characterization. • Basis for initial reservoir simulation model.	(Brown, IBDP Update on Petrel Models, 2008)
2010 Update	• Layer cake stratigraphy: well tops from CCS1. • No discrete features.	• Stochastic zonal porosity and permeability. • Conditioned to CCS1 well logs.	• Basis for initial reservoir simulation plume predictions.	(Brown, ADM-Update of Base Case Modeling Decatur Project, 2010)
2011 Update	• Stratigraphy: 2010 3D seismic survey and well top control from CCS1 and VW1. • No discrete features.	• Stochastic zonal porosity and permeability. • Conditioned to CCS1 and VW1 well logs and 2010 seismic inversion products.	• Basis for final Class VI permit reservoir simulation area of review. • Basis for preliminary finite element model (FEM).	(Smith, IBDP Geomodeling Review, 2012)
2013 Update	• Stratigraphy: 2011 extended 3D seismic survey and well top control from CCS1, VW1, and VW2. • Provisional fault interpretation. • Structural features such as faults were inferred from microseismic data.	• Stochastic zonal porosity and permeability. • Conditioned to CCS1, VW1, and VW2 well logs and 2011 seismic inversion products.	• Basis for updated FEM and preliminary microseismic prediction research.	(Smith, IBDP 2013_07_24_Model_IBDP-ICCS Geomodeling Overview, 2013)
2016 Update	• Stratigraphy: 2015 seismic survey was completed to be a time lapse survey for CCS1 injection and baseline survey for CCS2 injection with a 0.41-mile extension to the north.	• Updated stochastic zonal porosity and permeability based on the addition of updated structure. • Conditioned to CCS2, CCS1, VW1, and VW2 well logs and 2011 seismic inversion products and monitoring data.	• Update site characterization for reservoir simulations.	(Zaluski, IDBP Static Geological Model Development, 2016)
2018 Update	• Reservoir simulation cases of CO_2 migration were completed to match observed CO_2 migration with simulated CO_2	• Updated stochastic zonal porosity and permeability based on the addition of updated structure and the inclusion of faults.	• Update site characterization for history matching of reservoir simulations.	(Zaluski & Lee, 2018 IBDP/ICCS Static Geological Model Development and Dynamic Modelling Updates, 2019)

		Structure/Stratigraphy/ Discrete Features	Hydrodynamic Properties	Reference
	migration. Where the simulated and observed CO_2 migration did not match, geomodel refinements were performed until a reasonable match was obtained.	• Conditioned to CCS2, CCS1, VW1, and VW2 well logs and 2011 seismic inversion products and monitoring data. • Added low-permeability baffle layers into the Mt. Simon to achieve better history matching results.		
2020 Final Model	• In 2019, the baseline 3D seismic survey was reprocessed to provide much higher resolution for more precise interpretation of horizons and faults. Combined with reprocessed petrophysical well logs, the 3D seismic inversion was used to develop a much more detailed static geological model, which was used to complete CO_2 migration history matching.	• Updated structural model based on the horizons and faults interpreted from the reprocessed 3D seismic. • Reprocessed petrophysical properties (facies, porosity, and permeability) for CCS2, CCS1, VW1, and VW2. • Refined geocellular model (facies, porosity, and permeability) using the 2020 structural model, the 2020 petrophysical properties and the 2020 seismic inversion products. • Completed CO_2 migration history matching.	• Update site characterization for history matching of reservoir simulations. • Finalize project.	Content of this report

4 2020 Geomodel Construction

4.1 Workflow Overview

The general workflow used for the 2020 final model is presented in Figure 5. In 2020, the reprocessed baseline seismic (2019 Seismic Reprocessing Volume described in Table 4) was used to first refine the structural framework of the geological model. Then, using the 2019 Seismic Reprocessing Volume inversion products and the 2020 petrophysics reprocessing, a finalized property model of the subsurface was developed that represents the facies, effective porosity, and permeability of the subsurface. The below steps briefly describe the workflow:

1. The ISGS provided the 2019 3D seismic volume, which included depth-converted volumes of amplitude, acoustic impedance, and porosity.
2. The ISGS completed fault and horizon interpretation on the 2019 3D seismic and delivered it to Schlumberger.
3. Schlumberger worked with the ISGS to refine these interpretations so they could be used in the geomodel.
4. A structural framework model was built on these interpretations.
5. The ISGS provided a discrete fracture model that represented the natural fracture corridors in the Precambrian Formation.
6. Petrophysical reprocessing of CCS1, VW1, CCS2, and VW2 was completed. Updated logs of porosity, permeability, facies, and mineral fractions were developed.
7. Using the above data, a geocellular model representing the subsurface porosity, permeability, facies, and mineral fractions was developed.
8. Using this geocellular model, a coarser tartan model was also developed, which was used as the input for reservoir simulations (Section 5).
9. The final deliverables from the modeling were provided in the Petrel format and in exported formats that can be imported into other software.
10. This final report was prepared which summarizes the conclusions.

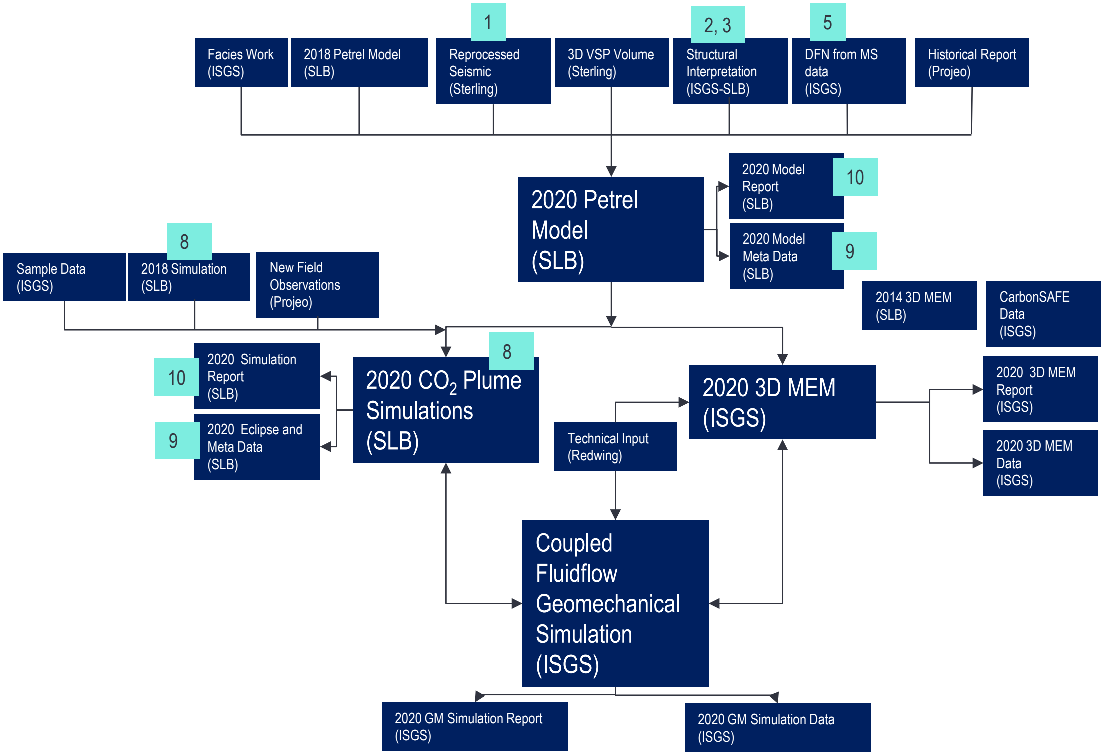

Figure 5. IBDP modeling and simulation workflow.

4.2 Data Support

4.2.1 Seismic Survey Data

Over the life of the project, several seismic surveys were performed at the IBDP site. The geomodel incorporated five seismic surveys (Table 4), and the associated processed outputs were used to develop geological models. Figure 6 outlines the reliable interpretation footprints of the 3D seismic surveys. The edges of the seismic surveys often have artifacts that must be excluded from interpretation; these boundaries vary because of the variation of processing methods used from 2010 to 2019.

Table 4. Seismic surveys

Seismic Survey		Description
Baseline Seismic	2010 Baseline Seismic Survey	- Pre-injection baseline and site characterization survey.
	2011 Baseline Seismic Survey	- Pre-injection baseline and site characterization survey (extension to north and northeast of 2010 survey area)
	2011 Baseline Porosity Cube	- Pre-injection baseline and site characterization survey to create 3D representation of porosity in the depth domain, which was the product of a post-stack seismic inversion, completed on the 2010 and 2011 seismic survey merged datasets. - Previous versions of the geomodel based on seismic interpretation from merged data from 2010 and 2011 acquisition.
	2011 Baseline Vertical Seismic Profile (VSP)	- Baseline VSP survey acquired in 2011 for time-lapse monitoring of the CO_2 plume development during several phases of injection. - Used to calibrate 3D seismic processing and to identify interbed multiples within the 3D surface seismic surveys. - Used to validate horizon interpretation completed for 2015 Seismic Baseline Reprocessing
	2019 VSP Reprocessed: Reprocessed 2011 Baseline VSP	- Reprocessed version of the 2011 Baseline Vertical Seismic - This was used to guide interpretation.
2015 Reprocessed	2015 Seismic Baseline Reprocessing	- Reprocessed version of the 2011 Baseline Seismic Survey. - Processed simultaneously with 2015 Seismic Survey to preserve time-lapse signature integrity. - Horizon and fault interpretations were used in the 2016 and 2018 reservoir characterizations. - A velocity model was used to convert this from the time to depth domain
	2015 Seismic Monitor Survey	- Post injection time-lapse survey designed to measure subtle differences between earlier surveys at and below the injection zone (may potentially represent the CO_2 plume extent in the subsurface). - This survey had 0.41 miles (400m) of data collected to the north (intended to establish a new baseline for the ICCS project). - 2011 and 2015 survey footprints were not identical (Figure 6) (differences were addressed and compensated for during processing). - A velocity model was used to convert this from the time to depth domain
2019 Reprocessed	2019 Seismic Reprocessing Volume:	- Sterling Seismic reprocessed version of the 2011 Baseline Seismic Survey for a much higher resolution amplitude volume. - This was delivered already converted from the time to depth domain.
	2019 Porosity Cube: 2019 Seismic Baseline Reprocessing Porosity Cube	- Sterling Seismic reprocessed version of 2011 Baseline Porosity Cube for a much higher resolution acoustic impedance and porosity volumes. - This was delivered already converted from the time to depth domain.

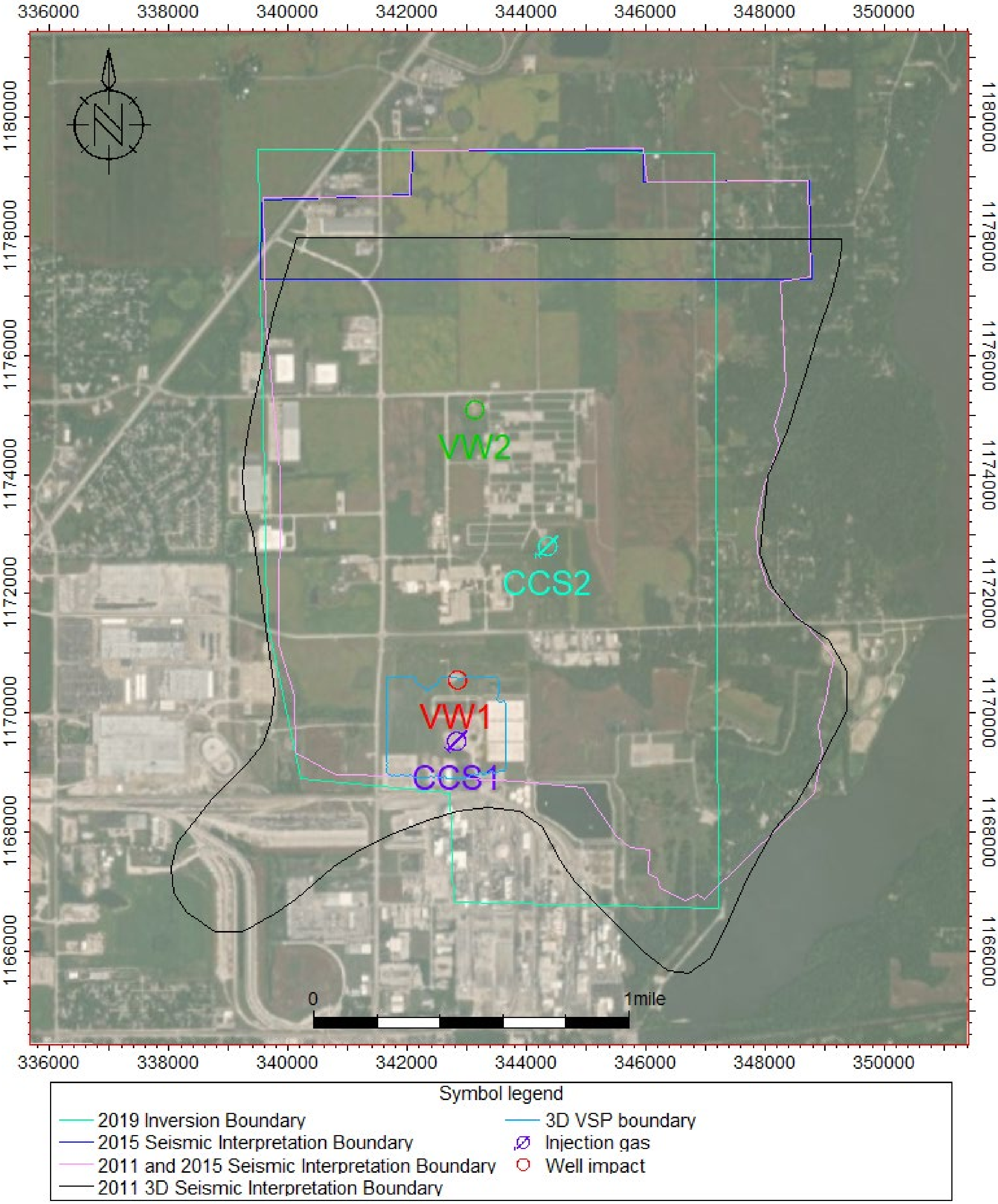

Figure 6. Map of seismic survey footprints clipped to reliable data.

4.2.2 Well Data

Data from CCS1, VW1, VW2, and CCS2 were used for the model development as follows:

- Formation tops to understand the formation structure.
- FMI* fullbore formation microimager logs to understand sedimentary bedding planes, fractures, and associated facies.
- Elemental log analysis to determine lithology fractions and, when combined with core analysis, estimate porosity and permeability. Elemental log analysis logs were reprocessed in 2020 and were included in this update.

4.3 Structural and Stratigraphic Framework

4.3.1 2019 Seismic Reprocessing Volume Horizon and Fault Interpretation

The 2019 processing provided much higher resolution of the subsurface than what was previously available (Table 4). Figure 7 and Figure 8 display a map of sample cross section interpretation lines and interpretation. Figure 9 and Figure 10 compare the 2019 Seismic Reprocessing Volume with the 2015 Seismic Baseline Reprocessing. These two vintages of the model were processed from the same 3D seismic survey; however, the 2019 Seismic Reprocessing Volume shows much higher vertical and horizontal resolution. This enhanced resolution of the 2019 Seismic Reprocessing Volume was used to interpreted faults and horizons with much more accuracy. Previously, the seismic volumes were blurry by comparison, resulting in reliable horizon interpretation with uncertain fault interpretation. With the 2019 Seismic Reprocessing Volume, the interpretation of these horizons, faults, and fault offsets was completed with much more confidence. Figure 11 displays higher quality processing of the 2019 Seismic Reprocessing Volume up to the ground surface without interpretation. Figure 12 is a close-up view of the Mt. Simon with horizon and fault interpretation.

Before the horizon interpretation, fault interpretation, and petrophysical property modeling (Section 4.4) were completed, a quality control process of the seismic was performed. The 2019 Seismic Reprocessing Volume was depth converted to the time domain by Sterling Seismic, and the interpretable horizons show good ties to the well tops (Figure 10). With the 2019 Seismic Reprocessing Volume, a new porosity cube (2019 Porosity Cube) was provided from an inversion completed by Sterling Seismic (Figure 13 and Figure 14). This was used primarily for petrophysical property modeling; however, it was also used to better interpret horizons and faults. To be effective, the 2019 Porosity Cube had to have a reasonable tie to the porosity logs from the wells; Figure 15 illustrates this good correlation. On Figure 15, the colored and depth-converted 2019 Porosity Cube ties well with the porosity log (thin black line) and the smoothed to seismic scale porosity log (thick black line). The magnitudes of the porosity values are similar and are generally on depth with each other, meaning that the 2019 Porosity Cube is a reliable representation of the porosity distribution within the Mt Simon. Figure 16 shows a cross-plot of the data from Figure 15 (2019 Porosity Cube versus the smoothed to seismic scale porosity log, which is the thick black line) colored by formation; this shows that there is a reliable correlation between the wells and seismic data. These correlations are never perfect and contain some vertical mismatch, however, the correlations are reliable enough to interpret structure and interpolate petrophysical properties.

The interpretation of faults and horizons were aided by the ant-tracking processing technique, which automatically extracts fault surfaces from the 2019 Seismic Reprocessing Volume (Figure 17). The algorithm uses the principles from ant colony systems to extract surfaces that appear as trends in very noisy data. The algorithm was tuned to highlight ant paths which represent the long vertical discontinuities (potential faults) observed in the 2019 Seismic Reprocessing Volume. These ant paths were overlain with the amplitude and porosity cube volumes and used only to guide the manual interpretation of 28 interpreted faults. Many smaller-scale ant paths were identified; however, only the longer ant paths correlated to interpretable faulting were used to guide the interpretation of these faults (Figure 18 to Figure 23). Ant tracking is a useful tool when identifying small-scale faults and fracture corridors; however, it is not substitute for manual interpretation of faults. Ant paths do not always extend the full length of the interpreted faults. Thus, the algorithm was adjusted many times to achieve a reliable correlation of the ant paths with the interpretable faulting while being careful to not omit smaller ant paths. The horizon and fault interpretation were completed in collaboration between the ISGS and Schlumberger.

The 2019 Seismic Reprocessing Volume amplitudes and the 2019 Porosity Cube were used to interpret the horizons. Generally, the events representing formation horizons were clear across the survey area. Interpretation was completed on the following horizons (Maquoketa, Base of New Albany, Eau Claire Lime Base, Eau Claire Shale, Mt. Simon, Mt. Simon B, Mt. Simon A-Upper, Mt Simon A-Lower, Argenta, and Precambrian). The strongest interpretable signals came from the Precambrian and Argenta Surfaces because of the strong acoustic impedance contrast between the surface tops. One area that remains uncertain is the subsurface high between VW1 and CCS2. Here, the Argenta becomes much thinner and the signal (red) representing the top of the Argenta and the signal (red) representing the top of the Precambrian begin to merge into one stronger signal (bright red) (Figure 10). Because of this signal tuning, it is difficult to know if the Argenta is present on top of this hill or not. Previously in 2015, the Argenta was interpreted to be missing here, meaning that the Mt. Simon was directly in contact with the Precambrian. With the 2019 Seismic Reprocessing Volume, the signal is much clearer and the Argenta on this subsurface high is interpretated to be very thin (~10ft; 3m) to absent in some small areas.

The seismic data show that many of these interpreted faults cut across the Mt Simon, the Argenta and extend into the Precambrian. The seismic signature within the Precambrian basement shows the expected structural complexity compared to the sedimentary deposits of the Mt Simon. Most of the interpreted faults had relatively small displacements (ranging from 0 to 30 ft (9.1m)) with only 9 faults interpreted to have relatively greater displacement ranging from approximately 30 to 59 ft (Table 5) (9.1 to 18.0m Table 6). Figure 24 shows the vertical displacement profile of the Precambrian formation for each of the 9 faults with a maximum displacement greater than 30ft (9.1m). Figure 25 shows the vertical displacement profile of the Precambrian formation for each of the faults with a maximum displacement less than 30ft (9.1m). All 28 interpreted faults are displayed in 3D in Figure 26 to Figure 35 to illustrate the displacement.

There is a loose correlation between these interpreted faults and the microseismic events (Figure 36, Figure 37 and Figure 38). Relocated events are primarily located within the Precambrian basement and trend to the northeast. The location and trend of these microseismic events was used to guide fault interpretation. Most of these events are located within the complex geology of the Precambrian. Therefore, the manual interpretation of so many small faults was far too complex. Instead, these fault splays and/or fracture corridors were represented with a discrete fracture model (DFN) (Williams-Stroud, 2020). The 28 faults manually interpreted here were the more extensive features that could be interpreted up through the Precambrian into the Mt. Simon.

Table 5. Fault Length and Maximum Vertical Displacement Summary (feet)

Fault Number	Maximum Vertical Displacement (m)	Horizontal Length of Fault (m)	3D Figures of Faults
Fault #1	59	2827	Figure 26
Fault #2	39	4211	Figure 27
Fault #3	45	3000	Figure 28
Fault #4	34	1541	Figure 29
Fault #5	50	2326	Figure 30
Fault #6	37	2453	Figure 31
Fault #7	29	4479	Figure 32
Fault #8	30	1880	Figure 33
Fault #9	29	2084	Figure 34
Fault #10 to Fault #28	<30	<2220	Figure 35

Table 6. Fault Length and Maximum Vertical Displacement Summary (meters)

Fault Number	Maximum Vertical Displacement (m)	Horizontal Length of Fault (m)	3D Figures of Faults
Fault #1	18.0	861.9	Figure 26
Fault #2	11.9	1283.8	Figure 27
Fault #3	13.7	914.6	Figure 28
Fault #4	10.4	469.8	Figure 29
Fault #5	15.2	709.1	Figure 30
Fault #6	11.3	747.9	Figure 31
Fault #7	8.8	1365.5	Figure 32
Fault #8	9.1	573.2	Figure 33
Fault #9	8.8	635.4	Figure 34
Fault #10 to Fault #28	<9.1	<676.8	Figure 35

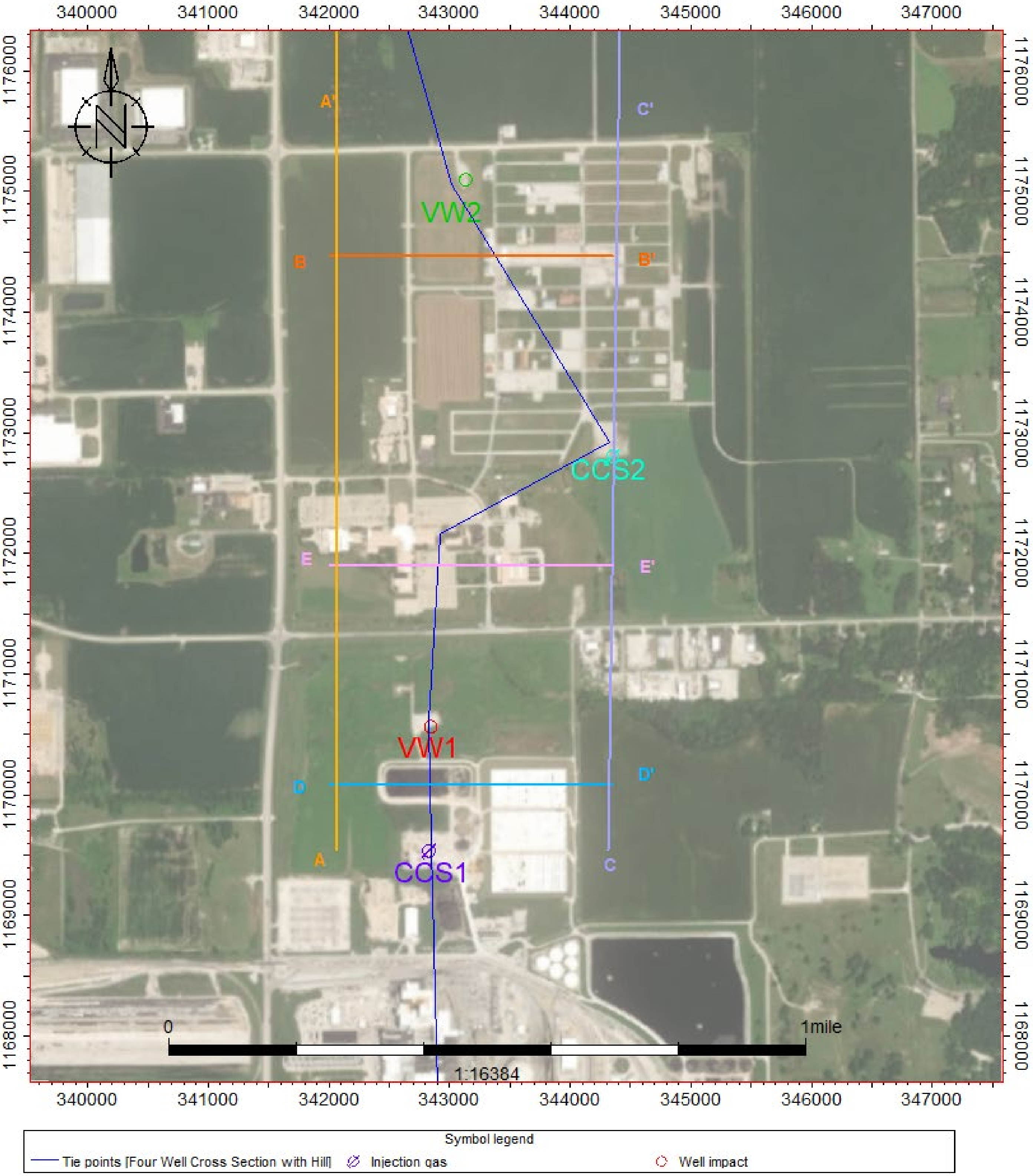

Figure 7. Seismic interpretation map showing the locations of the highlighted seismic interpretation sections.

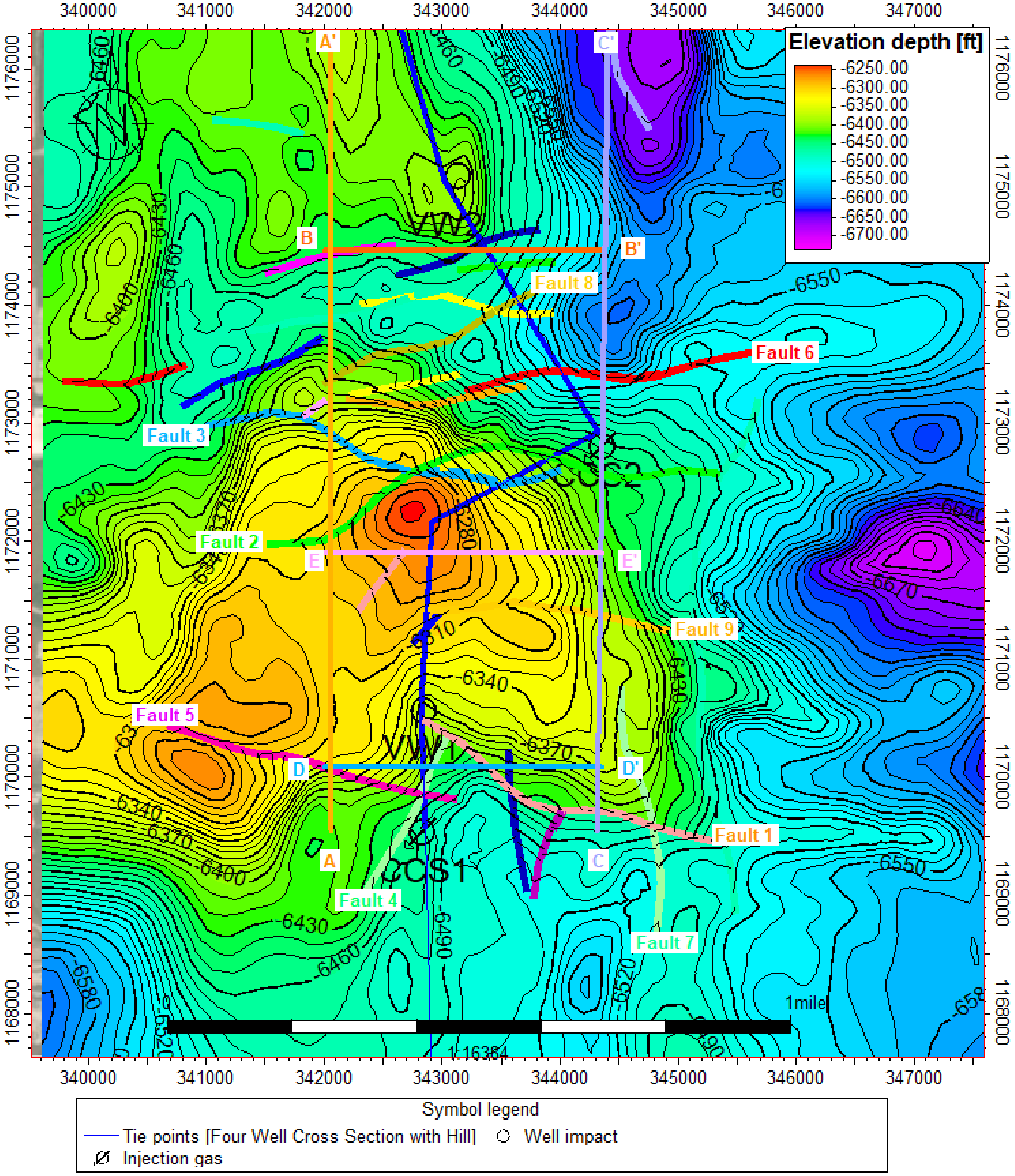

Figure 8. Seismic interpretation map of the Precambrian horizon showing the locations of seismic cross sections.

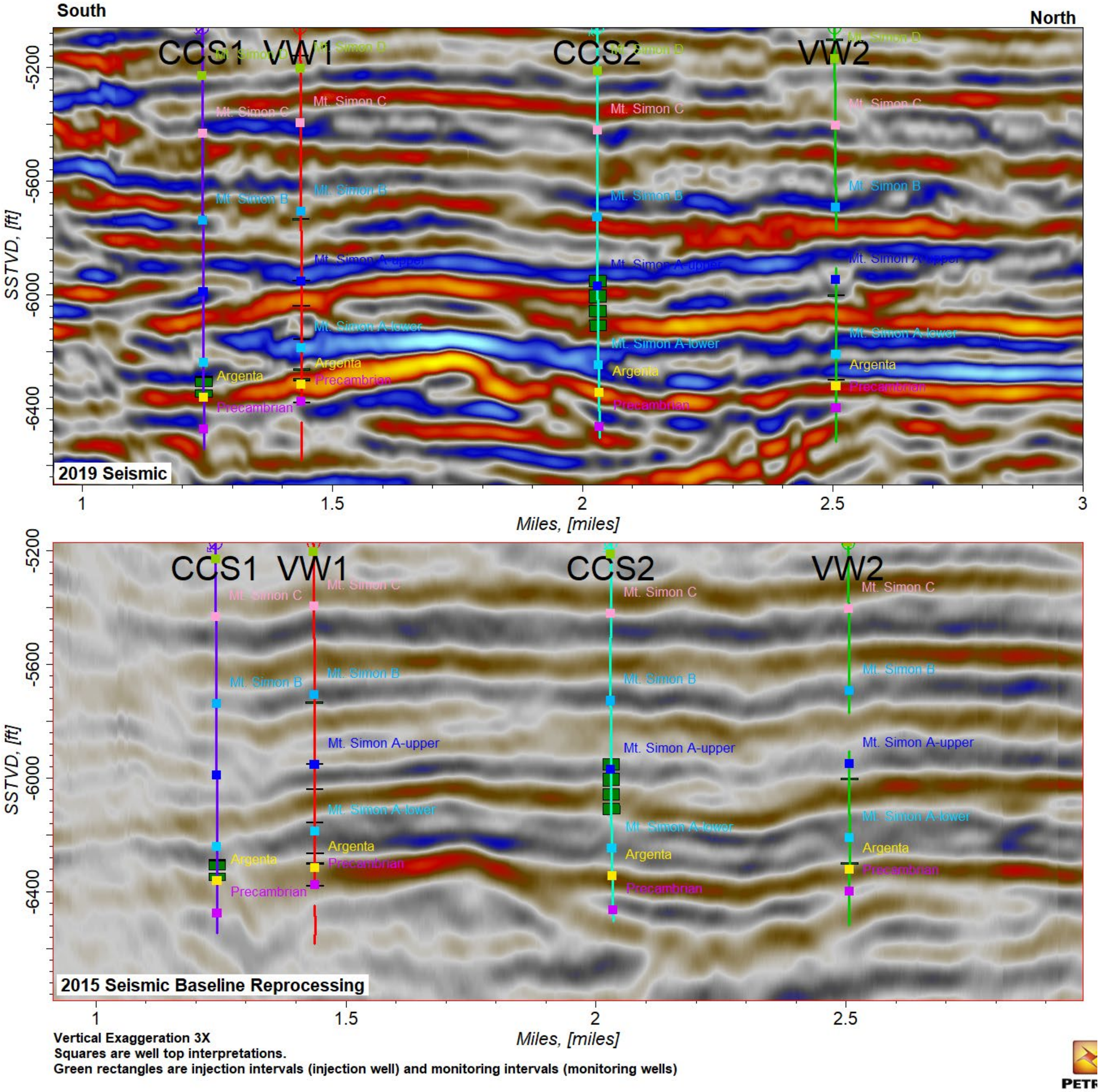

Vertical Exaggeration 3X
Squares are well top interpretations.
Green rectangles are injection intervals (injection well) and monitoring intervals (monitoring wells)

Figure 9. Four-well cross section. 3D seismic volume vintages (2019 Seismic Reprocessing Volume, top, and 2015 Seismic Baseline Reprocessed, bottom) without interpretation.

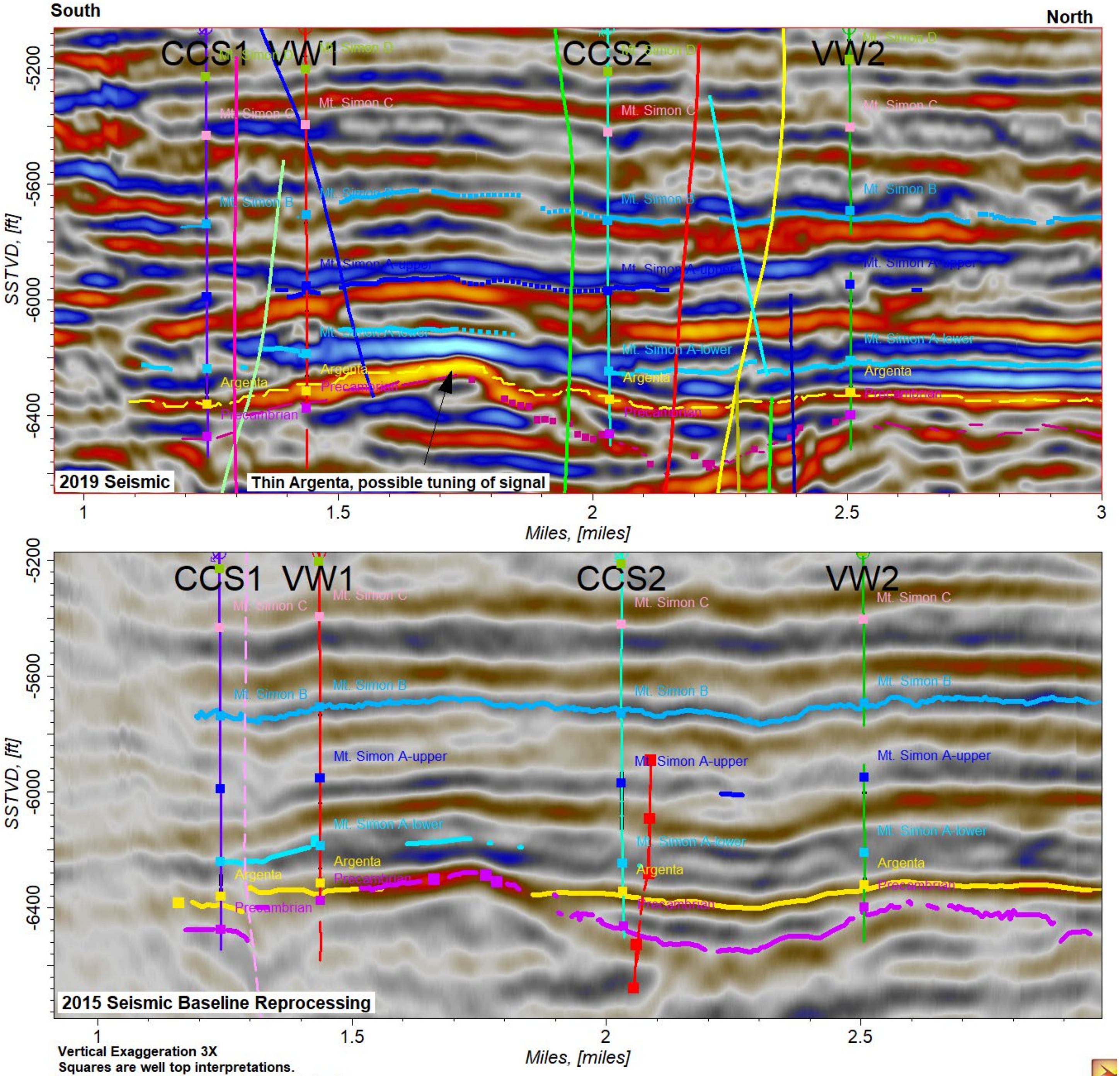

Vertical Exaggeration 3X
Squares are well top interpretations.
Horizontal lines are interpreted seismic horizons.
Vertical lines are seismic fault interpretation.
Green rectangles are injection intervals (injection well) and monitoring intervals (monitoring wells)

Figure 10. Four-well cross section. 3D Seismic volume vintages (2019 Seismic Reprocessing Volume, top, and 2015 Seismic Baseline Reprocessed, bottom) with interpretation.

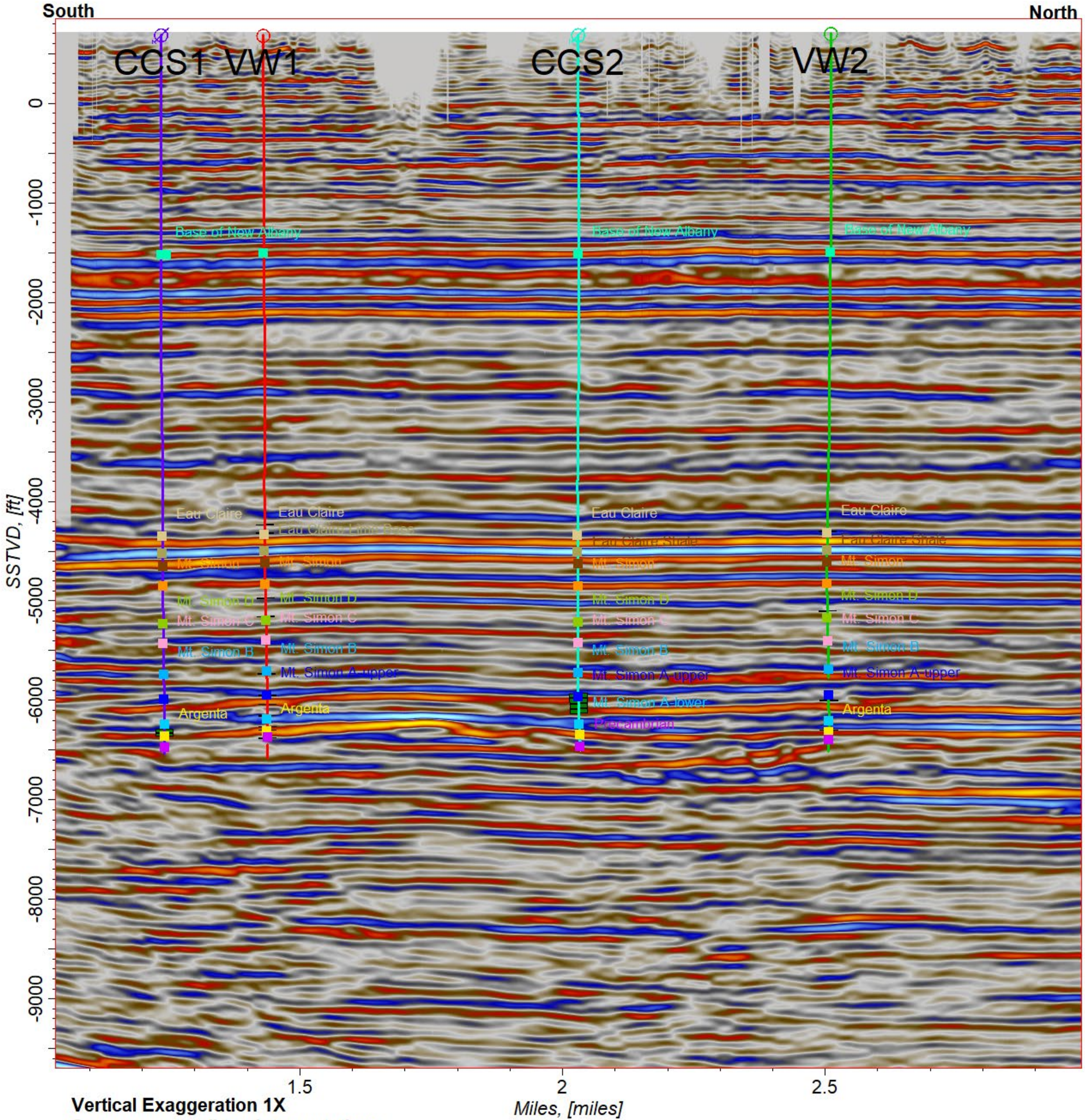

Vertical Exaggeration 1X
Squares are well top interpretations.
Green rectangles are injection intervals (injection well) and monitoring intervals (monitoring wells)

Figure 11. Four-well cross section. 2019 Seismic Reprocessing volume to surface.

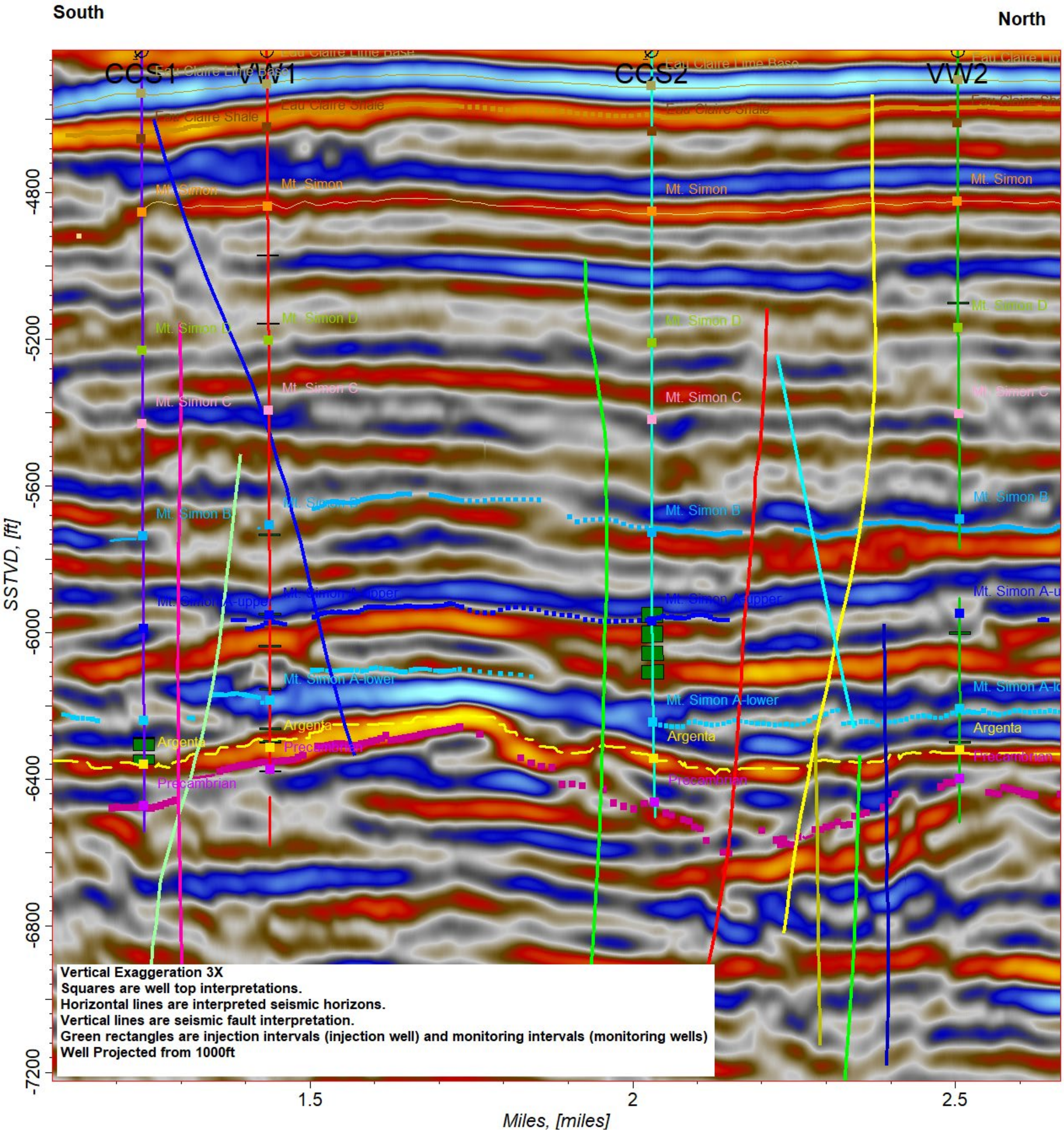

Vertical Exaggeration 3X
Squares are well top interpretations.
Horizontal lines are interpreted seismic horizons.
Vertical lines are seismic fault interpretation.
Green rectangles are injection intervals (injection well) and monitoring intervals (monitoring wells)
Well Projected from 1000ft

Figure 12. Four-well cross section. 2019 Seismic Reprocessing volume with interpretation displaying injection interval.

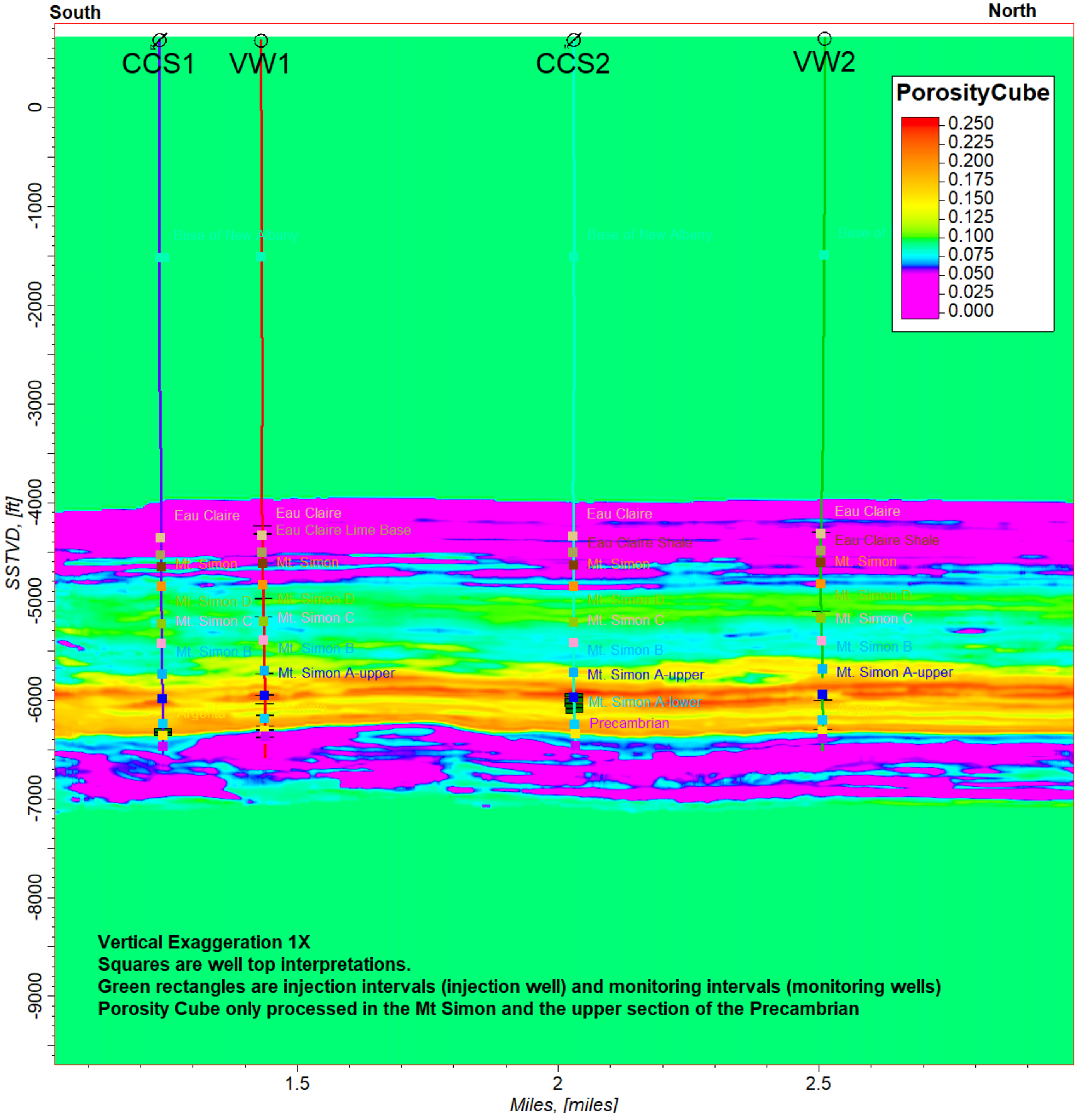

Vertical Exaggeration 1X
Squares are well top interpretations.
Green rectangles are injection intervals (injection well) and monitoring intervals (monitoring wells)
Porosity Cube only processed in the Mt Simon and the upper section of the Precambrian

Figure 13. Four-well cross section. 2019 Porosity Cube to surface.

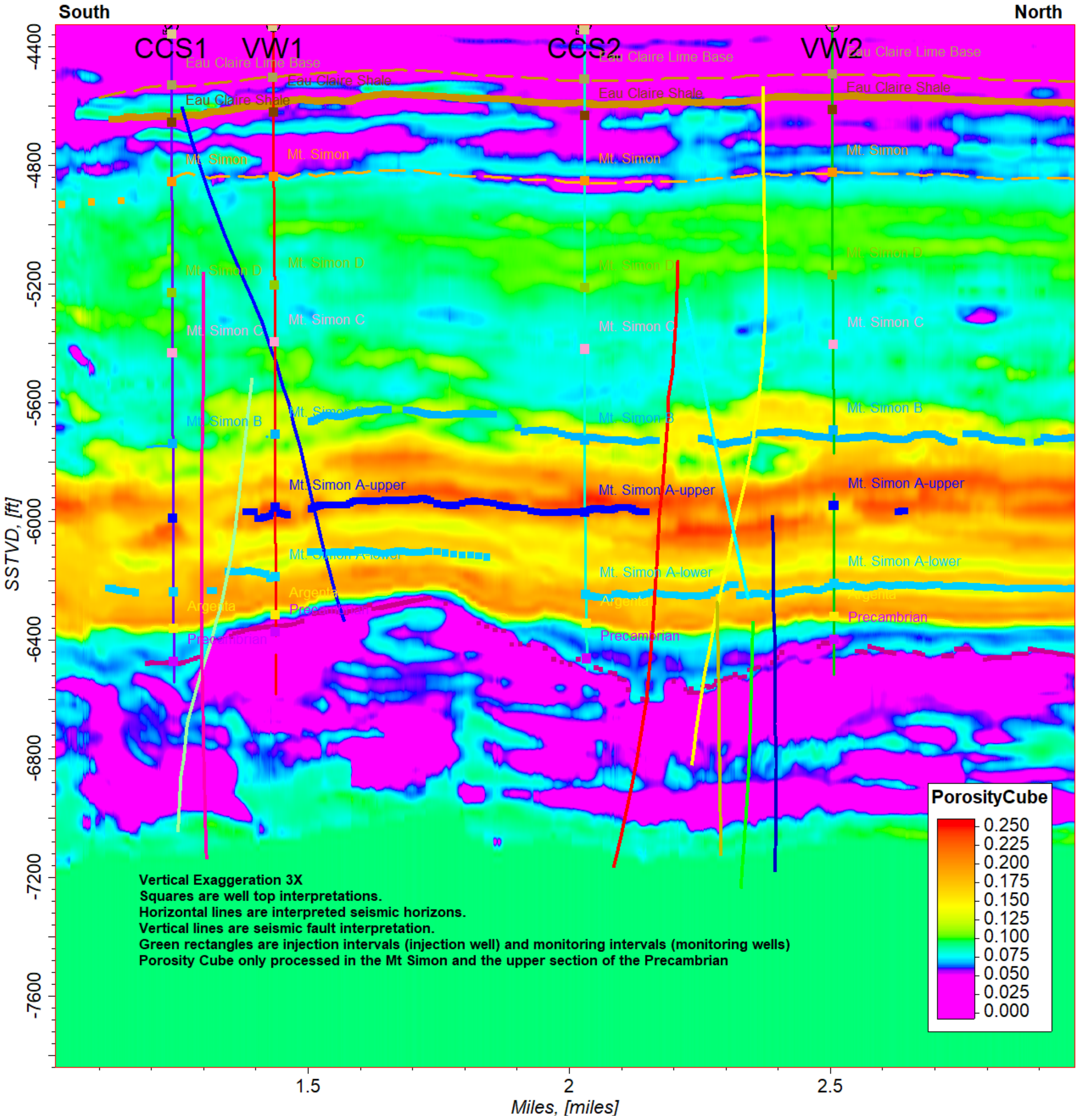

Vertical Exaggeration 3X
Squares are well top interpretations.
Horizontal lines are interpreted seismic horizons.
Vertical lines are seismic fault interpretation.
Green rectangles are injection intervals (injection well) and monitoring intervals (monitoring wells)
Porosity Cube only processed in the Mt Simon and the upper section of the Precambrian

Figure 14. Four-well cross section. 2019 Porosity Cube with interpretation displaying injection interval.

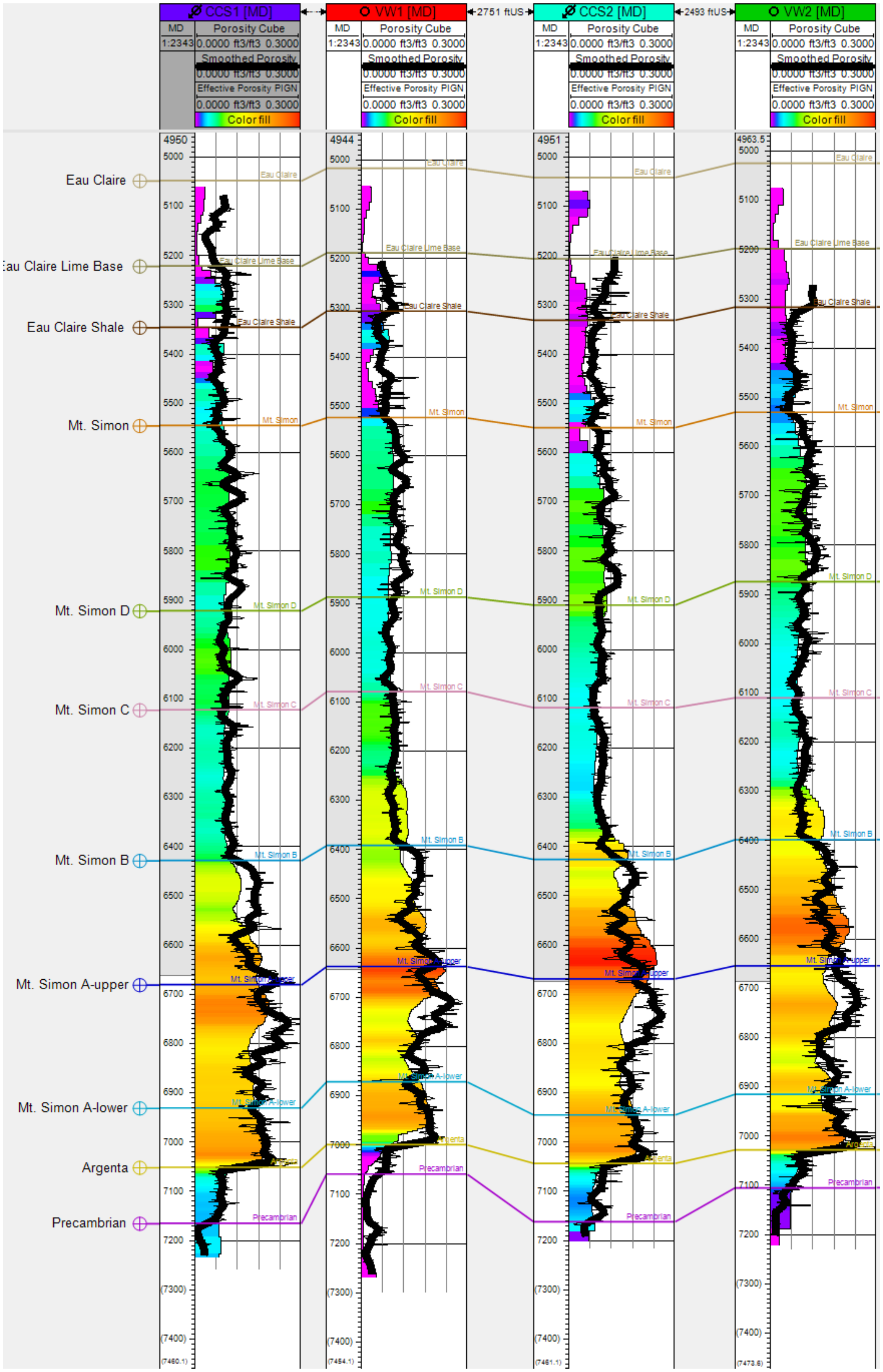

Figure 15. Seismic quality correlation. four-well section window cross section of 2019 Porosity Cube showing the well log effective porosity and seismic scale porosity log (smoothed porosity).

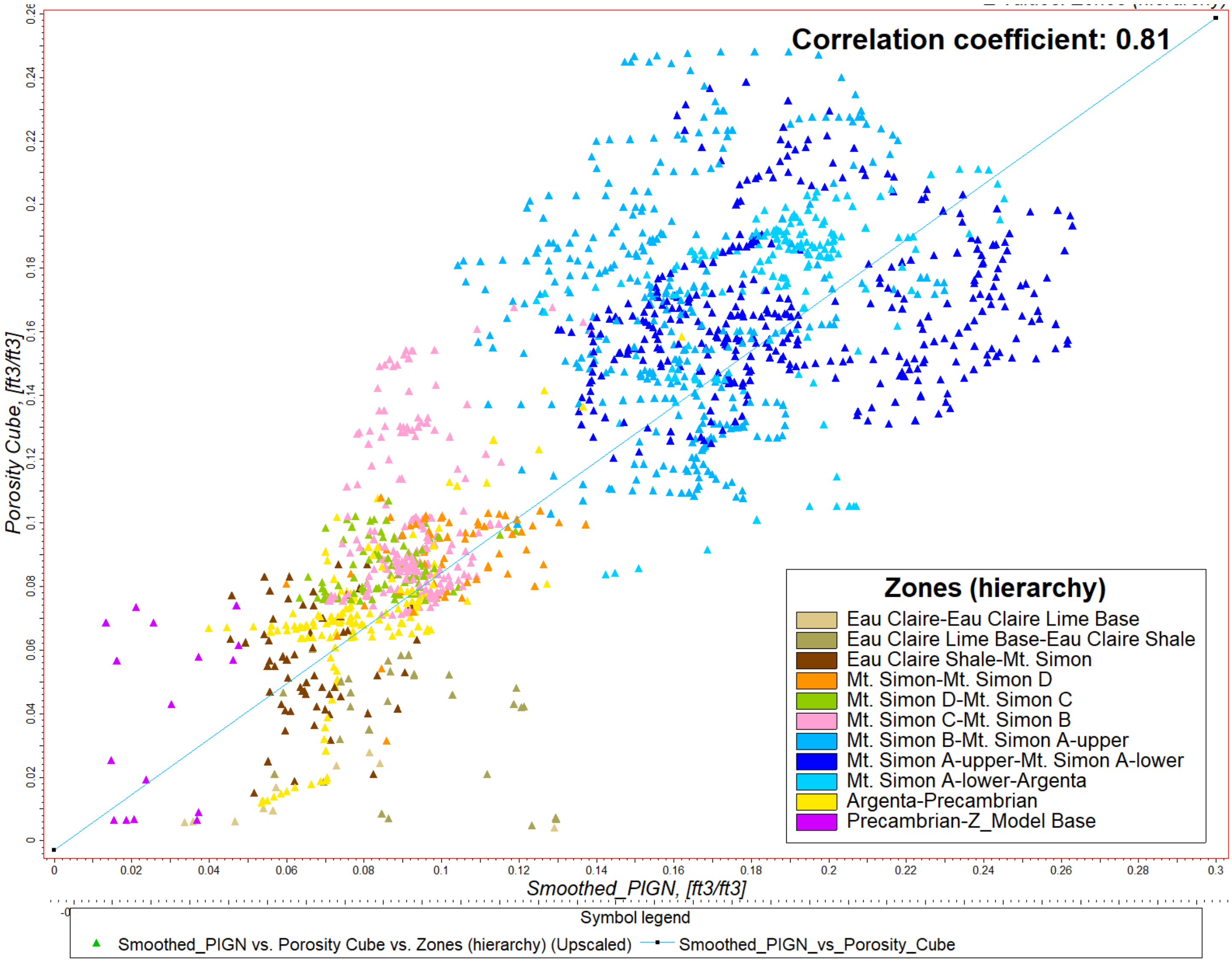

Figure 16. 2019 Seismic Reprocessing Volume well correlation quality control cross-plot.

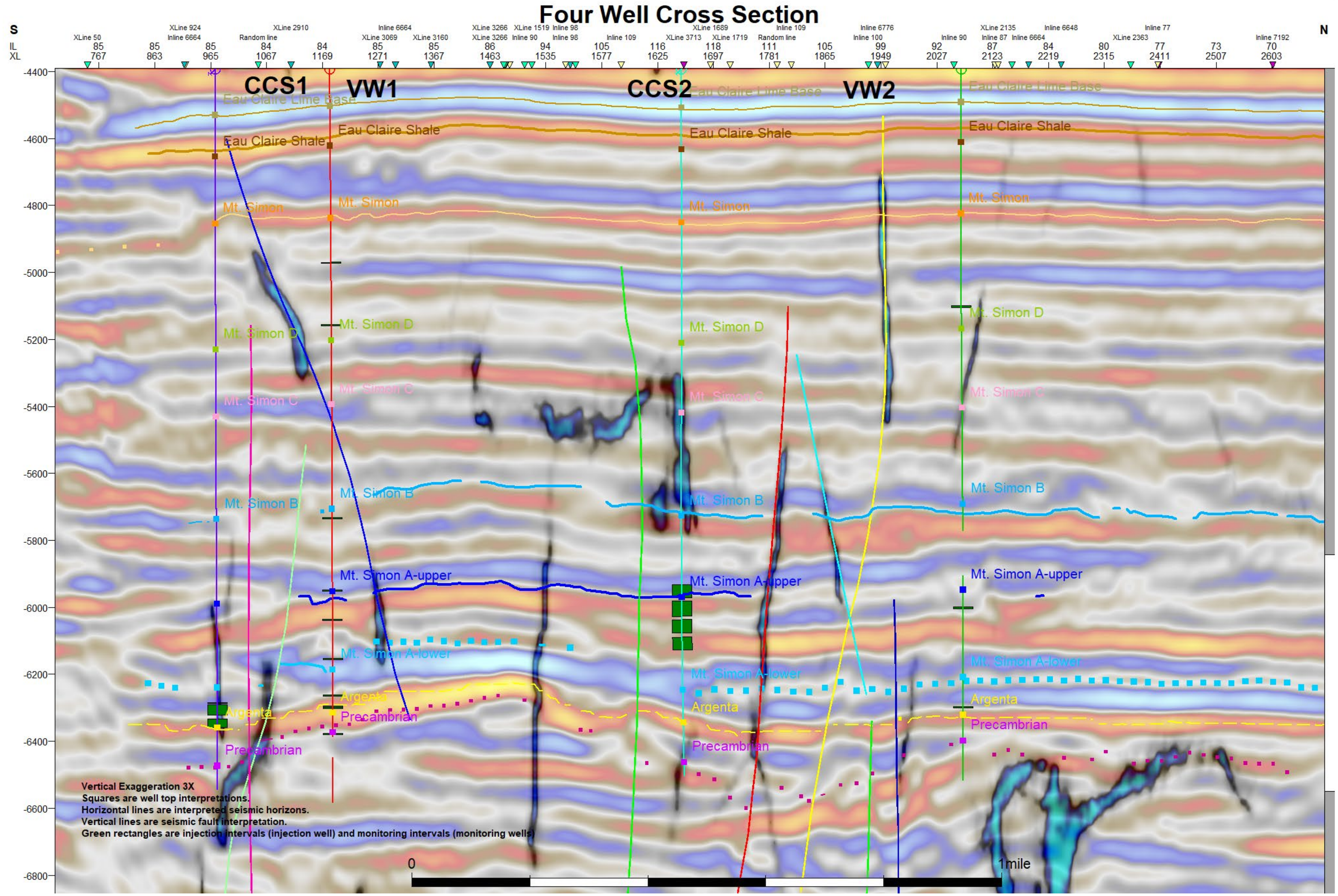

Vertical Exaggeration 3X
Squares are well top interpretations.
Horizontal lines are interpreted seismic horizons.
Vertical lines are seismic fault interpretation.
Green rectangles are injection intervals (injection well) and monitoring intervals (monitoring wells)

Figure 17. Four-well cross section. 3D 2019 Seismic Reprocessing Volume with ant tracking overlay, horizon interpretation and fault interpretation.

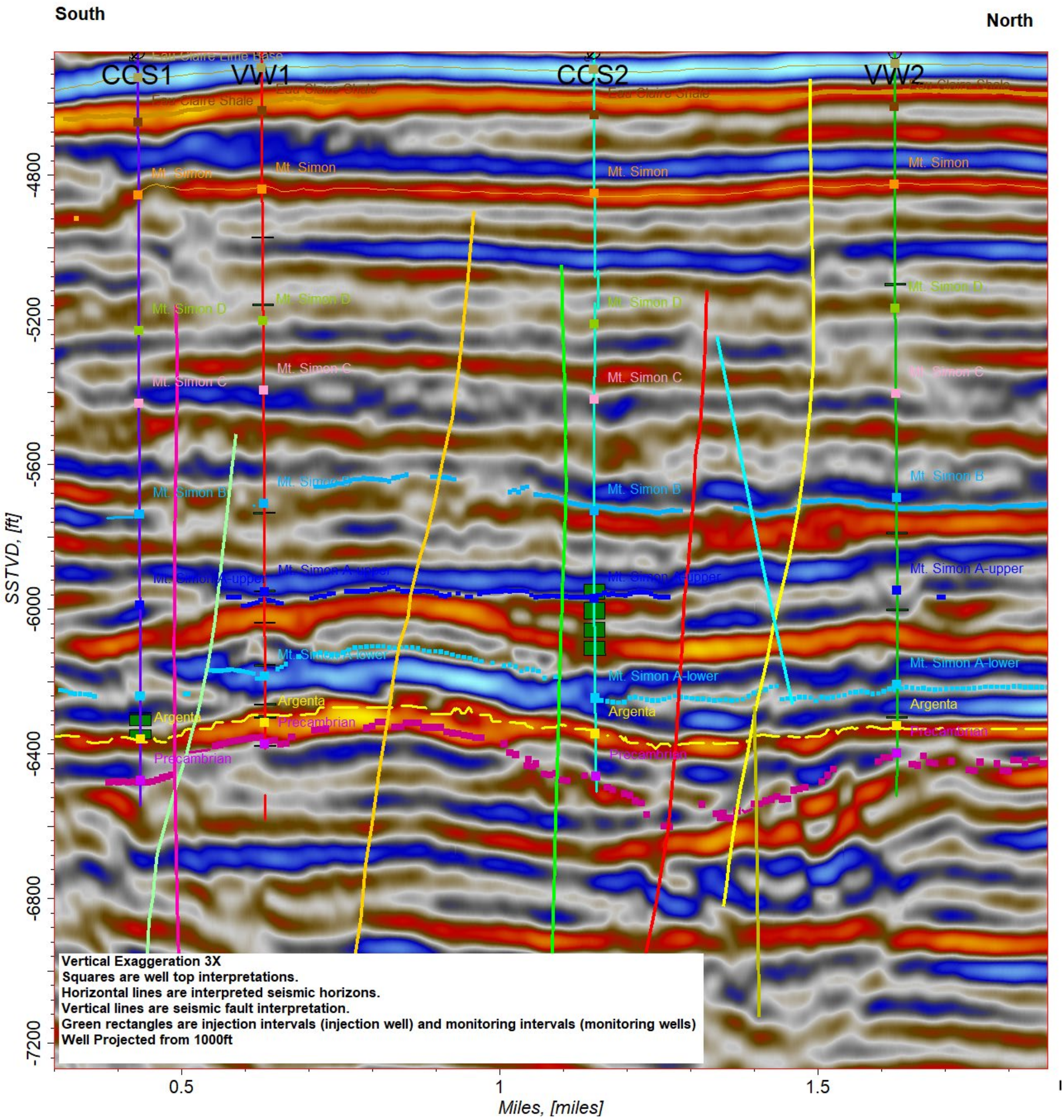

Vertical Exaggeration 3X
Squares are well top interpretations.
Horizontal lines are interpreted seismic horizons.
Vertical lines are seismic fault interpretation.
Green rectangles are injection intervals (injection well) and monitoring intervals (monitoring wells)
Well Projected from 1000ft

Figure 18.Four-well cross section. 2019 Seismic Reprocessing Volume with horizon interpretation and fault interpretation.

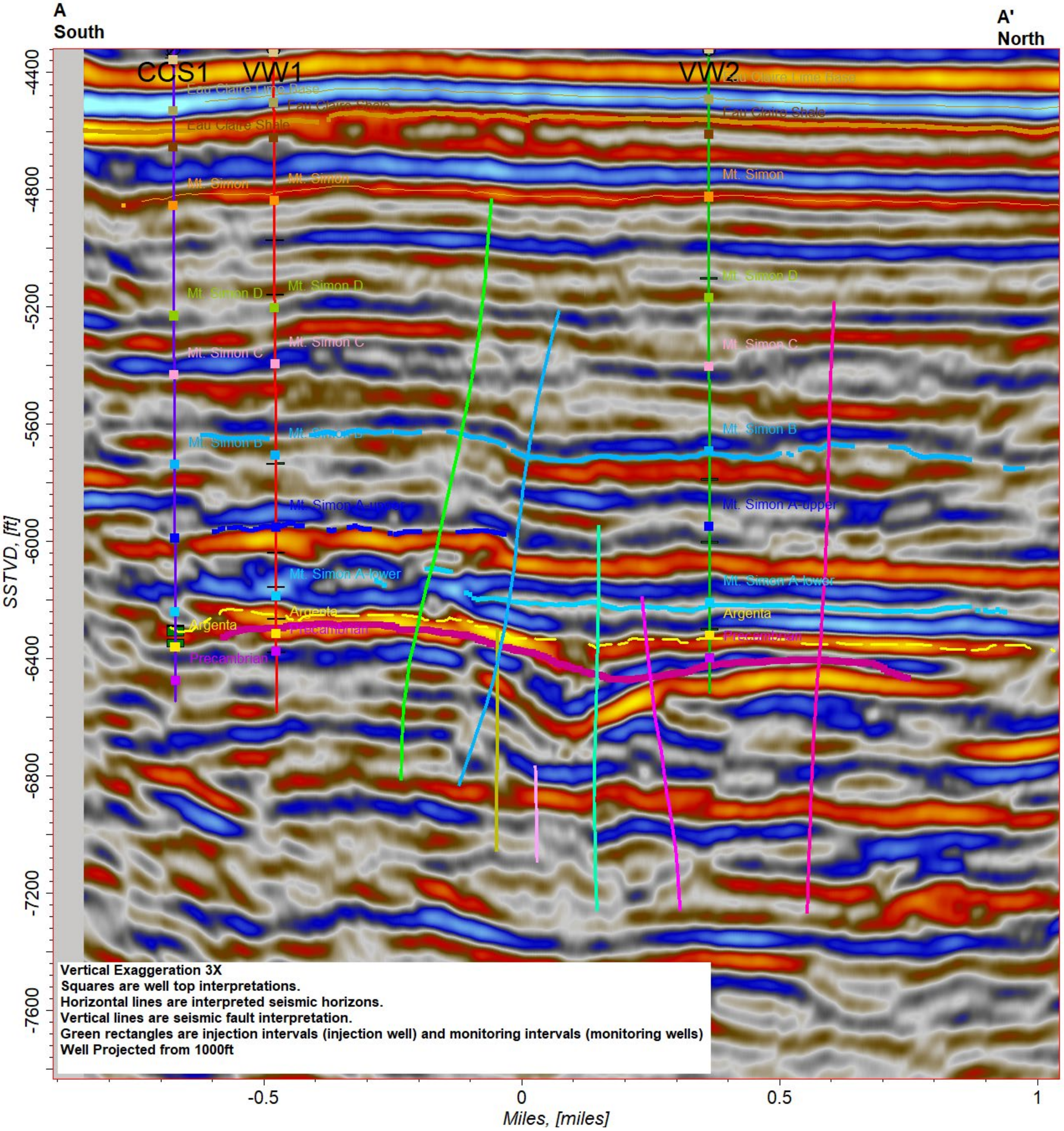

Vertical Exaggeration 3X
Squares are well top interpretations.
Horizontal lines are interpreted seismic horizons.
Vertical lines are seismic fault interpretation.
Green rectangles are injection intervals (injection well) and monitoring intervals (monitoring wells)
Well Projected from 1000ft

Figure 19. A-A'. 2019 Seismic Reprocessing Volume with horizon interpretation and fault interpretation.

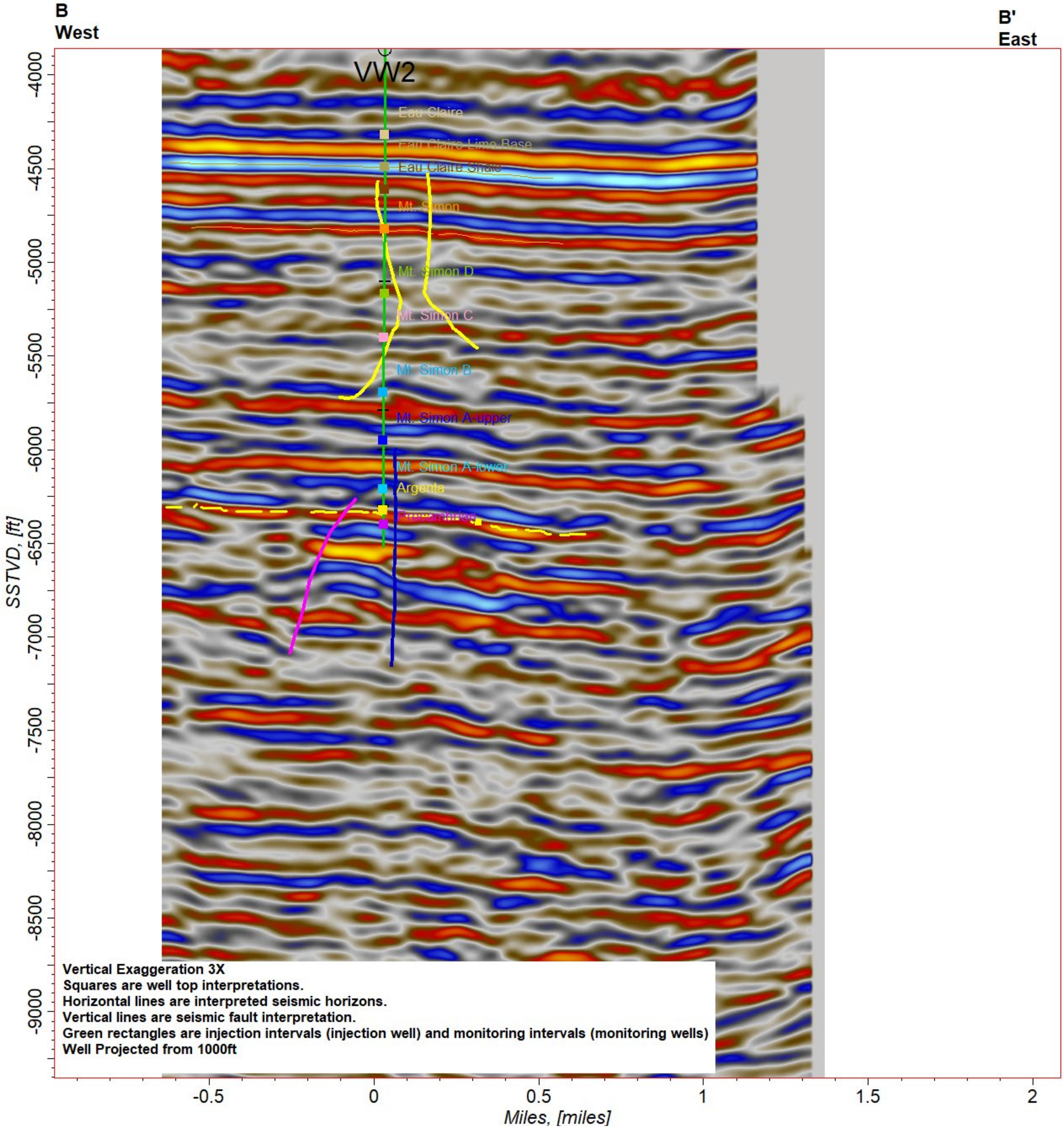

Vertical Exaggeration 3X
Squares are well top interpretations.
Horizontal lines are interpreted seismic horizons.
Vertical lines are seismic fault interpretation.
Green rectangles are injection intervals (injection well) and monitoring intervals (monitoring wells)
Well Projected from 1000ft

Figure 20.B-B'. 2019 Seismic Reprocessing Volume with horizon interpretation and fault interpretation.

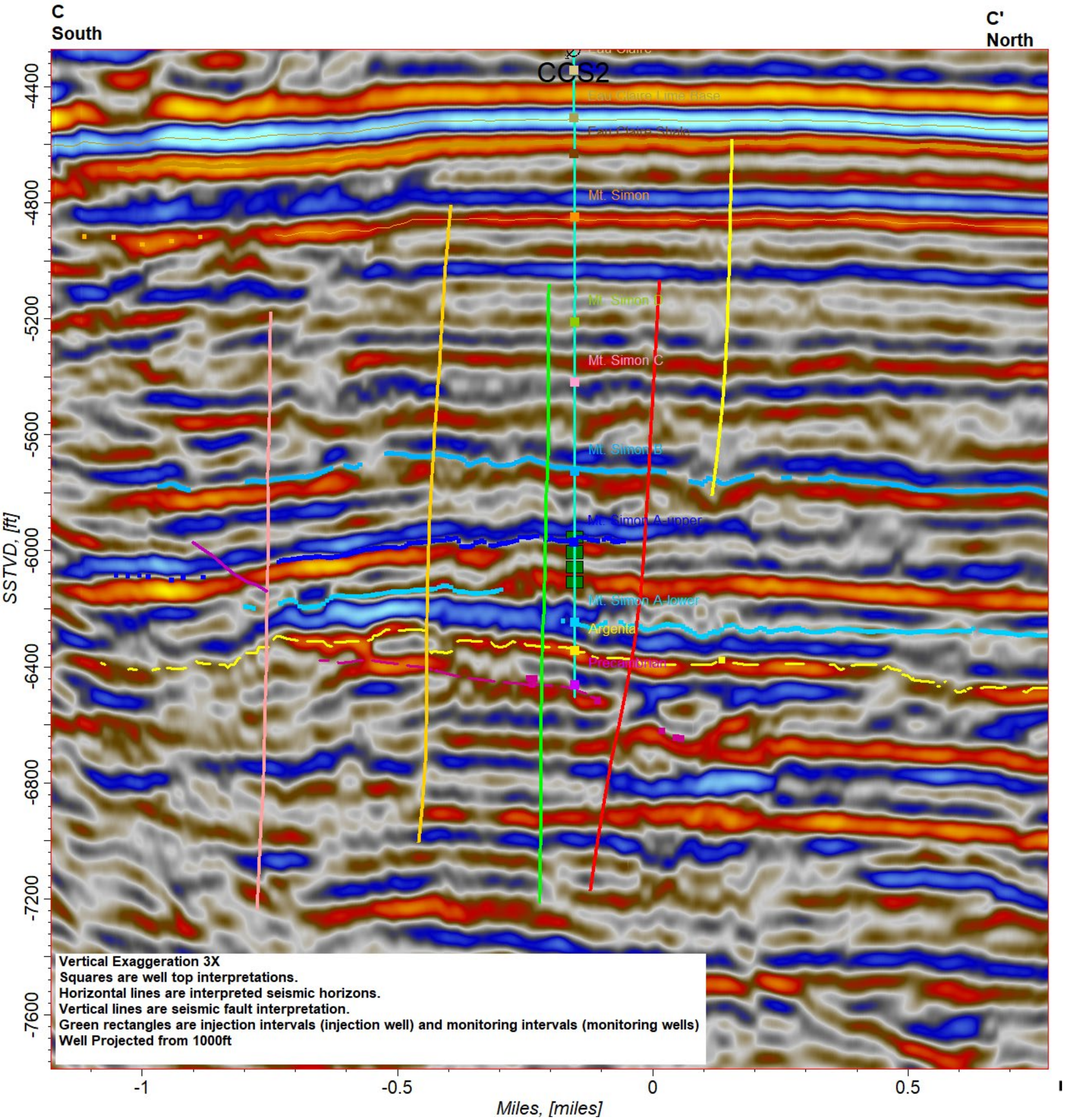

Vertical Exaggeration 3X
Squares are well top interpretations.
Horizontal lines are interpreted seismic horizons.
Vertical lines are seismic fault interpretation.
Green rectangles are injection intervals (injection well) and monitoring intervals (monitoring wells)
Well Projected from 1000ft

Figure 21. C-C'. 2019 Seismic Reprocessing Volume with horizon interpretation and fault interpretation.

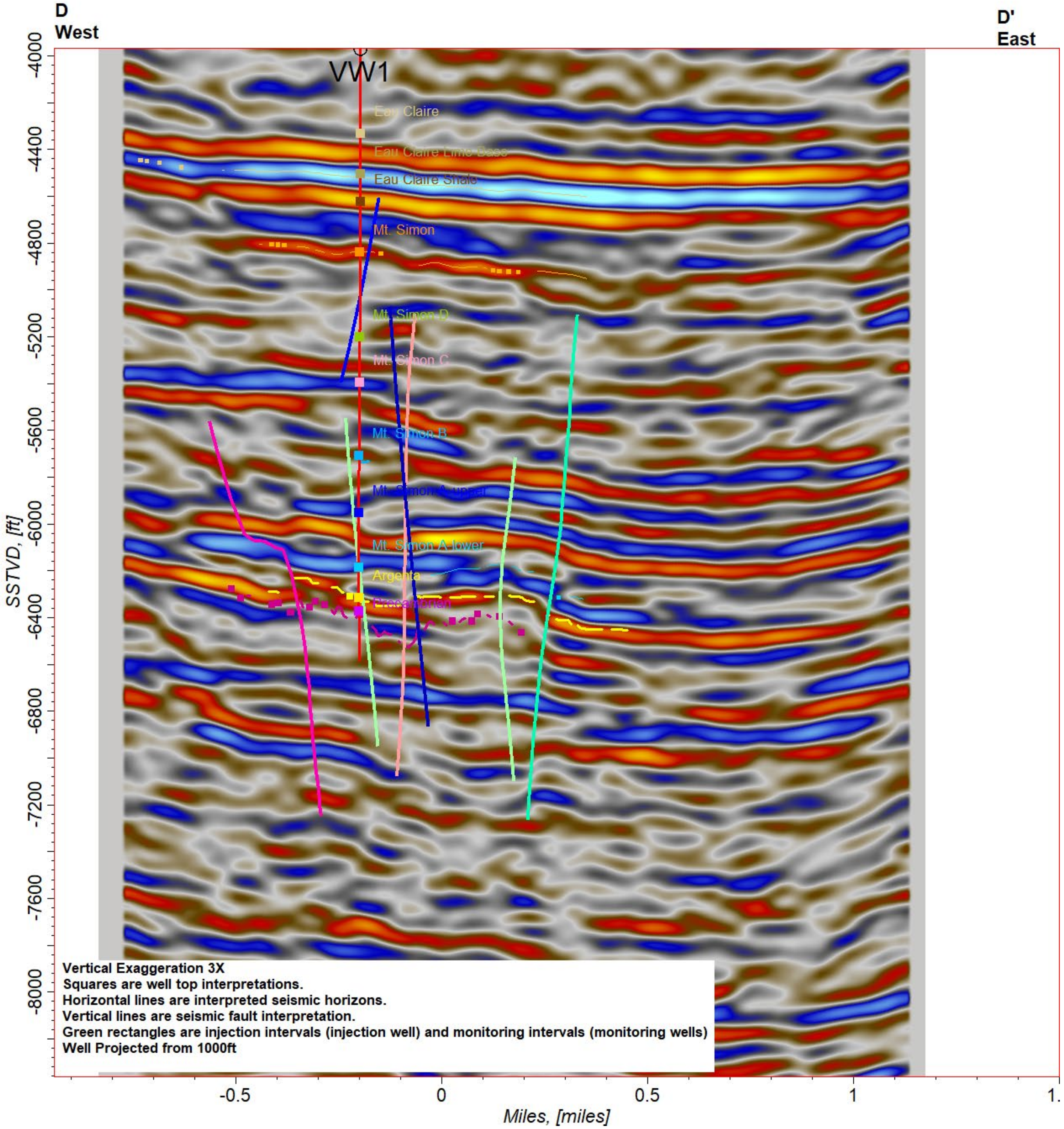

Vertical Exaggeration 3X
Squares are well top interpretations.
Horizontal lines are interpreted seismic horizons.
Vertical lines are seismic fault interpretation.
Green rectangles are injection intervals (injection well) and monitoring intervals (monitoring wells)
Well Projected from 1000ft

Figure 22. D-D'. 2019 Seismic Reprocessing Volume with horizon interpretation and fault interpretation.

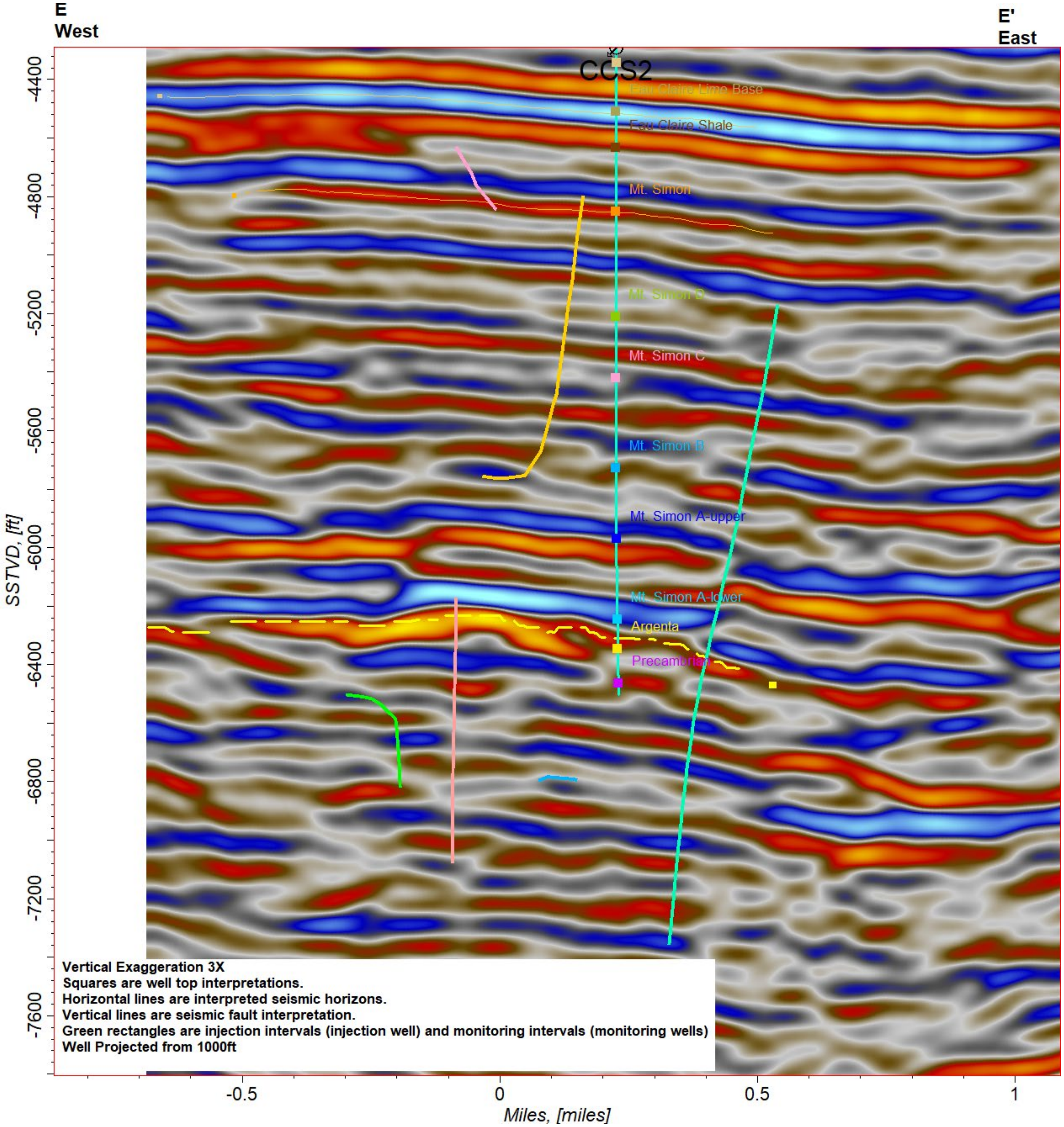

Vertical Exaggeration 3X
Squares are well top interpretations.
Horizontal lines are interpreted seismic horizons.
Vertical lines are seismic fault interpretation.
Green rectangles are injection intervals (injection well) and monitoring intervals (monitoring wells)
Well Projected from 1000ft

Figure 23. E-E'. 2019 Seismic Reprocessing Volume with horizon interpretation and fault interpretation.

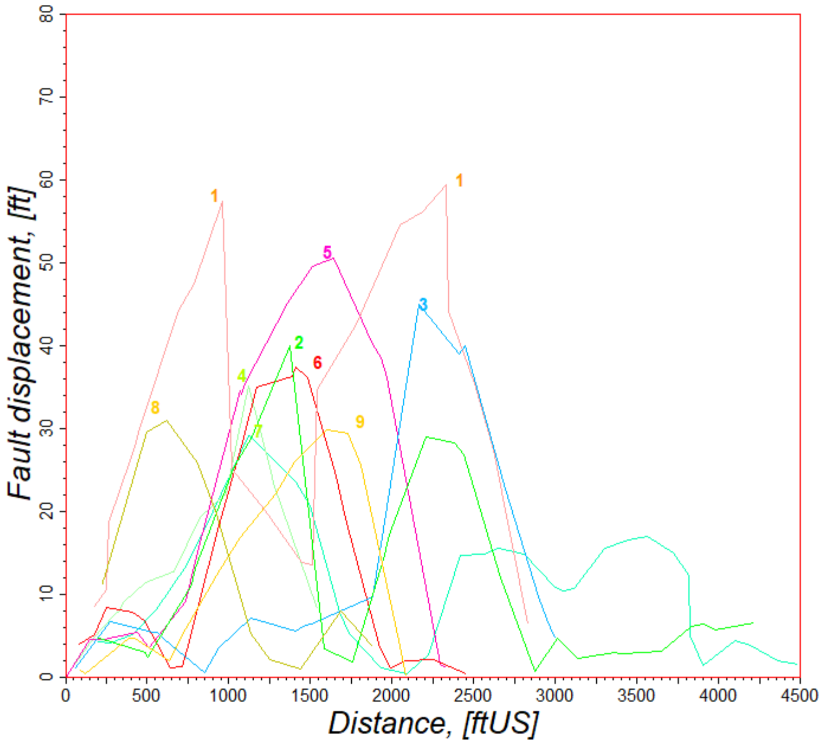

Figure 24. Fault displacement vs fault length. Faults (1-9) with a maximum displacement greater than 30 feet.

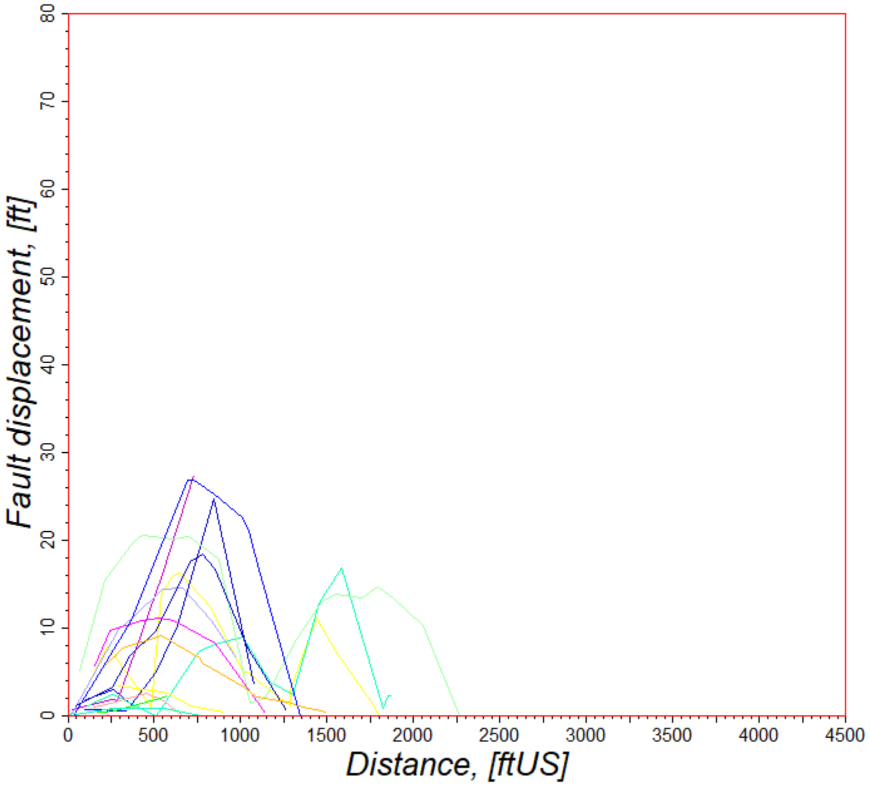

Figure 25. Fault displacement vs fault length. Faults (10-28) with a maximum displacement greater less than 30 feet.

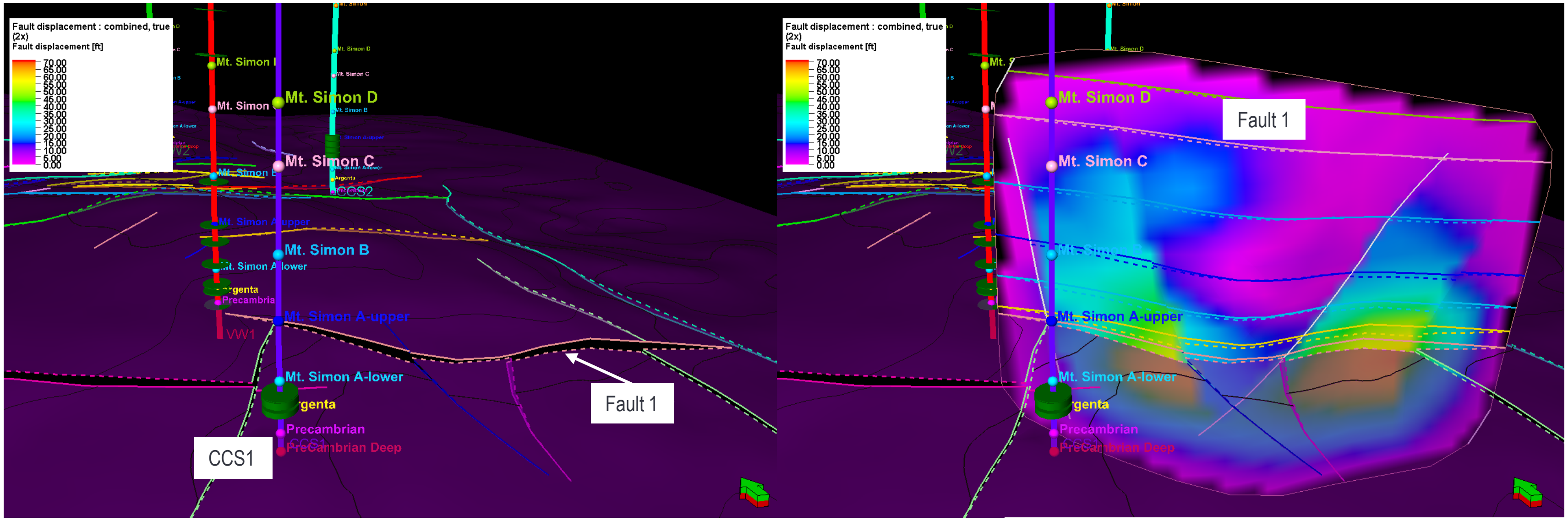

Vertical Exaggeration 1X
Surface is Precambrian
Circles are well top interpretations.
Green circles are injection intervals (injection well) and monitoring intervals (monitoring wells)
50ft contours

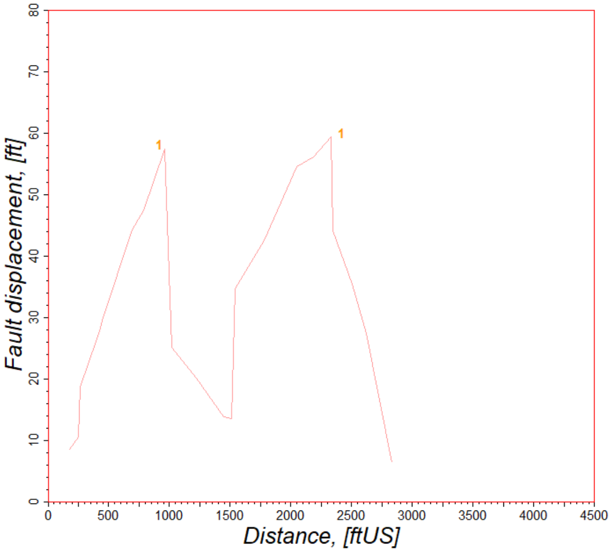

Figure 26. Fault #1 displacement

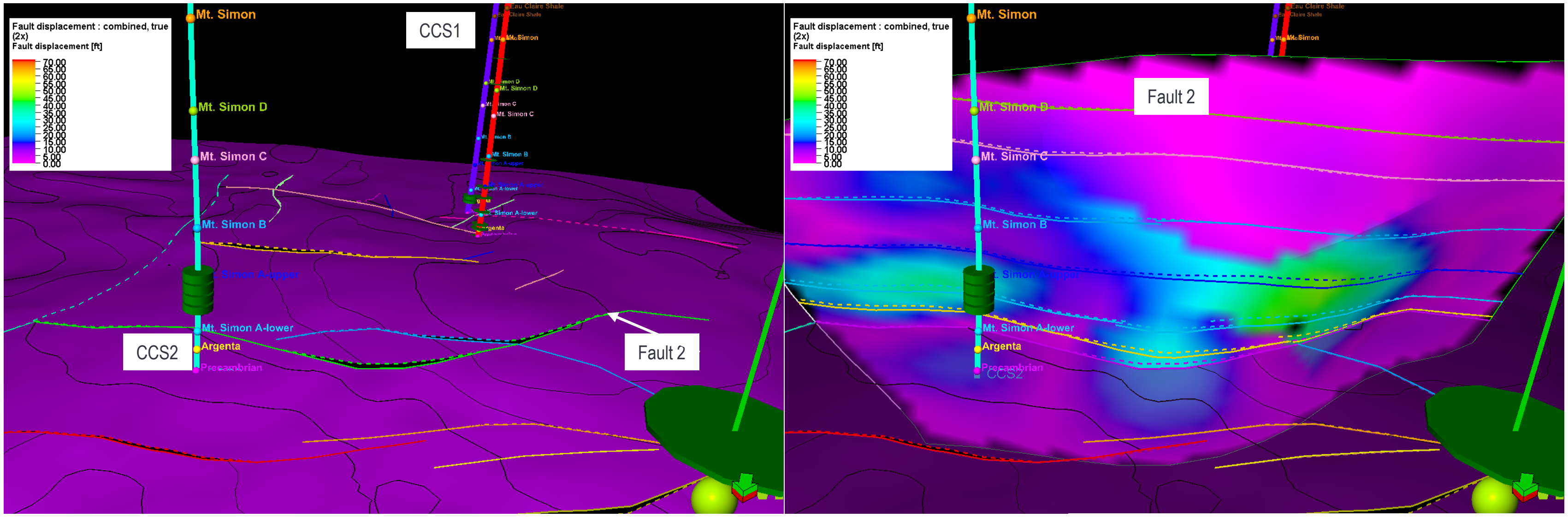

Vertical Exaggeration 1X
Surface is Precambrian
Circles are well top interpretations.
Green circles are injection intervals (injection well) and monitoring intervals (monitoring wells)
50ft contours

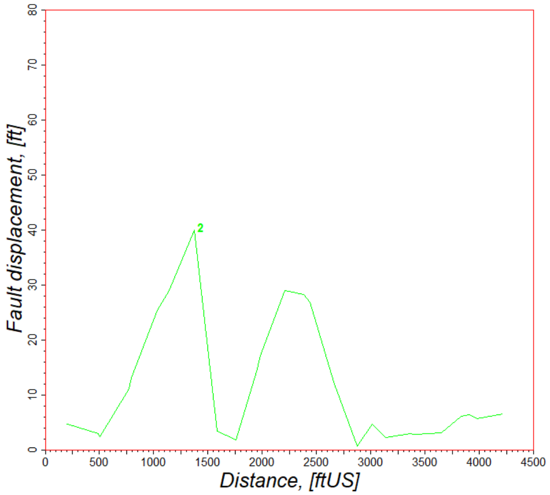

Figure 27. Fault #2 displacement

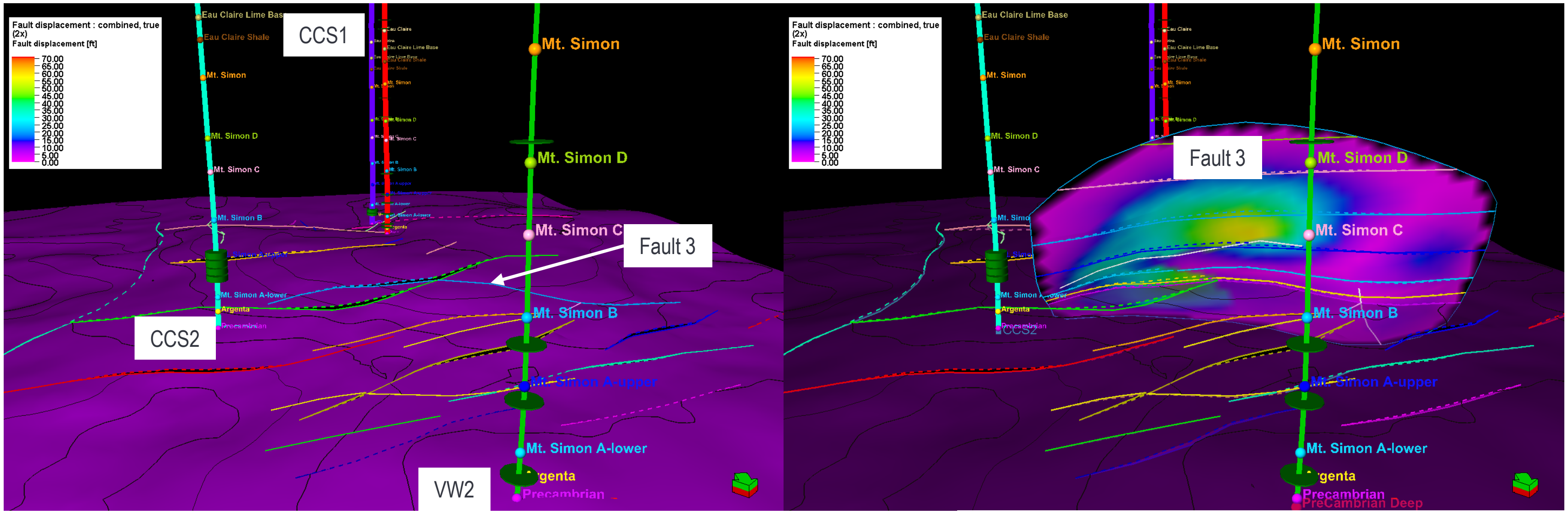

Vertical Exaggeration 1X
Surface is Precambrian
Circles are well top interpretations.
Green circles are injection intervals (injection well) and monitoring intervals (monitoring wells)
50ft contours

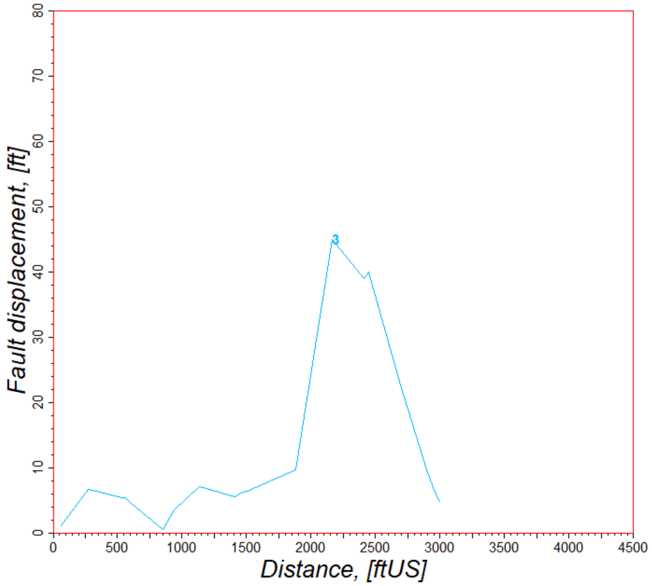

Figure 28. Fault #3 displacement.

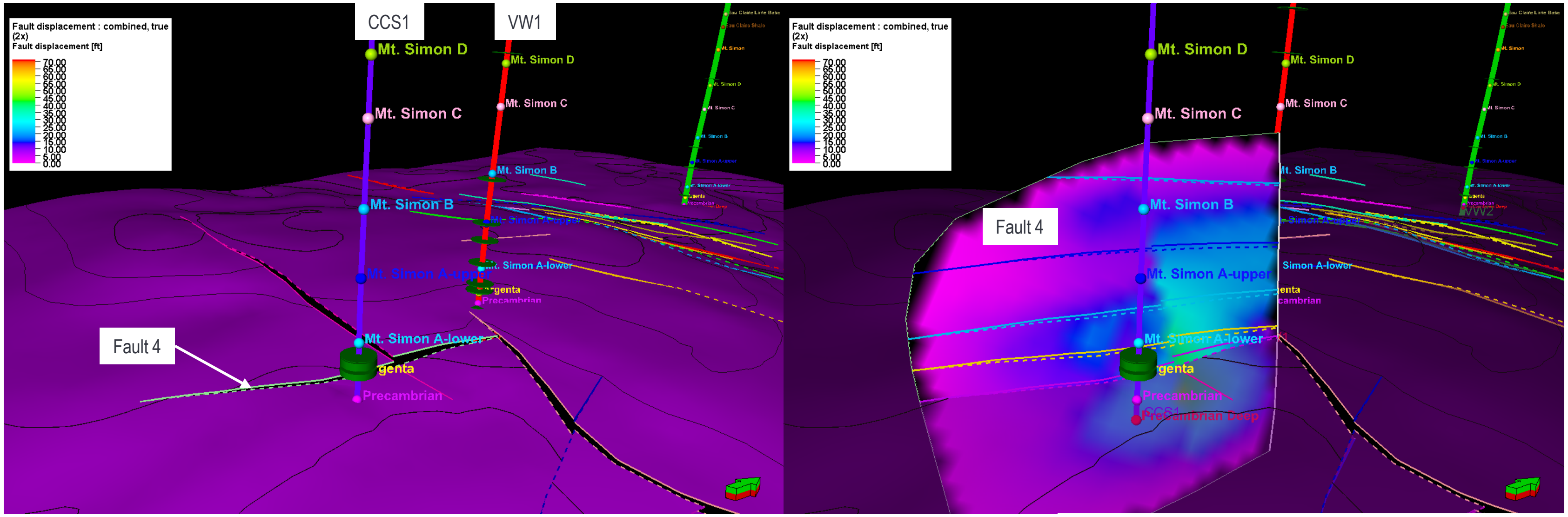

Vertical Exaggeration 1X
Surface is Precambrian
Circles are well top interpretations.
Green circles are injection intervals (injection well) and monitoring intervals (monitoring wells)
50ft contours

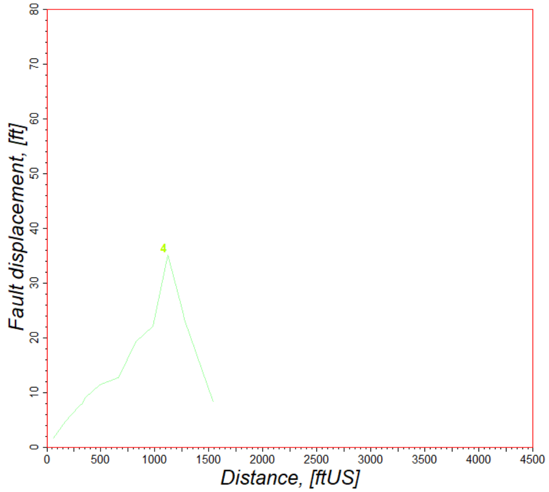

Figure 29. Fault #4 displacement

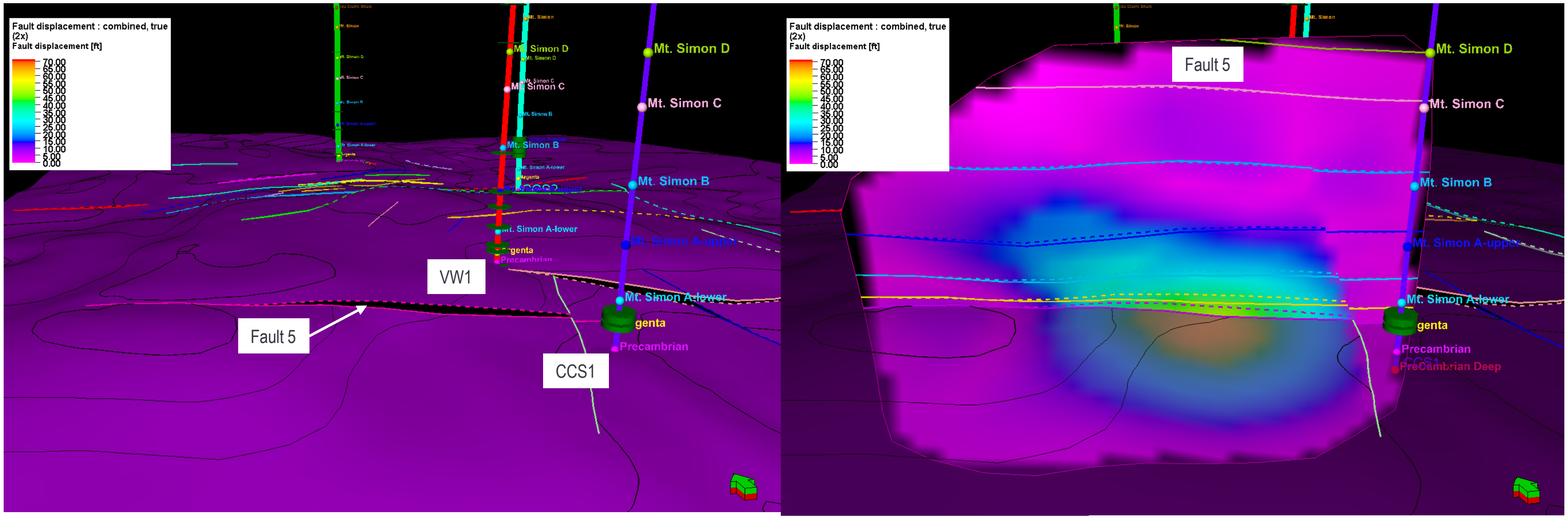

Vertical Exaggeration 1X
Surface is Precambrian
Circles are well top interpretations.
Green circles are injection intervals (injection well) and monitoring intervals (monitoring wells)
50ft contours

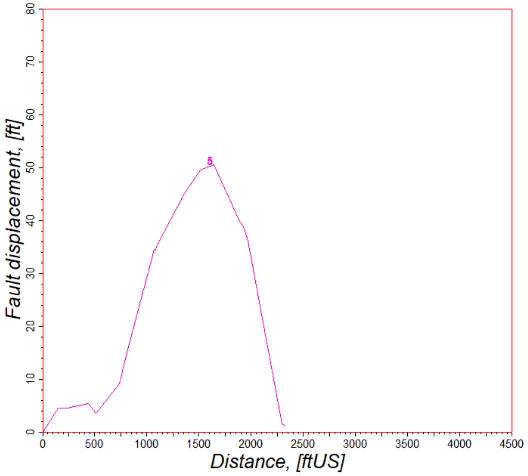

Figure 30. Fault #5 displacement

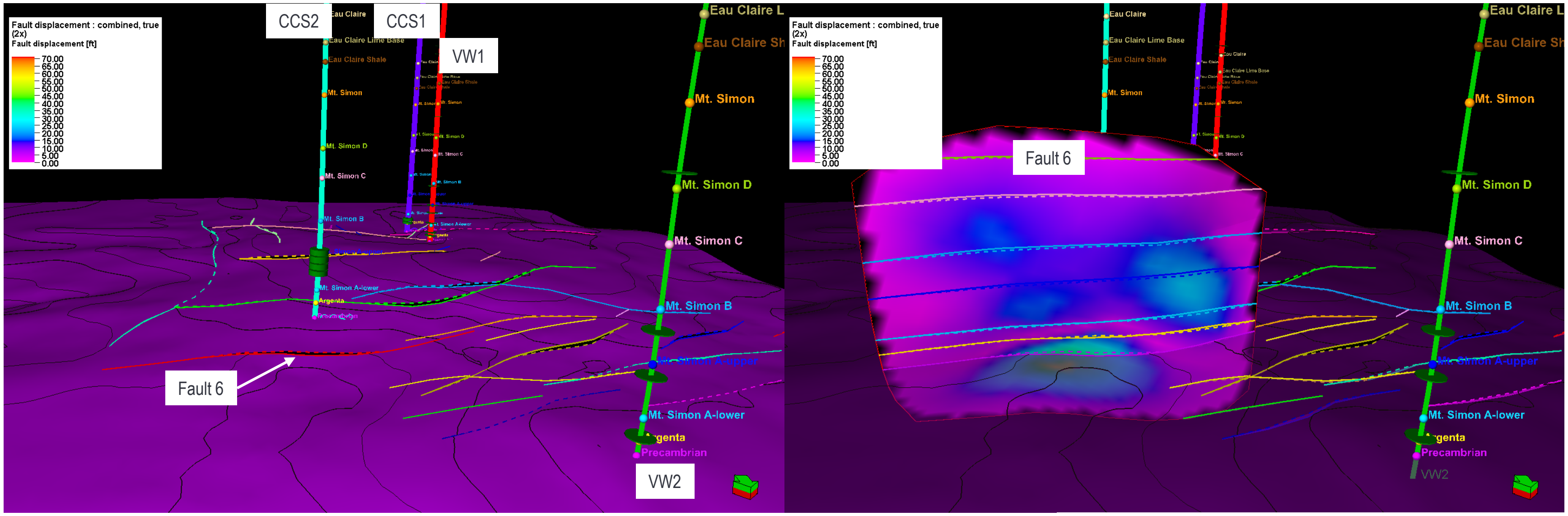

Vertical Exaggeration 1X
Surface is Precambrian
Circles are well top interpretations.
Green circles are injection intervals (injection well) and monitoring intervals (monitoring wells)
50ft contours

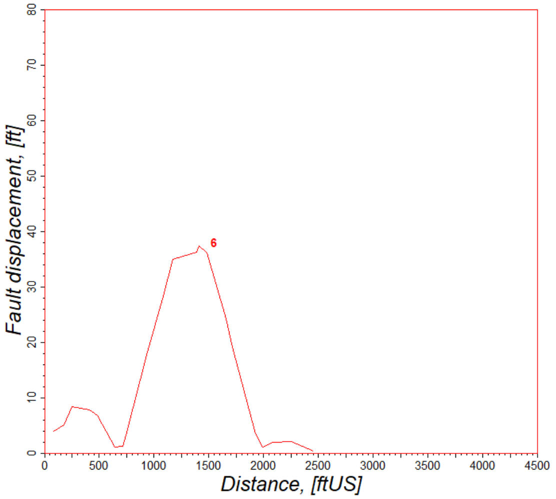

Figure 31. Fault #6 displacement

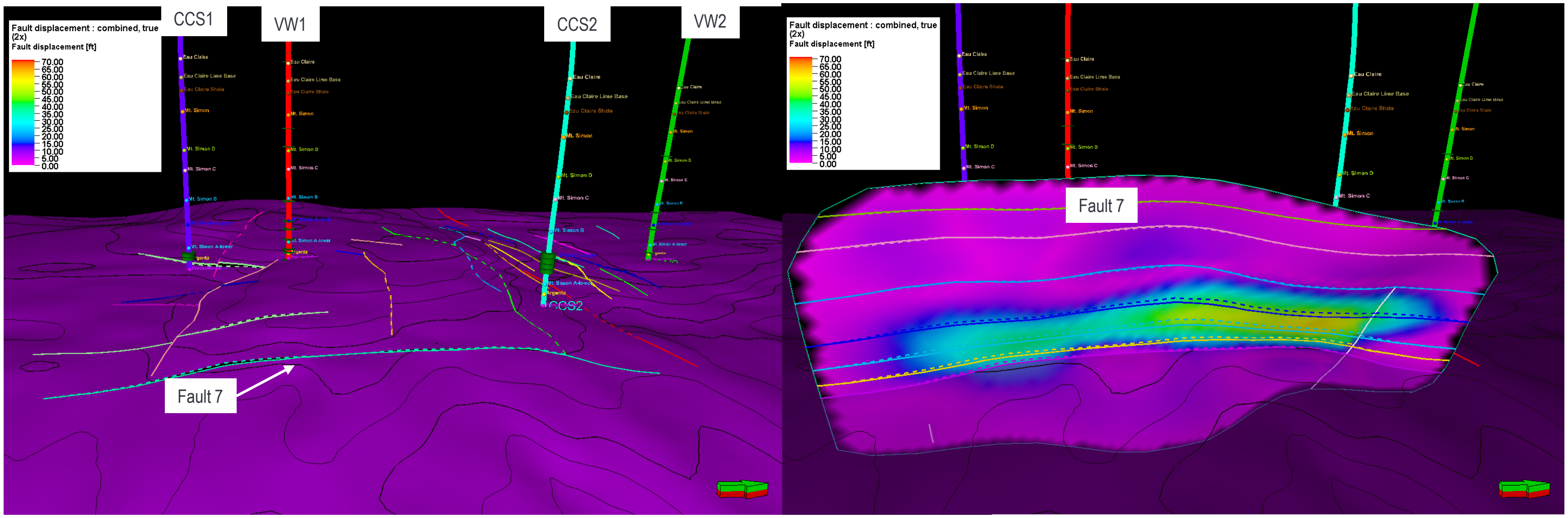

Vertical Exaggeration 1X
Surface is Precambrian
Circles are well top interpretations.
Green circles are injection intervals (injection well) and monitoring intervals (monitoring wells)
50ft contours

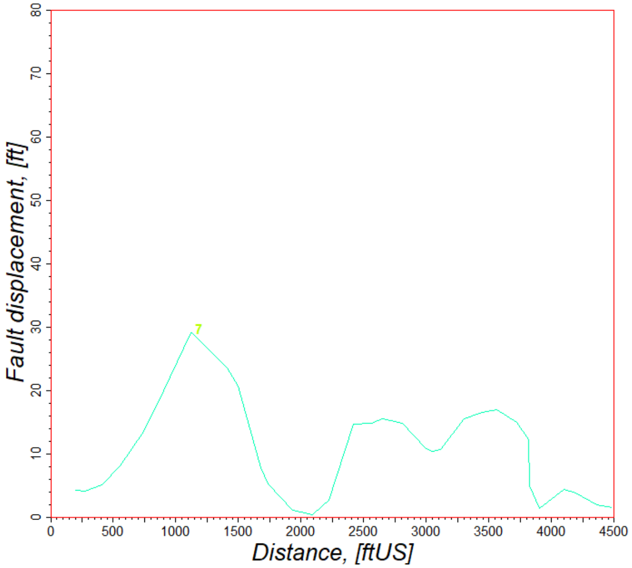

Figure 32. Fault #7 displacement

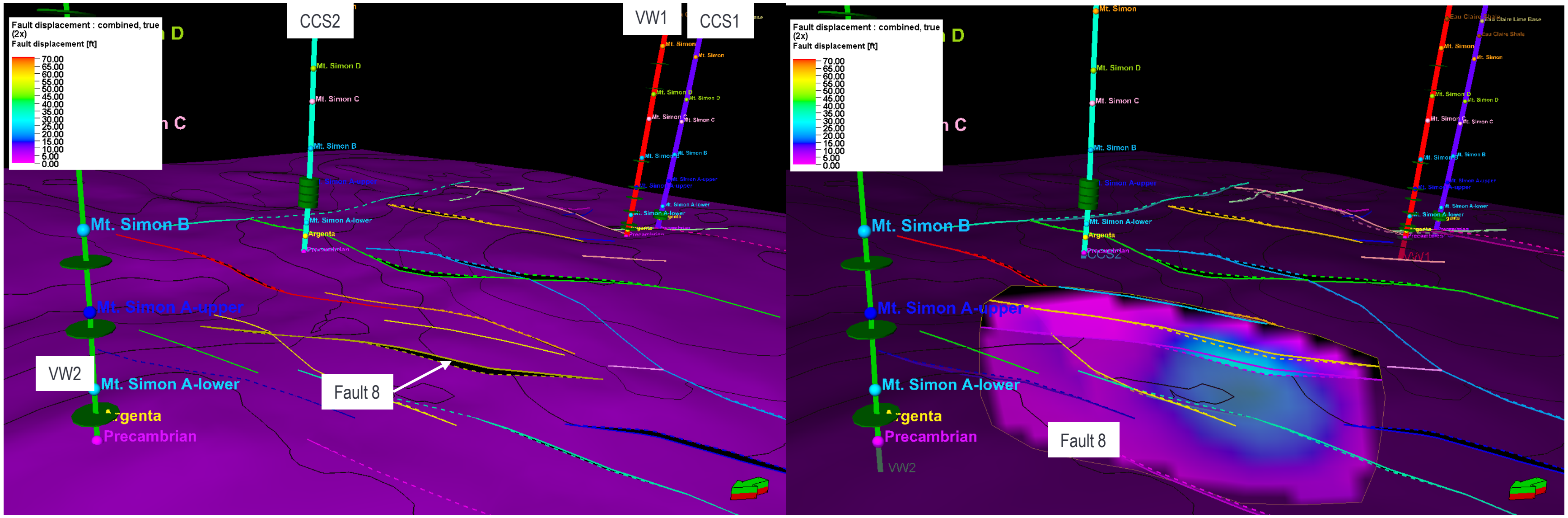

Vertical Exaggeration 1X
Surface is Precambrian
Circles are well top interpretations.
Green circles are injection intervals (injection well) and monitoring intervals (monitoring wells)
50ft contours

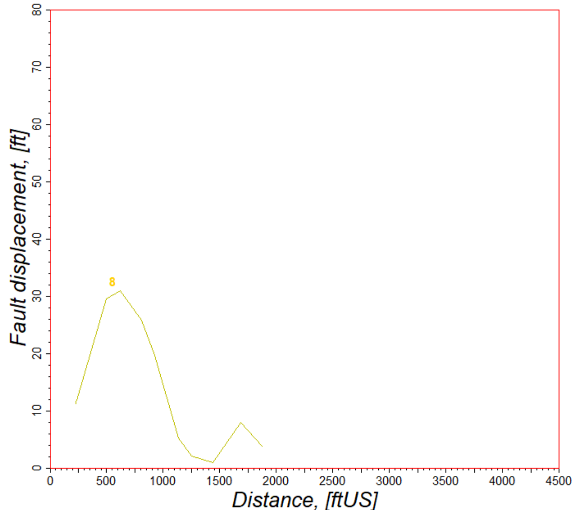

Figure 33. Fault #8 displacement

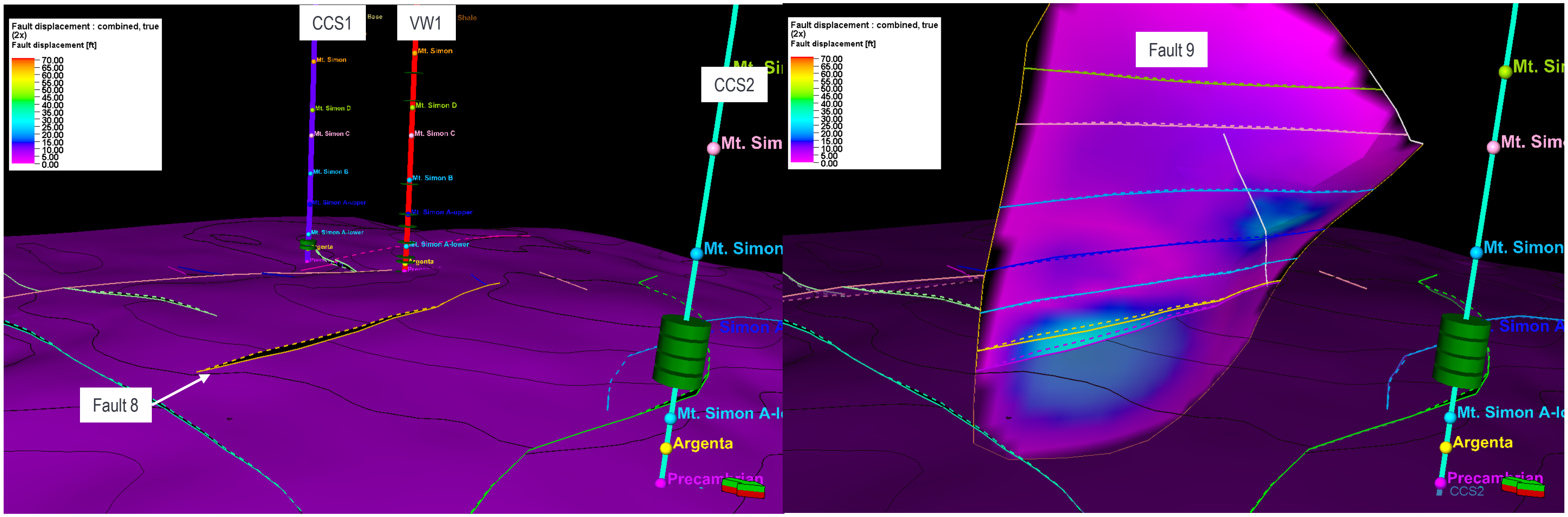

Vertical Exaggeration 1X
Surface is Precambrian
Circles are well top interpretations.
Green circles are injection intervals (injection well) and monitoring intervals (monitoring wells)
50ft contours

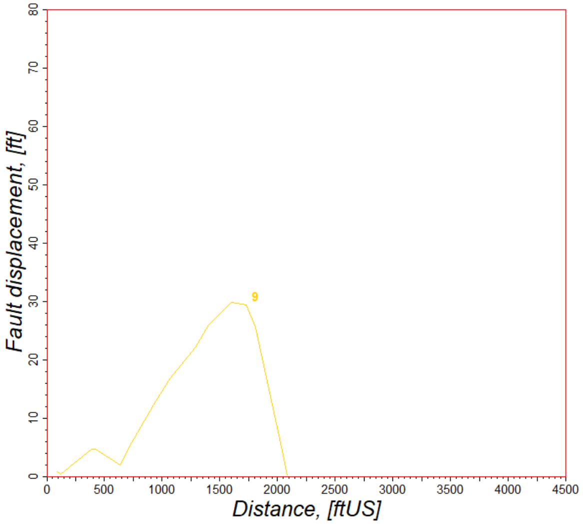

Figure 34. Fault #9 displacement

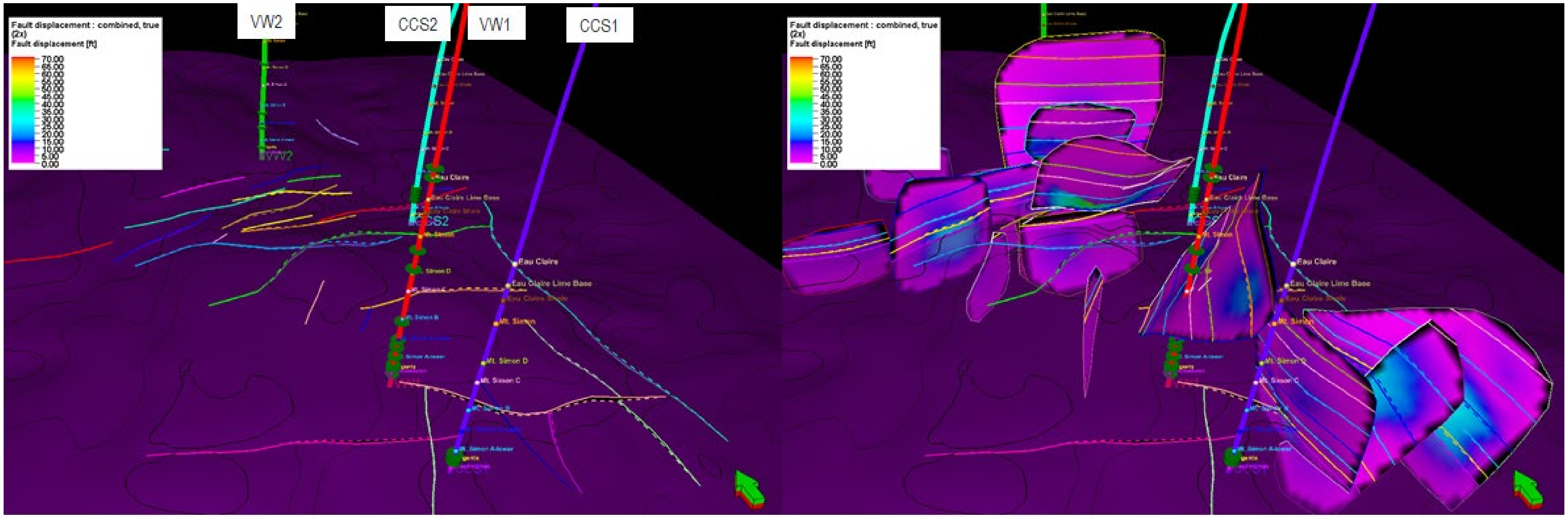

Vertical Exaggeration 1X
Surface is Precambrian
Circles are well top interpretations.
Green circles are injection intervals (injection well) and monitoring intervals (monitoring wells)
50ft contours

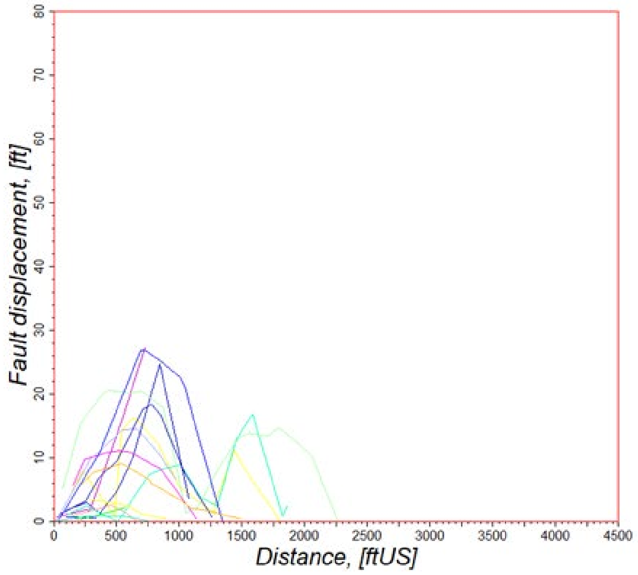

Figure 35. Fault #10 to Fault #28 displacement

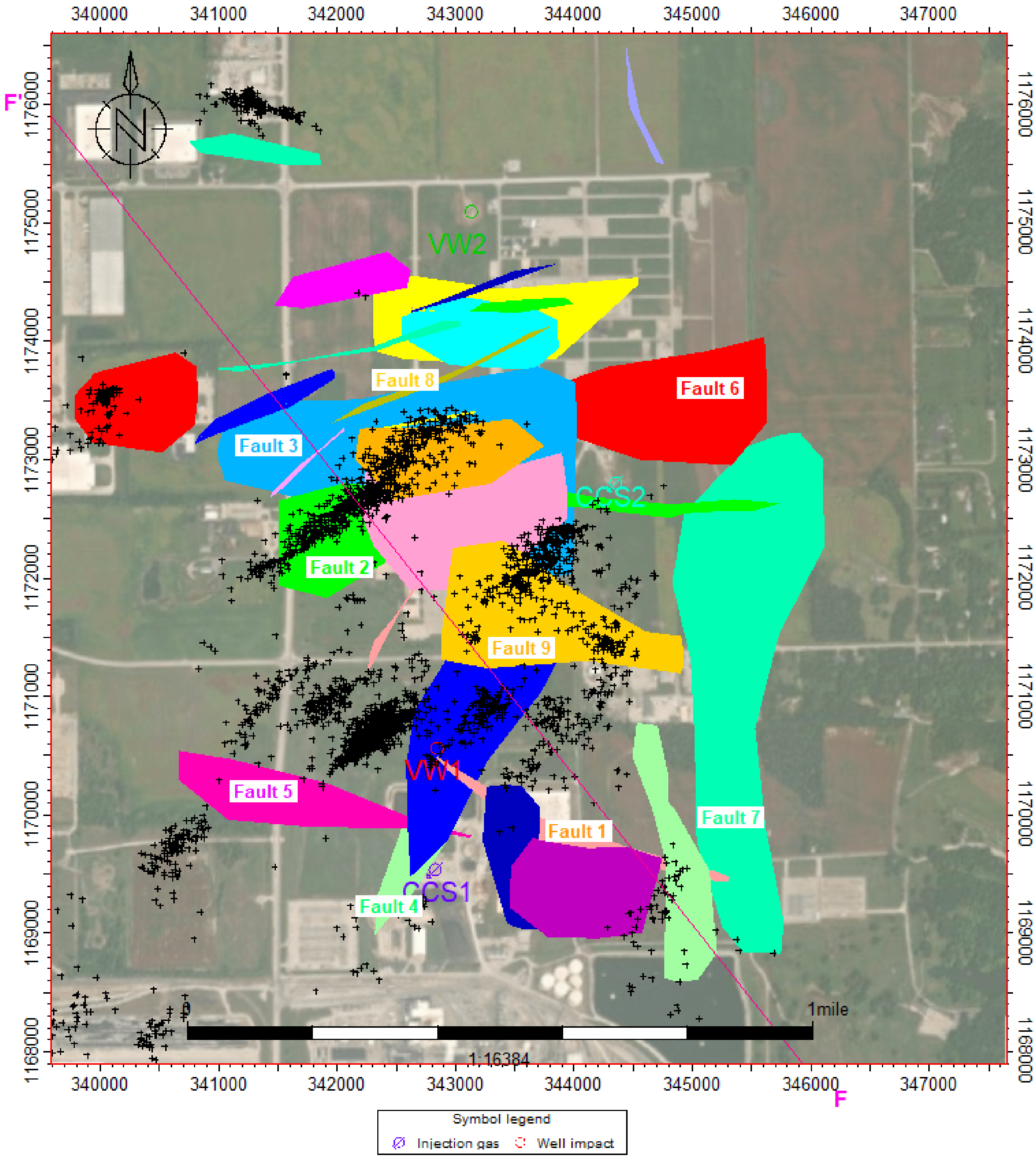

Figure 36. Injection-induced microseismic events with five interpreted faults.

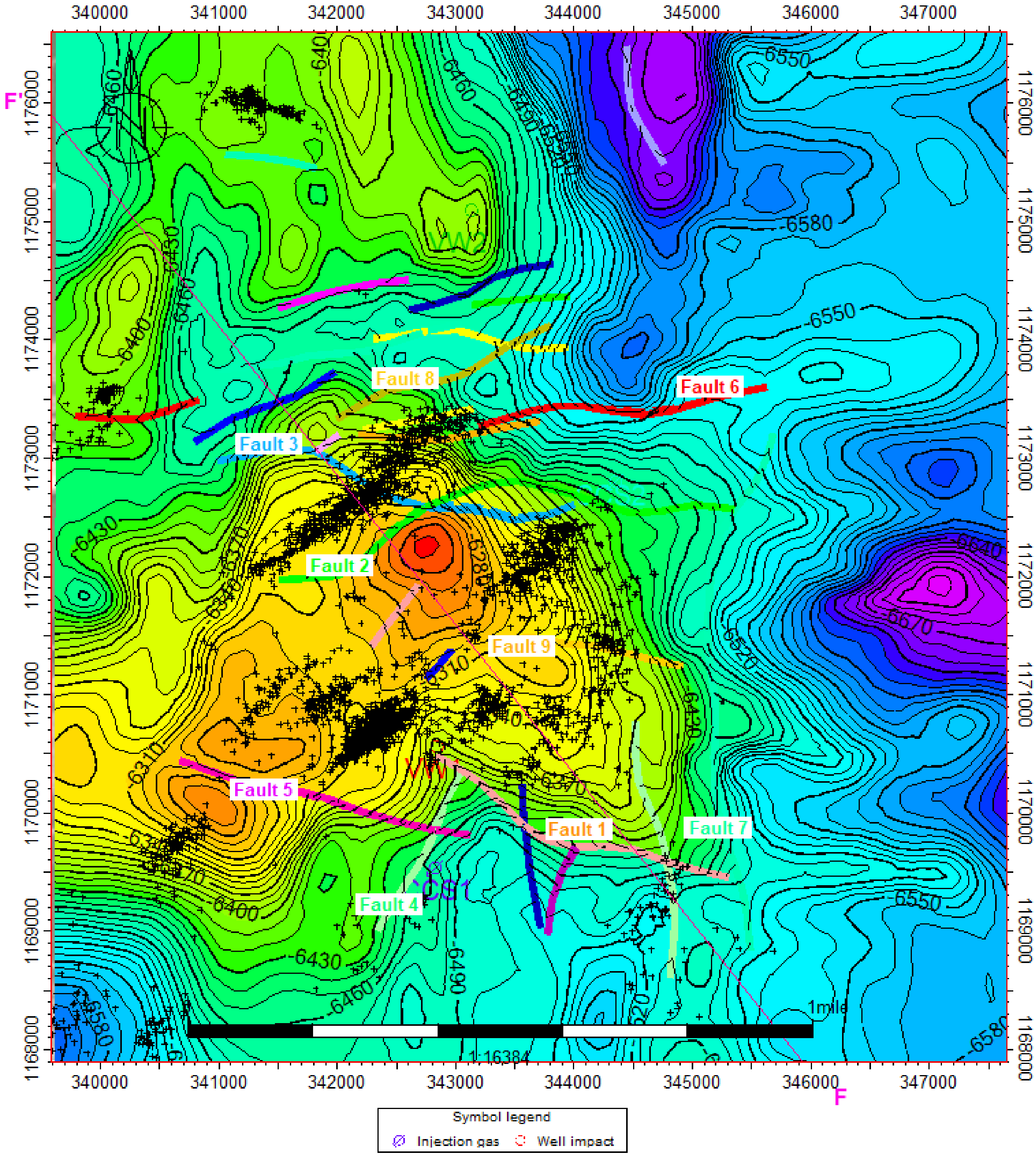

Figure 37. Injection-induced microseismic events with interpreted faults and Precambrian surface.

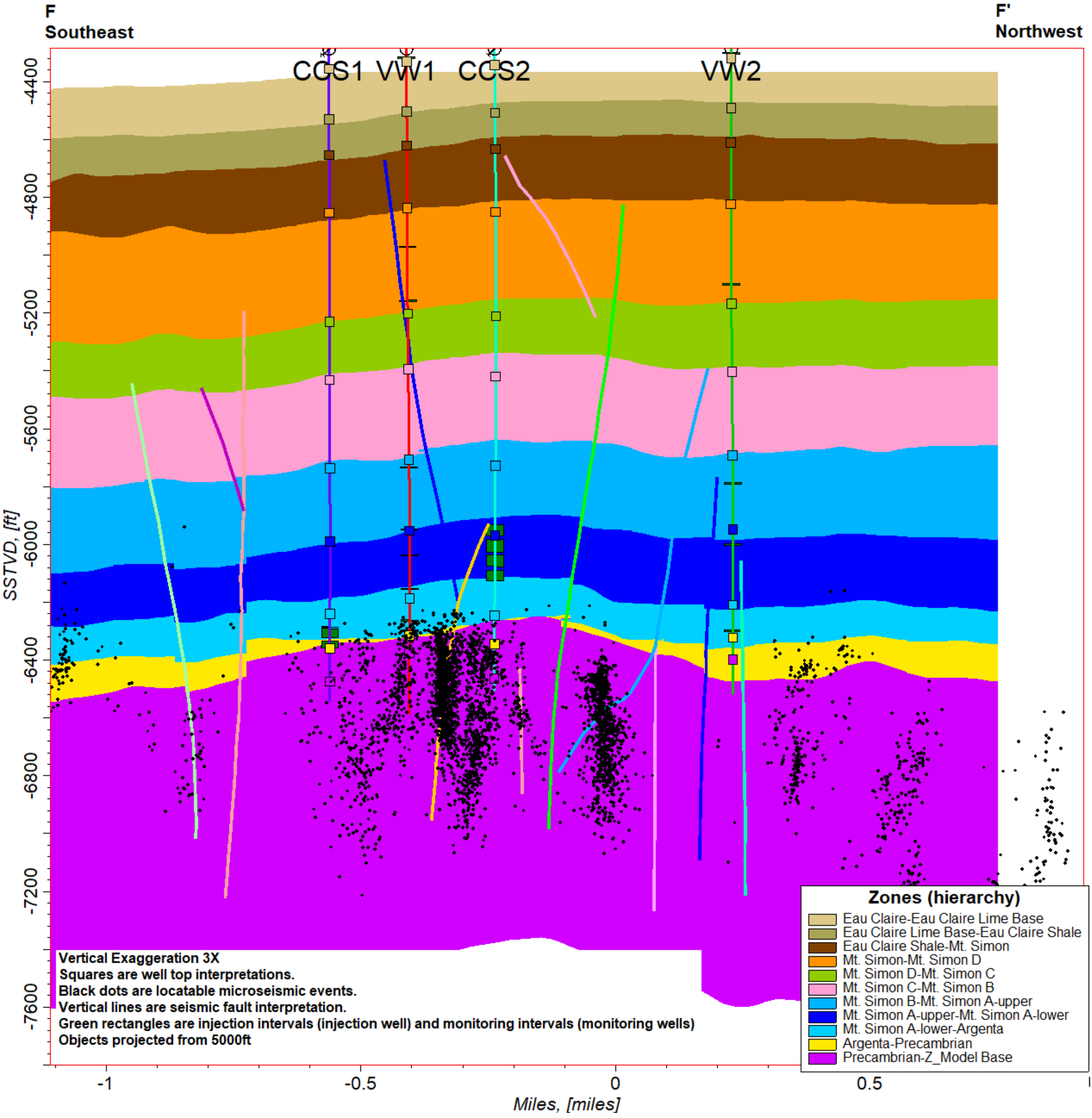

Vertical Exaggeration 3X
Squares are well top interpretations.
Black dots are locatable microseismic events.
Vertical lines are seismic fault interpretation.
Green rectangles are injection intervals (injection well) and monitoring intervals (monitoring wells)
Objects projected from 5000ft

Figure 38. F-F′ cross section displaying microseismic events.

4.3.2 Geocellular Grid Development

4.3.2.1 Lateral grid resolution

A geocellular 3D grid (9.7 mile × 9.3 mile) (15.5km × 14.9km) was generated with a horizontal cell size of 100 ft x 100 ft (30.5m x 30.5m) and a vertical cell size of 3 ft (0.9m) to be used for the geocellular modeling. This resolution was appropriate to capture the detail of the subsurface and was not too high to hinder reservoir simulations. The grid was rotated 20° to better represent the subtle dip of the Illinois Basin.

4.3.2.2 Surface extrapolation

The model size of 9.7 mile × 9.3 mile required extending the true vertical depth (TVD) surfaces outside the seismic area. The Illinois Basin near the project site has a regional dip of 0.5%, trending from the southeast to the northwest. This regional dip was statistically added to the TVD depth formation surfaces to extend the model out to the 9.7-mile × 9.3-mile extent (Figure 39). Figure 40, Figure 35, and Figure 42 display the 3D structural surfaces of the Precambrian, Argenta, and Mt. Simon A-Lower, respectively.

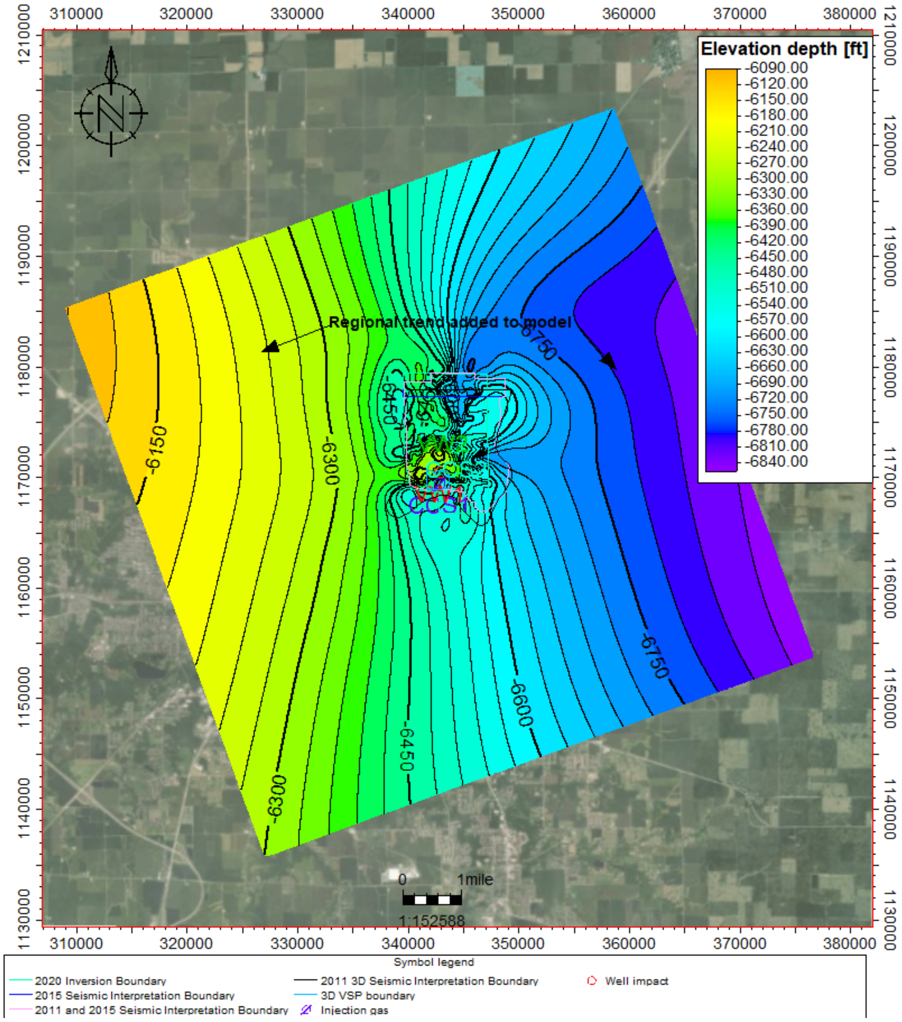

Figure 39. Precambrian surface (TVD) extrapolated to model area, which includes the regional dip.

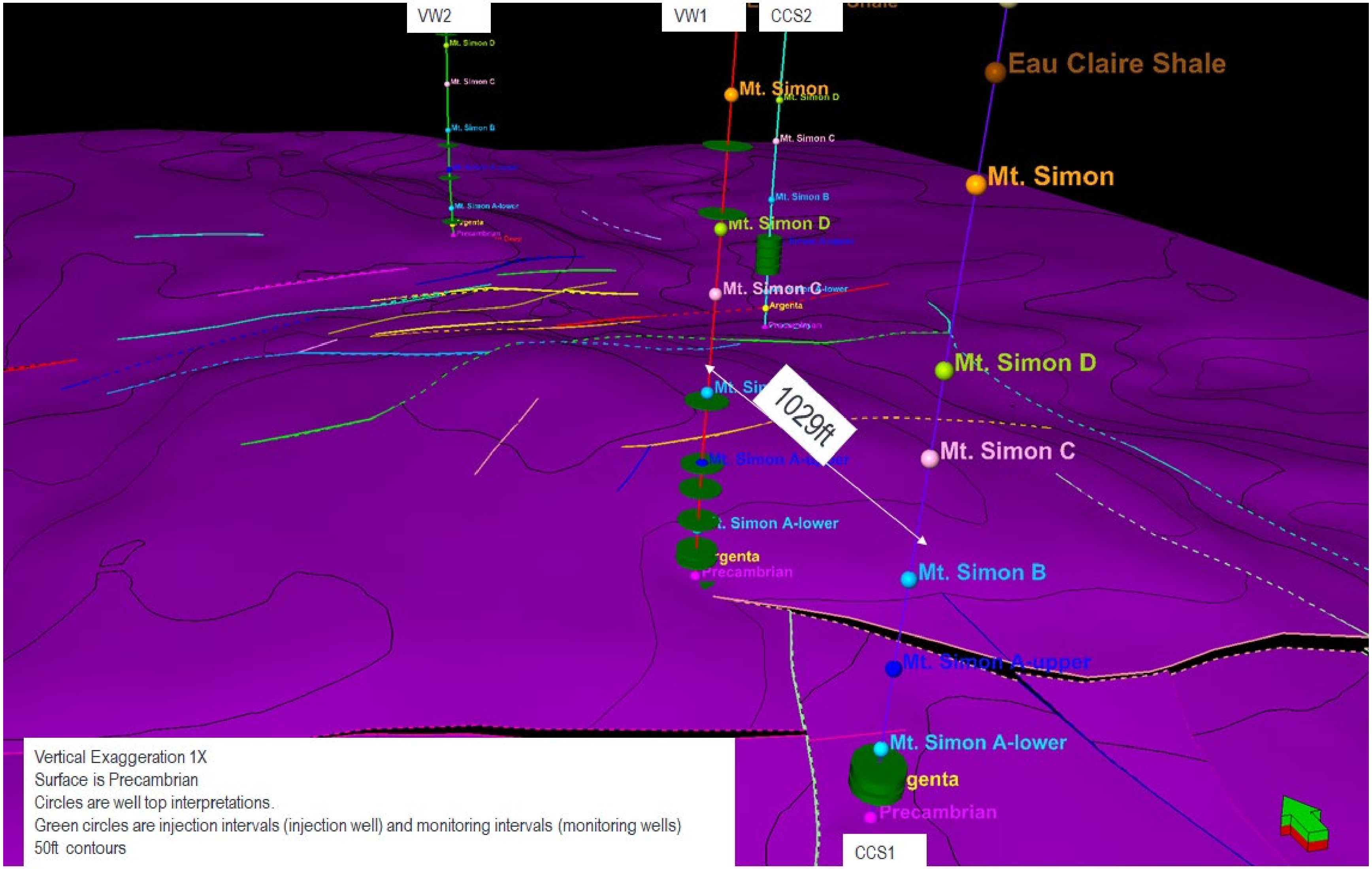

Vertical Exaggeration 1X
Surface is Precambrian
Circles are well top interpretations.
Green circles are injection intervals (injection well) and monitoring intervals (monitoring wells)
50ft contours

Figure 40. Structural Surface of the Precambrian.

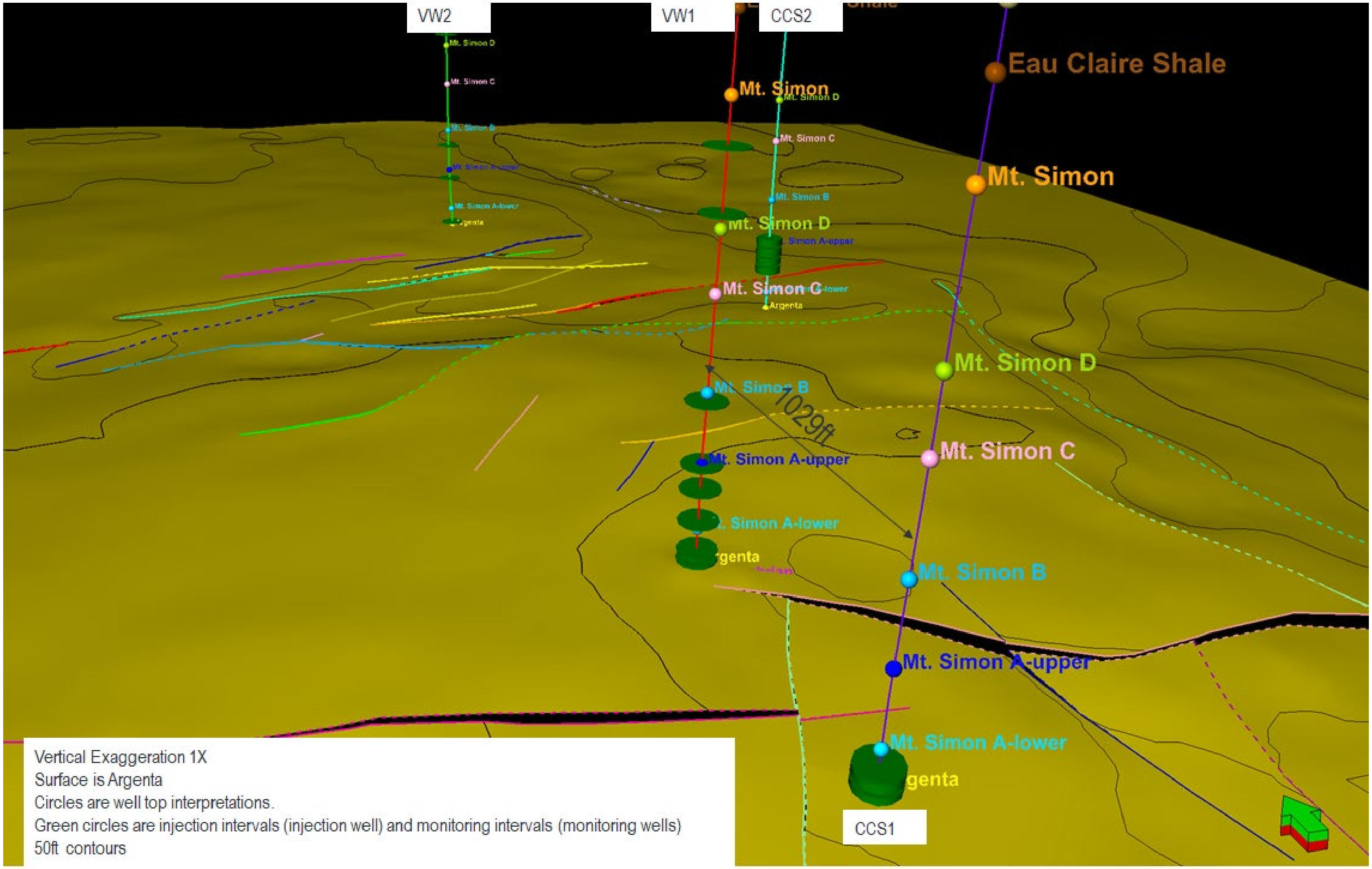

Vertical Exaggeration 1X
Surface is Argenta
Circles are well top interpretations.
Green circles are injection intervals (injection well) and monitoring intervals (monitoring wells)
50ft contours

Figure 41. Structural Surface of the Argenta.

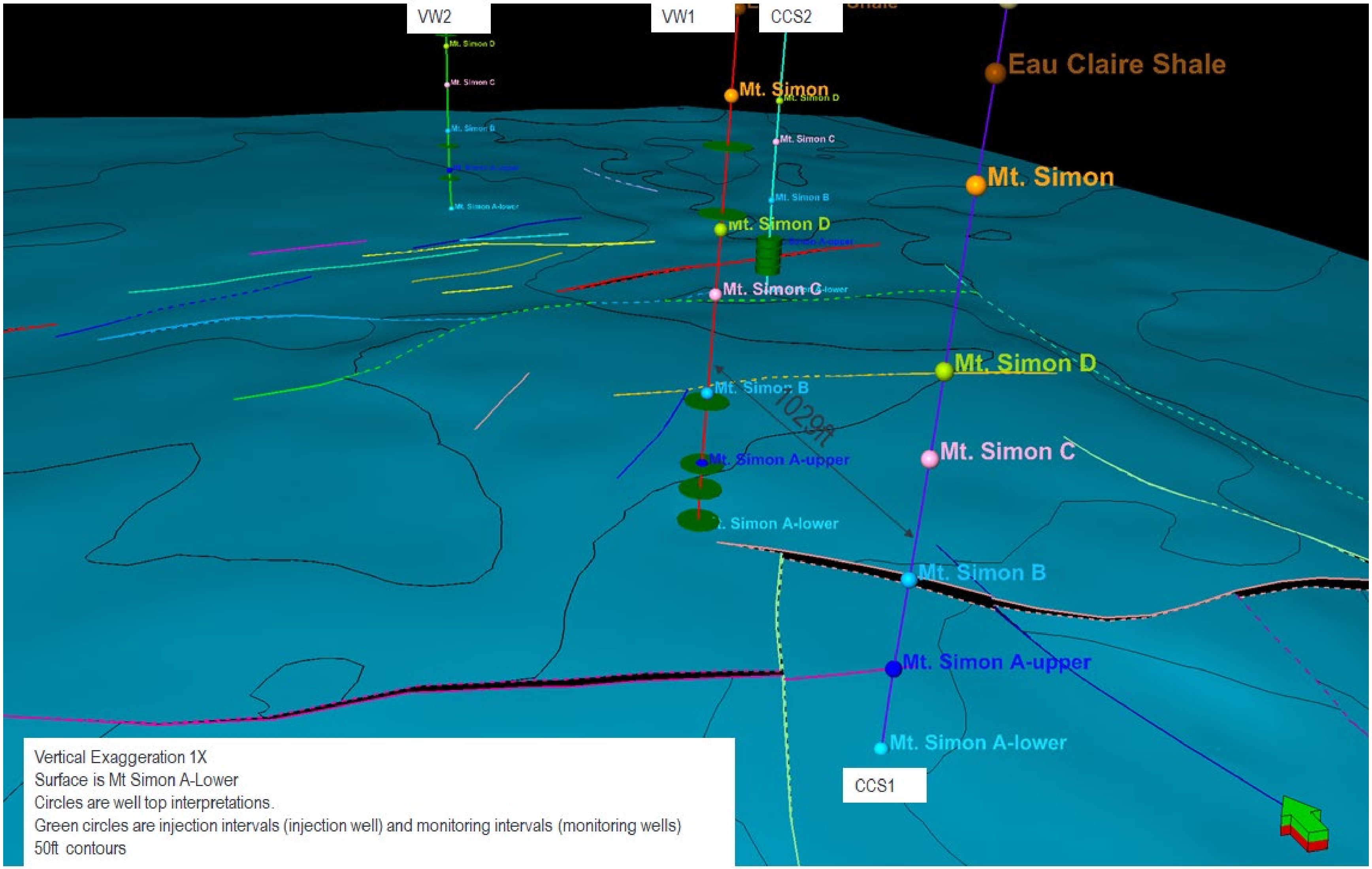

Vertical Exaggeration 1X
Surface is Mt Simon A-Lower
Circles are well top interpretations.
Green circles are injection intervals (injection well) and monitoring intervals (monitoring wells)
50ft contours

Figure 42. Structural Surface of the Mt. Simon A-Lower.

4.3.2.3 Main zone and layering

The formations (zones) that were modeled and the number of layers in each zone are summarized in Table 7. Model layering was as thin as 3 ft (0.9m) through the injection reservoir interval (Mt. Simon B to Mt. Simon A- Lower). With this 9.7- mile × 9.3-mile model, it was important to have a model cell count that represented the subsurface heterogeneity and that, at the same time, kept the number of model cells to a manageable count. Models with an excessive number of cells becomes too cumbersome to work with. To balance this, thinner cells were used in the formations where CO_2 history matching would be completed.

Table 7. Table of modeled formations and cell count

Formation (Zone)	Model Cell Layer Thickness (feet)	Model Cell Layer Thickness (meters)
Eau Claire	6	1.8
Eau Claire Lime Base	5	1.5
Eau Claire Shale	5	1.5
Mt. Simon	5	1.5
Mt. Simon D	5	1.5
Mt. Simon C	4	1.2
Mt. Simon B	3	0.9
Mt. Simon A-Upper	3	0.9
Mt. Simon A-Lower	3	0.9
Argenta	3	0.9
Precambrian	6	1.8

4.4 Petrophysical Property Modeling

4.4.1 Workflow Overview

An essential feature of the petrophysical model was the requirement for properties (facies, porosity, and permeability) to be distributed in a geologically reasonable fashion within two domains, inside the seismic survey volumes and outside the seismic survey volume. The following steps describe the workflow that was used to generate the final property model:

1. **Baffle facies interpretation:** A facies interpretation of reservoir (relatively higher-permeability facies).and baffles (relatively lower-permeability facies). This interpretation was completed within the Mt. Simon B, Mt. Simon A-Upper, and Mt. Simon A-Lower.
2. **Upscale facies, effective porosity, permeability, and 2019 Porosity Cube into the grid:** The 2019 Porosity Cube and well logs (baffle logs, effective porosity logs, and permeability) were upscaled into the grid.
3. **Relationships between porosity logs and 2019 Porosity Cube:** As discussed in Section 4.3.1, because there was a reliable correlation between the 2020 Porosity Cube and the porosity well logs, the 2019 Porosity Cube was used as a cokriging variable to interpolate the well log effective porosity into the interwell space.
4. **Variogram analysis**: Variogram maps of each formation were extracted from the upscaled 2019 Porosity Cube to determine the major and minor variogram ranges and major direction of each formation. Vertical variogram ranges were extracted from upscaled well logs.
5. **Petrophysical modeling of facies, effective porosity and permeability interpolation:** Using geostatistics from the variogram analysis, Sequential Indicator Simulation (SIS) was used to interpolate the baffle facies. Gaussian

random function simulation (GRFS) effective porosity co-kriged to the 2020 porosity property. GRFS was used to interpolate permeability co-kriged to effective porosity.

6. **ISGS fracture model properties from the Precambrian:** The ISGS completed discreet fracture modeling in the Precambrian Formation (Williams-Stroud, 2020). This model was imported into the Petrel model.
7. **Quality control:** Effective porosity and permeability properties were cross-plotted to verify a reasonable relationship.

4.4.2 Baffle Facies Interpretation

When the reservoir simulations began in 2008, there were challenges with history matching between the observed data and the simulation results. This will be discussed in detail in Section 5. The history matching helped refine the geomodel by using the discrepancies between the observed and the simulated CO_2 migration to highlight regions of the geomodel that required modification. These model modifications were changes to structure and property distribution (porosity and permeability) that were not clear or had been uncertain earlier. The interpretation of the faults on the IBDP geomodel was a good example of this.

In the 2018 model update, adding baffle facies layers became necessary for history matching. These baffle facies are areas of relatively lower porosity and relatively lower permeability barriers, which were interpreted layers within the Mt. Simon Formation. When the reservoir simulations were run, the baffle layers were used as discontinuous barriers to CO_2 and pressure migration. On the well logs, these baffles have been interpreted in intervals where the porosity and permeability are low. From this log interpretation, the baffles were not always continuous between wells (dark green baffles with yellow reservoir on track 6 of Figure 43). Some baffles could be correlated from well to well and some could not. The justification for adding these baffle facies into the model was as follows; the details will be discussed in Section 5:

- The first recognized influence of layered baffles was the pressure reactions at VW1 during the CCS1 injection, with the highest formation pressure increases of about 5.1% in the lowest three gauges, highs of only about 1.7% increase in gauge 4, and less going higher. Also, CO_2 was detected in VW1 at Zone 3 and lower but not at Zone 4 and higher.
- When CCS2 injection began in the lowest perforation, there was a higher-pressure response at the injection interval at CCS1 than was modeled. This indicates there may be a preferential pathway from CCS2 to CCS1; however, such a high-pressure response at VW1 compared to the previous modeled response did not occur, suggesting a different degree of connection between CCS2 to CCS1 and CCS2 to VW1. A directional preferential pathway was seen by CCS2 pressure response first arriving at VW1 far before VW2 which is closer to CCS2.
- The pressure response at VW2 (Zone 2) indicated that reservoir interval including VW2 (Zone 2) and CCS2 might be locally confined by the low-permeability baffles.
- Although the Mt. Simon A-Lower was believed to be undifferentiated, repeat pulsed neutron logs at VW1 show that high-permeability sand packages and interlayered low-porosity and low-permeability layers (baffles) strongly control vertical CO_2 plume geometry at distance from the injector.
- These observed preferential pathways/flow barriers suggested that strong heterogeneity (porosity and permeability) exists in the reservoir. Adding the baffle facies allowed for better history matching results in all the simulation scenarios.

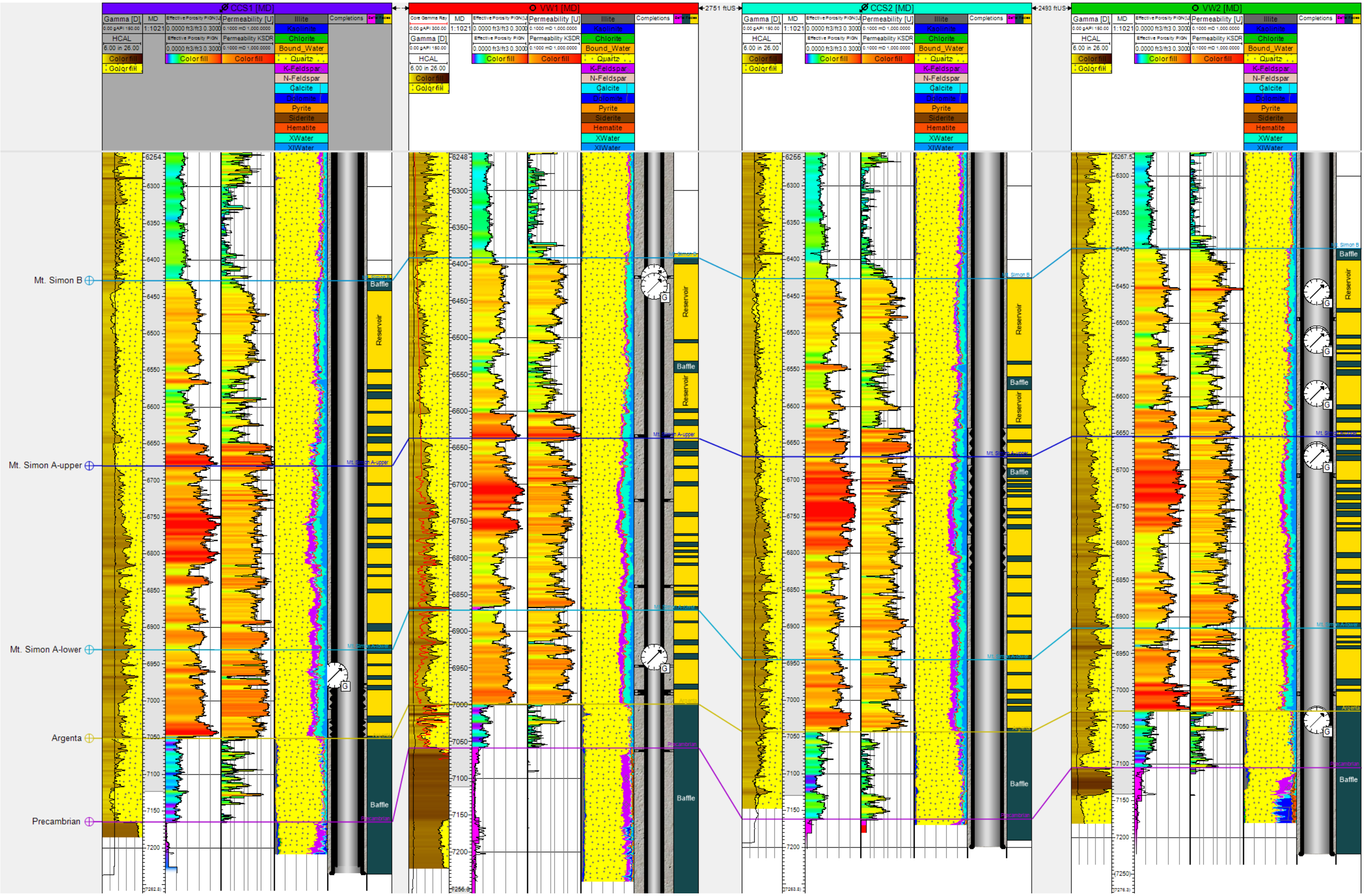

Figure 43. Petrophysics, completions, and baffle facies interpretation on low-porosity and low-permeability layers.

4.4.1 Upscale Facies, Effective Porosity, and Permeability

Upscaling well logs is a method in which an algorithm is applied to the high-vertical-resolution well logs to produce one log value for each model cell that is penetrated by the well. In upscaling well logs, cell height plays a significant role in how porosity and permeability logs are upscaled. Cell height selection (i.e., vertical layering) is a balance between capturing vertical heterogeneity and keeping the model's cell-count at a manageable level. Effective porosity, permeability, and the baffle facies logs from all four wells were upscaled into the grid (Figure 44). The arithmetic method was determined to be the most appropriate for effective porosity, permeability, and facies. Table 7 summarizes the formations that were modeled and the layer in each formation. Model layering was as thin as 3 ft (0.9m) through the injection reservoir interval (Mt. Simon A-Upper and Mt. Simon A-Lower). This high-resolution cell height helped capture the variability observed in the porosity and permeability logs. The intent was to honor thin intervals that may represent significant permeability streaks and thus play a significant role in dynamic reservoir behavior.

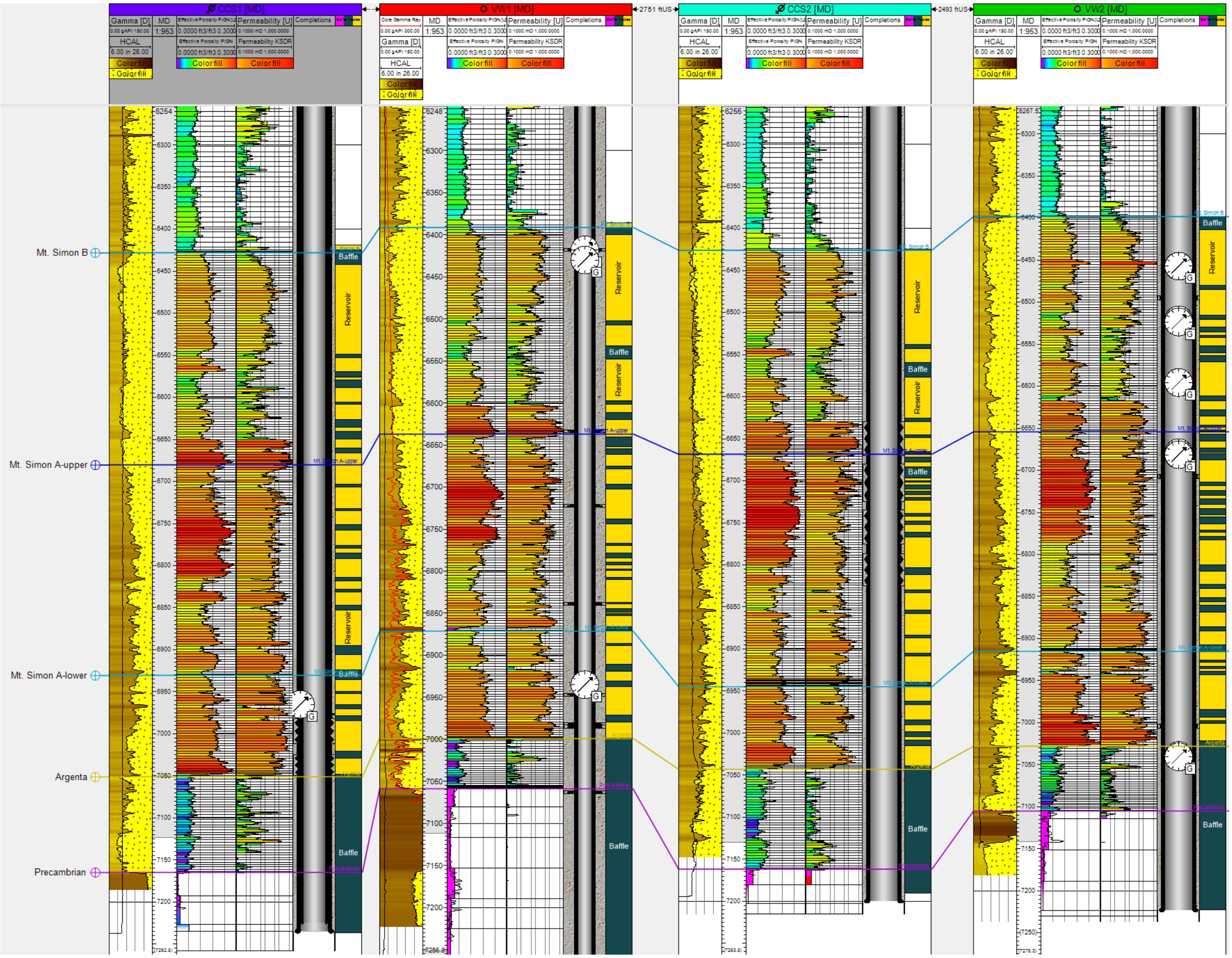

Figure 44. Upscaled well logs (effective porosity, permeability, and baffle facies) and completions.

4.4.2 Variogram Analysis

The effective porosity logs from the four wells used in modeling provided high vertical resolution at each well; however, without using other data, little was known about the porosity values between the wells. To complete geological modeling, it was necessary to properly interpolate the data from the wells into the interwell space in a way that represented the geological setting. Variogram analysis was used to properly evaluate the geological setting, and it was used to interpolate the porosity well logs into the interwell space in a way that properly represented the geology. Variograms are often determined from well data; however, this analysis could not be completed on only four wells. To complete the modeling, variogram analysis was done on the upscaled 2019 Porosity Cube (Figure 45) because it has a high horizontal sampling rate. The 2019 Porosity Cube was only processed for the Eau Claire Shale down to the upper section of the Precambrian. The upscaling process used an averaging algorithm to define one porosity cube value for each model cell. This provided a way to calculate a series of zone-specific parameters, which included a variogram map, major azimuth, range, sill, nugget, and function types (Figure 45 and Figure 46). The quantified variogram parameters that were generated for each formation are explained below and shown in Table 8:

- **Variogram map**: In variogram analysis, deciding on the direction of the variogram is one of the first decisions that must be made. This was completed using variogram maps (Figure 46). Theoretically, the direction of maximum continuity (major direction) and direction of minimum continuity (minor direction) are found after the variograms are calculated in all possible directions (from 0 degree to 359°). Then, the ones that show minimum and maximum range are selected as the variograms that represent the minor and major directions.
    - The major direction defines the direction where the sample points have the strongest correlation. The azimuth angle of this major direction can be changed interactively by editing the direction in the search cone. Azimuth angle is specified as the clockwise angle from the north (in degrees).
    - The minor search direction is perpendicular to the major direction.
- **Range**: The range describes where the variogram model reaches its plateau (i.e., the separation distance where there is no longer any change in the degree of correlation between pairs of data values). The range is specific in each direction for the model variogram. A large range means greater continuity and a small range means less continuity. The larger the range, the smaller the heterogeneity. Major and minor ranges were extracted from the highly horizontal sampled 2019 Porosity Cube, and the vertical range was taken from the well log analysis.
- **Sill:** The sill is the semi-variance where the separation distance is greater than the range (on the plateau). This describes the variation between two unrelated samples.
- **Nugget:** The nugget is the semi-variance where the separation distance is zero.
- **Variogram types**: Different methods (variogram types) exist. The types used in this project were:
    - Spherical: The curve is linear at shorter distances and then makes a sharp transition to a flat sill.
    - Exponential: The curve has an exponential behavior, with a rapid variation at shorter distances.

Table 8. Variogram parameters extracted from the 2019 Porosity Cube and well logs

Zone	Major Azimuth	Major Range (ft)	Minor Range (ft)	Vertical Range (ft)	Sill	Nugget	Variogram Type
Eau Claire	0	1846	1053	14	0.9	0.0001	Spherical
Eau Claire Lime Base	133	1415	481	17	0.8	0.0001	Exponential
Eau Claire Shale	111	2917	1928	19	0.9	0.0001	Exponential
Mt. Simon	127	1653	1049	13	1.0	0.0001	Exponential
Mt. Simon D	121	2844	2194	15	1.0	0.0001	Exponential
Mt. Simon C	123	1461	1260	12	0.8	0.0001	Exponential
Mt. Simon B	127	2670	1937	18	1.0	0.0001	Spherical
Mt. Simon A-upper	127	2349	2175	44	0.6	0.0001	Exponential
Mt. Simon A-lower	127	2294	2120	9	1.0	0.0001	Spherical
Argenta	140	1831	1743	9	0.9	0.0001	Exponential
Precambrian	132	2481	2075	17	0.6	0.0001	Exponential

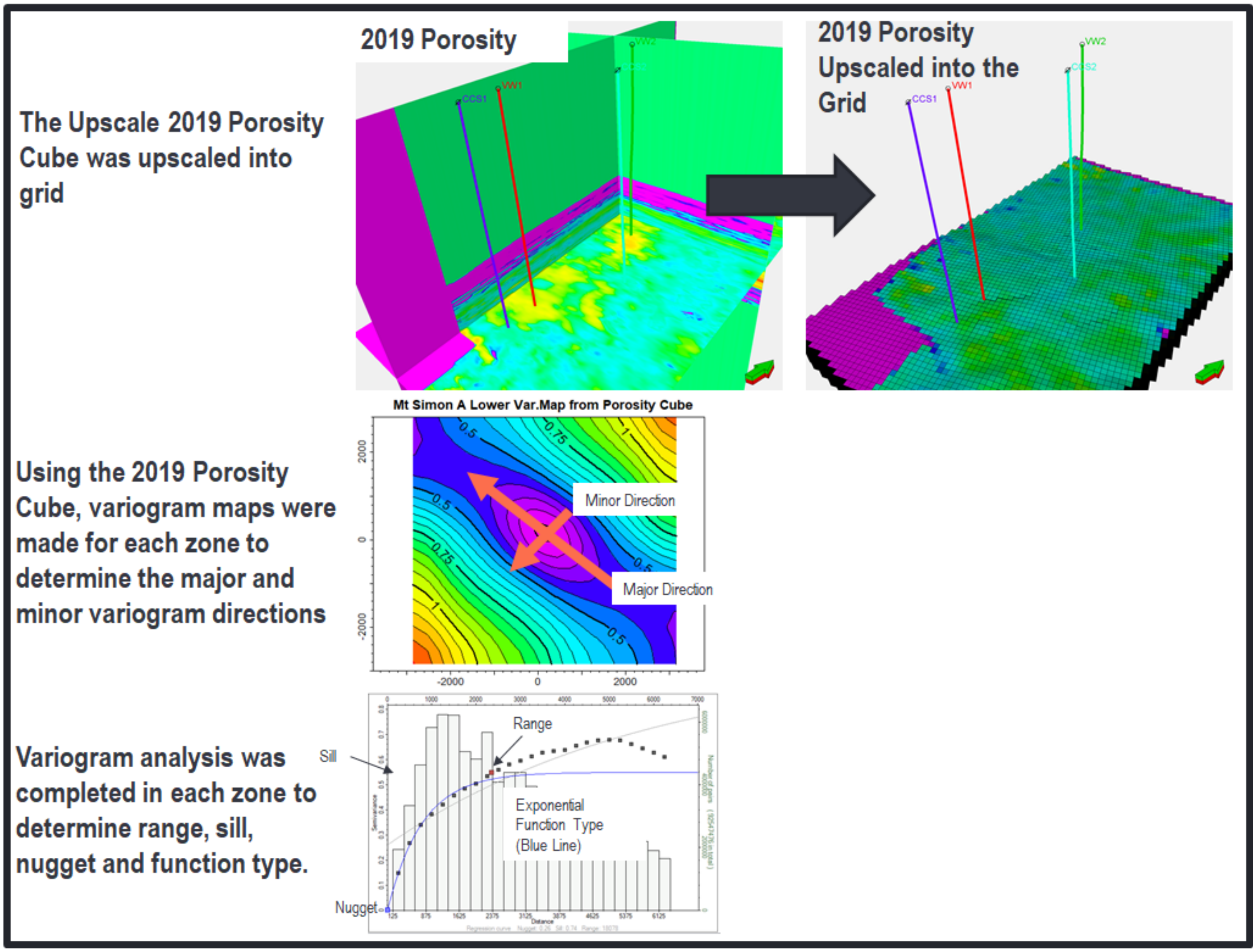

The Upscale 2019 Porosity Cube was upscaled into grid

Using the 2019 Porosity Cube, variogram maps were made for each zone to determine the major and minor variogram directions

Variogram analysis was completed in each zone to determine range, sill, nugget and function type.

Figure 45. Steps used to generate the mini grid for geostatistical extraction.

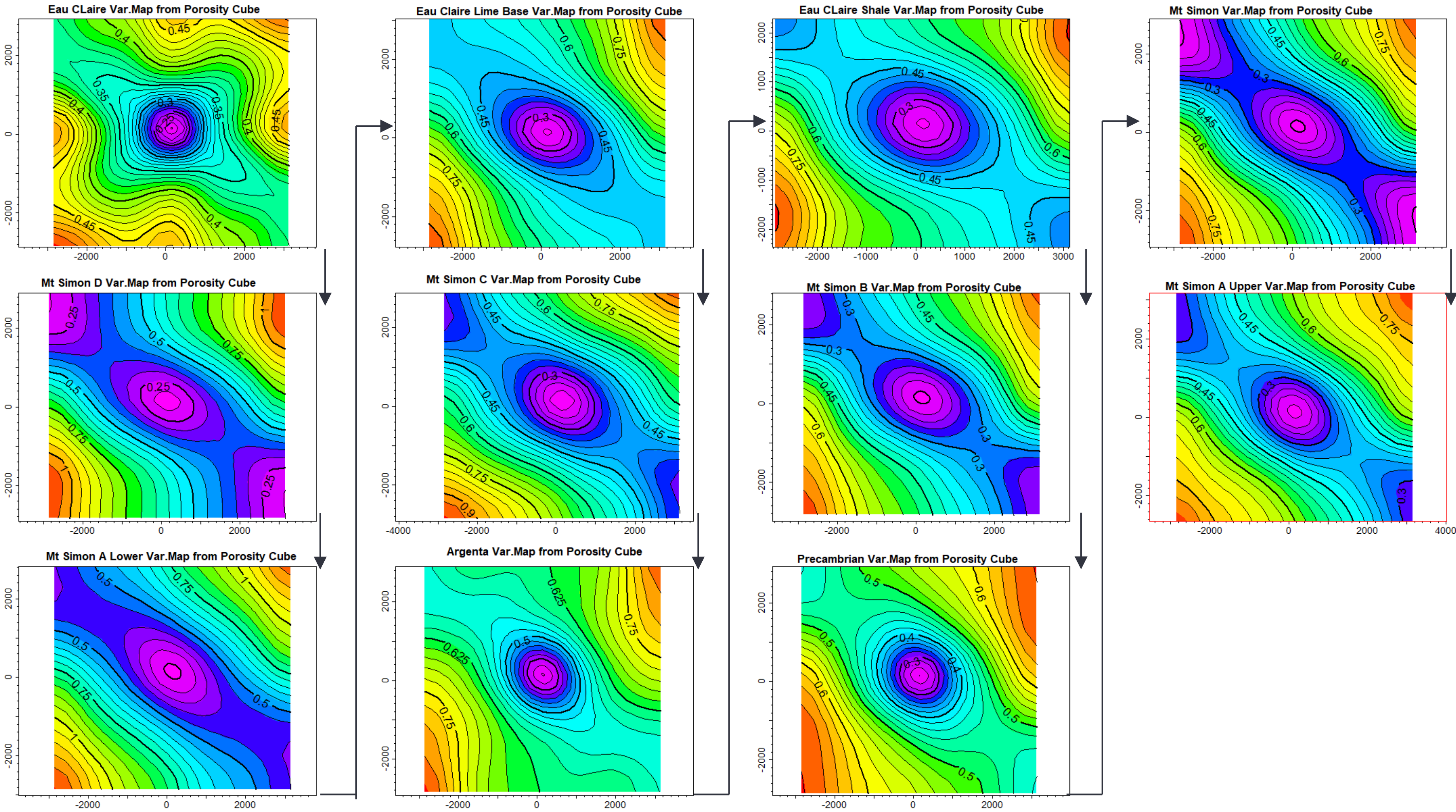
Eau CLaire Var.Map from Porosity Cube

Eau Claire Lime Base Var.Map from Porosity Cube

Eau CLaire Shale Var.Map from Porosity Cube

Mt Simon Var.Map from Porosity Cube

Mt Simon D Var.Map from Porosity Cube

Mt Simon C Var.Map from Porosity Cube

Mt Simon B Var.Map from Porosity Cube

Mt Simon A Upper Var.Map from Porosity Cube

Mt Simon A Lower Var.Map from Porosity Cube

Argenta Var.Map from Porosity Cube

Precambrian Var.Map from Porosity Cube

Figure 46. Variogram maps extracted from the 2019 Porosity Cube.

4.4.3 Petrophysical Modeling of Facies and Effective Porosity and Permeability Interpolation

The effective porosity logs from the four wells used in modeling provided high vertical resolution at each well; however, little was known about the porosity values between the wells. Using the variogram analysis described in Section 4.4.2, the 2019 Porosity Cube was used to guide the petrophysical modeling of effective porosity. This was used because there is a correlation of seismic inversion properties (porosity and acoustic impedance, AI) with the well log properties (porosity and AI). Seismic inversion requires a relationship to be defined between the AI observed in the 3D seismic survey and the total porosity in the well logs. The relationship is then used to transform the 3D acoustic impedance (AI) volume into a porosity volume (2019 Porosity Cube). A reliable correlation between the porosity well log and the 2019 Porosity Cube was found (Figure 16).

The baffle facies were interpolated using sequential indicator simulation (SIS) between wells using the previously described statistics in the Mt. Simon A-Upper and Mt. Simon A-Lower. The facies model consists of two discrete facies (reservoir and baffle). As observed with the discontinuous well log correlation of baffle facies and to achieve a better history match (Section 5), the baffle facies were interpolated to be discontinuous.

Effective porosity and permeability were interpolated using the above-described geostatistics. Because of the presence of reservoir and non-reservoir facies types, the porosity and permeability were modeled separately within each zone and facies type. Cokriging was used to take advantage of the covariance between the effective porosity logs and the 2019 Porosity Cube. This method is appropriate here because the primary data (effective porosity logs) has high vertical resolution but is not present between wells; the related secondary data (2019 Porosity Cube) lacks high vertical resolution but has abundant horizontal sampling between the wells. Using this relationship, in 2020, a more-reliable reservoir model was developed because it capitalizes on the strengths of both the high vertical resolution well log with the higher horizontal sampling seismic data. A plot of the upscaled porosity versus the porosity cube is shown to have a reasonable correlation coefficient of 0.81 (Figure 16); therefore, the porosity cube can be used as a reliable cokriging variable (Figure 47). Using the geostatistics from each formation from the variogram analysis, permeability was cokriged using Gaussian random function simulation (GRFS) against the effective porosity property (Figure 47). Cokriging was used to take advantage of the known covariance between effective porosity and permeability. Figure 48 to Figure 52 display the workflow properties on the four-well cross section. Figure 53 to Figure 58 display 3D views of the effective porosity property and geologic structure on the various cross section lines (Cross-section lines on Figure 7).

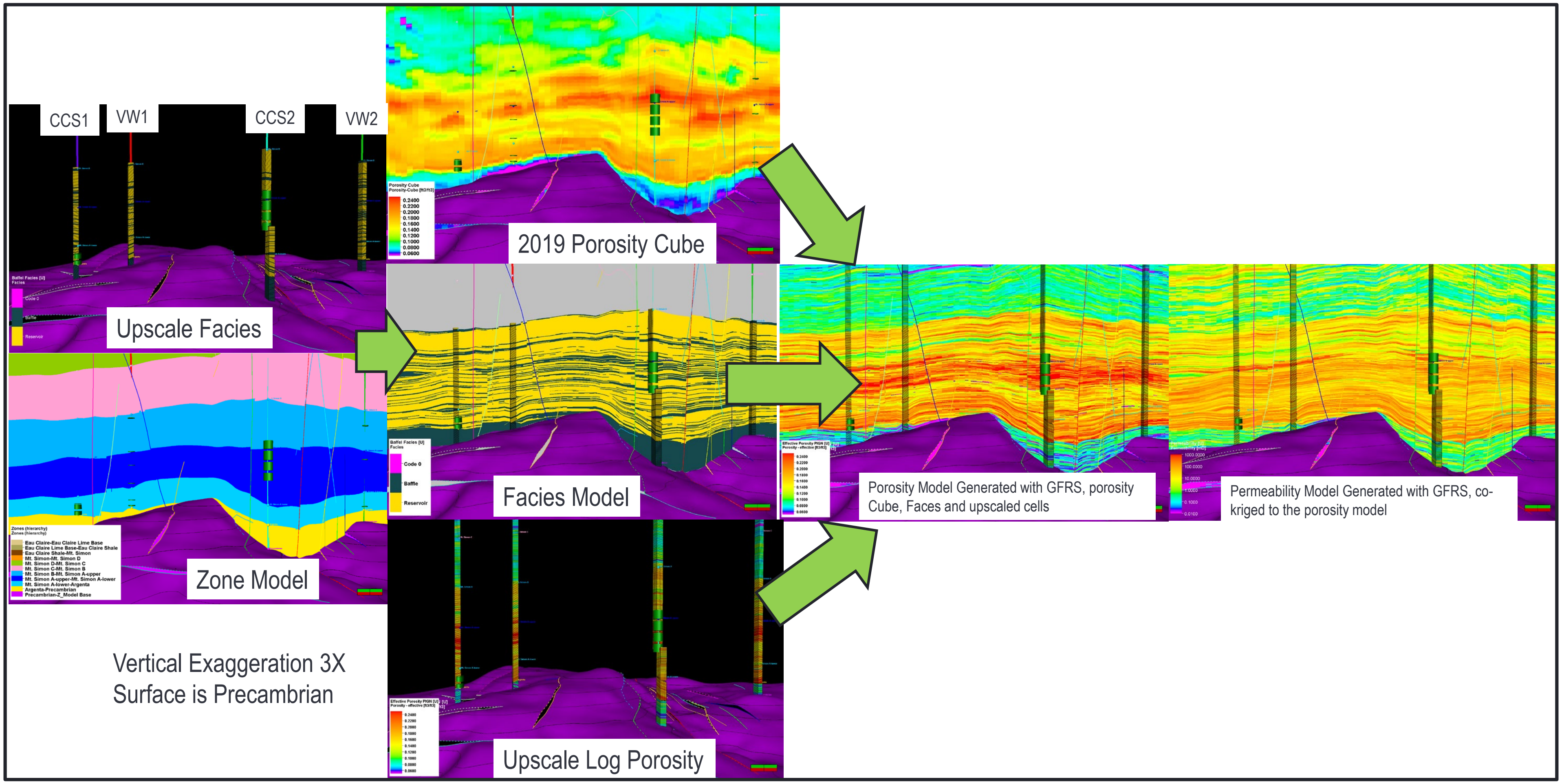

Figure 47. Property model workflow.

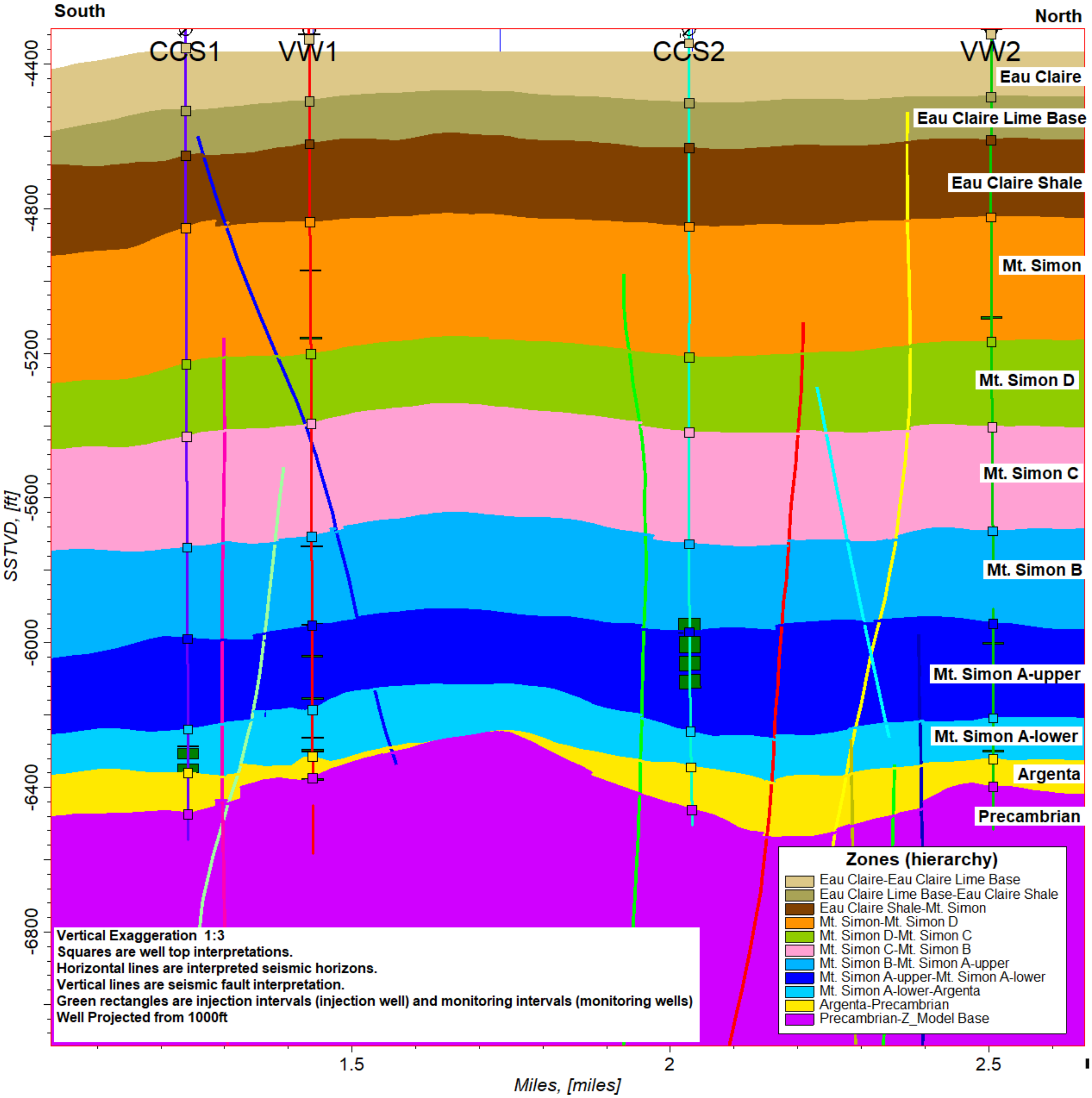

Vertical Exaggeration 1:3
Squares are well top interpretations.
Horizontal lines are interpreted seismic horizons.
Vertical lines are seismic fault interpretation.
Green rectangles are injection intervals (injection well) and monitoring intervals (monitoring wells)
Well Projected from 1000ft

Figure 48. Four-well cross section displaying zones.

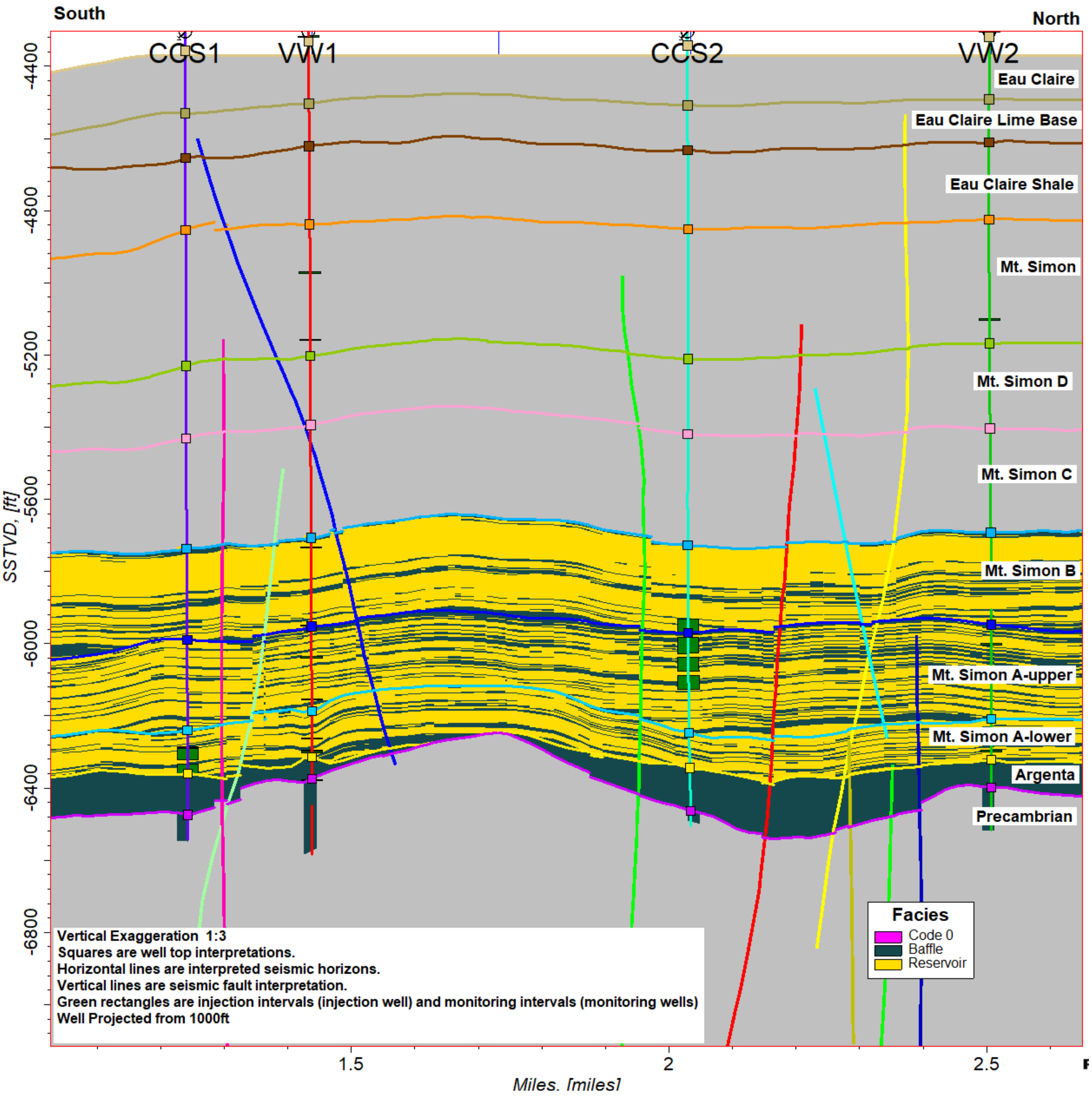

Vertical Exaggeration 1:3
Squares are well top interpretations.
Horizontal lines are interpreted seismic horizons.
Vertical lines are seismic fault interpretation.
Green rectangles are injection intervals (injection well) and monitoring intervals (monitoring wells)
Well Projected from 1000ft

Figure 49. Four-well cross section displaying facies.

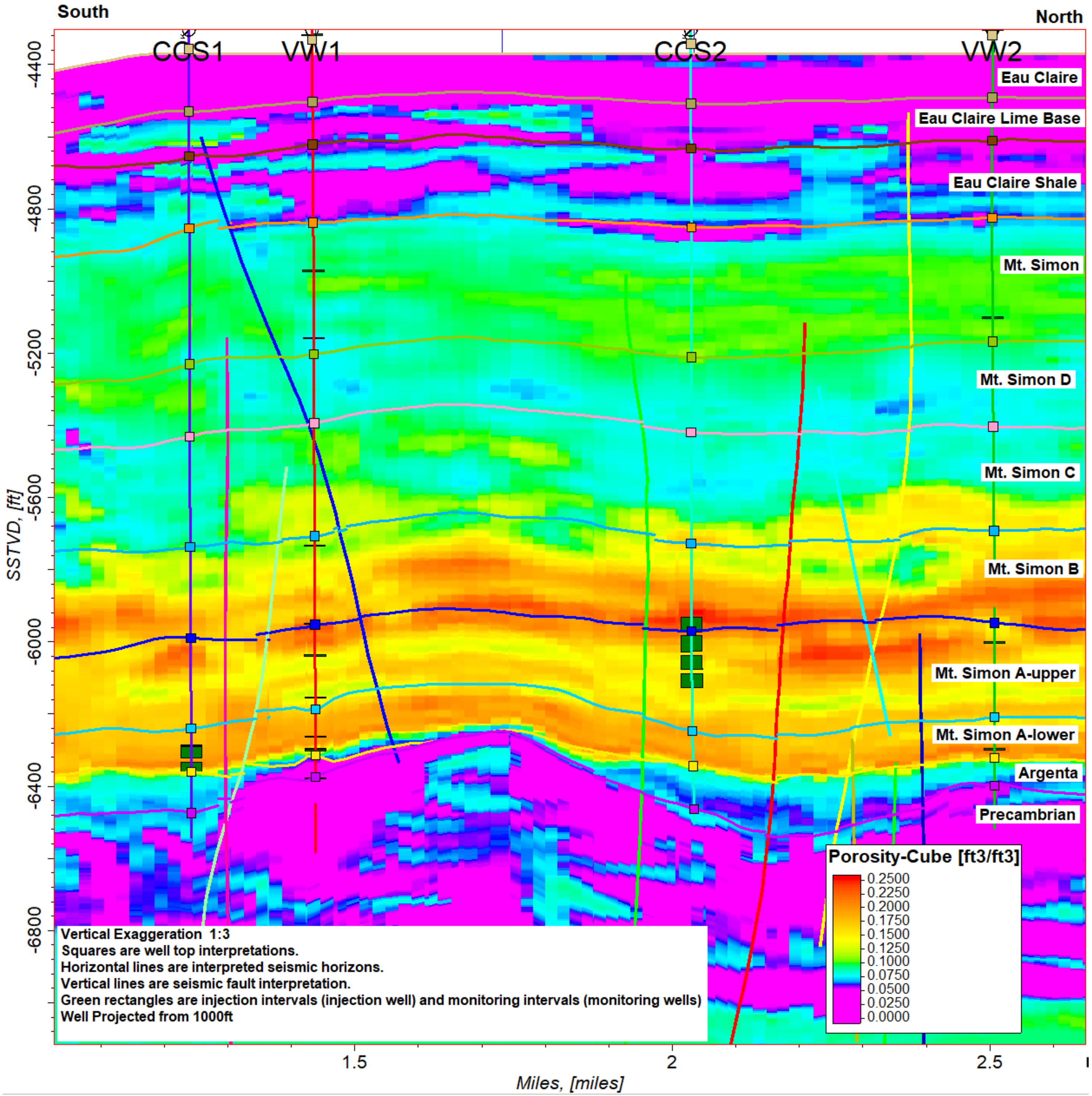

Vertical Exaggeration 1:3
Squares are well top interpretations.
Horizontal lines are interpreted seismic horizons.
Vertical lines are seismic fault interpretation.
Green rectangles are injection intervals (injection well) and monitoring intervals (monitoring wells)
Well Projected from 1000ft

Figure 50. Four-well cross section displaying 2019 Porosity Cube.

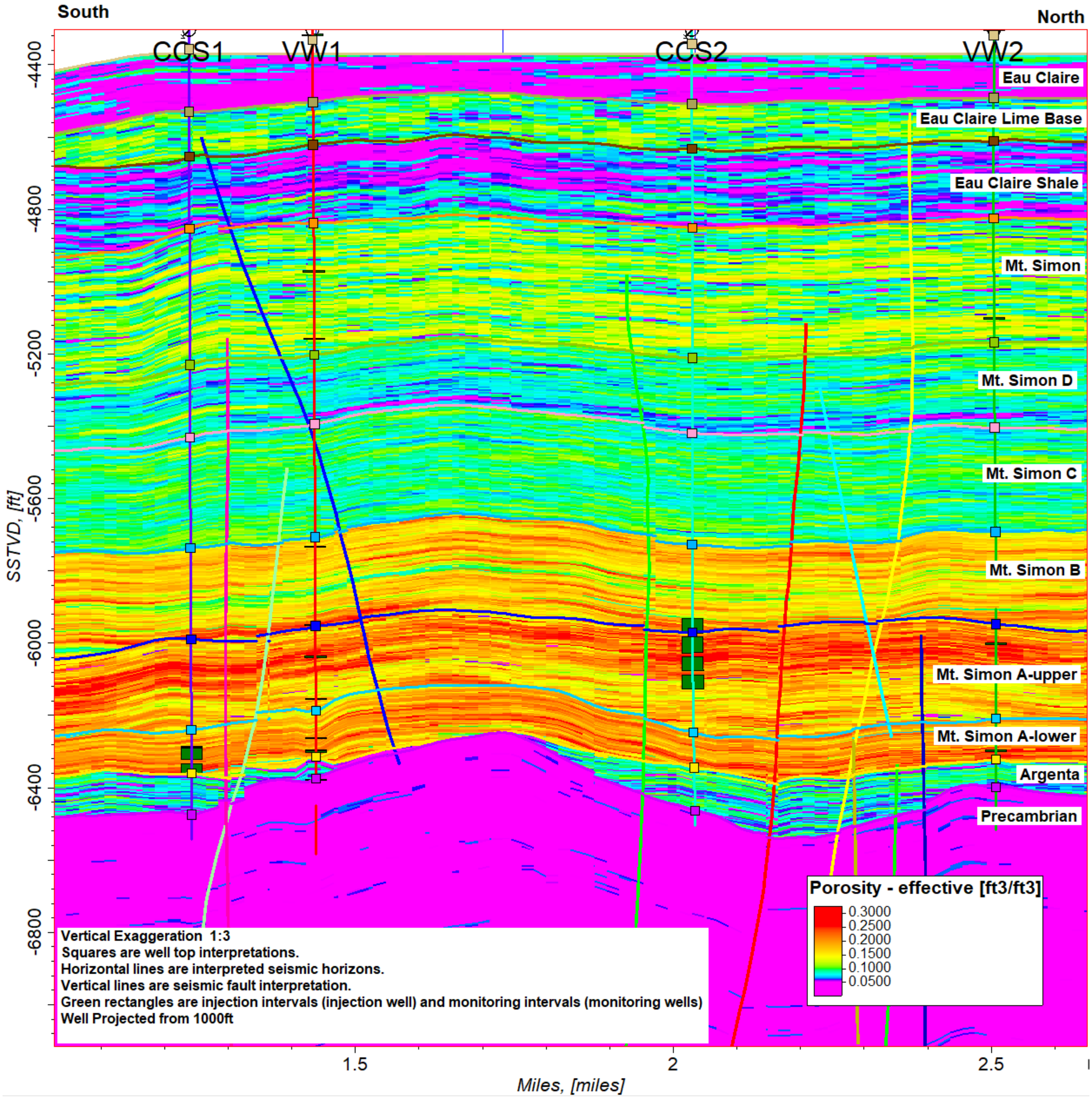

Vertical Exaggeration 1:3
Squares are well top interpretations.
Horizontal lines are interpreted seismic horizons.
Vertical lines are seismic fault interpretation.
Green rectangles are injection intervals (injection well) and monitoring intervals (monitoring wells)
Well Projected from 1000ft

Figure 51. Four-well cross section displaying modelled effective porosity guided by the 2019 Porosity Cube.

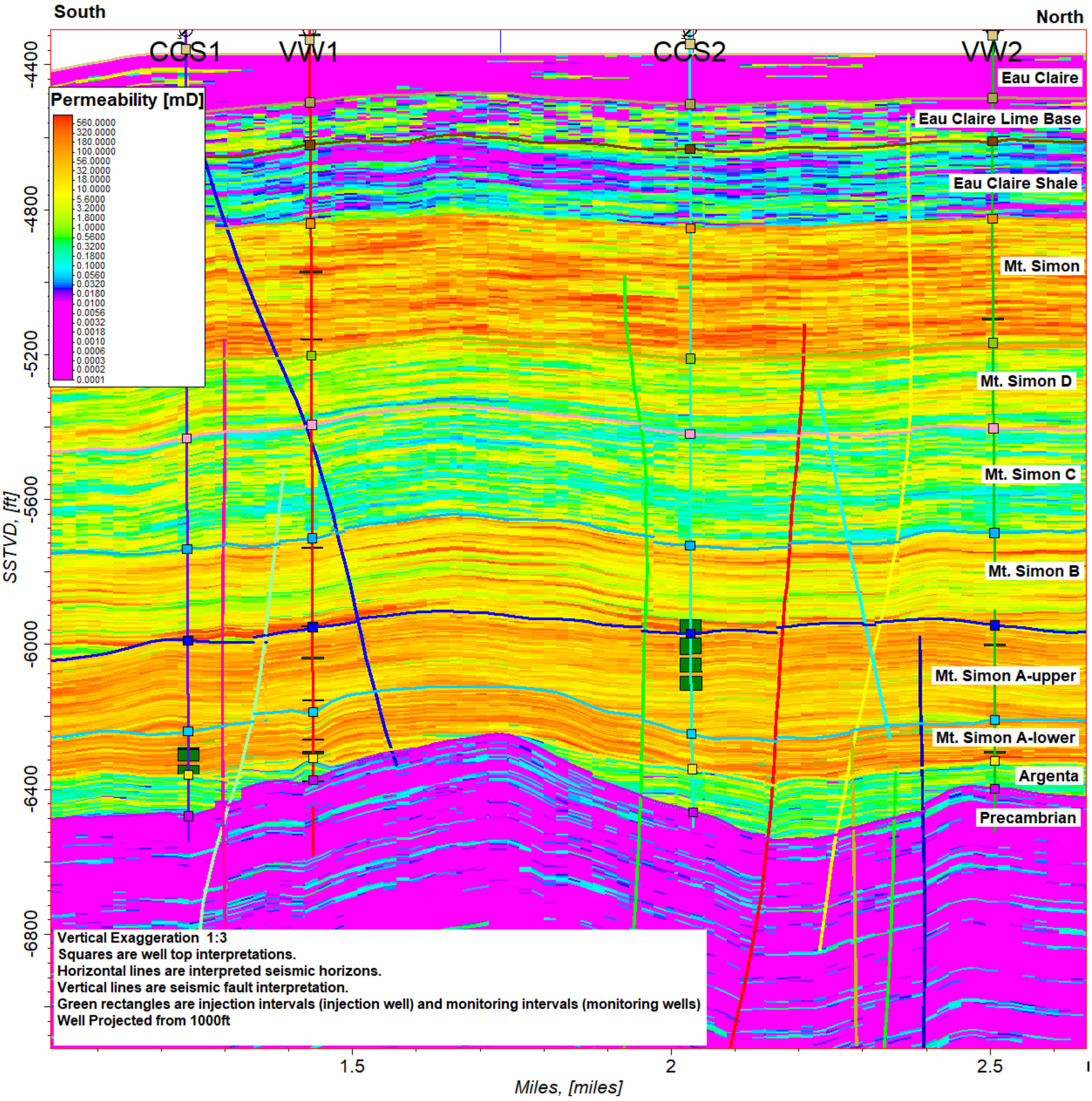

Vertical Exaggeration 1:3
Squares are well top interpretations.
Horizontal lines are interpreted seismic horizons.
Vertical lines are seismic fault interpretation.
Green rectangles are injection intervals (injection well) and monitoring intervals (monitoring wells)
Well Projected from 1000ft

Figure 52. Four-well cross section displaying permeability.

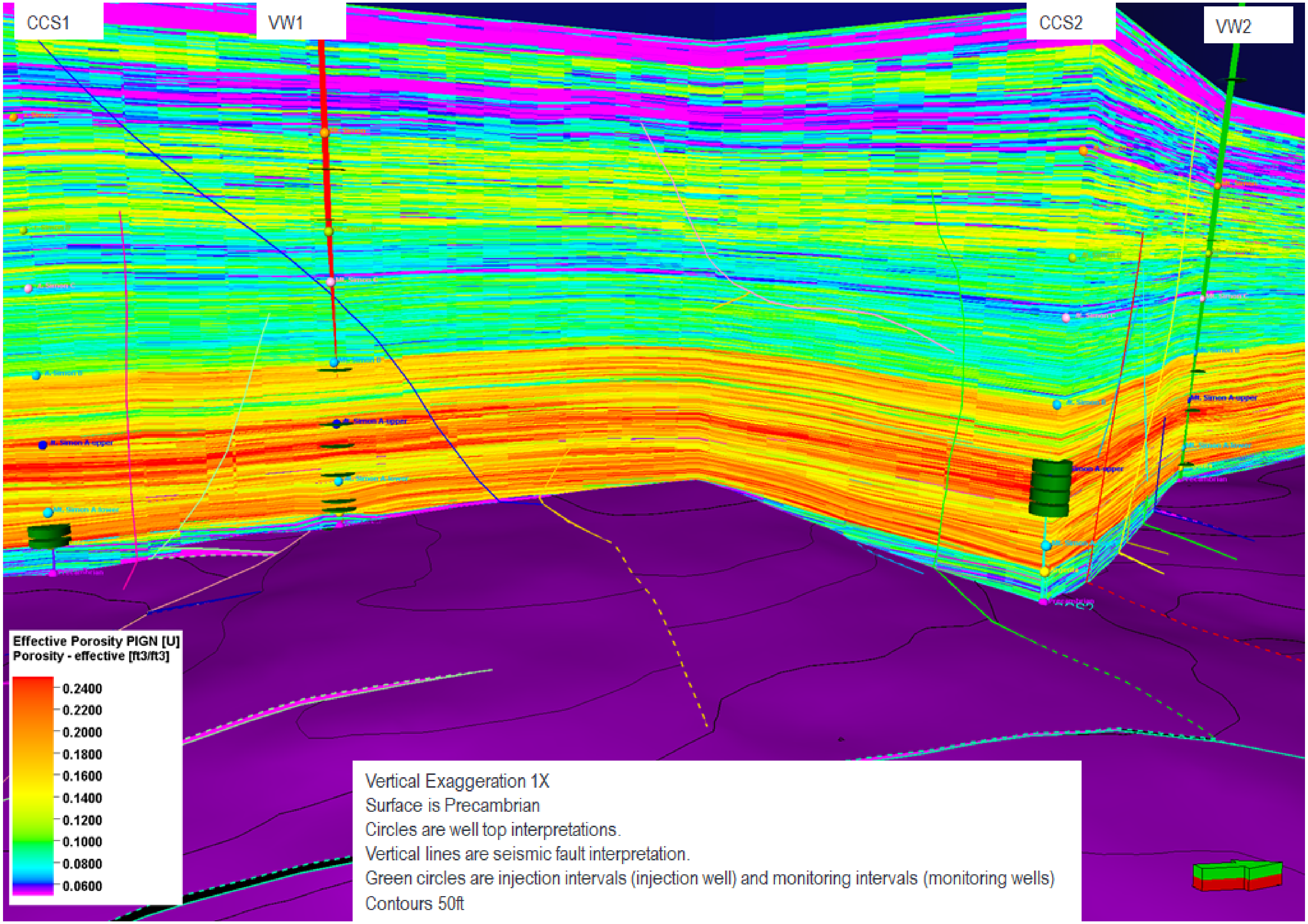

Vertical Exaggeration 1X
Surface is Precambrian
Circles are well top interpretations.
Vertical lines are seismic fault interpretation.
Green circles are injection intervals (injection well) and monitoring intervals (monitoring wells)
Contours 50ft

Figure 53. Four-well cross section effective porosity.

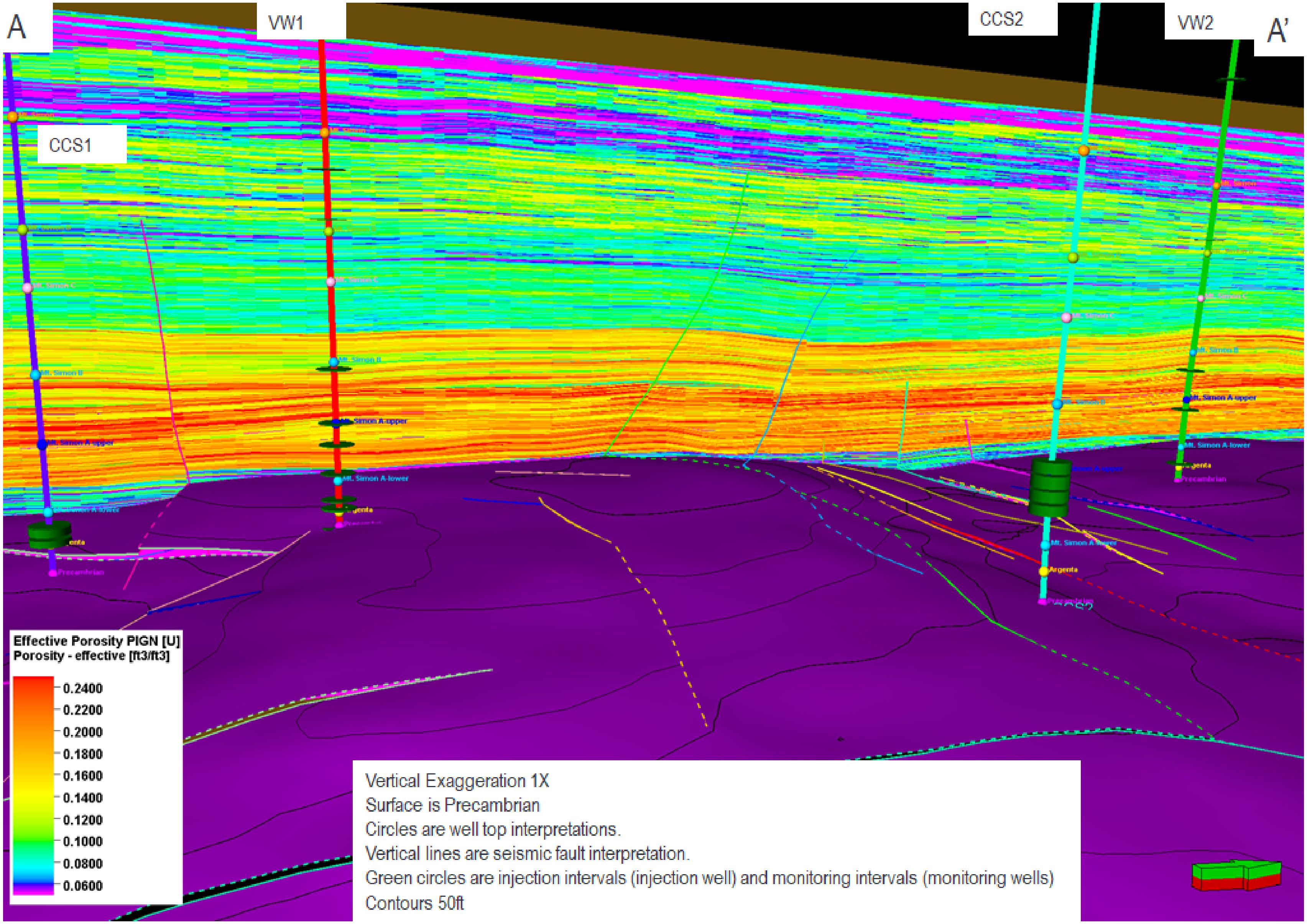

Vertical Exaggeration 1X
Surface is Precambrian
Circles are well top interpretations.
Vertical lines are seismic fault interpretation.
Green circles are injection intervals (injection well) and monitoring intervals (monitoring wells)
Contours 50ft

Figure 54. A-A' effective porosity.

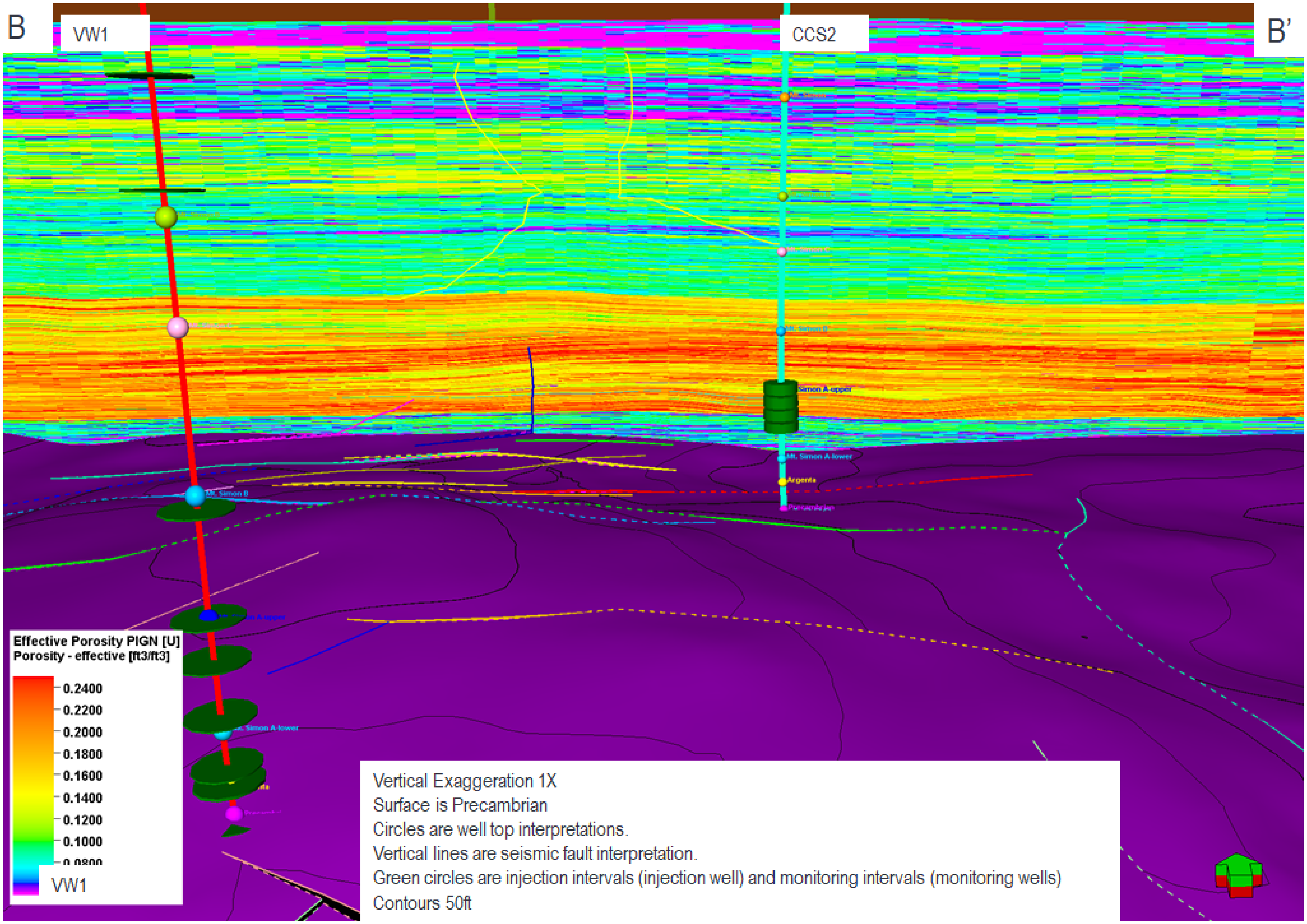

Vertical Exaggeration 1X
Surface is Precambrian
Circles are well top interpretations.
Vertical lines are seismic fault interpretation.
Green circles are injection intervals (injection well) and monitoring intervals (monitoring wells)
Contours 50ft

Figure 55. B-B' effective porosity.

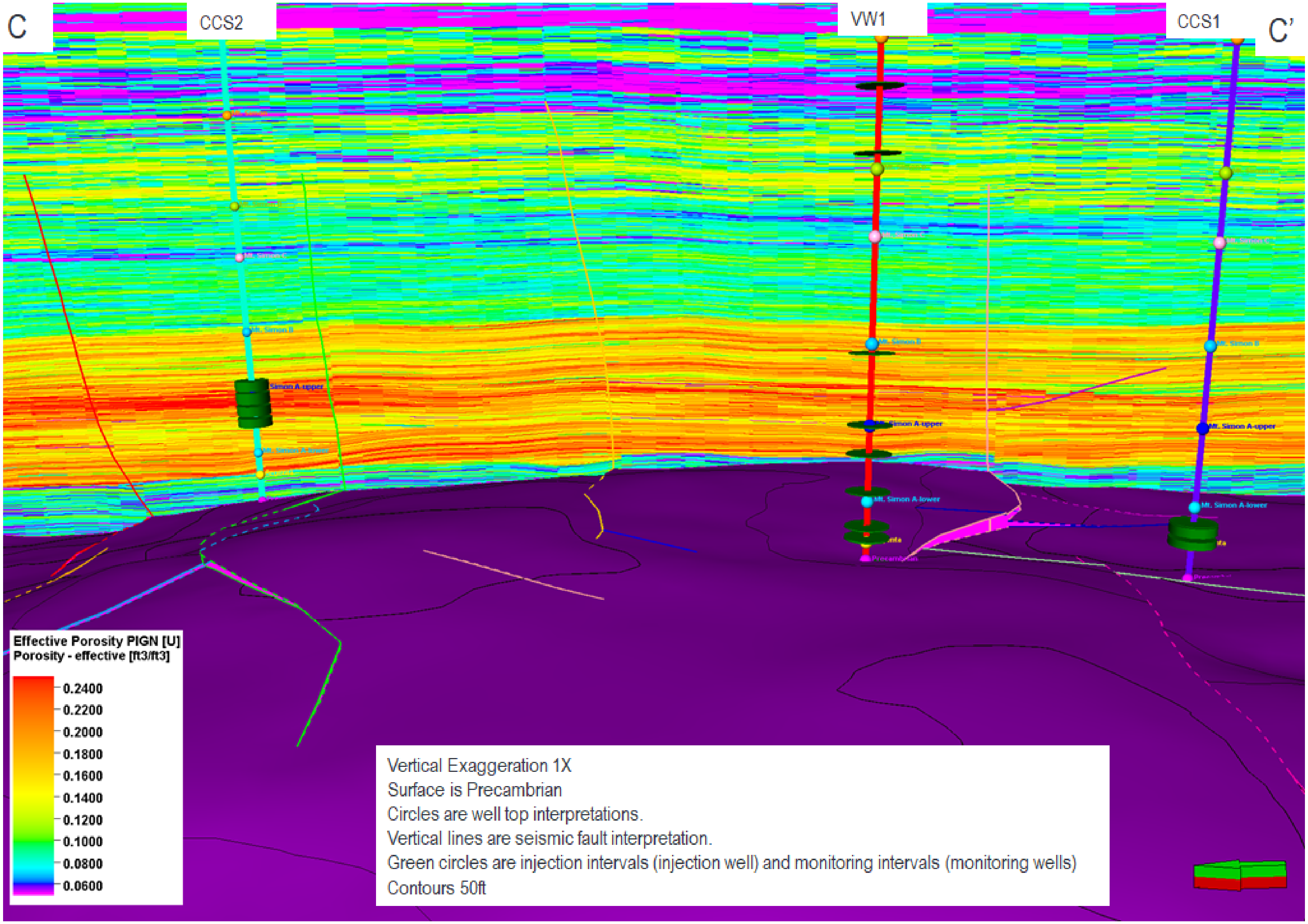

Vertical Exaggeration 1X
Surface is Precambrian
Circles are well top interpretations.
Vertical lines are seismic fault interpretation.
Green circles are injection intervals (injection well) and monitoring intervals (monitoring wells)
Contours 50ft

Figure 56. C-C' effective porosity.

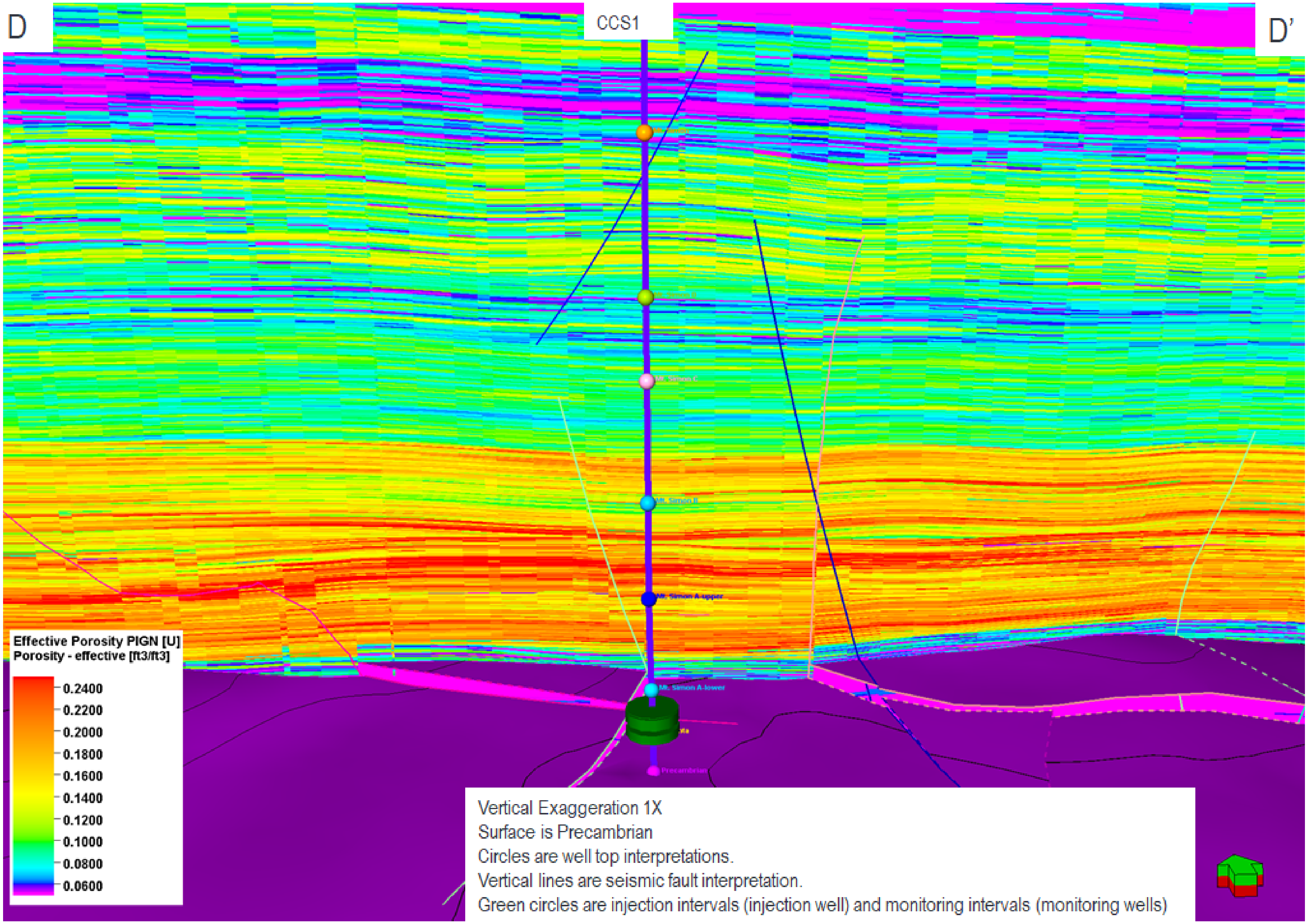

Vertical Exaggeration 1X
Surface is Precambrian
Circles are well top interpretations.
Vertical lines are seismic fault interpretation.
Green circles are injection intervals (injection well) and monitoring intervals (monitoring wells)

Figure 57. D-D' effective porosity.

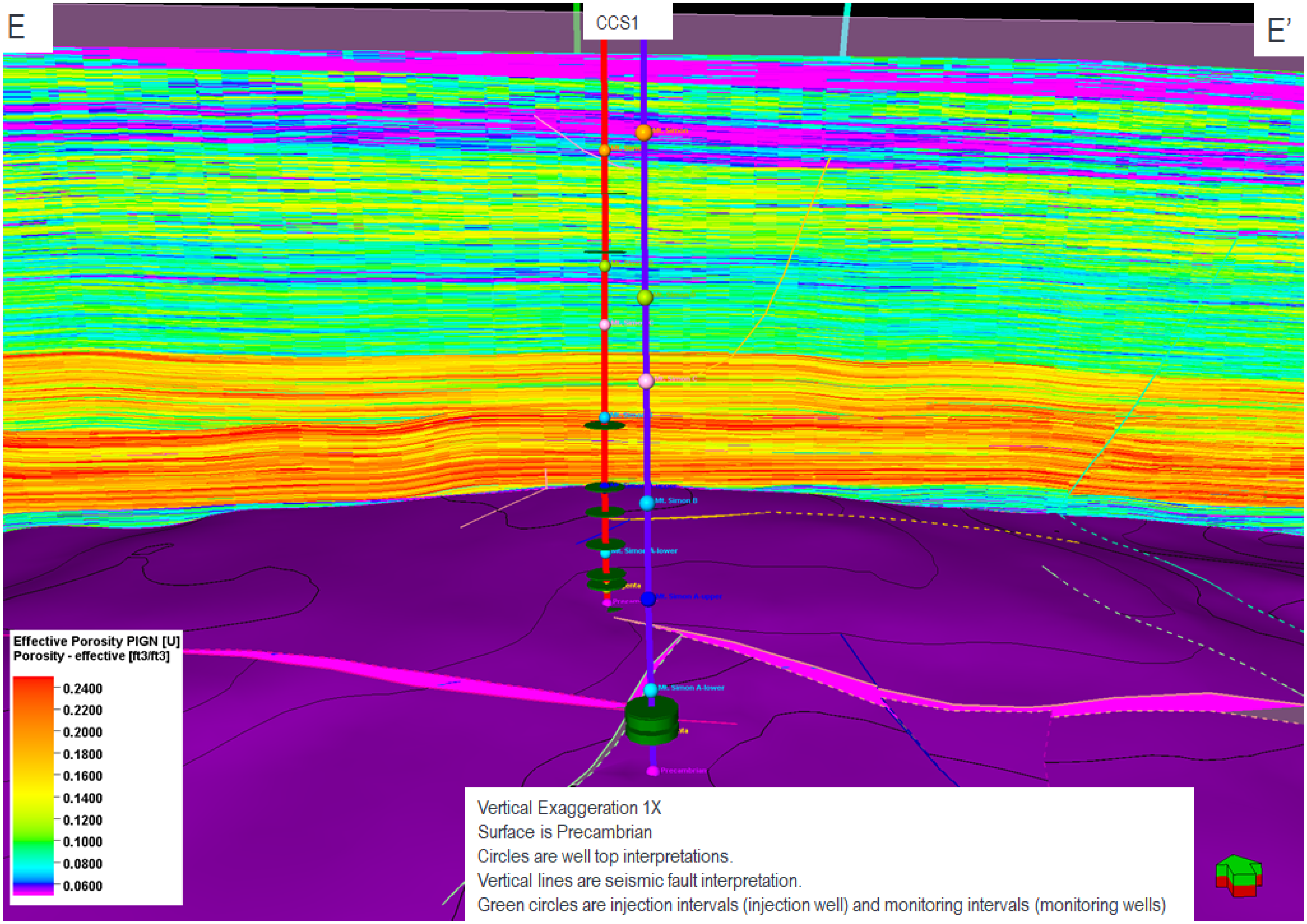

Vertical Exaggeration 1X
Surface is Precambrian
Circles are well top interpretations.
Vertical lines are seismic fault interpretation.
Green circles are injection intervals (injection well) and monitoring intervals (monitoring wells)

Figure 58. E-E' effective porosity.

4.4.4 ISGS Discrete Fracture Network Model (DFN)

The figure below shows a discrete fracture network model (DFN) constrained by the microseismic events recorded during pre-injection injection and post-injection phases. More than 90% of the events occur in the Precambrian Formation (Figure 59). Fractures were modeled by calculating from each event a fracture plane size by using the relationship between the moment magnitude of the event, the shear modulus of the rock, and an estimated slip, as described in (Williams-Stroud, 2020):

$$M = \mu A D \qquad \text{(Eqn. 1)}$$

Where
M = moment
μ = shear modulus (2.34×10^9 MPa)
A = fracture surface area in meters^2
D = average displacement in meters

The DFN calculates fractures stochastically according to fracture driver properties, for example surface curvature, seismic coherency, fault proximity, or lithology that can be used to populate a simulation grid. For this simulation, two different DFNs were generated, 1) a DFN constrained by the microseismic events to model fractures and faults that were reactivated by the pressure perturbations, and 2) a stochastic DFN for the entire volume of the Precambrian using fracture orientations measured from image logs. A stochastic DFN in the Precambrian was generated to provide a background permeability to that unit; the measured permeability was too small for fluid transmission in the model for a history match.

DFN 1 was calculated using the induced seismicity, using the 72 focal mechanism inversions that were available from event data collected from seismometers installed on the ground surface in the Decatur area as modeling constraints. The estimated failure planes from these focal mechanisms were used to constrain the fracture orientations within the DFN. The first four clusters develop prior to the installation of the seismometers. For each subsequent cluster, at least one source mechanism inversion was available, and the orientations of the fractures in that cluster were assigned according to either the orientation statistics of the failure planes from the focal mechanism solution (where more than one focal mechanism was available) or a statistical scatter in orientations was assigned to the one fault plane from the focal mechanism solution in order to generate a DFN with fractures of different but similar orientations. The stochastically generated fractures were then sorted by size and centered on the microseismic event locations according to size. DFN 2 was constrained by the image log fracture orientations which were distributed uniformly within the Precambrian. The generated fractures followed the statistics of the image log fracture orientations, and a power law size distribution was applied. Combining the resulting DFNs creates porosity and permeability that is higher in the locations of the induced seismicity. The porosity and permeability properties of the 2 fracture models were upscaled into the geocellular model.

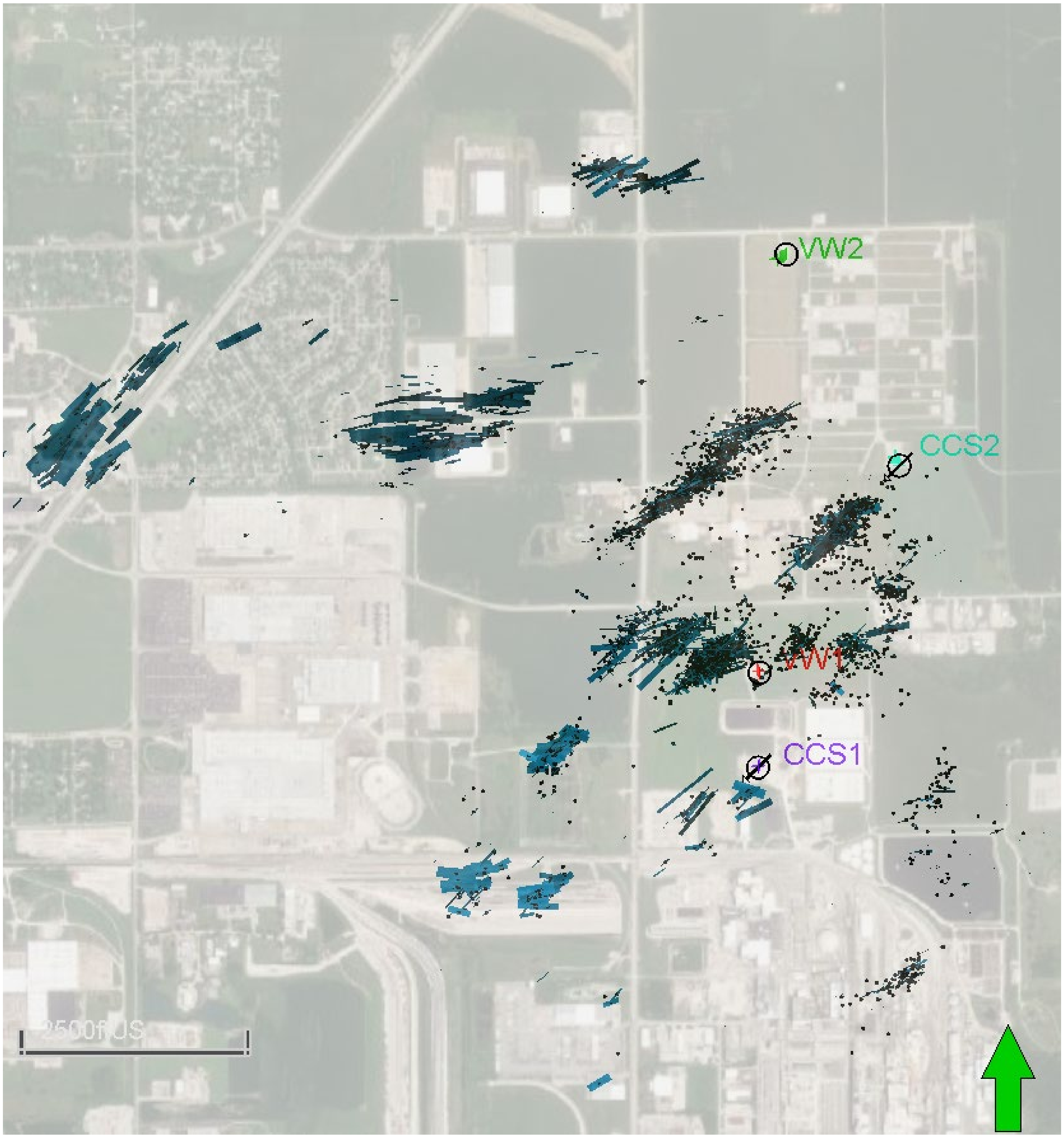

Figure 59. ISGS Discrete Fracture Model 1 showing fractures and their associated microseismic events

4.4.5 Quality Control

With effective porosity and permeability properties generated, it was important to cross-plot them and to analyze the histograms to ensure there was a realistic relationship. This section displays many zone-specific statistical views of the input and output data which were analyzed during the modeling process to make sure that the geological modeling made statistical sense. Geological property modeling is a complex process with many variables to tune for each zone (variograms, co-kriging variables, data transformations etc). With all these variables, for each zone, it is very easy to miss one setting that will generate a poor model.

These errors are not noticible in the above cross sections and maps and can only be seen using the below statistical plots. During the modeling process, with these plots readily available, these relationships were quality checked, errors were quickly identified and corrected. It is easy to generate a model that is statistically representative but does not make any geological sense. To properly quality control this geomodel, the below statistical plots were analyzed while looking at maps and cross sections of the data (sections above). The below plots display a reliable statical relationship while at the same time made geological sense as observed in the property model cross sections.

Figure 60 displays cross-plots of the injection zones, Mt. Simon A-Upper and Mt. Simon A-Lower. Figure 61 displays histograms of the same data. In Figure 60, the top left the plot displays the high vertical resolution input log data (blue) with the data upscaled into the model cells (green) and the final modeled properties (red). This plot (Figure 60) and the histograms of Figure 61 were made to check how the upscaling process represents the input well log. In Figure 60, the green (upscaled cells) matches the blue (logs) in a way the represents the heterogeneity of the reservoir. Because the cells are 3 feet (0.9 m) thick, the fine scale low and high reflections of the well logs could not be captured. This is a something that every geomodel must balance, thinner cells will capture more heterogeneity; however, the cost is a very high cell count and cumbersome geomodel. For the IBDP model, this relationship was observed as the upscaling methods were being selected. In this case, the averaging upscale method was able to achieve a good balance between capturing the heterogeneity and keeping the cell count manageable. The remaining plots display the upscaled cells colored by zone and facies. The lower left plot shows how the sands (yellow) have a higher porosity/permeability than the baffles (green). The next step was to interpolate the upscaled cells into the empty model cells (red) as described in Section 4.3. This interpolation was co-kriged to the 2019 Porosity Cube. The relationship of the model cells follows the same trends as the upscaled cells and with the analysis of the model cross sections, is a reliable statistical representation of the subsurface. This relationship is expected to deviate in places because the model cells (red) represent the entire model domain while the upscaled cells only represent the petrophysics properties at the four well locations (CCS1, VW1, CCS2 and VW2). The geology, as seen in the 2019 Porosity Cube will vary and will not be the same as what is seen at the four well locations; therefore, there is some expected deviation in the model cells (red) when compared to the upscaled cells (green). Figure 61 displays separated porosity and permeability histograms of these above-described relationships.

Figure 62, Figure 63, Figure 64 and Figure 65 display a series of zone specific cross-plots and histograms. Following the same process as described above, these plots were analyzed during the modeling process along with the cross sections to ensure that the modeled cells properly represent the geologic setting. In zones above the Mt Simon D and the Precambrian, there is a deviation of the upscaled cells (green in cross-plots, dark blue in histograms) from the well logs (dark blue in cross-plots, light blue in histograms) and modeled cells (red cells in cross-plots and pink in histograms). This is because the vertical thickness the model cells in these zones was increased to reduce the model cell size count to keep the model to a manageable size. Because of this, the high and low ranges of the well logs could not be captured in the upscaling process. To achieve a geological representation of the model cells, instead of using the upscaled cells, the well log data distribution was used in the GRFS data transformations.

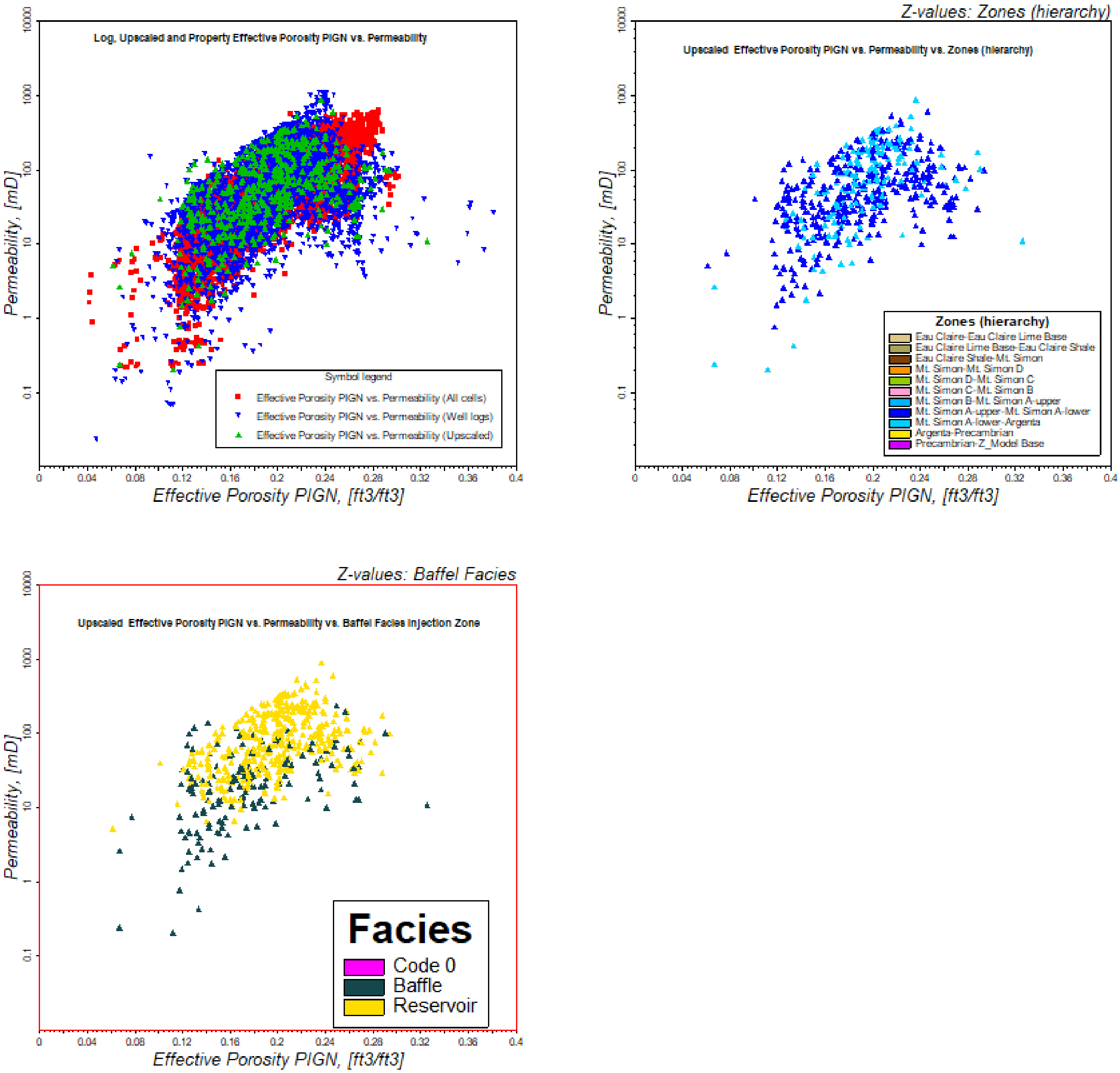

Figure 60. Mt. Simon A and B cross-plots of effective porosity and permeability.

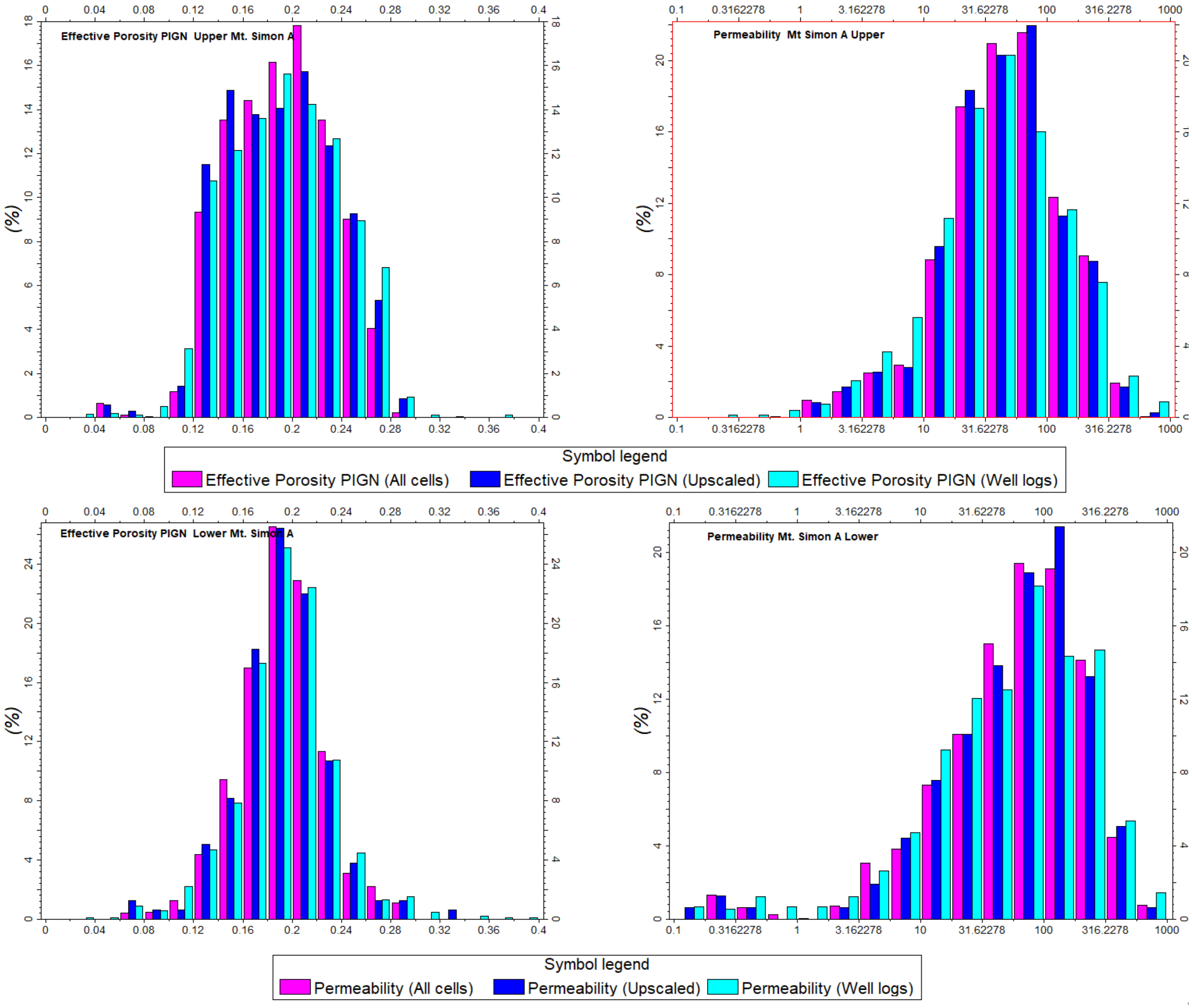

Figure 61. Mt. Simon A histograms of porosity and permeability.

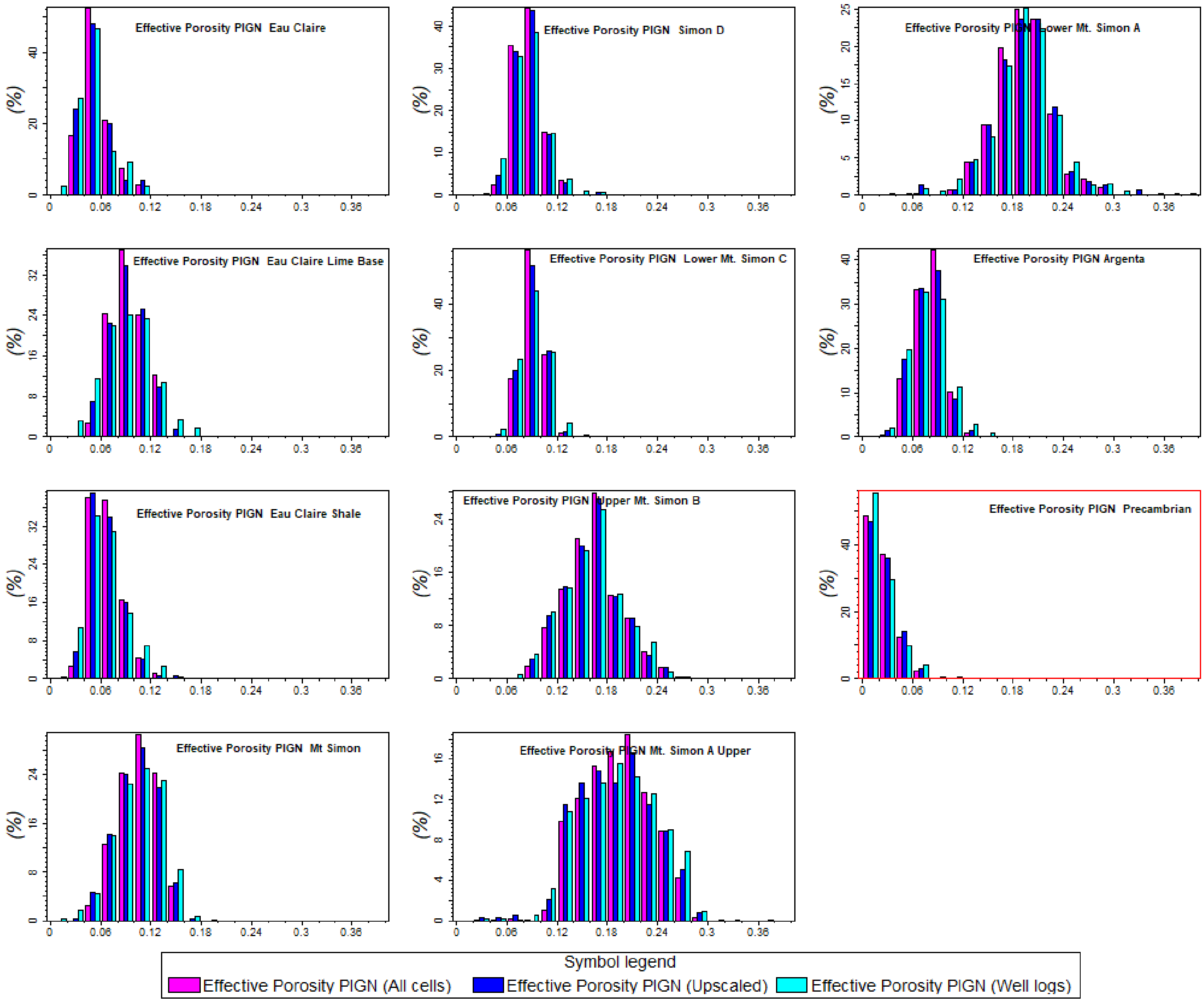

Figure 62. Effective porosity histograms for all zones.

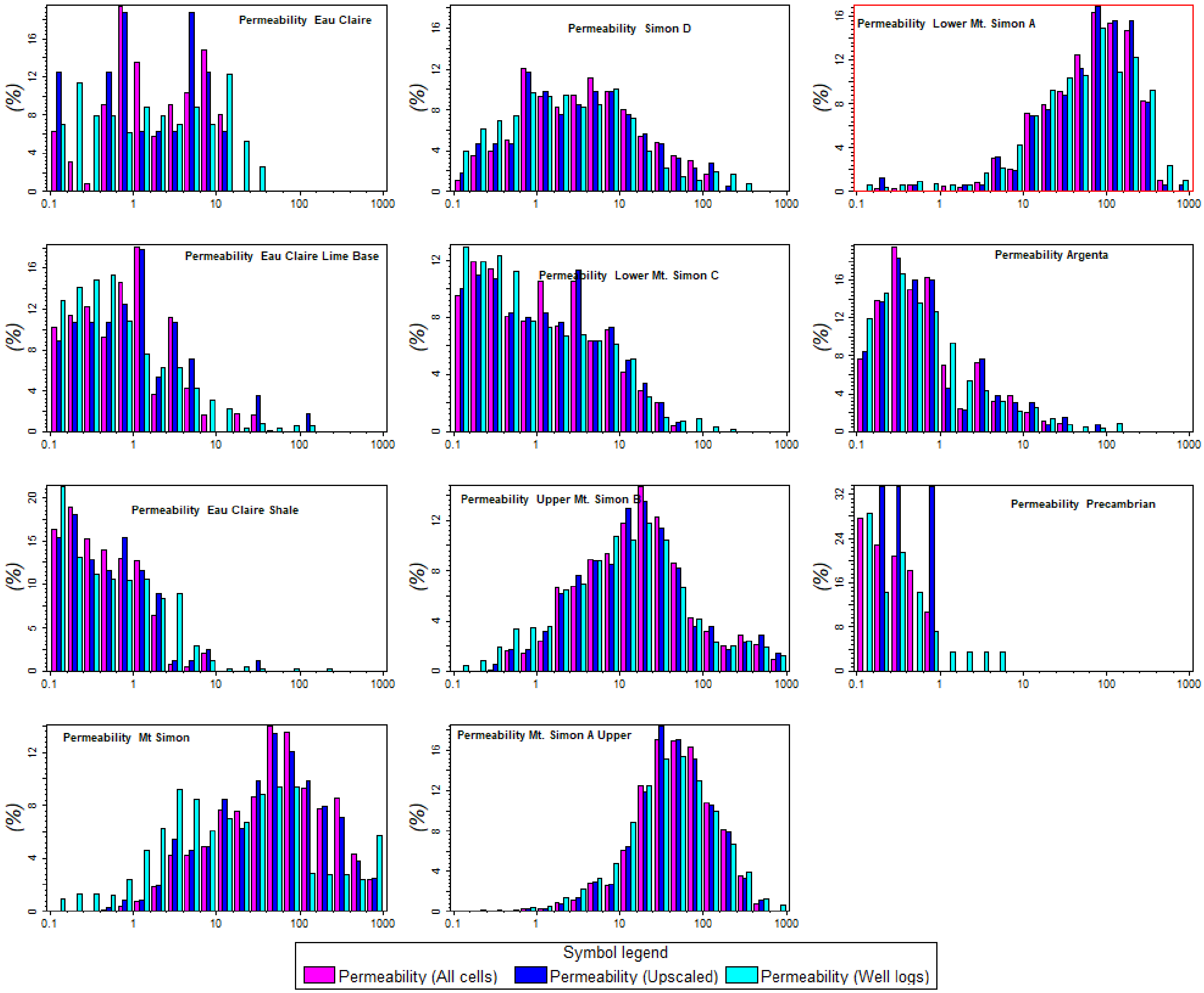

Figure 63. Permeability histograms all zones.

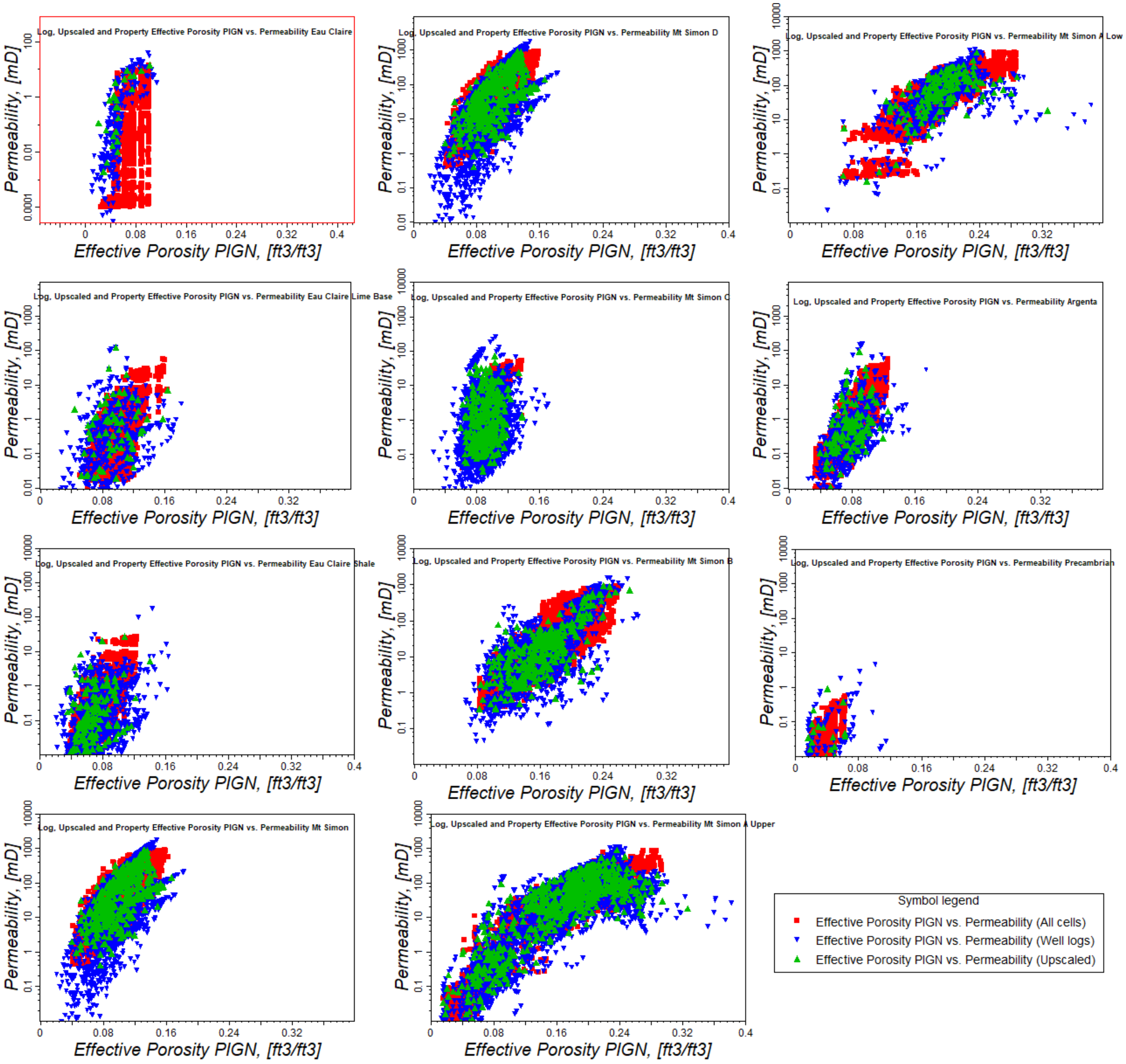

Figure 64. Porosity vs. permeability for all zones.

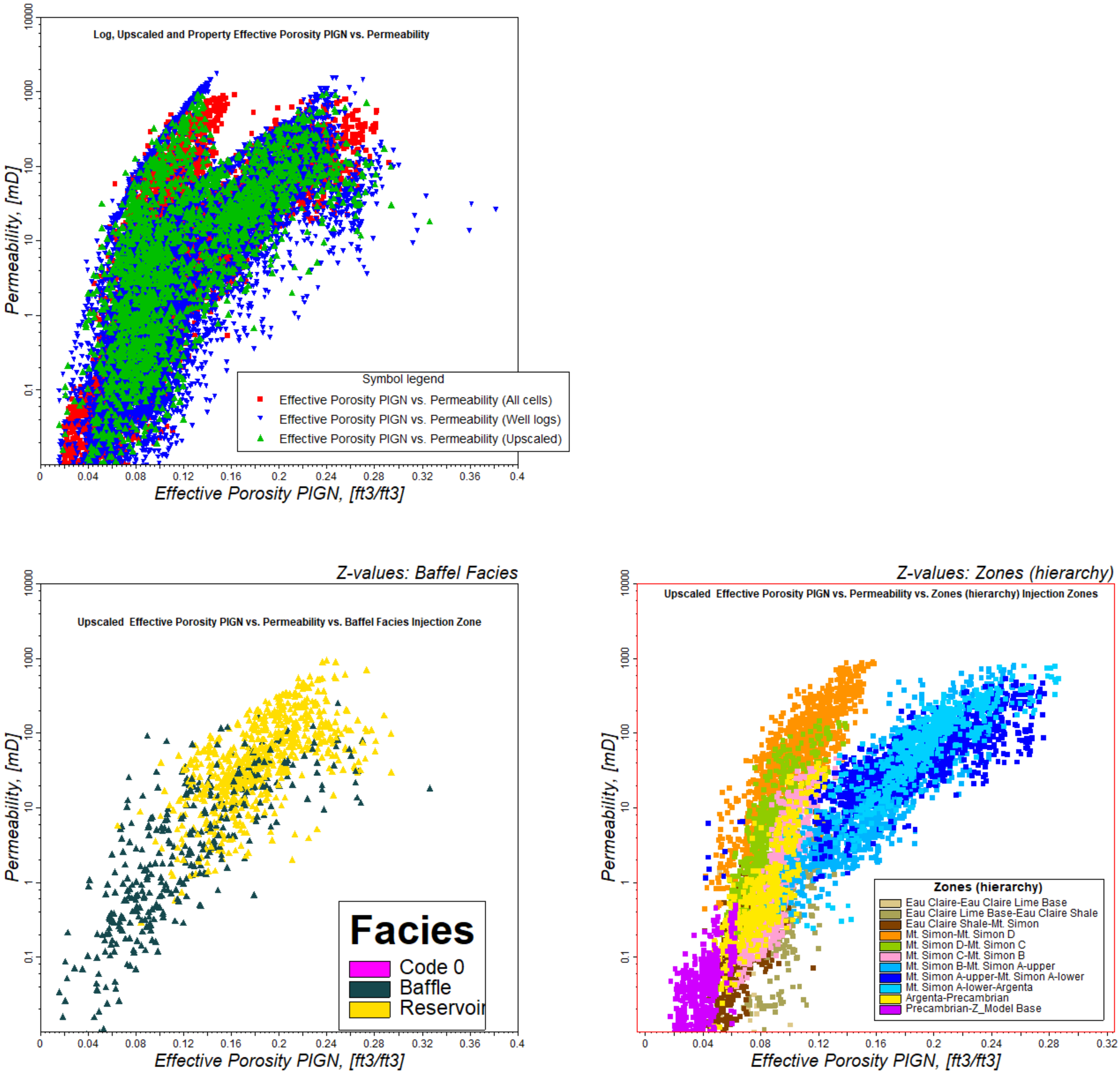

Figure 65. Porosity vs. permeability cross-plots for all zones.

4.5 Geomodel Summary

From the beginning of the IBDP project, the 9.7-mile × 9.3-mile geomodel was an integral component for reservoir characterization of the CO_2 storage site. This geomodel was successfully developed to represent the Eau Claire Shale (confining unit), the Mt. Simon Sandstone (reservoir), and the underlying formations. A structural framework was built using the true vertical depth (TVD) surfaces and the interpreted faults. The interpreted horizons were extrapolated out beyond the 3D seismic coverage area with a regional trend to cover the model domain because the 9.7-mile x 9.3-mile model domain is larger than the seismic survey footprint. In collaboration with the ISGS, the higher resolution 2019 Seismic Reprocessing Volume was used to interpret 28 faults in the seismic footprint, only 9 of these faults had maximum displacement between 30 and 60 feet, the remaining faults had a maximum displacement of less than 30 feet.

Baffle facies were interpreted on well logs as areas of relatively lower porosity and relatively lower permeability barriers which were interpreted layers within the Mt. Simon B, Mt. Simon A-Upper and Mt. Simon A-Lower. Because these baffle layers could not be always correlated between the wells and because history matching results (Discussed in Section 5) showed that CO_2 and pressure migration was moving around discontinuous barriers, these baffle layers were interpolated between these wells in a discontinuous way. The 2019 Porosity Cube, effective porosity, permeability and the baffle facies logs from all four wells were upscaled into the grid. A 3-foot cell height was chosen (Mt. Simon B to Mt Simon A-Lower) to keep the model's cell-count at a manageable level while still capturing vertical heterogeneity.

Using the 2019 Porosity Cube, variogram analysis was completed to properly evaluate how the petrophysical properties vary within the interwell space. Using these variogram parameters, within each zone and within each facies, the geocellular property model was populated for the Eau Claire to Precambrian Formations with petrophysical logs (porosity and permeability) from the wells (CCS1, VW1, CCS2 and VW2). To guide the interpolation of porosity in the interwell space, geological knowledge and the 2019 Porosity Cube was used as a co-kriging variable because an effective correlation of the porosity logs and 2019 Porosity Cube was found.

Co-kriging of permeability against the recently generated porosity property was used to take advantage of the known covariance between effective porosity, 2019 Porosity Cube and permeability. With effective porosity and permeability properties generated, cross sections, histograms, cross-plots for each formation were generated to ensure that the results make geological and geostatistical sense. This geomodel was then ready for use as the primary input for reservoir simulations of CO_2 migration in the Mt. Simon Formation which is discussed in the following sections.

5 Dynamic Modeling Updates

The IBDP and ICCS Projects have performed extensive field monitoring efforts compiling vast amounts of dynamic data. Continuous pressure monitoring at the injectors and multilevel monitoring wells, saturation estimates from repeat pulsed neutron logs, production logging (spinner survey), and time-lapse seismic data have been collected and incorporated into the simulation model calibration (history matching). Each of these dynamic data provided insights into the architecture of the reservoir and confining units beyond the information that can be captured through the static characterization process. This section summarizes the tasks performed to update dynamic modeling with history matching to observed behavior in IBDP and ICCS projects starting from the commencement of CCS1 injection on November 17, 2011, cessation of CCS1 injection on November 26, 2014, through the onset of injection from CCS2 from April 4, 2017, to cessation of IBDP monitoring program on March 31, 2020.[1]

5.1 2020 Final Model Updates

For the simulation of saline storage, the ECLIPSE* E300 compositional reservoir simulator with the CO_2 storage module (CO2STORE) was used with Petrel E&P suite as the pre-and post-processing platform in DELFI* environment. The DELFI environment is a secure, cloud-based environment that can provide the users a workspace for a vast number of simulation runs. Sensitivity and history matching work were conducted with the aid of the Petrel Uncertainty & Optimization tool.

The static model including petrophysical properties was updated with the reprocessed 3D seismic data, as described in Section 4.3.1. Based on the recent 3D seismic reinterpretation, newly identified faults were included in the static model. The model domain was expanded vertically for the geomechanical modeling work to be conducted by ISGS (see Section 4.3.2.3). Permeabilities of Precambrian rock were also updated according to the fracture permeabilities obtained from the ISGS' discrete fracture network (DFN) modeling work. See Zaluski and Lee (2019) for the details of fluid properties, relative permeability curves, and model equilibrium used for dynamic modeling.

In addition to the model updates, additional surveys such as pulsed neutron logging and spinner survey were conducted in March 2019. Downhole pressure data from CCS1, VW1, CCS2, and VW2 and injection history at CCS2 since the previous report (Zaluski & Lee, 2018 IBDP/ICCS Static Geological Model Development and Dynamic Modelling Updates, 2019) were also included in this work for history matching.

5.1.1 Grid Settings

A high-resolution static geologic model was constructed through integration of 3D seismic data, geophysical logs, and core analysis, as described in Section 4. A subset of the heterogeneous reservoir model covering a 9.7-mile × 9.3-mile area with the injection wells centered in the model domain (Figure 66) was used for the dynamic modeling. Based on the previous work, a vertical extension to the static model above Mt. Simon C and below the Precambrian rocks was made for dynamic modeling, resulting in the vertical expansion of the model size (5 layers at the top and 17 layers at the bottom). Starting with the Eau Claire at the top, the global tartan grid configuration, with variable cell sizes, is 126 × 125 × 110 cells (totaling 1,732,500) in the x, y, and z direction, respectively. Note that the lateral grid setting remains the same as the previous work (Figure 67). The smallest grid cells around the injectors and observation wells are 125 ft × 125 ft (38.1m x 38.1m) laterally. The vertical thickness of each cell depends

---

[1] Data are continued to be collected from CCS1 and CCS2 beyond the periods identified here. For the purposes of IBDP, data used for models ends on March 31, 2020.

on the vertical thickness of each formation at a cell's location. The detailed description of the model zones can be found in Section 4.4.

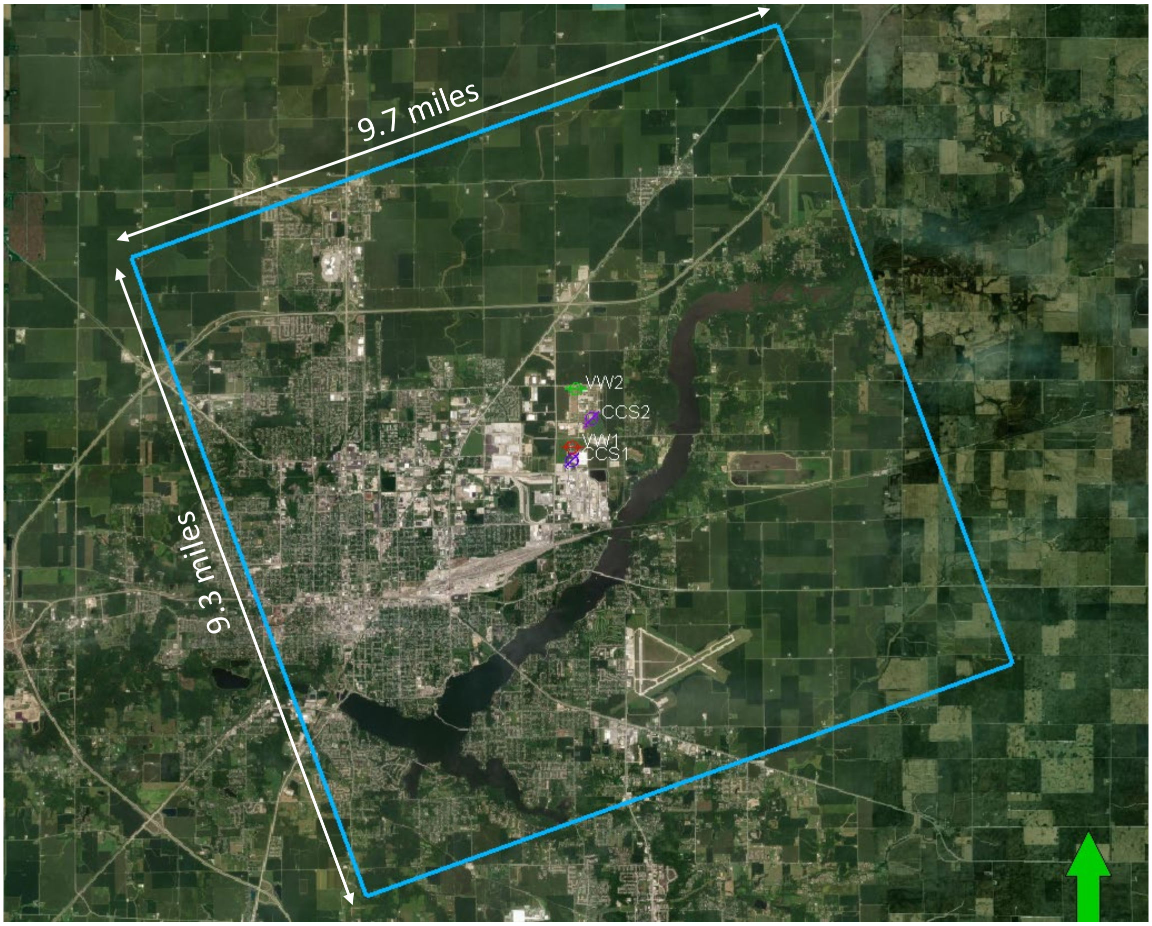

Figure 66. Satellite imagery showing the dynamic model boundary and location of injectors and monitoring wells.

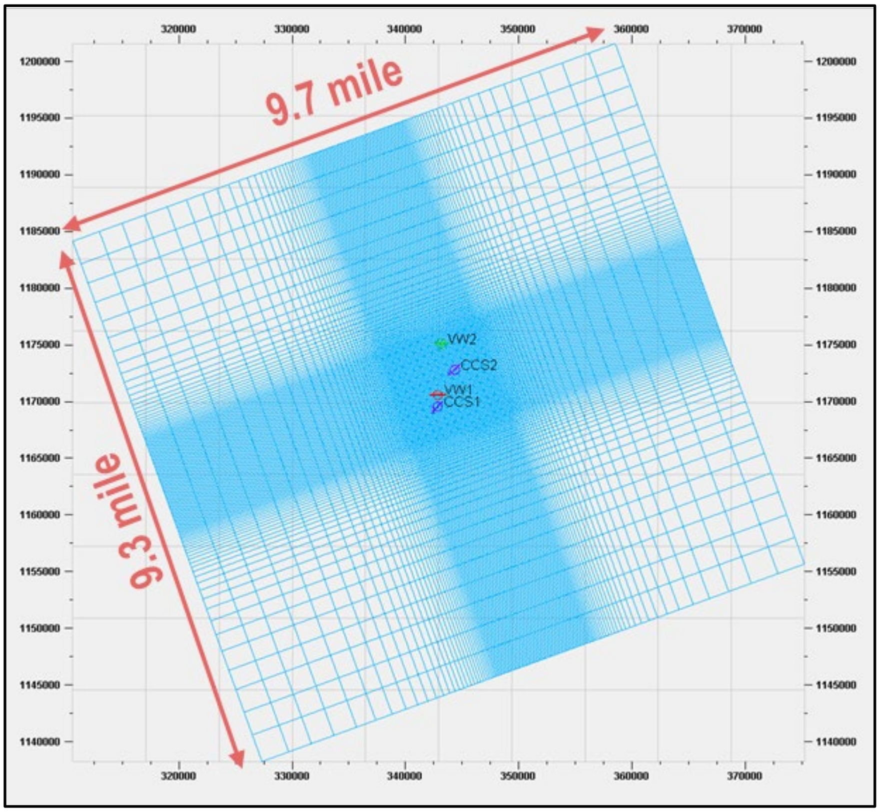

Figure 67. Dynamic model domain and tartan grid.

Figure 68 shows the spatial distribution of the two CO_2 injection wells (CCS1 and CCS2) and two monitoring wells (VW1 and VW2). Cross-sectional lines I-I′ along CCS1, VW1, and VW2, II-II′ along CCS2 and VW2, and III-III′ along CCS1 and CCS2 are used to show the internal distribution of various properties in the following sections. Multiple perforation intervals of injectors and multilevel pressure gauges of monitoring wells are shown in Figure 69 along the I-I′ and II-II′ cross-sections. Figure 70 and Figure 71 illustrate the 3D upscaled porosity and permeability distributions along II-II′ and III-III′ cross-sections.

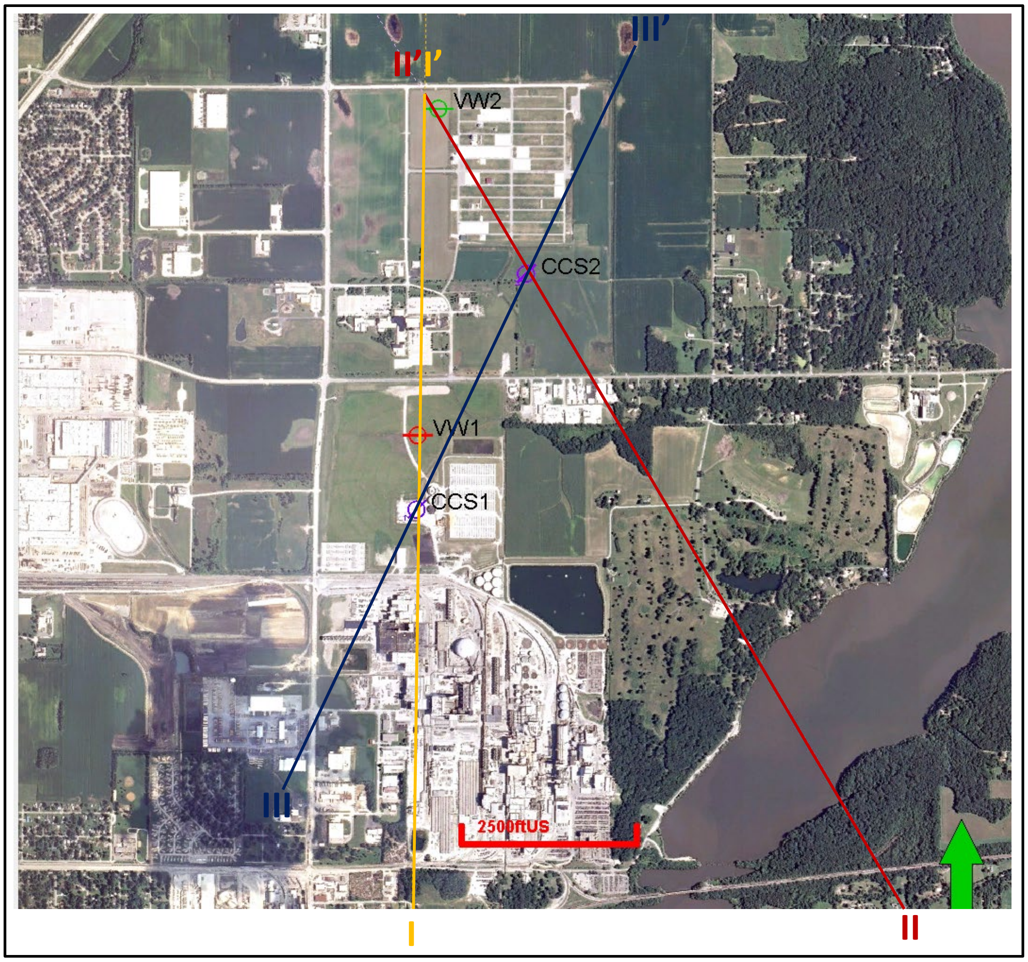

Figure 68. Location of injectors (CCS1 and CCS2), monitoring wells (VW1 and VW2) and cross-section lines.

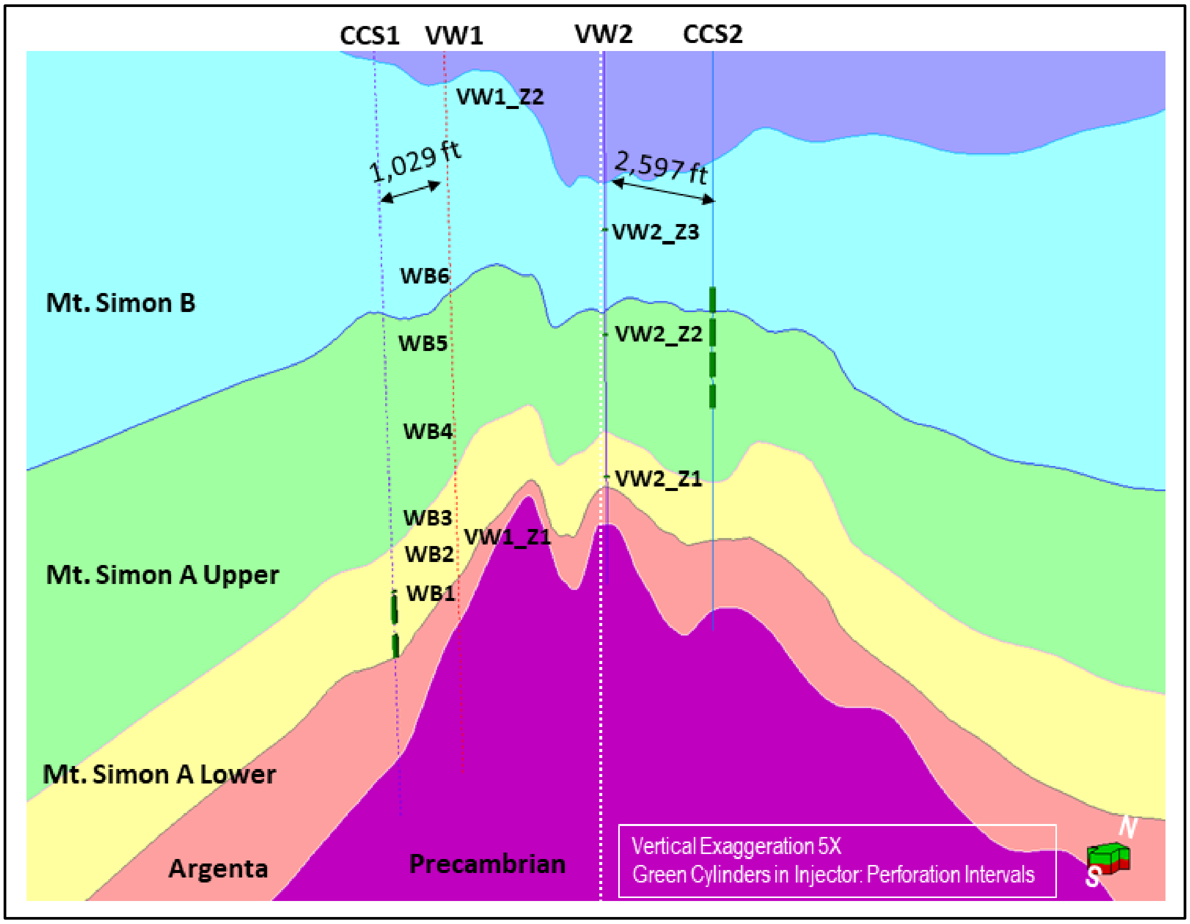

Figure 69. Location of perforation intervals in injectors (green cylinders) and pressure gauges in monitoring wells along the cross- sections I-I′ (left) and II-II′ (right).

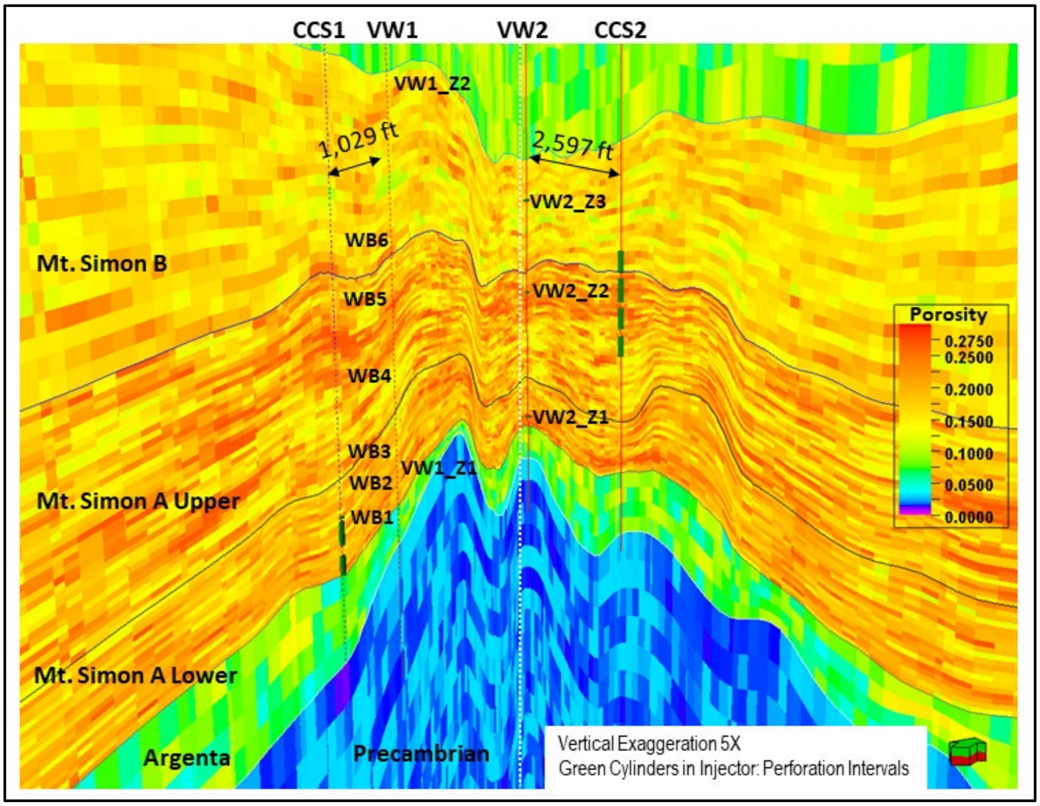

Figure 70. Upscaled porosity profiles along the cross-section I-I′ (left) and II-II′ (right).

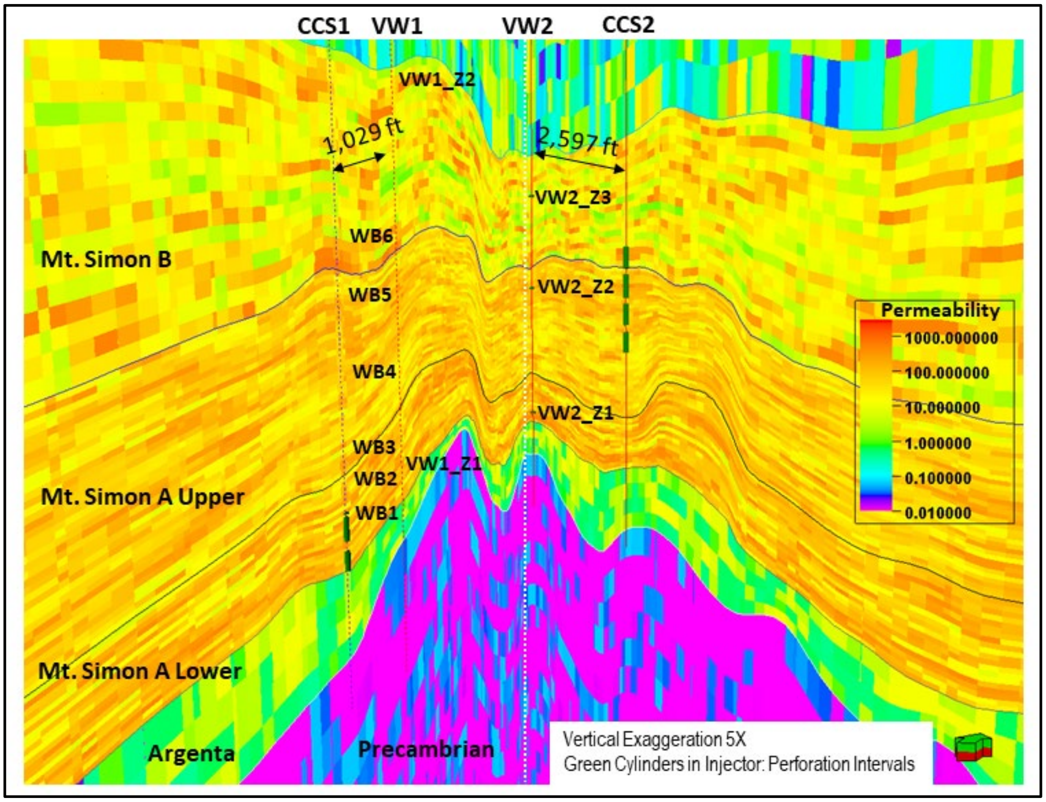

Figure 71. Upscaled permeability profiles along the cross-section I-I′ (left) and II-II′ (right).

5.1.2 Reservoir Boundaries

In the previous study (Zaluski & Lee, 2018 IBDP/ICCS Static Geological Model Development and Dynamic Modelling Updates, 2019), an infinite-acting boundary was assigned at the bottom of the model due to the short distance between injection intervals and the top of the fractured Precambrian basement in addition to the limited inclusion of upper Precambrian layers in the model. Because this 2020 final model was vertically extended substantially to include the Precambrian rock and updated permeabilities were upscaled from a DFN provided by the ISGS, the infinite-acting boundary was no longer assigned at the bottom of model. Infinite-acting conditions were assumed at the lateral boundaries of the simulation model. The lateral infinite-acting boundary was modeled by applying a pore multiplier of 10^6 in the cells at the model perimeters to account for a near-infinite aquifer volume. These boundaries would act as pressure sinks/source during and after the injection. No-flow boundaries are assumed at the top and bottom of the model.

5.1.3 Baffle Facies

Prior to the CCS2 injection and introduction of the VW2 data, the dynamic model required a thin and continuous low-permeability baffle zone between Mt. Simon A-Lower and -Upper to isolate the pressure response above to the Mt. Simon A-Lower. However, as described in Section 4.4.2, additional monitoring data required the revisit of the geologic model for better history matching. As a result, additional low-porosity and low-permeability baffle facies were introduced into the dynamic model. The 3D architecture of the baffle facies would provide a local flow barrier and/or preferential pathway. Figure 72 illustrates the newly introduced baffles along the I-I′ and II-II′ cross-sections. Discontinuity/holes in the baffle zone were achieved according to the baffle facies modeling described in Section 4.4.2 and are shown in Figure 72.

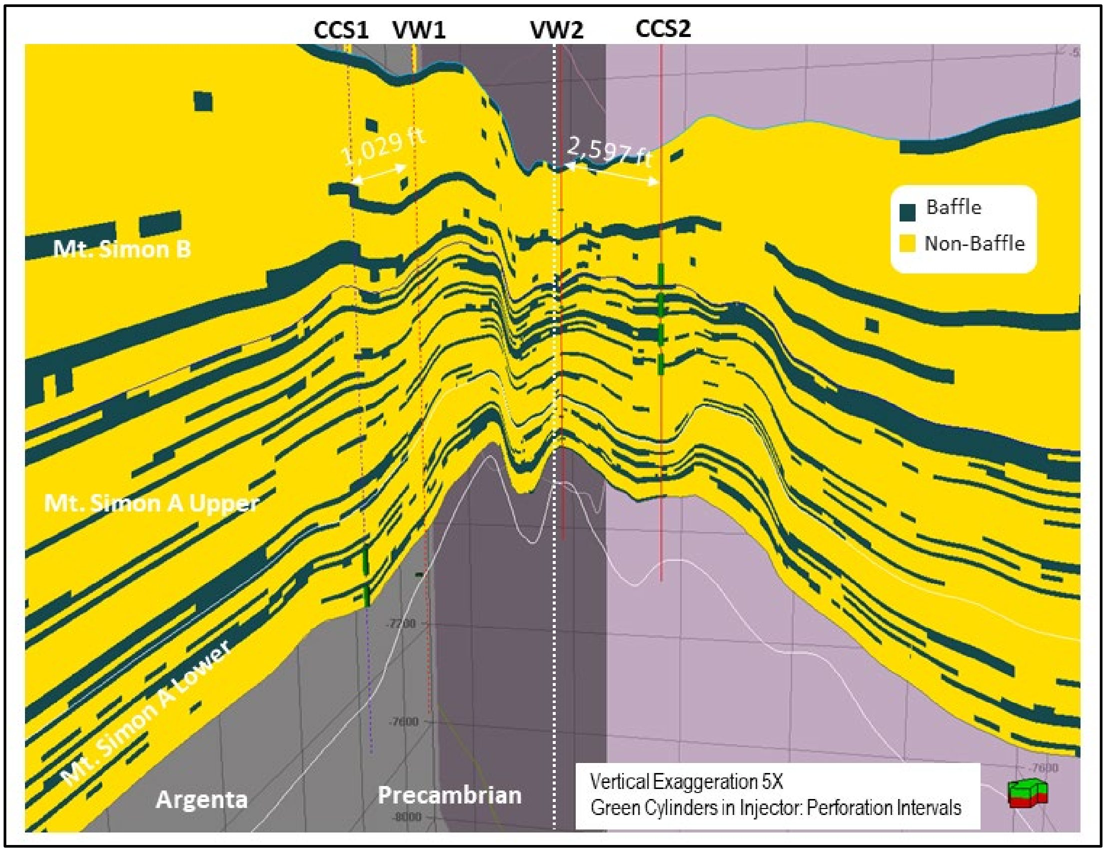

Figure 72. Low-permeability baffles along the cross-section I-I′ (left) and II-II′ (right) in a perspective view. Green cylinders along CCS1 and CCS2 represent the perforation intervals.

5.1.4 Permeabilities of Precambrian Rocks

A DFN constrained by the induced seismicity was used to create permeability properties in the Precambrian rocks. Wellbore images indicate the basement rocks are highly fractured. Fracture size distribution of DFN within the Precambrian rocks was constrained by the microseismic event magnitudes, and fracture permeabilities were calculated from the DFN. In Figure 73, the permeabilities of the Precambrian rocks were updated according to the fracture permeabilities and porosity.

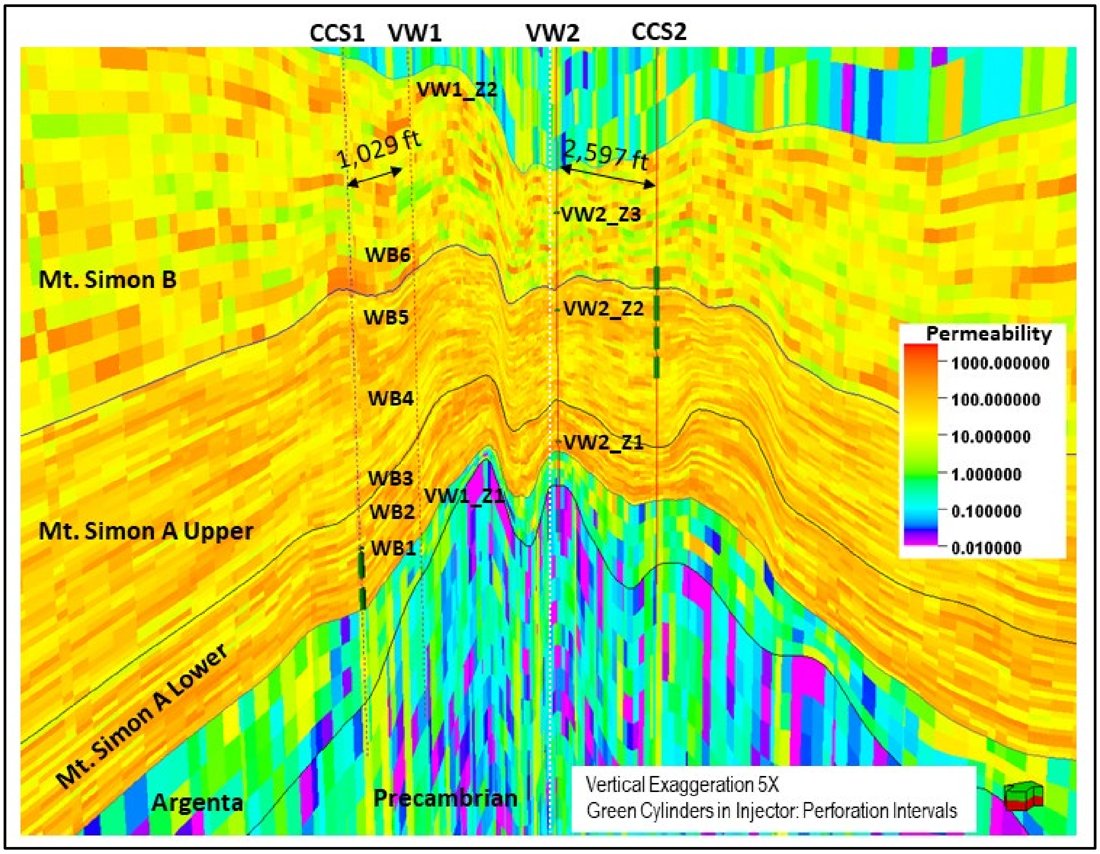

Figure 73. X-dir Permeability (K_x) profiles after Precambrian fracture permeability updates along the cross-section I-I′ (left) and II-II′ (right) in a perspective view.

5.1.5 Faults

Major updates to the 2020 version of the dynamic modeling were related to the presence of an updated structural framework with newly captured faults based on the seismic re-interpretation since the previous study (Zaluski & Lee, 2019). A study of the static model and available well-data gave focus to the inclusion of structural faults in the tartan grid used in dynamic simulation. Figure 74 shows the process utilized to model the faults within the Tartan gird as modified transmissibility zones. Twenty-eight faults were mapped into the model. The transmissibility multipliers for these faults were evaluated with sensitivity analysis and used for history matching.

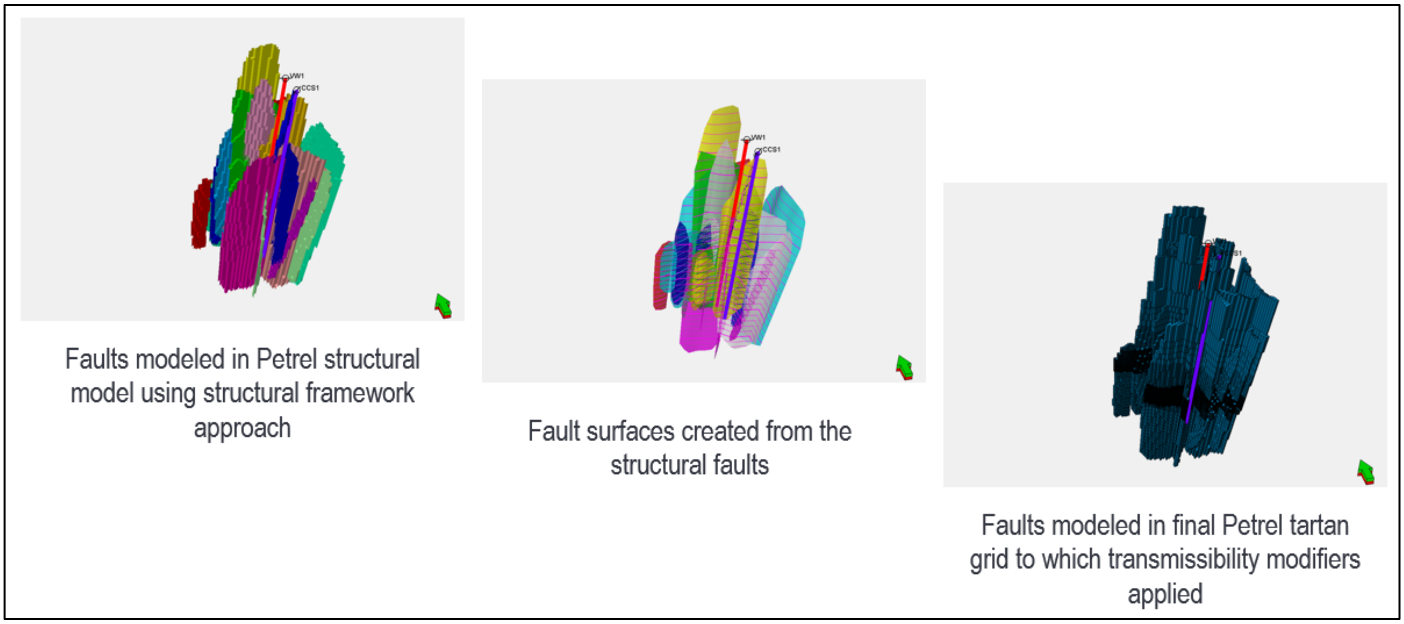

Faults modeled in Petrel structural model using structural framework approach

Fault surfaces created from the structural faults

Faults modeled in final Petrel tartan grid to which transmissibility modifiers applied

Figure 74. Faults modeled in Tartan grid (right) from structural grid model (left).

5.2 History Matching

History matching and model calibration was used to help refine the reservoir parameters. This history matching allowed the model to predict the reservoir performance in future operations. In the IBDP/ICCS projects, after model initialization, sensitivity analysis and history matching were primarily focused on the multi-well and multi-level BHP data: Time-lapse saturation logs, CO_2 spinner survey, and seismic results were addressed secondarily in terms of history matching because the BHP data were continuous and direct, and thus the most reliable. Time-lapse saturation logs, the spinner survey, and seismic data are discrete measurements in time and sparse in frequency. In addition, seismic data are challenging to acquire and process, and the data have a limited threshold or resolution in terms of detection of CO_2. Similarly, there exists a threshold of detection (>~5%) in the saturation logs. The deviation from observed data was used to study the parameters that influence the match of the dynamic model.

Figure 75 shows the BHP and CO_2 injection rate (Q) history observed through March 31, 2020. Cumulative CO_2 injection of CCS1 was 999,231 tonnes, and injection of CCS2 through March 31, 2020 was 1,716,754 tonnes. In addition to the BHP gauges at the CCS1 and CCS2 injectors, there existed multilevel pressure data available at the VW1 and VW2 monitoring wells (see Figure 69 for the location of gauges). The Westbay (WB) multilevel groundwater characterization and monitoring systems were originally installed at VW1 and removed in May 2017. New pressure gauges at VW1 (VW1_Z1, VW1_Z2, and VW1_Z3) were installed after the recompletion of VW1, and data from these gauges were available starting on July 11, 2017. As shown in Figure 75, WB pressure recordings at VW1 prior to the system's permanent removal are intermittently absent due to sampling events, probe malfunctions, communication loss, system removal for maintenance, or accidental power outages. In addition, a month prior to and after CCS2 injection commencement, only the data from WB4 and WB6 for the VW1 downhole data are available. WB2 did not function correctly after November 2016.

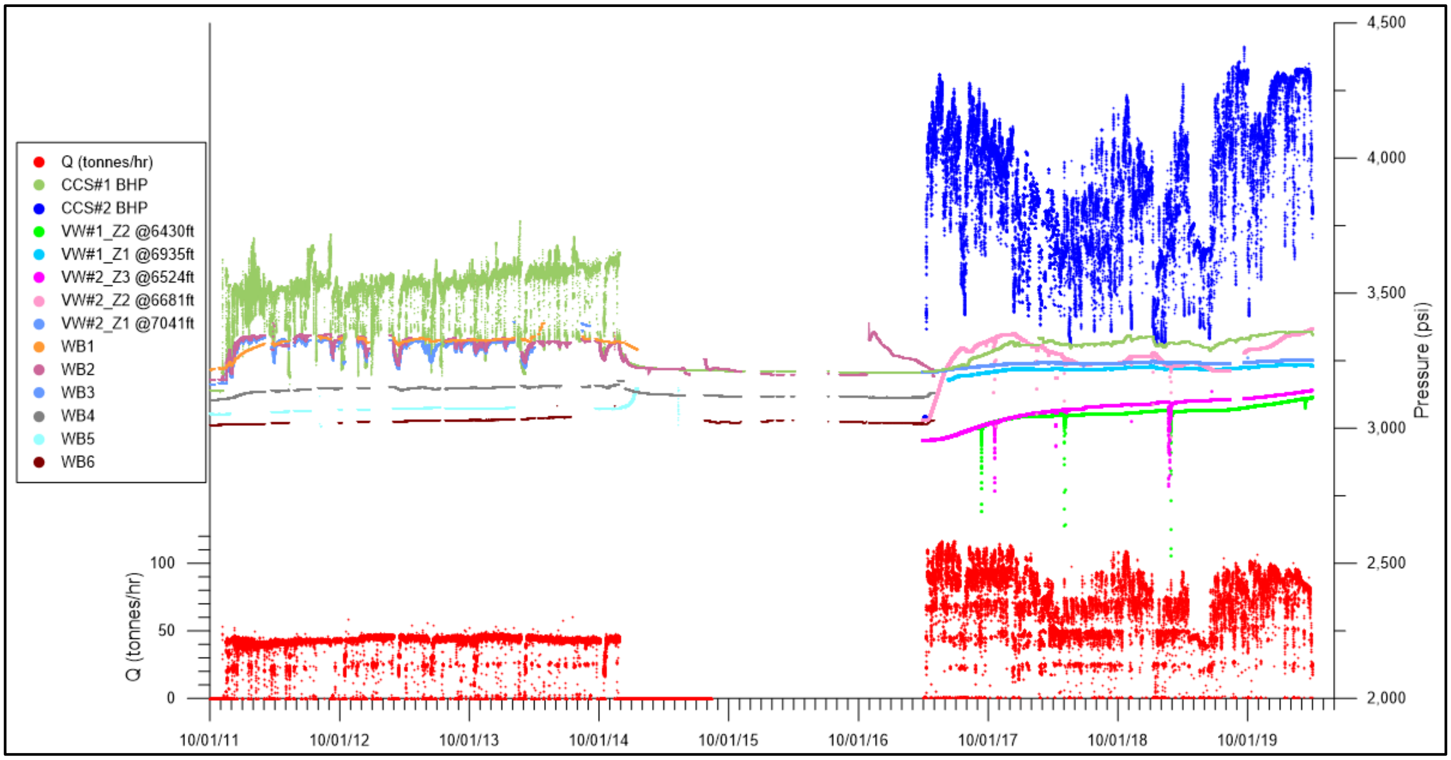

Figure 75. BHP and CO_2 injection history.

5.2.1 Evolution of CO_2 Injectivity

In the previous work (Zaluski & Lee, 2018 IBDP/ICCS Static Geological Model Development and Dynamic Modelling Updates, 2019) to examine the temporal change of well performance quantitatively, injectivity was defined as

$$\text{Injectivity} = Q/(P\text{–}P_o)\times 10 \qquad \text{(Eqn. 2)}$$

Where:
Q = CO_2 mass injection rate, tonnes/day
P = injection well BHP (psi)
P_o = initial reservoir pressure (psi)

The injectivity values represent the injection rates corresponding to the pressure change. In other words, given the change in pressure, higher injection rates indicate greater injectivity. Figure 76 and Figure 77 plot the injectivity values for CCS1 and CCS2, respectively. It appears that injectivity at CCS1 started deteriorating from May 2013. This may be due to salt precipitation, scaling, or solids buildup into the perforation and injection intervals. In the previous work (Zaluski & Lee, 2018 IBDP/ICCS Static Geological Model Development and Dynamic Modelling Updates, 2019), CCS2 injection did not show a clear trend in the injectivity plot until April 7, 2018, suggesting no change in well performance at CCS2 during the reporting period. However, with the additional data through March 31, 2020 it is noted that the injectivity of CCS2 also decreases beginning in February 2019.

In addition to injectivity values, Figure 78 shows the BHP vs. Q data plot to confirm the injectivity change at CCS2. The slope (dP/dQ) in the plot demonstrates the injectivity (or pressure response to the change in injection rate). Slightly higher slope was found in the data grouped after March 2019, indicating the lower injectivity. In other words, higher pressure (*P*) is required to achieve the same injection rate (*Q*) under the lower injectivity condition. The change of injectivity both in CCS1 and CCS2 was represented in the simulation by reducing the well connection transmissibility factors.

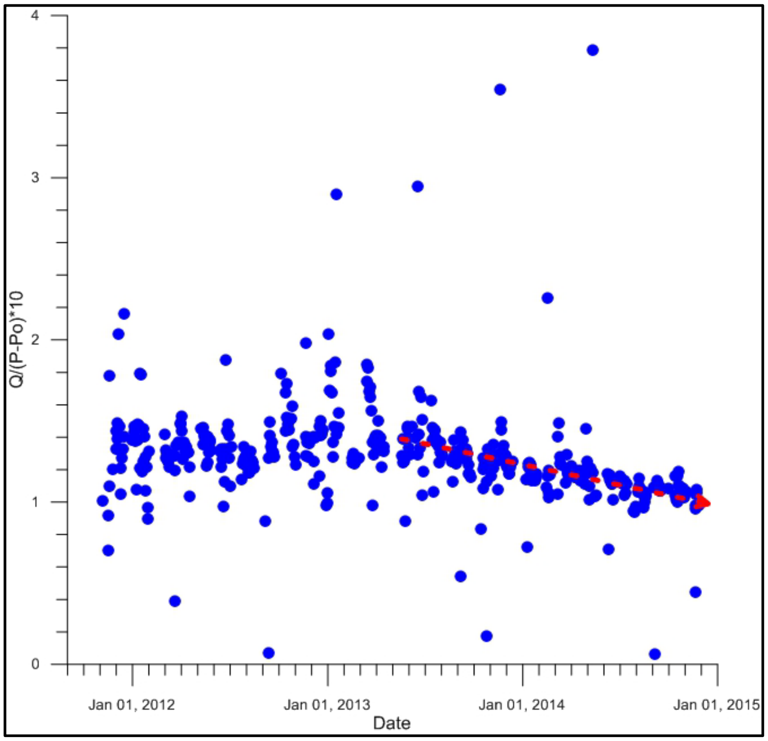

Figure 76. Injectivity of CCS1.

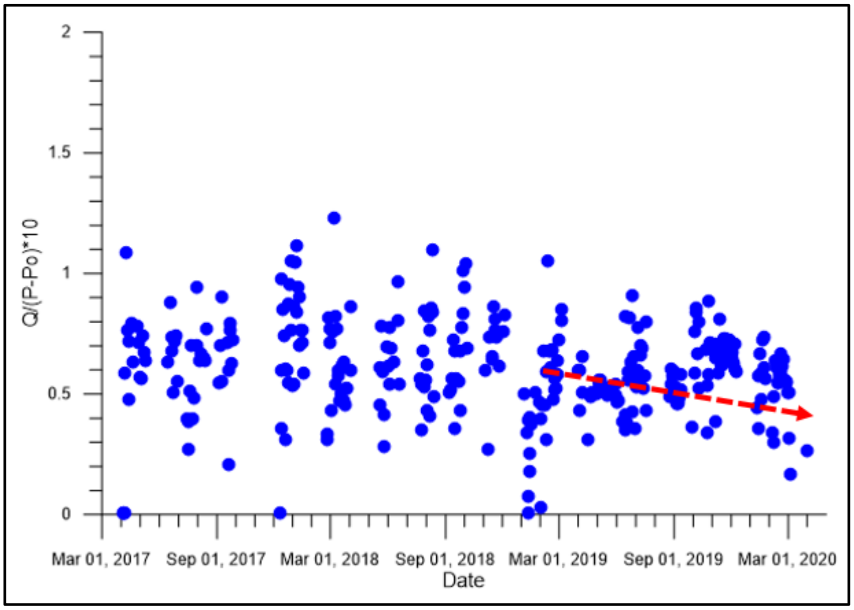

Figure 77. Injectivity of CCS2.

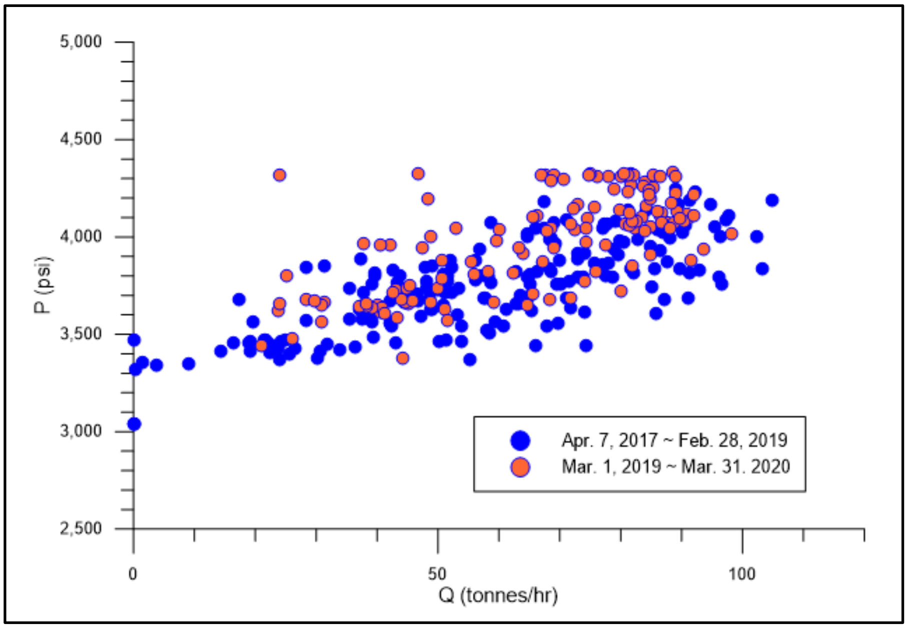

Figure 78. Scatter plot of downhole pressure (*P*) vs. injection rate (*Q*) of CCS2.

5.2.2 Methodology

A two-step approach was used to perform the history matching:

1) Conducting a sensitivity analysis to screen the influential parameters in the simulation study
2) Optimizing the history matching runs to minimize the mismatch between the observed and simulated data

The approach was to initially delineate the independent variables that would impact the dynamic modeling results and then define a mismatch parameter to check the progress of the reliability of the model with respect to observed data available through March 31, 2020. Subsequent sections of the report detail this methodology.

5.2.2.1 Independent Variables of the Study

Four key variables were identified to focus the simulation efforts on. They are as follows:

- **Structural faults** based on 2019 reprocessed seismic interpretation
  A total of 28 faults are included in the updated structural model and incorporated into the tartan grid using the workflow described in Section 5.1.5. In addition to the effects of the individual fault, groupings of these faults according to their orientation and proximity to CCS1 and CCS2 were done initially to evaluate the geologic impact of the faults (Figure 79 and Figure 80). For history matching, faults trending N-S and NW-SE were assumed to be sealing, and all other faults were assumed to be transmissive according to regional stress direction after discussion with ISGS. Later, technical discussion with ISGS on the grouping of these faults led to the grouping of faults based on the fault orientation relative to the regional stress direction. Faults trending N-S and NW-SE were assumed to be sealing, and faults trending E-W and NE-SW were assumed to be transmissive for history matching.

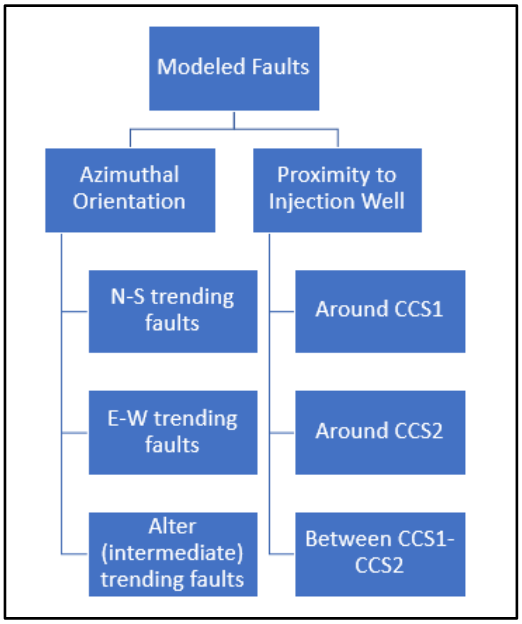

Figure 79. Grouping of faults based on their orientation and proximity to CCS1 and CCS2.

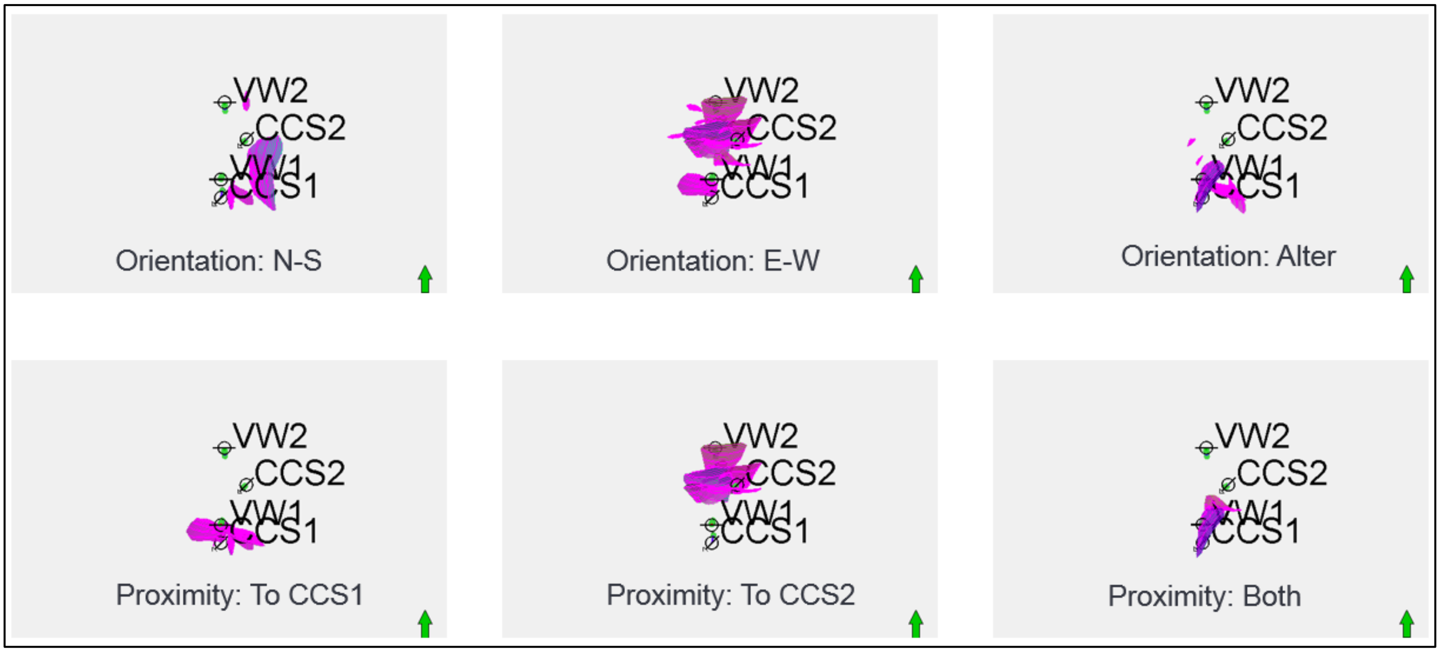

Figure 80. Faults distribution according to orientation and proximity grouping.

- **Baffle facies** properties from geological input

  The porosity and permeability of the baffle facies can have a significant impact on the modification of flow behavior around the wells. They are also considered as an independent parameter in the study.

- **Reservoir heterogeneity** (permeability)

  Due to the heterogenous nature of the formations, the geologic formations vertically subdivided by the positions of the pressure gauges and completions in the injection and verification wells were considered. Zone-wise modifiers for permeability in the lateral and vertical directions were used for the sensitivity analysis and history matching.

- **Well Connection Transmissibility Factor**

  Connection transmissibility factors of CCS1 and CCS2 were modified according to the well injectivity described in Section 5.2.1. In the Eclipse simulator, the following relationship was used for connection transmissibility factor (T_{wj}) in a Cartesian grid:

$$T_{wj} = \frac{c\theta Kh}{\ln\left(\frac{r_0}{r_w}\right)+S} \qquad \text{(Eqn. 3)}$$

Where:
c is a unit conversion factor (0.001127 in oilfield units)
θ is the angle of the segment connecting with the well, in radians
Kh is the effective permeability times net thickness of the connection
r_0 is the pressure equivalent radius of the grid block
r_w is the wellbore radius
S is the skin factor

5.2.2.2 Objective Function Definition

The objective (or mismatch) function is defined as the root-mean-square-error of the simulated and observed data. It was used to analyze the impact of the independent variables on the history-match result. Multiple mismatch functions were created, with a focus on CCS1 and CCS2 individually, and combined with the gauges at VW1 and VW2. Components of the objective function included the ability to give higher weight to the injector wells as compared to verification wells in calculating the mismatch function because there are more data sources from the observation wells (with equal weight), and it is more difficult to history match at injection wells. In addition, time-weights were applied to allow for higher consideration of the initial well response as compared to late-time behavior in the simulation timeline due to the temporal change in injectivity described in Section 5.2.1.

5.2.2.3 Sensitivity Analysis

A suitable combination of the independent variables with specified, geologically reasonable, ranges was used to perform one-variable-at-a-time sensitivity analysis. Based on the sensitivity results for the different objective functions, significant independent variables for a specific objective function were identified and used for history matching. Results from tornado plots of all individual wells/gauges based on suitably defined objective functions were obtained. In addition, correlation analysis also provided the relationship (positive or negative) between the independent variables and specific objective function, which helped to understand which variables affected which pressure gauges in positive or negative way. Figure 81 and Figure 82 are examples of tornado charts for the mismatch function at CCS2 and WB3, respectively. The tornado chart graphically represents the degree of sensitivity of all the variables to an output/objective function from top (greatest) to bottom (smallest) row. Bars from the center to the left or right also indicate the deviation from a base case due to the change of a variable. Bars to the left show the decrease in a mismatch function or better history matching, whereas bars to the right from the center represent the increase in the mismatch.

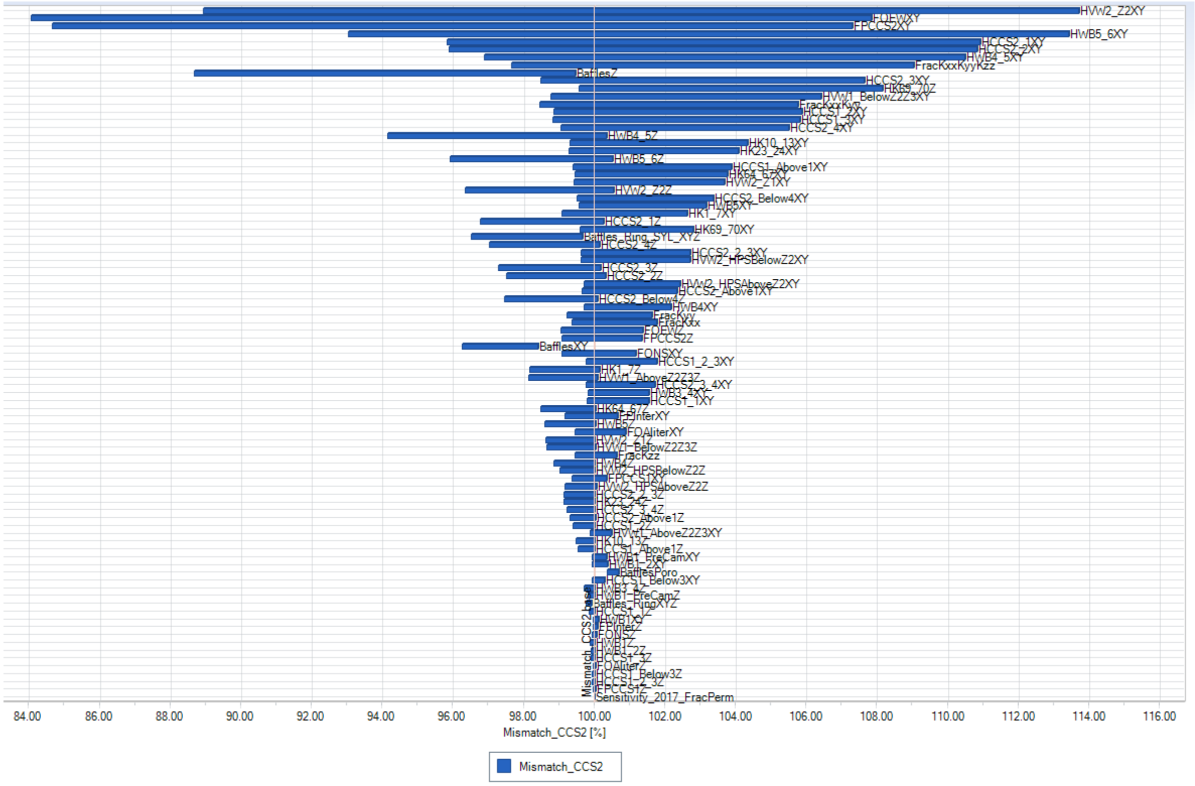

Figure 81. Tornado chart for the mismatch function at CCS2.

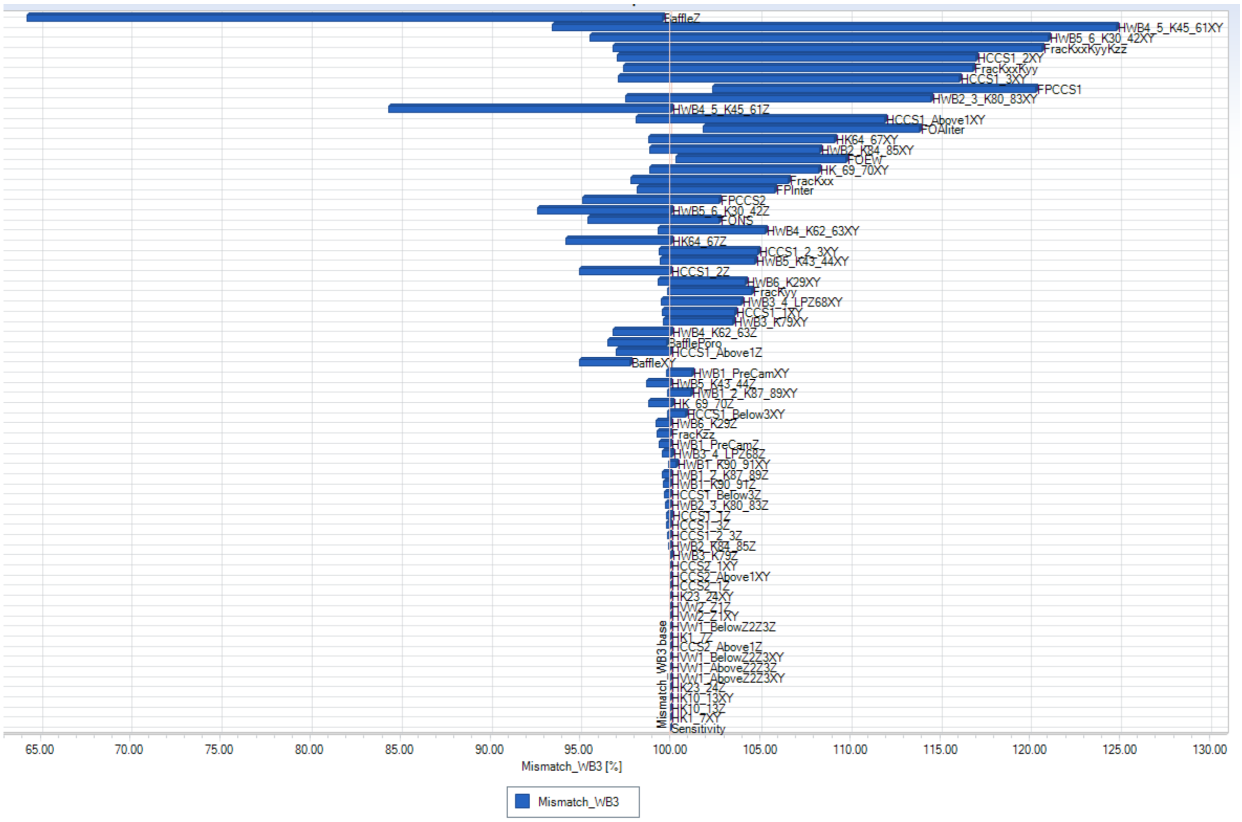

Figure 82. Tornado chart for the mismatch function at WB3.

5.2.2.4 History Match Optimization

After the initial uncertainty spread was obtained from the sensitivity analysis and initial uncertainty runs, an evolutionary strategy optimizer was used with the new ranges. The evolution strategy optimization technique used primarily mutation and selection as search operators. The operator was applied in a loop called a generation. The sequence of generations continued until a specified criterion was satisfied.

5.2.3 Bottomhole Pressure

BHP data in the injection and monitoring wells were used as the primary datasets in history matching. Continuous pressure measurements at the injector within the reservoir zone and at multiple depths in a monitoring well spanning the stratigraphic section from Precambrian basement to the Eau Claire Shale provided valuable information about spatial connectivity within and above the injection zone that was not captured in geophysical logs.

Figure 83 shows the simulated pressure responses after history matching with the observed data of CCS1, CCS2, WB4, WB5, and WB6. Simulated pressure at WB5 and WB6 is slightly higher and lower, respectively, than the observed data. A discrepancy in CCS1 BHP data after about 4 months of CCS2 injection occurred and could not be matched to the observed data. The observed response at CCS1 after the commencement of CCS2 injection suggests that there seems to be a preferential pathway (transmissive faults/fractures zones) connecting CCS1 and CCS2 that are not present in the model. Observed BHP response at CCS2 after late 2019 is greater than the simulated results, which might be due to deterioration of well injectivity. This can be confirmed with additional data and can be better matched with the corresponding adjustment of the well connection transmissibility factor. Other than these exceptions, history matching to CCS1, CCS2, and WB4 shows good agreement.

Figure 84. contains the simulation results and observed data for WB1, WB2, and WB3. WB2 and WB3 show a better match compared to WB1, which is slightly higher than the observed data. Overall, the simulated results of new pressure gauges (VW1_Z1 and VW1_Z2) after VW1 recompletion are a good match to the observed data (Figure 85). Figure 86 also shows good agreement between the simulated results of VW2 gauges (VW2_Z1, VW2_Z2, and VW2_Z3) and the observed data. Note that the VW1_Z1 is located at slightly shallower depth than the top perforation of CCS1 and spatially closer to CCS2. However, the pressure response at VW1_Z1 is significantly different from the response at CCS1, indicating the presence of preferential pathway/channels and/or flow barriers around these wells to make the responses totally different. Similar to the previous work, the pressure response at VW2_Z2 was increased and better matched by the local confinement added manually with the baffles around CCS2 and VW2. The simulated response of VW2_Z2 emphasizes the important role of low-permeability baffles and requires better characterization of them, especially around those wells.

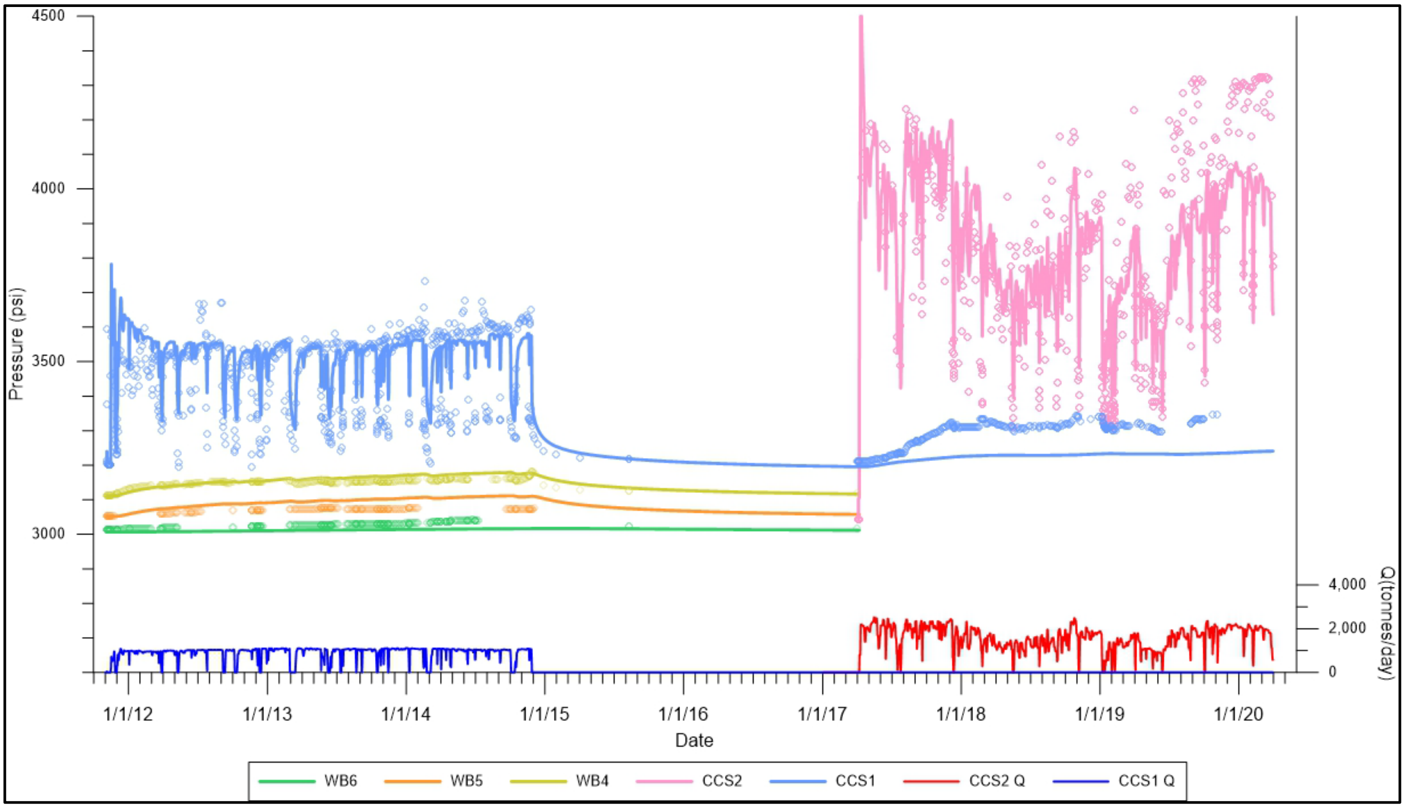

Figure 83. Simulation results and observed data of CCS1, CCS2, WB4, WB5, and WB6 to March 31, 2020.

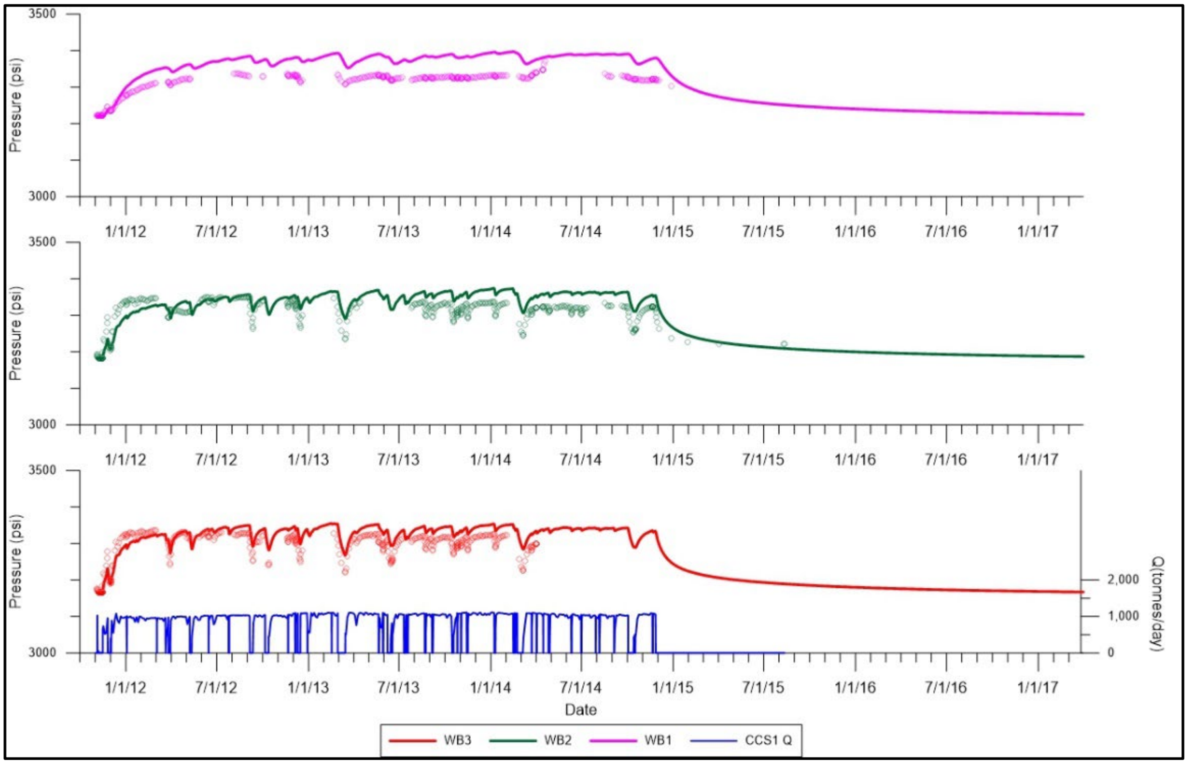

Figure 84. Simulation results and observed data of WB1, WB2, and WB3 to April 7, 2017.

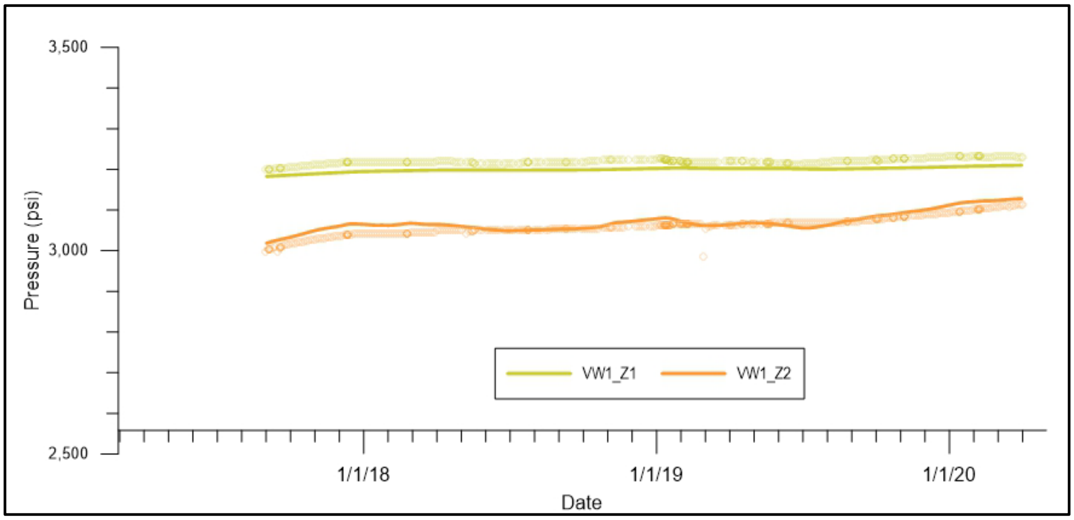

Figure 85. Simulation results and observed data of VW1_Z1 and VW1_Z2 to March 31, 2020.

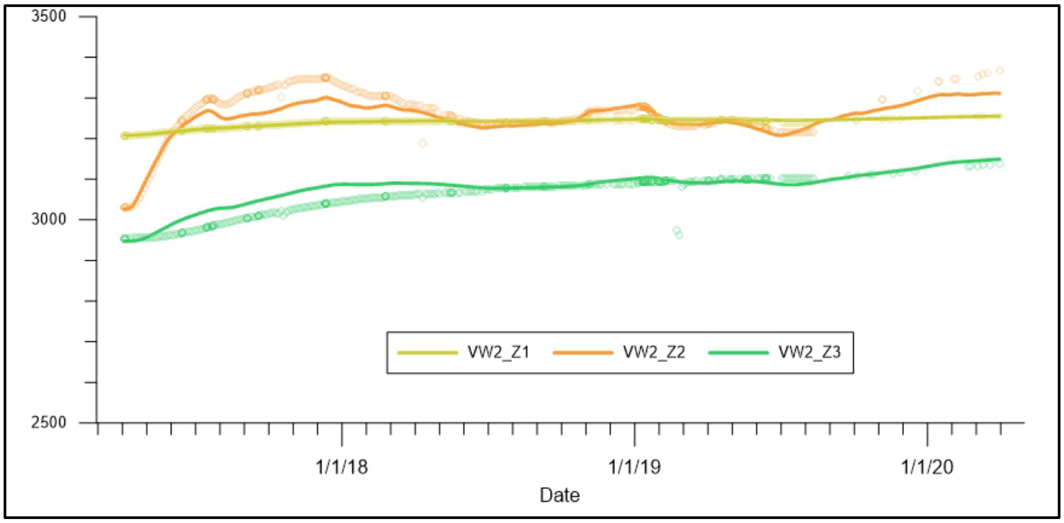

Figure 86. Simulation results and observed data of VW2_Z1, VW2_Z2, and VW2_Z3 to March 31, 2020.

5.2.4 Time-Lapse Pulsed Neutron Capture Logs

Pulsed neutron capture logging (PNL) tools are capable of several different measurements sensitive to CO_2 in the formation and in the tubing-casing annulus. Therefore, PNL logs can be used to monitor the formation fluids and to identify mechanical integrity problems that may allow the CO_2 to migrate up the casing annuli. For monitoring changes in the formation fluids and mechanical integrity monitoring, the PNL logs are most effective when used as a time-lapse measurement comparing a base pass to subsequent monitoring passes.

For the CCS1 and VW1, PNL base passes run in March and September 2011 prior to CO_2 injection provided the baseline. Multiple saturation monitoring logs were run at VW1 (Figure 87) and CCS1 (Figure 88) since the commencement of CO_2 injection to measure the temporal change in the formation CO_2 saturation and to evaluate well integrity. The first PNL monitor logs were run using the RST* reservoir saturation tool on CCS1 and VW1 in March and September 2012. Subsequent RST monitor logs were run in both CCS1 and VW1 in March, July and November 2012, July 2013, July 2014, and December 2014. A new-generation PNL tool, the Pulsar* multifunction pulsed neutron service, was run in July 2014 in addition to the RST and used for all PNL monitoring from 2015. The most current Pulsar logs were conducted in March 2019. Based on the repeat PNL logs of VW1, it appears that three high-permeability sand packages (upper, middle, and lower) and interbedded low-porosity and low-permeability layers (baffles) strongly control CO_2 plume migration/geometry at distance from the injector. Because of these observations and for reasons previously described in Section 4.4.2, baffle facies were added to the simulation model and parameterized for history matching.

Using the maximum CO_2 saturation value in each sand package, Figure 89 shows the breakthrough curve at VW1. The fastest arrival and highest CO_2 saturation occur in the middle zone of the Mt. Simon A-Lower. The slowest arrival and lowest CO_2 saturation occur in the upper zone. Note that spinner surveys at CCS1, to be discussed in the following section, are inconsistent with the PNL logs in that most of the flow goes into the bottom perforation, which corresponds to the lower sand package, whereas the first arrival of CO_2 at VW1 appears in the middle zone and consistently has higher CO_2 saturation than in the lower zone. Simulated breakthrough curves in Figure 89 show the delayed arrival for the middle (~0.5 year) and lower sand (~ 1 year) packages compared to the observed logs, which is also indicative of the presence of a strong preferential pathway between CCS1 and VW1. The simulated breakthrough curves reach their peak at the end of 2014 and decline afterwards. Although the simulation results do not perfectly agree with observations from PNL logs, the simulated breakthrough curves could capture the general trend found in three different sand packages.

Detailed CO_2 saturation profiles along the cross-section I-I′ and II-II′ (see Figure 68 for the location) are shown in Figure 90–Figure 94 for November 1, 2012, 2014, 2016, 2018, and March 1, 2020, respectively. As shown in Figure 89, CO_2 migrates faster in the middle zone. There was no vertical migration pathway found from the lower to middle zone towards the north along the cross-section I-I′. Figure 95 is a simulated CO_2 saturation profile along the cross-section III-III′ connecting CCS1 and CCS2 well on March 1, 2020.

The May 2018 and March 2019 saturation logs of CCS1 confirmed a new interval with CO_2 at 6,840 to 6,830 ft (2085.4m to 2082.3m) in the Mt Simon A-Upper (Figure 88). However, simulated results show no CO_2 arrival at CCS1 due to CCS2 injection (Figure 94 and Figure 95). It is likely that the origin of CO_2 at this interval is CCS2 injection. Better history matching of this CO_2 occurrence in the CCS2 injection intervals at CCS1 would improve the simulated BHP responses at CCS1 due to CCS2 injection.

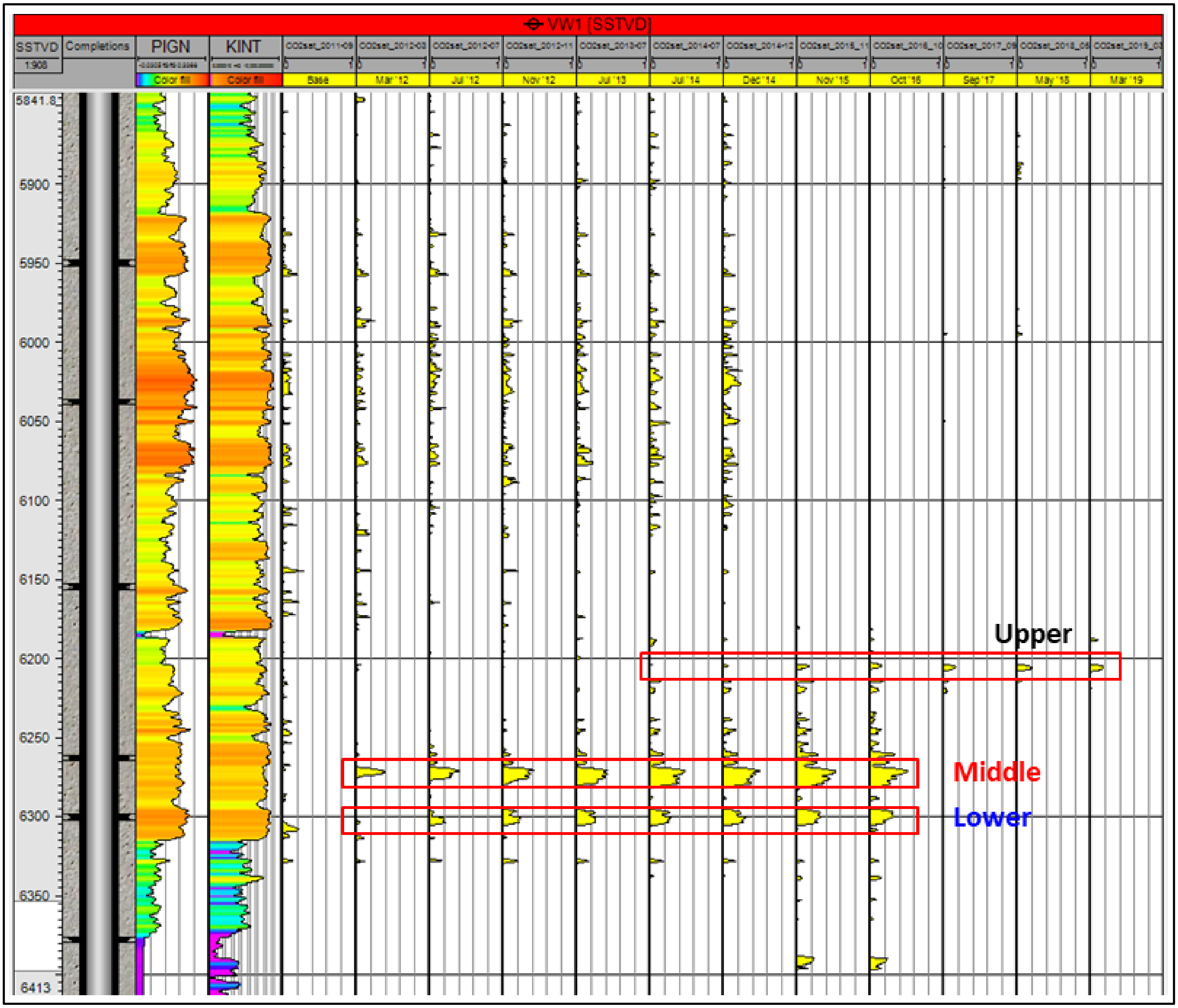

Figure 87. Well section showing time-lapse PNL CO_2 saturation profile at VW1 well.

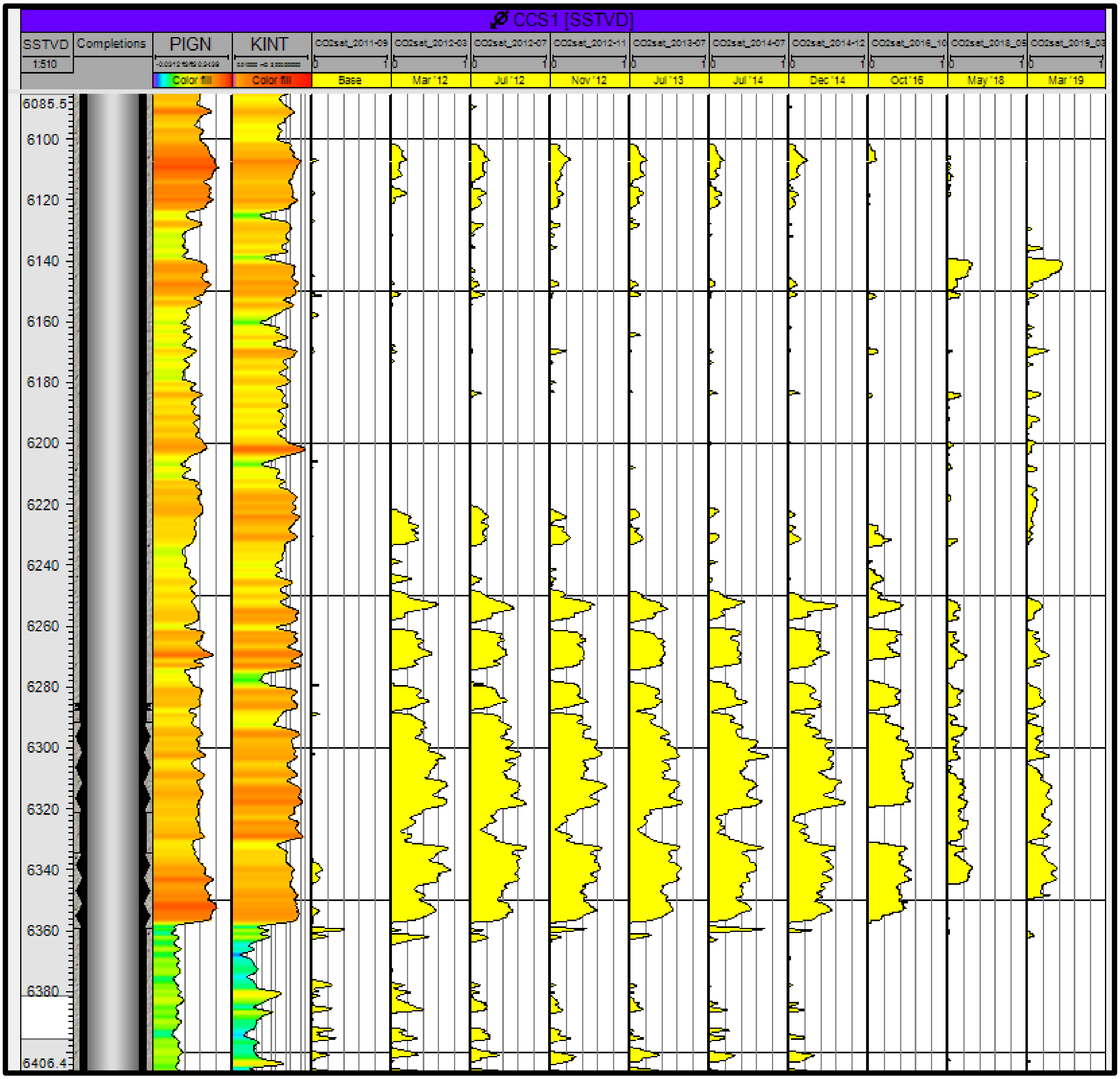

Figure 88. Well section showing time-lapse PNL CO_2 saturation profile at CCS1 well.

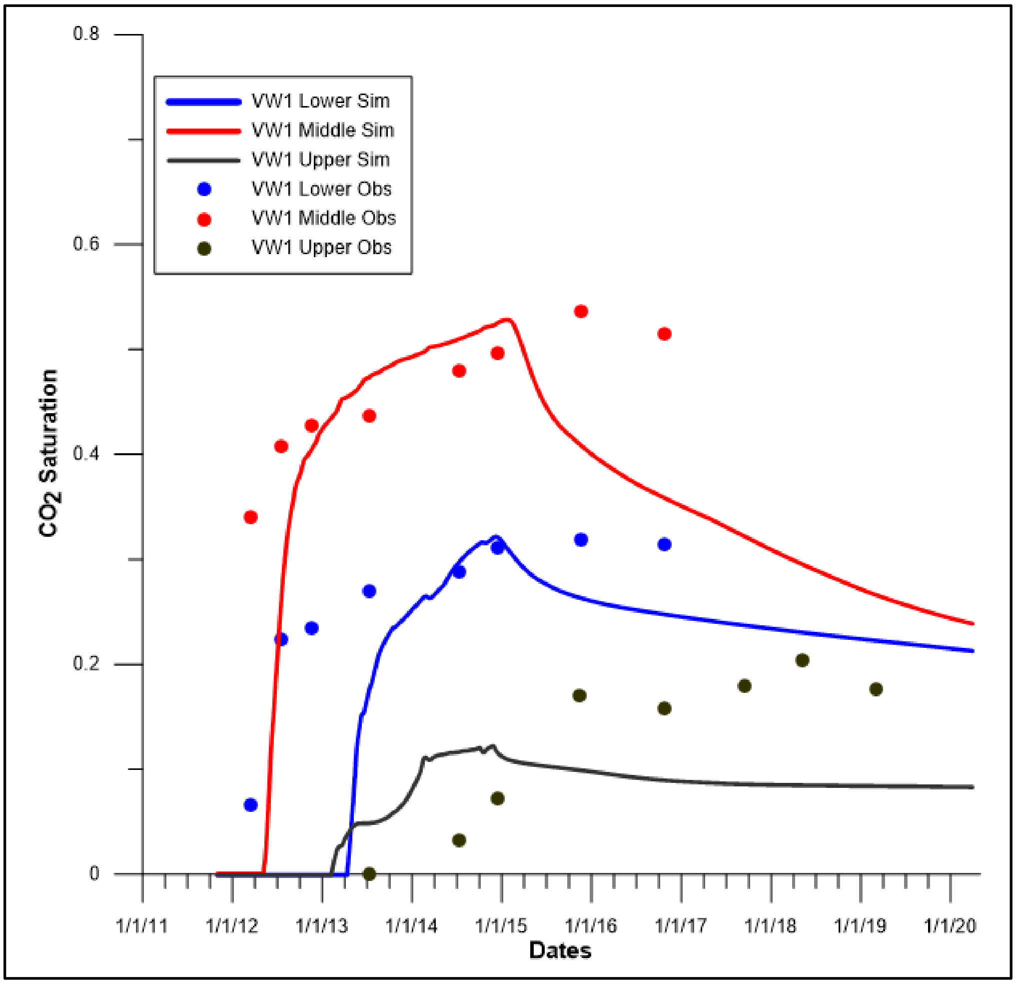

Figure 89. CO_2 breakthrough at VW1 according to time-lapse PNL logs.

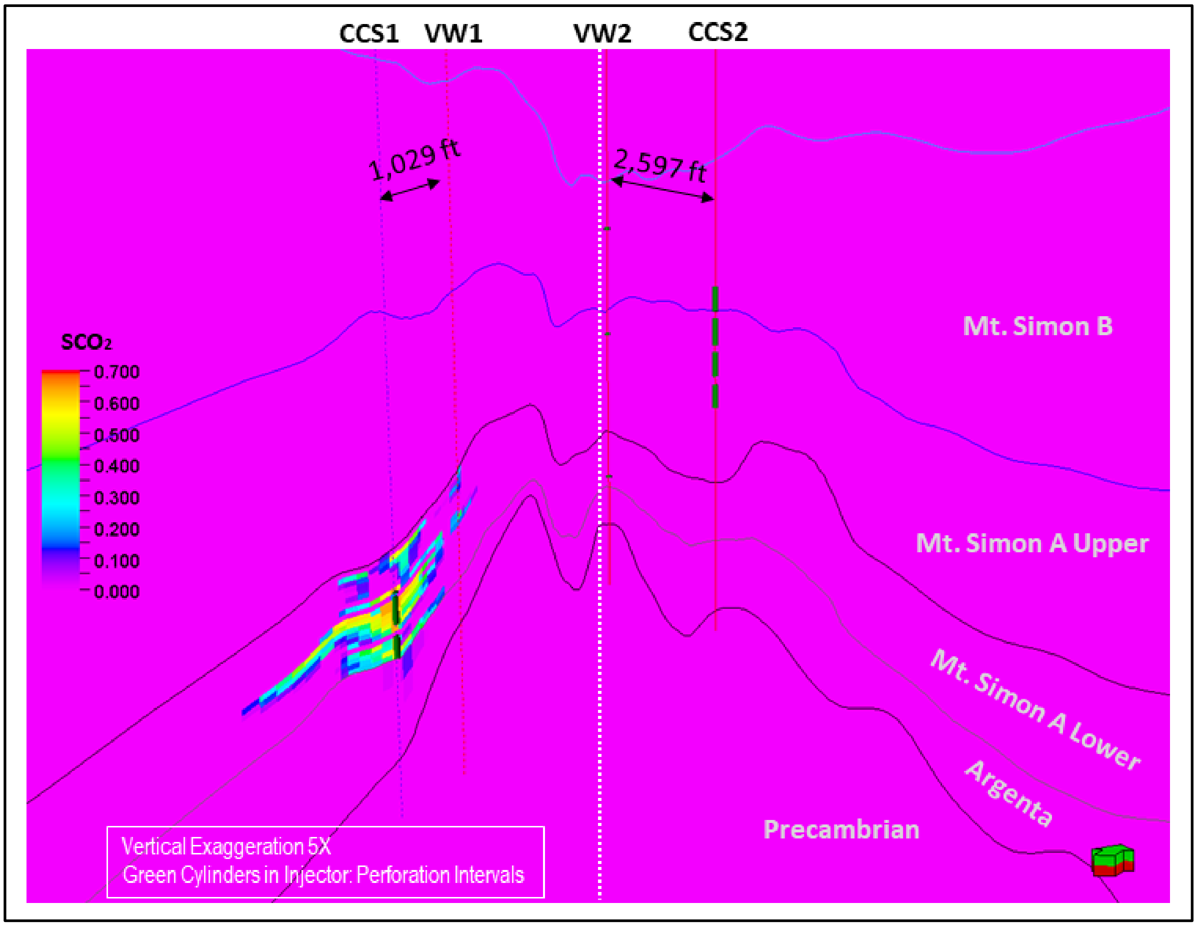

Figure 90. Simulated CO_2 saturation profile along the cross-section I-I′ (left) and II-II′ (right) on November 1, 2012.

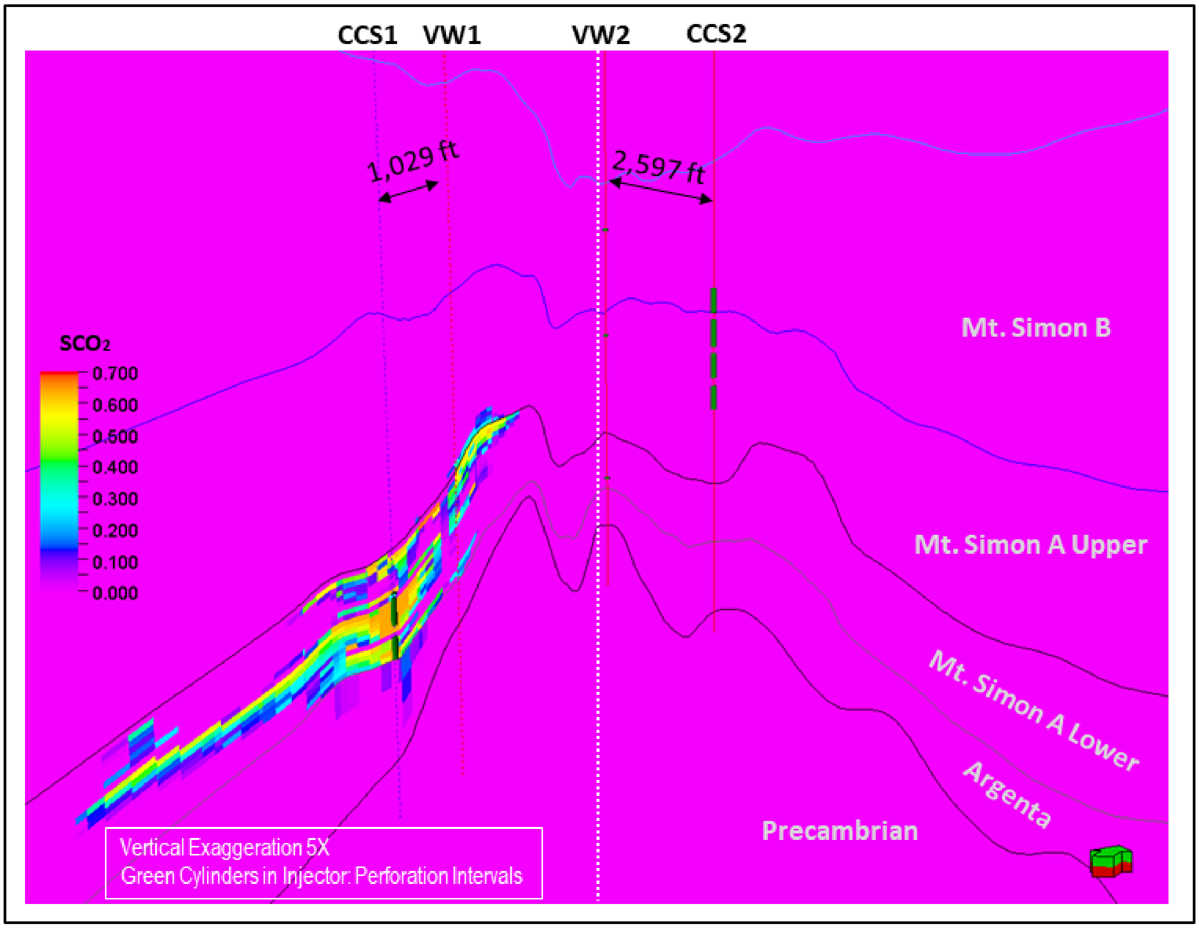

Figure 91. Simulated CO_2 saturation profile along the cross-section I-I' (left) and II-II' (right) on November 1, 2014.

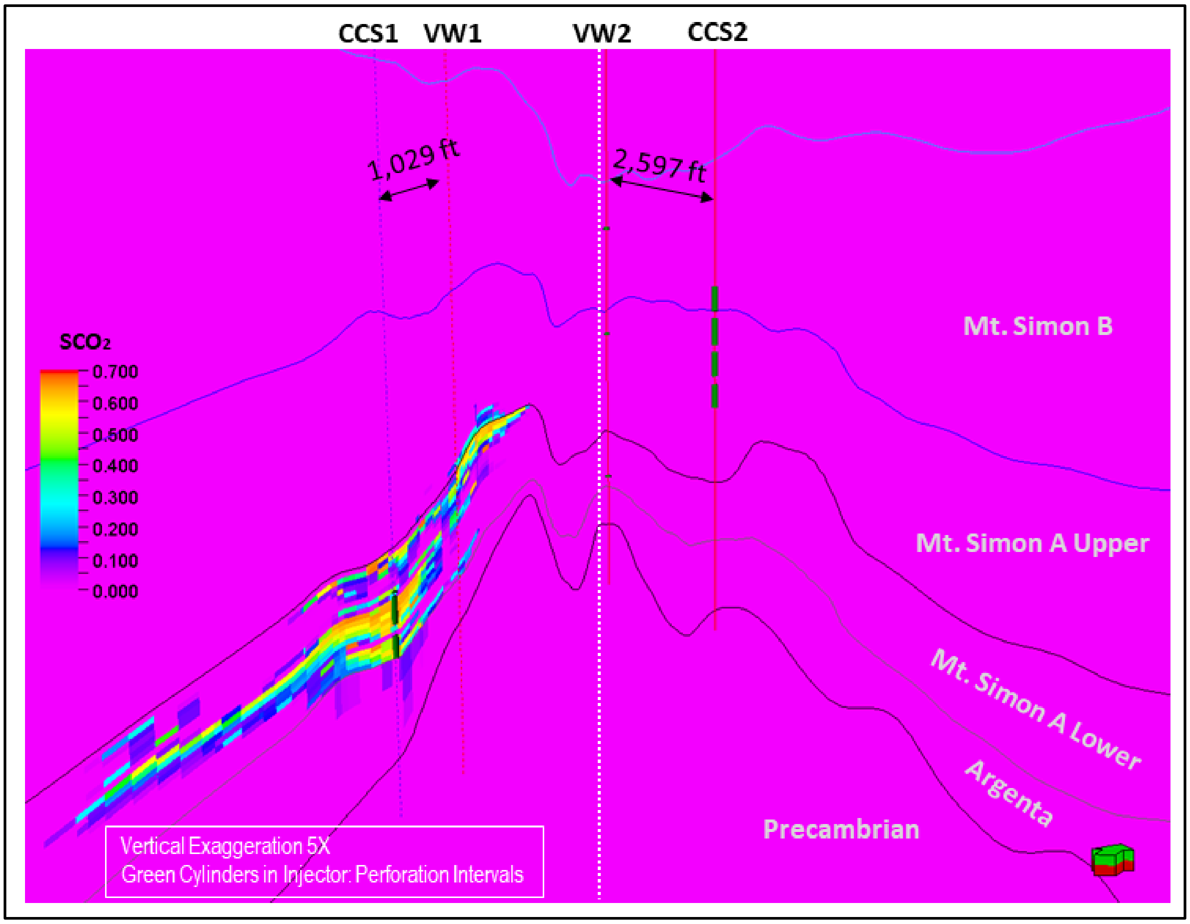

Figure 92. Simulated CO_2 saturation profile along the cross-section I-I′ (left) and II-II′ (right) on November 1, 2016.

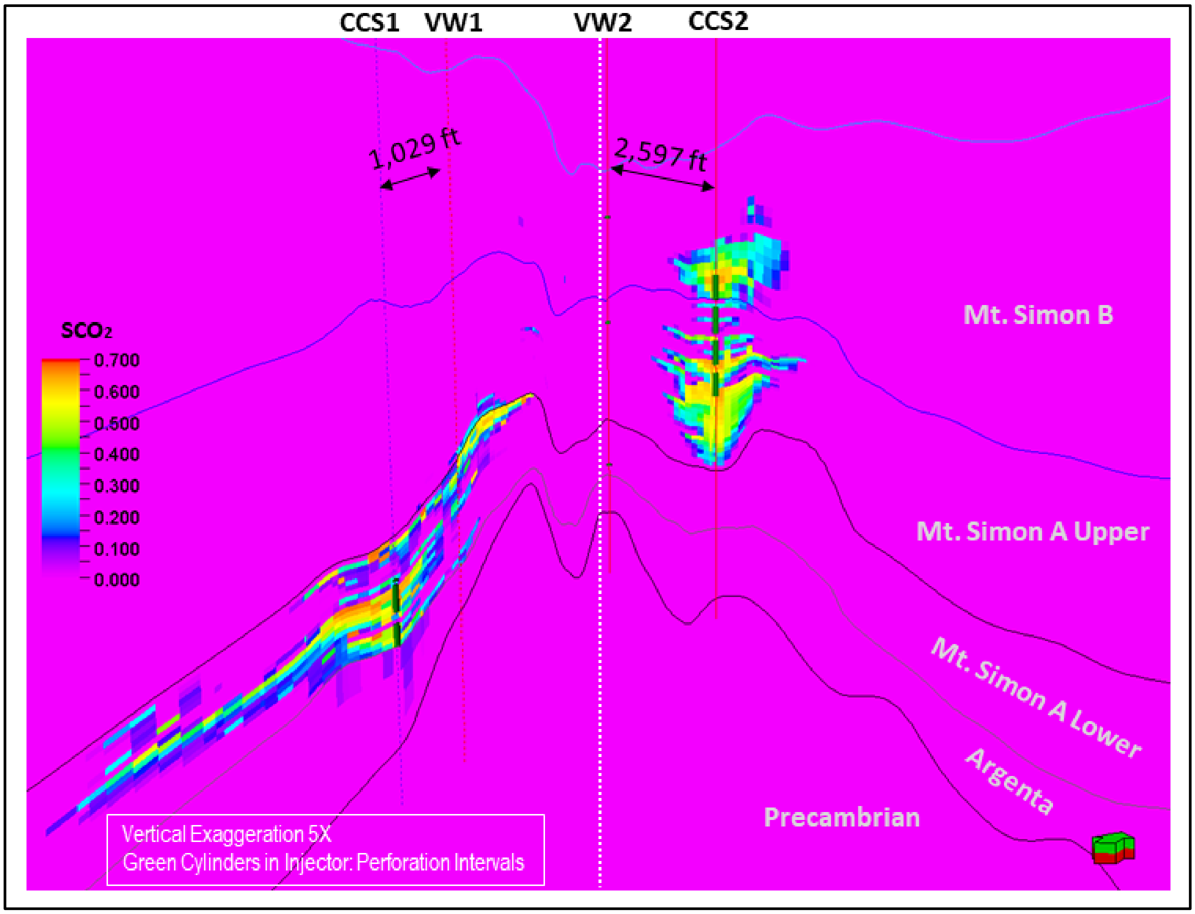

Figure 93. Simulated CO_2 saturation profile along the cross-section I-I′ (left) and II-II′ (right) on November 1, 2018.

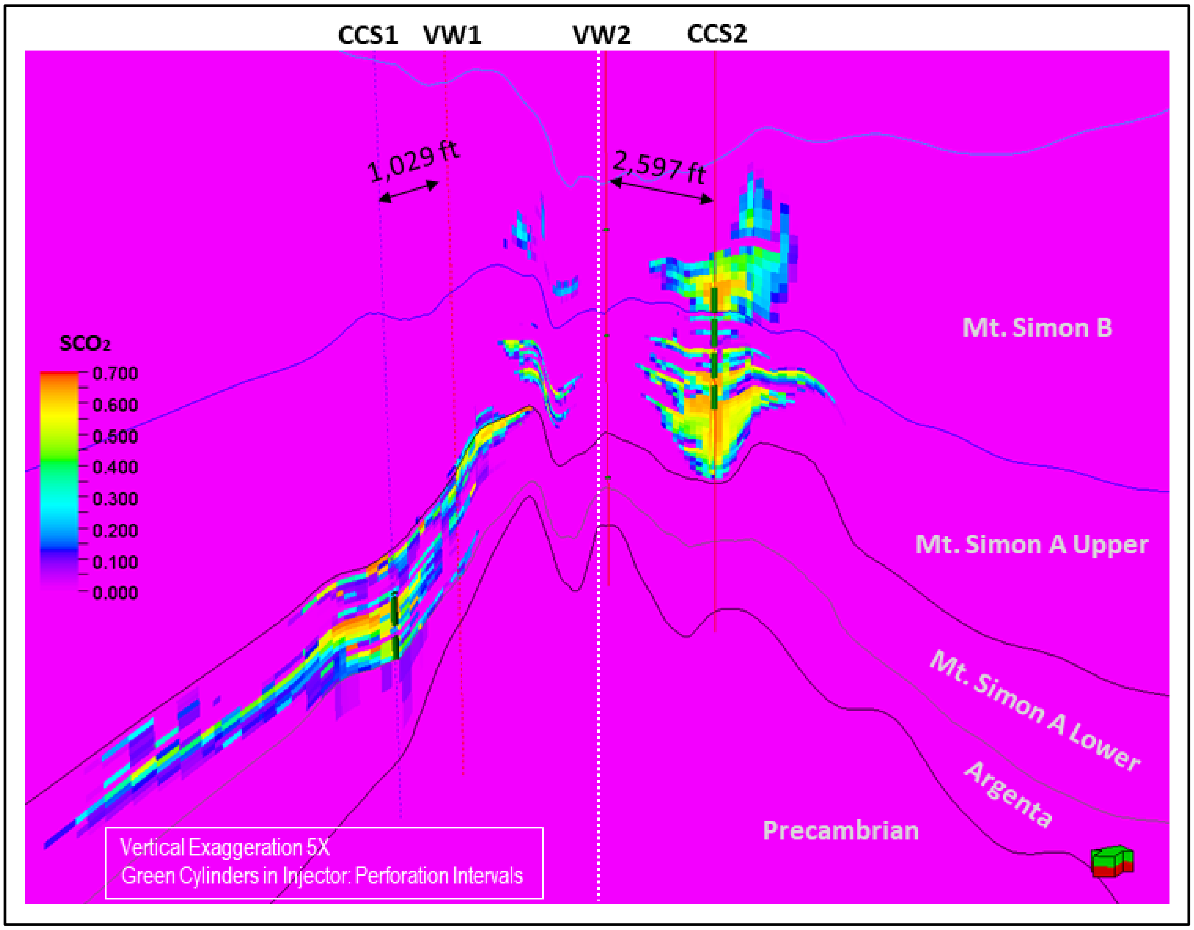

Figure 94. Simulated CO_2 saturation profile along the cross-section I-I′ (left) and II-II′ (right) on March 1, 2020.

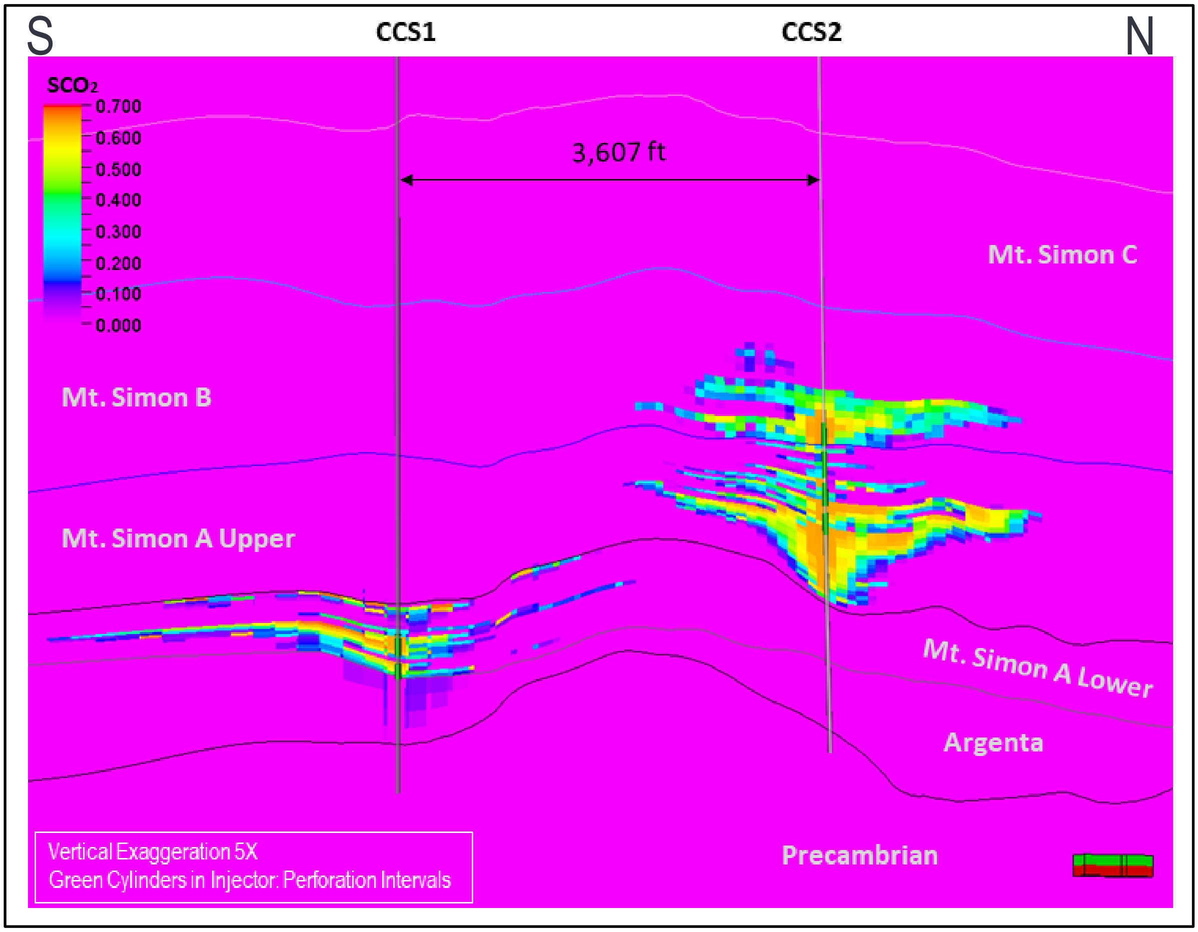

Figure 95. Simulated CO_2 saturation profile along the south to north cross-section III-III′ on Mar. 1, 2020.

5.2.5 Spinner Surveys

A production logging tool or spinner survey is used to evaluate the fluid movement in and out of wellbores, quantify flow rates, and determine fluid properties at downhole conditions. The first spinner survey was run in the CCS1 well on March 2, 2012, and the second was conducted on July 19, 2014 (Table 9). There exist three perforation intervals in the CCS1 (see Figure 96). Each survey was performed at two different injection rates (about 500 and 1,000 tonnes/day).

Table 9 summarizes the partitioning of CO2 inflow at CCS1 as determined from the production logging obtained from the two surveys. Both results showed that Perforation 3 (7,025 ft to 7,050 ft) (2141.7m to 2149.3m) takes about 75 to 85% of total flow, which is not consistent with the saturation logs at VW1. Perforation 1 (6,976 ft to 6,978 ft) (2126.8m to 2127.4m) and Perforation 2 (6,981 ft to 7,012 ft) (2128.3 to 2137.8m) take about 6 to 9% and 9 to 16%, respectively. Figure 96 shows the simulated flow rates where only 11 to 18 % of total flow goes into the Perforation 3. Perforation 1 and 2 take 6 to 9% and 76 to 80% of the simulated flow. Simulated fractional flow rates to Perforation 2 and 3 are not in agreement with the spinner survey at CCS1. However, it should be noted that the higher flow rates to Perforation 2 lead to better match in terms of PNL logs at the VW1.

Table 9. Spinner survey results at CCS1 well on March 2, 2012 and July 19, 2014.

Perforation	Perforation Top (MD, ft)	Perforation Bottom (MD, ft)	Fractional Flow Rate	
			Minimum (%)	Maximum (%)
1	6,976	6,978	6.2	9.2
2	6,981.5	7,012	9.1	15.7
3	7,025	7,038	10	18
3	7,038	7,050	57.3	69.7

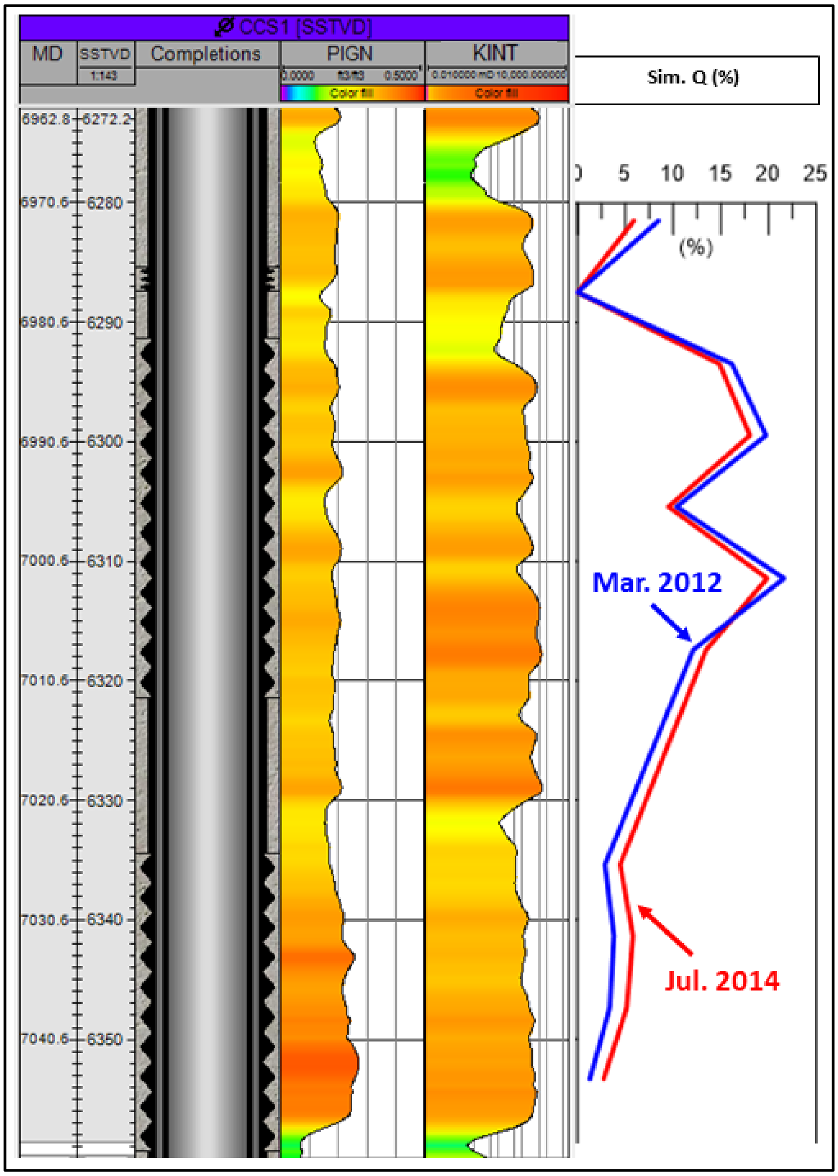

Figure 96. Well section window showing perforation intervals of CCS1 well and simulated flow rate.

There were three spinner surveys conducted on the CCS2 well—April 7 to 11, 2017; March 29, 2018; and March 8, 2019. The results of these surveys are summarized in Table 10. The first survey in 2017 was done with multiple injection rates from 541 tonnes per day to 2,471 tonnes per day with an increment of about 500 tonnes per day. The second and third surveys in March 2018 and March 2019 were performed with a single injection rate of 1,040 and 1,200 tonnes/day (TPD) due to the limitation of CO_2 availability at the time of the logging. There are four perforation intervals in the CCS2 (Figure 97). The survey in 2017 showed that as injection rates increased, flow in the shallow perforation tended to increase. Perforation 4 (bottom) took more than 50% of the total flow. However, the 2018 survey disagreed with the 2017 survey. In the 2018 survey, the bottom 13 ft (3.9m) of Perforation 4 takes more than 91% of total flow, and there was almost no flow in the shallow perforation intervals. The 2019 survey showed similar results to the 2018 survey.

Table 10. Spinner survey results at CCS2 well April 2017, March 2018, and March 2019.

Perforation	Injection Interval, Top (MD, ft)	Injection Interval, Bottom (MD, ft)	4/7/2017	4/8-9/2017	4/9-10/2017	4/10-11/2017	4/11/2017	3/29/2018	3/8/2019
			541 TPD	1,004 TPD	1,554 TPD	2,106 TPD	2,471 TPD	997 TPD	1,121 TPD
			Fractional Flow Rates (%)						
1	6,630	6,670	18.4	18.5	21.4	34	42	0	0
2	6,680	6,725	5.8	6.9	6.6	5.8	6.2	0	0
3	6,735	6,760	1.7	1.1	1.2	1	0.5	0	0
	6,760	6,775	2.6	1.5	2.3	2.2	1.4	4.7	6.5
4	6,787	6,798	2	1.7	1.3	1.2	0.3	0	0
	6,798	6,805	0	0	0	0	0	4	5.5
	6,805	6,812	8.1	6.4	5.8	3.8	4.4	0	0
	6,812	6,817	9.9	11.1	8.5	9	6.6	20.6	16
	6,817	6,825	51.6	52.8	52.9	43	38.7	70.6	72

The injectivity values discussed in Section 5.2.1 show clear signs of deterioration in the CCS2 well performance, and the caliper log during the spinner survey in March 2018 and 2019 confirmed the buildup of solids at the top perforation. However, for the history matching, the entire closure of shallow perforations could not achieve the BHP responses at VW2. Thus, the perforation intervals were partially closed to mimic the spinner data as of March 1, 2018. Downhole pressure data at VW_Z2 (Figure 86) required non-negligible flow rates at the Perforation 2 and the top of Perforation 3 under the current static model. It is recommended to perform additional spinner surveys annually to monitor the well performance at CCS2. Figure 97 shows the change in the simulated flow rates before and after this partial closure of perforation intervals. Simulated results for April 2017 show 44% of total flow goes into Perforation 1. Perforations 2 and 3 take 18% and 12%, respectively, of total flow. The remaining 26% flows into Perforation 4. After the application of partial perforation closure, 54 to 61% go into Perforation 4 whereas 34 to 40% still flow into the Perforation 1.

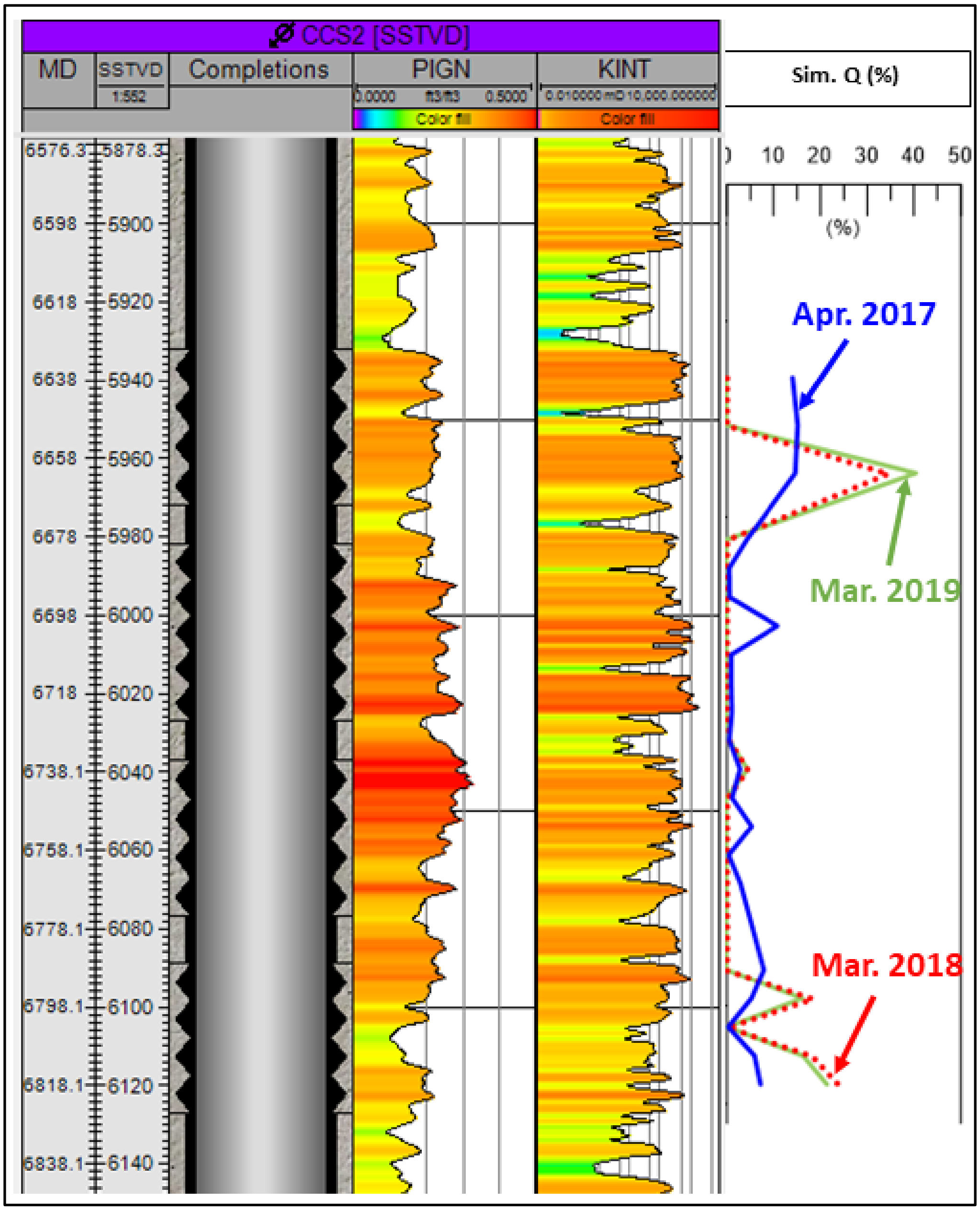

Figure 97. Well section window showing perforation intervals of CCS2 well and simulated flow rate.

5.2.6 CO_2 Plume Extent

To show the temporal CO_2 plume evolution within the model domain, a series of 3D distributions of simulated CO_2 saturation is shown in Figure 98–Figure 106 for each year from November 1, 2012 to March 1, 2020. In addition, Figure 107 illustrates the temporal evolution of the CO_2 plume during the reporting period by plotting the plume edge as CO_2 gas saturation of 0.02 (or 2%). Due to the removal of the flow barrier north of VW1 applied to the previous work, the CO_2 plume edge tends to migrate toward the NW rather than exhibit radial growth from the injector after the commencement of CCS1 injection. There is no noticeable change in the plume's north edge within the CCS1 injection zone after November 2014 whereas the simulated edge of the CO_2 plume extends approximately 5,250 ft NW-SE and 3,500 ft NE-SW (1600 m NW-WE and 1067.1 m NE-SW).

In the previous history matching (Zaluski & Lee, 2018 IBDP/ICCS Static Geological Model Development and Dynamic Modelling Updates, 2019) to the CO_2 plume outline from the non-rigid matching (NRM) anomaly mapping, a hypothetical flow barrier was introduced in the dynamic model whereas the 2020 Final Model excluded the flow barrier north of VW1 given the introduction of new faults. However, with the sealing faults only trending N-S and NW-SE, there is no flow barrier present to prevent the flow to the north in the model. The net CO_2 saturation (summation of SCO2*h) map shown in Figure 108 is displayed as a proxy to the NRM anomaly. Unlike previous results, even with higher net CO_2 saturation values, the plume outline does not match the NRM anomaly outline. It seems the sealing faults (those trending N-S and NW-SE) added in this work could not replace the previous flow barrier in terms of history matching of the NRM anomaly outline. It is possible that a critically stressed fault analysis would indicate whether the newly identified faults are transmissive or sealing; however, this still requires the verification with the model. The current classification is based on orientation relative to regional stress direction, which could be updated with additional work.

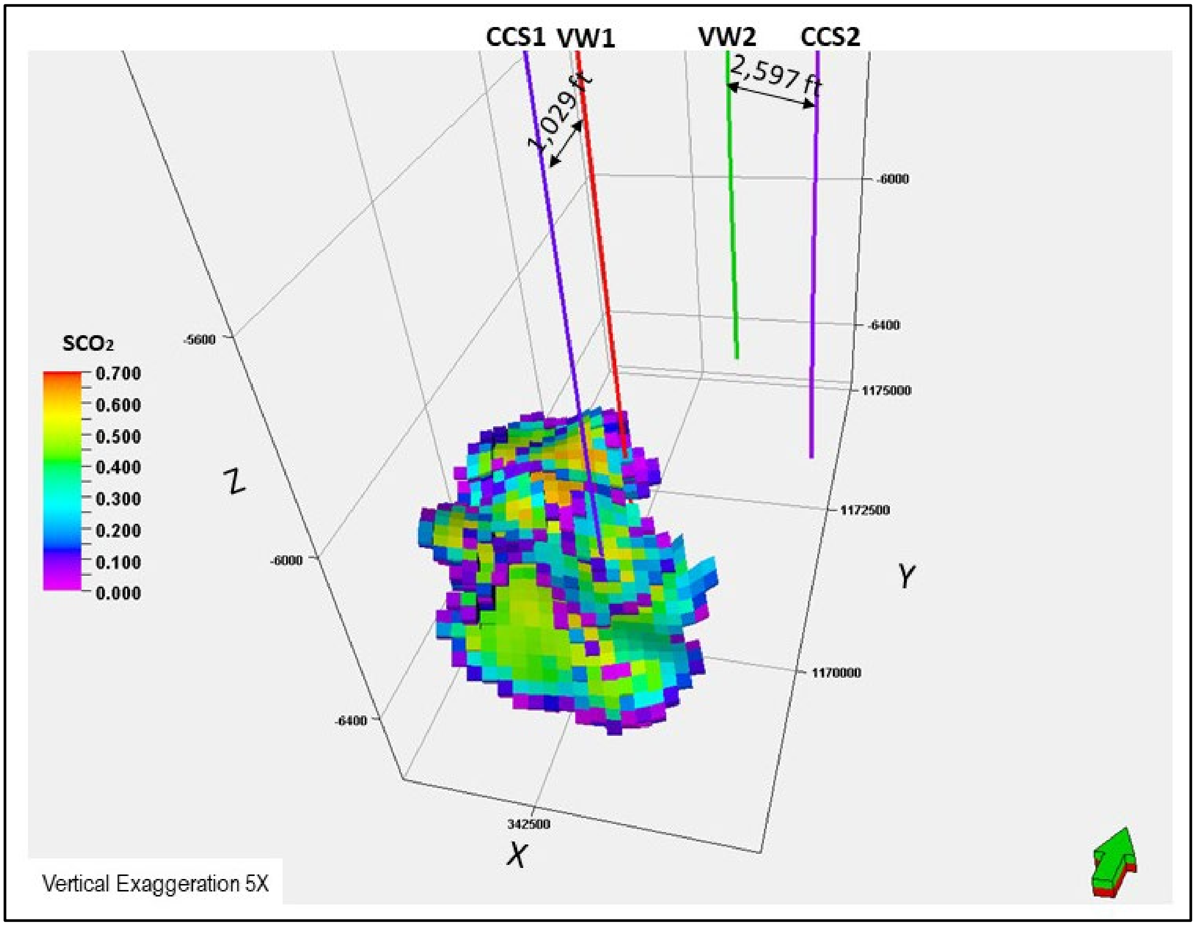

Figure 98. 3D simulated CO_2 plume distribution on November 1, 2012.

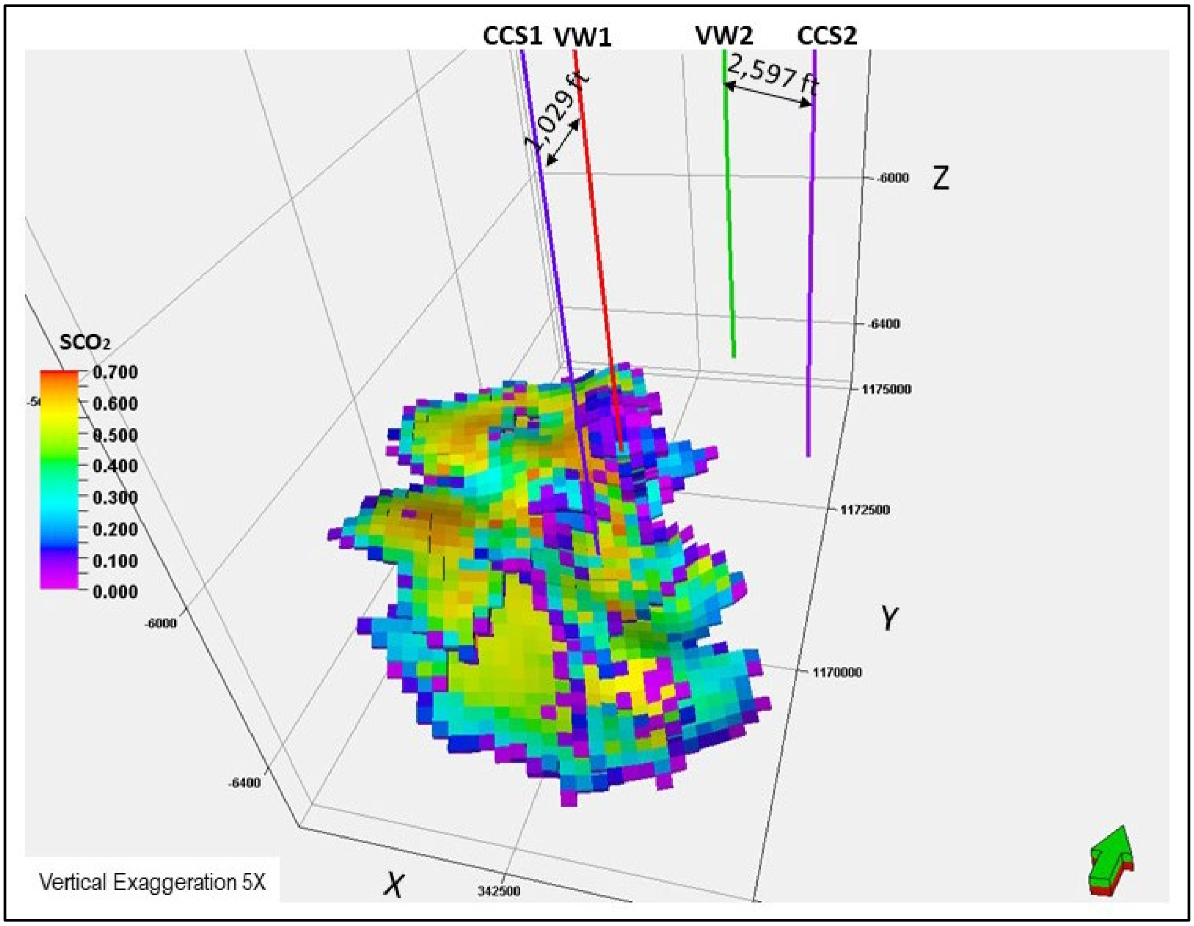

Figure 99. 3D simulated CO_2 plume distribution on November 1, 2013.

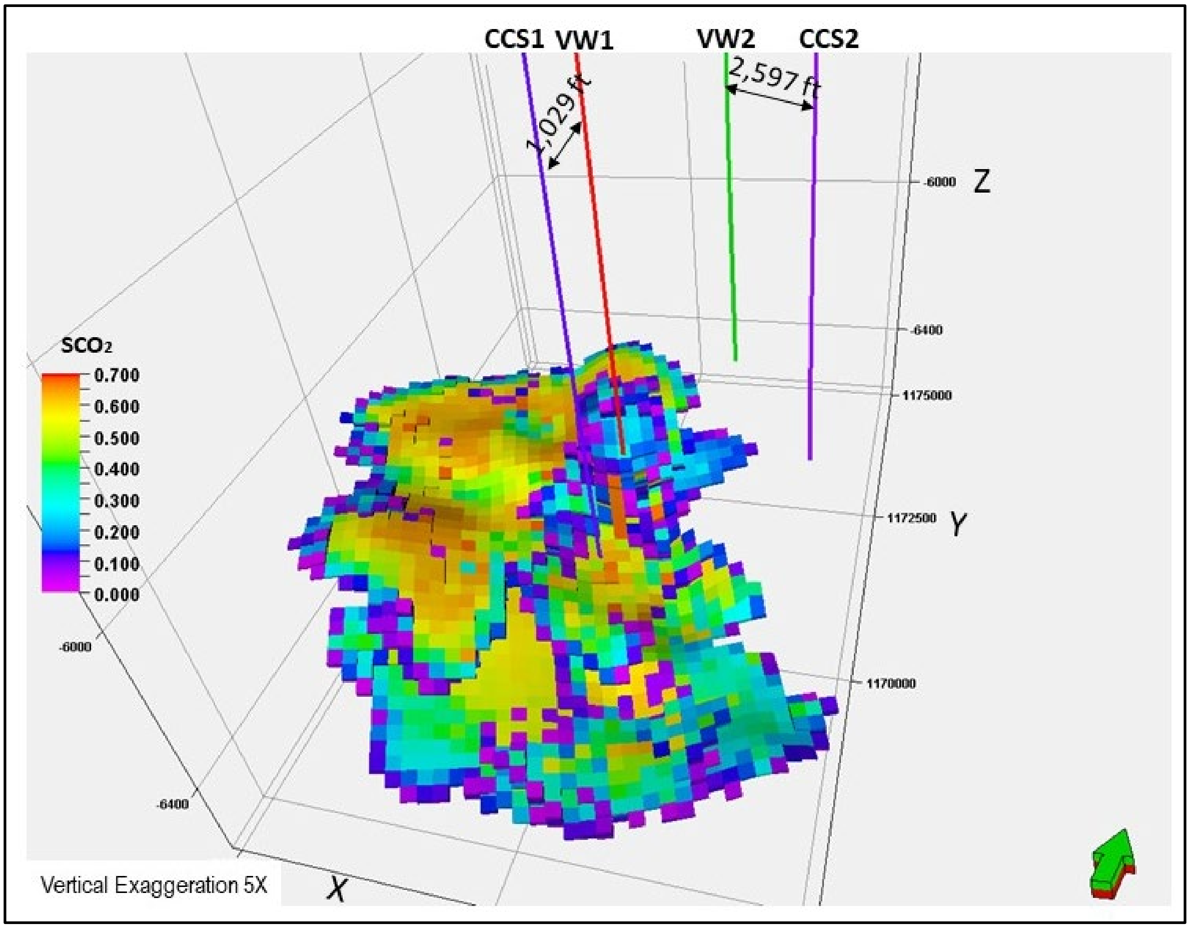

Figure 100. 3D simulated CO_2 plume distribution on November 1, 2014.

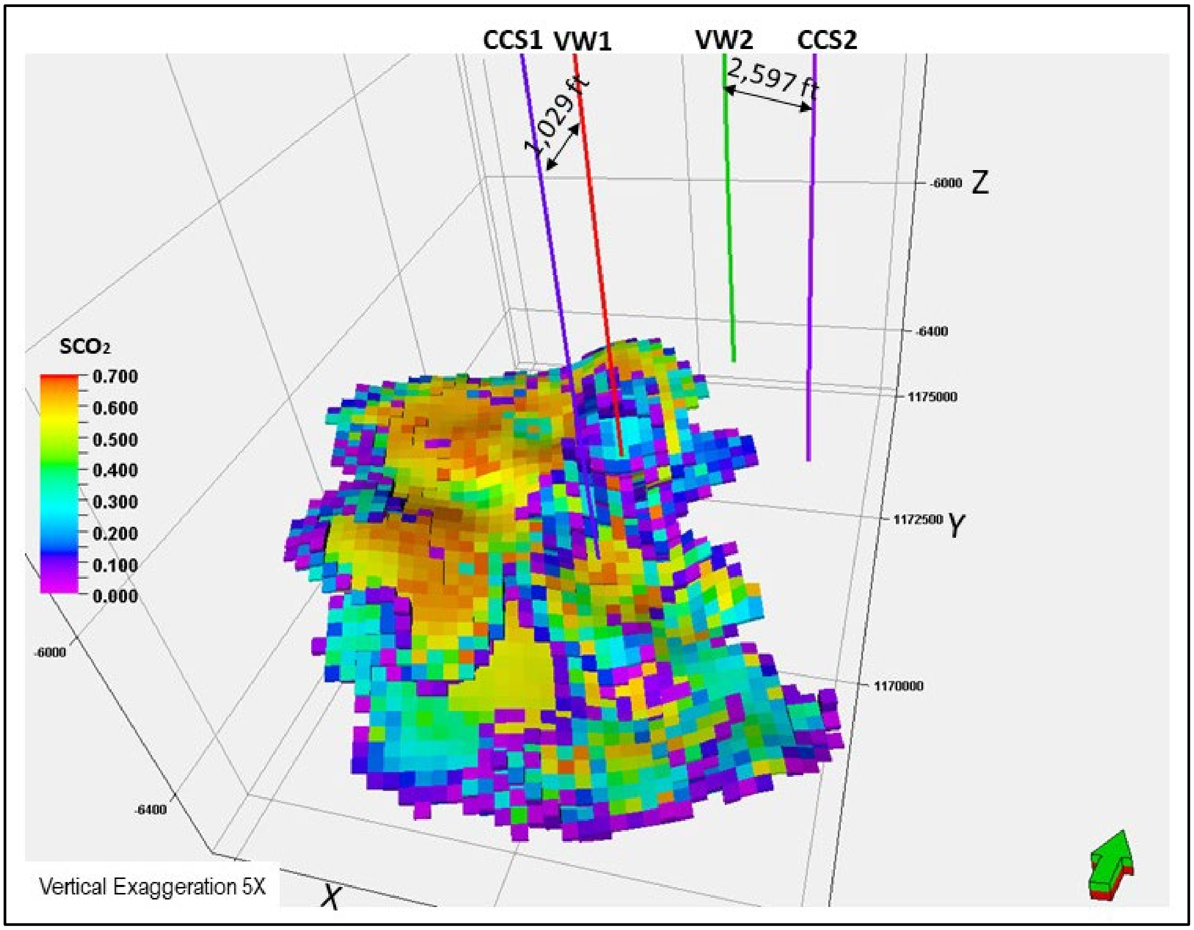

Figure 101. 3D simulated CO_2 plume distribution on November 1, 2015.

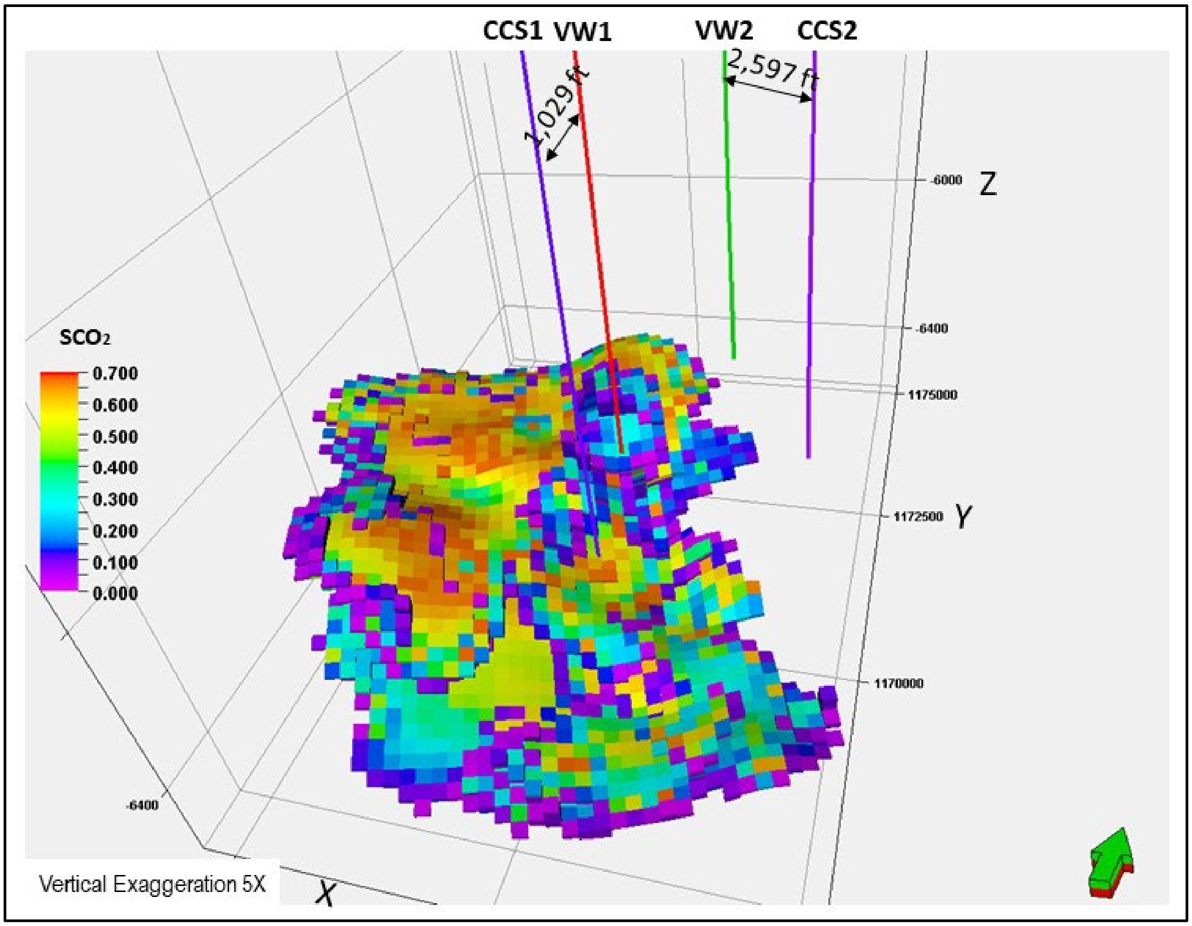

Figure 102. 3D simulated CO_2 plume distribution on November 1, 2016.

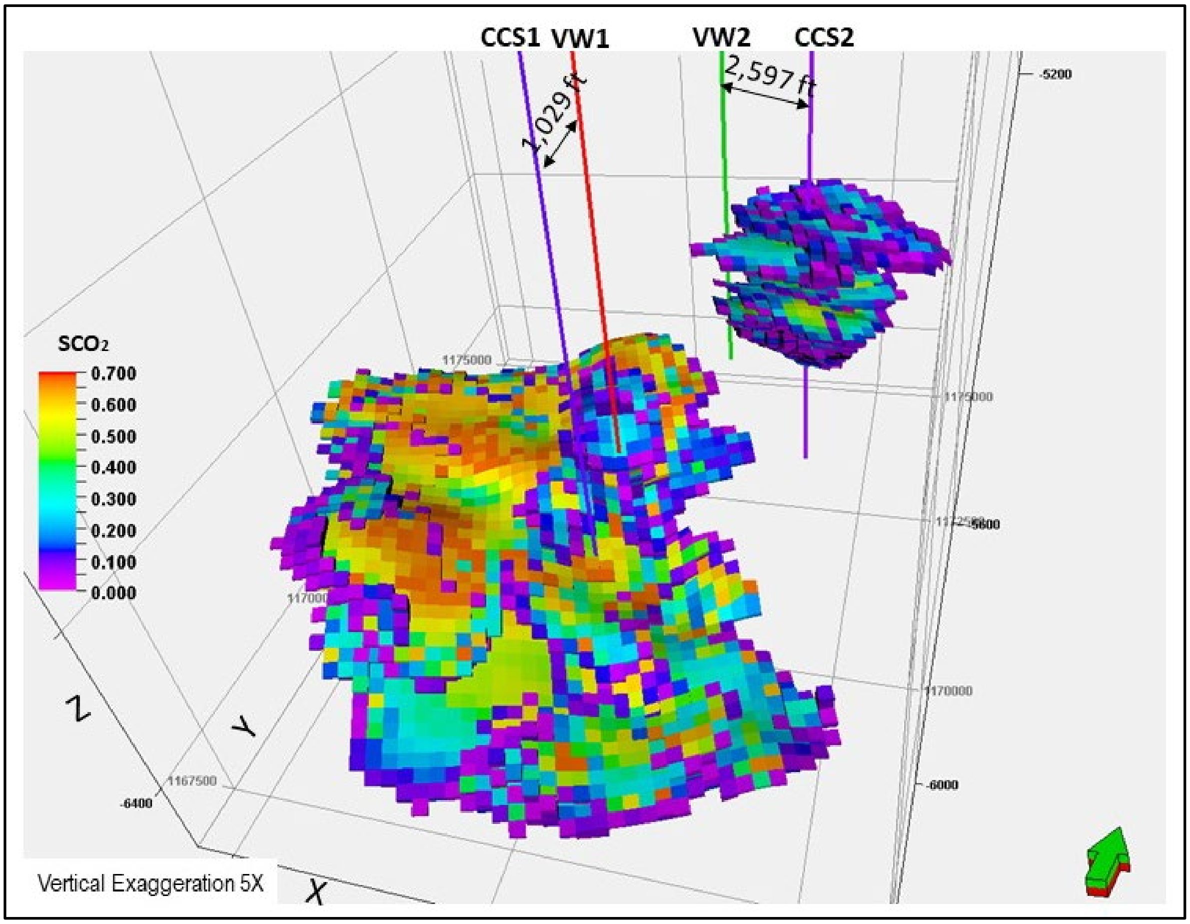

Figure 103. 3D simulated CO_2 plume distribution on November 1, 2017.

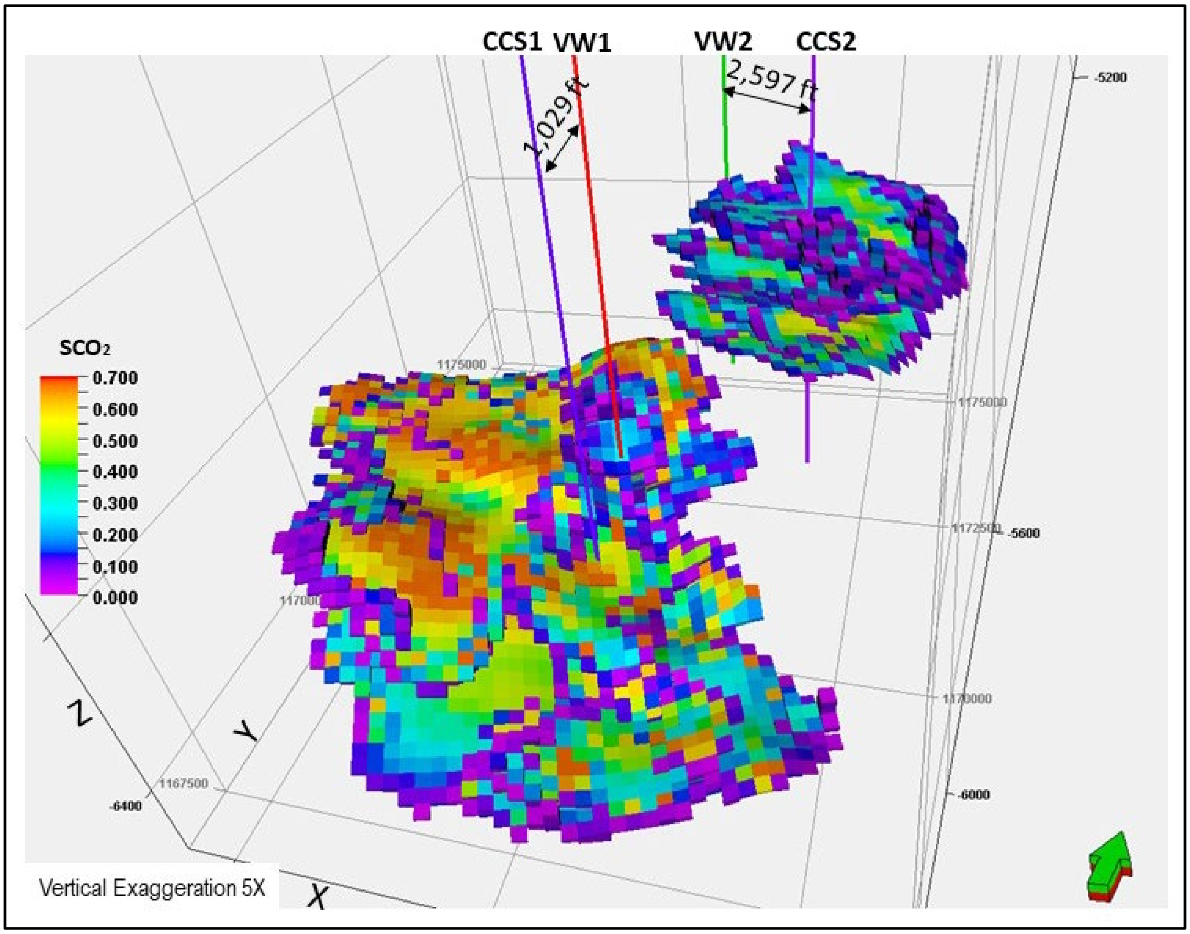

Figure 104. 3D simulated CO_2 plume distribution on November 1, 2018.

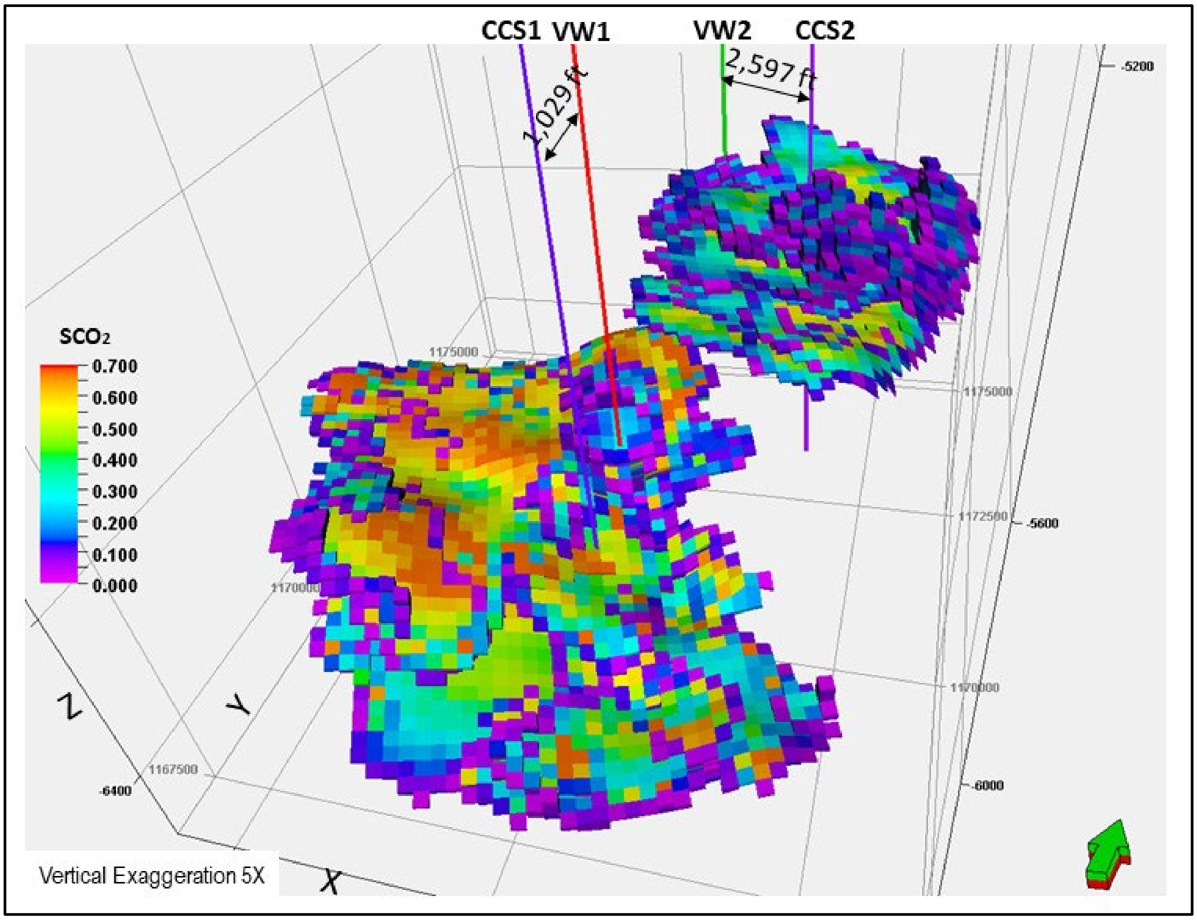

Figure 105. 3D simulated CO_2 plume distribution on November 1, 2019.

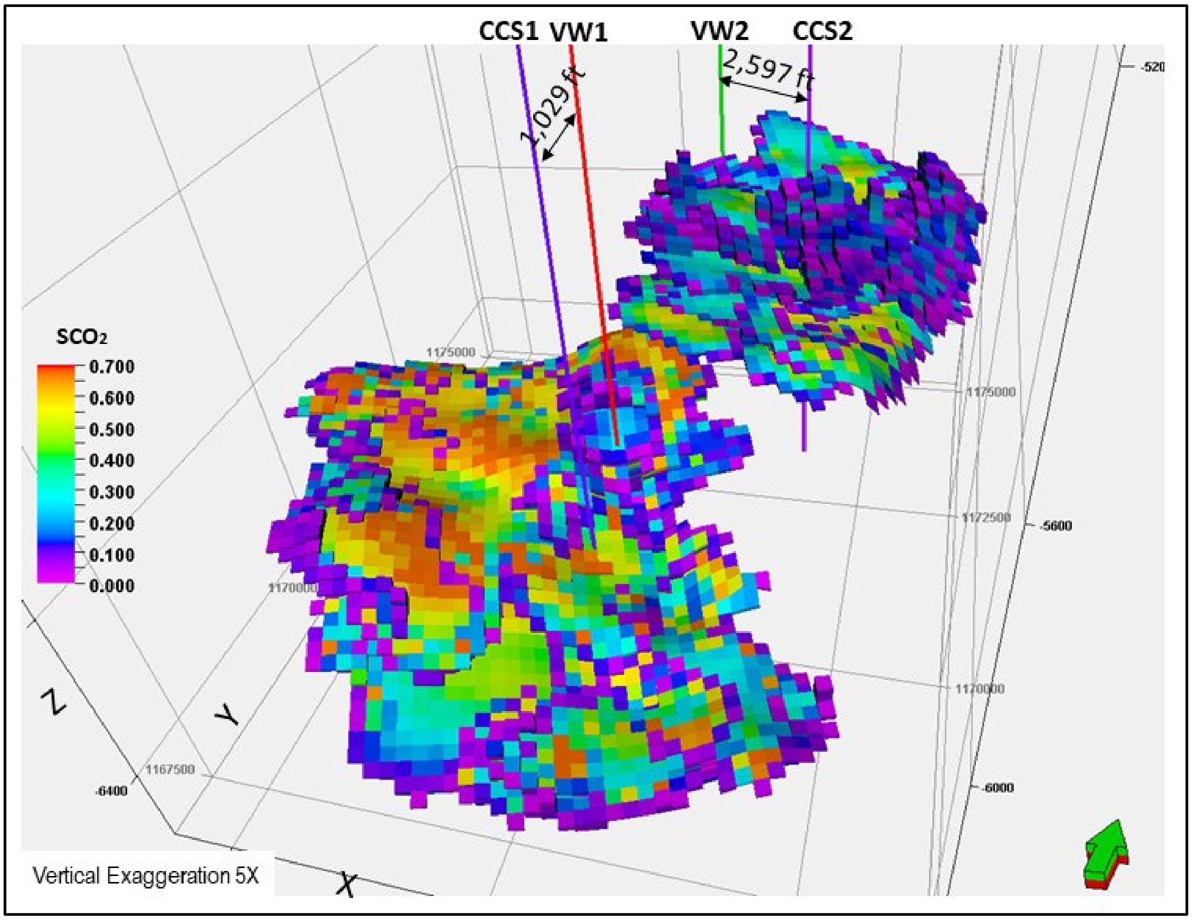

Figure 106. 3D simulated CO_2 plume distribution on March 1, 2020.

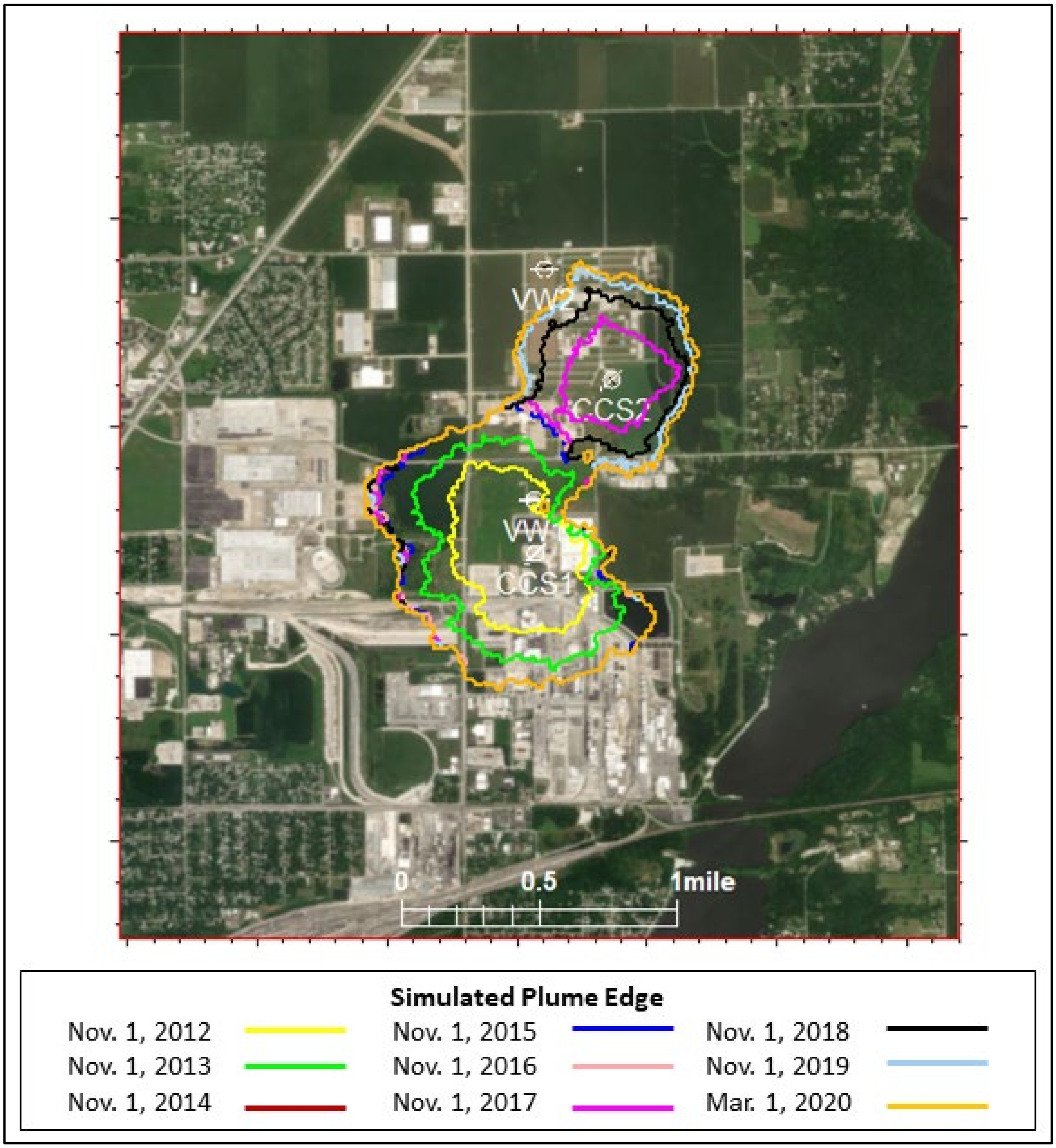

Figure 107. Simulated plume edge (CO_2 concentration >2%).

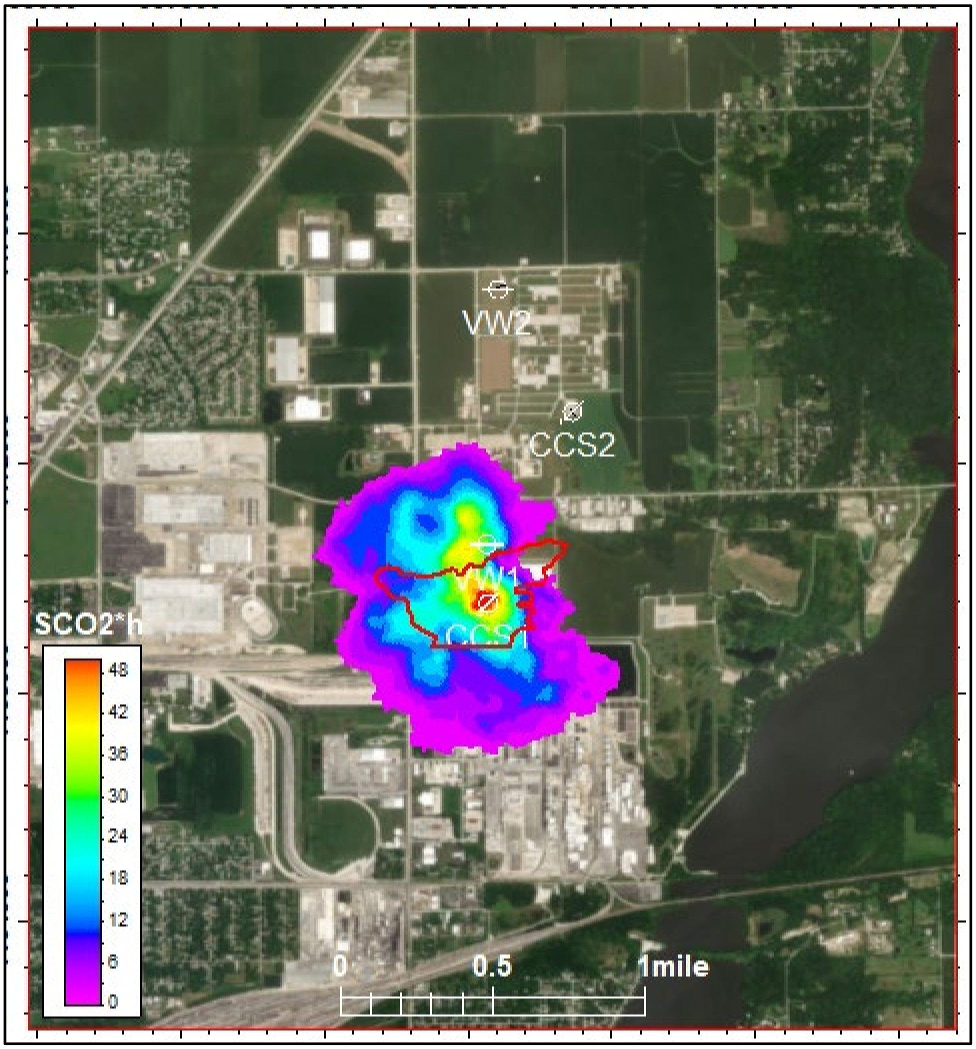

Figure 108. Outline of NRM anomaly (red polygon) and CO_2 net saturation map in January 2015.

5.3 CO_2 Injection Simulation Summary

The following observations result from the history matching to the observed behavior from the IBDP and ICCS projects:

- The iterative process of modeling and simulation has successfully incorporated and integrated new observed data to refine, improve, and honor the complex geologic features at the site.
- When the seismic reprocessing (2019 Seismic Reprocessing Volume) and new seismic inversion processing was completed, the associated structural interpretation of formation horizons and the fault framework interpretation provided the structural detail necessary for better history matching. The inversion products better guided the interpolation of log properties and identified geological features to produce a better history match.
- Simulation results after history matching show that injected CO_2 are confined within the Mt. Simon target Formations and there exists no leakage (pathway) of CO_2.

- According to observed BHP responses, injectivity of the CCS1 injection well deteriorated starting in May 2013. This was possibly due to salt precipitation, scaling, or solids buildup into the perforation and injection intervals as observed by the caliper log during the spinner surveys. In addition, CCS2 shows a similar trend in the well injectivity data plot and caliper log, compared to CCS1. Continuous monitoring of CCS2 injectivity and additional spinner surveys are recommended to evaluate the temporal evolution of well performance.
- After approximately 4 months of CCS2 injection, there exist discrepancies in measured CCS1 BHP data in relation to expected results based on modeling with CCS1 injection. This suggests there exists geologic features between CCS1 and CCS2 not captured in this study.
- BHP response at CCS1 is significantly different from the downhole pressure of VW1_Z1, suggesting the presence of strong heterogeneity (preferential pathway/channel) between wells. Further characterization of spatial heterogeneity/architecture of fluvial channel/baffles with the guidance of the ISGS would help better history match the downhole pressure responses at CCS1 and VW1.
- Although the May 2018 and March 2019 saturation logs showed a new interval with CO_2 at 6,840 ft to 6,830 ft (2085.3m to 2082.3m) in the Mt Simon A-Upper of CCS1 (Figure 88), simulated results showed no CO_2 arrival at CCS1 due to CCS2 injection (Figure 95). It is likely that the origin of CO_2 at this interval is CCS2 injection. However, the confirmation of CO_2 origin (CCS1 or CCS2) in the CCS2 injection intervals at CCS1 would help improve the history matching. Of interest also is that WB4 at a depth of 6,838 ft (2084.7m) in VW1 is the first sensor to detect a formation pressure increase from the CCS2 injection, but CO_2 arrival was not detected in the May 2018 or the March 2019 PNL.
- An inconsistency in the interpretation from the spinner survey at CCS1 and CO_2 saturation logs at VW1 exists. Higher injection rates at the bottom perforation of CCS1 were not confirmed by the fastest CO_2 arrival at the middle zone of Mt. Simon A-Lower at the VW1 (WB3). Inconsistencies also exist with the spinner surveys at CCS2. The caliper log showed the closure of Perforation 1 at CCS2; however, the full closure of top perforations could not be history-matched to the pressure of shallow gauges at VW2. Thus, for history matching, less weight was applied to spinner survey data compared to other data used.
- Even after the removal of a flow barrier north of VW1 (introduced in the previous work), first arrival time of CO_2 at VW1 is still delayed about 0.5 year compared to the PNLs. This indicates that CO_2 migrates much faster than expected through a preferential pathway.
- Applying critically stressed fault analysis to newly identified faults may provide information to support whether a fault is transmissive or sealing. The current classification based on their orientation relative to regional stress direction could be updated with additional work.
- History matching for the IBDP and ICCS projects involved a suite of observed dynamic data including downhole pressure data, time-lapse CO_2 saturation logs, spinner surveys, and time-lapse seismic data. The reservoir model parameters were adjusted until they closely reproduced the observed data. Overall, history matching to multiwell and multilevel downhole pressure data showed good match except for the CCS1 response due to CCS2 injection whereas history matching to less frequent data (time-lapse saturation logs and spinner surveys) is not in strong agreement.
- History matching efforts with each of the dynamic data provided valuable insights into the architecture of the reservoir and confining units that could not be captured through the static characterization process. Additional data after CCS2 injection showed the significant effect of geologic heterogeneity (preferential pathway/channel and/or low-permeability baffles) between wells. The repeat PNL logs at VW1 also indicated that three high-permeability sand packages and interbedded low-porosity and low-permeability layers (baffles) strongly control vertical CO_2 plume geometry.

6 Conclusions 2020 Final Geomodelling and Simulation

This report concludes the 2020 final round of geological modeling and reservoir simulations for the IBDP project. The modeling and simulation work has come a long way since the first layer cake stratigraphy modeling was completed in 2008. Since then, the resolution of the model was periodically improved when new well, seismic, injection, logging and monitoring data became available over the years. During the life of the IBDP project, this modeling was always completed in collaboration with the ISGS who has expertise in the Illinois Basin. The geological model was finalized in 2020 with the integration of repossessed baseline 3D seismic (2019 Seismic Reprocessing Volume) and reprocessed petrophysics. The 2019 processing provided much higher resolution of the subsurface than what was previously available and made for much more accurate horizons and fault interpretation. 28 faults were interpreted with the seismic; however, most of the interpreted faults had relatively small displacements (ranging from 0 to 30 ft) (9.1 to 18.0m) with only 9 faults interpreted to have relatively greater displacement ranging from approximately 30 to 59 ft. These newly interpreted horizons and faults were used to develop a structural framework model from the surface to below the Precambrian.

The newly reprocessed petrophysics (facies, porosity, and permeability) of the formations provided more consistency with geocellular modeling of these petrophysical properties in the interwell space. Because relatively less permeable sandstones can act as vertical barriers (baffles) to CO_2 migration, a facies model was stochastically generated for sand (reservoir) and baffle (non-reservoir) facies. A discreet fracture model (DFN) within the Precambrian developed by the ISGS improved the permeabilities of the fractured Precambrian rocks. This updated geomodel was used as the primary input for reservoir simulations of carbon dioxide (CO_2) migration in the Mt. Simon Formation.

The geological model was used as the primary input for dynamic modeling of reservoir simulations which was completed primarily with the multiwell and multilevel BHP data. Variable parameters used for history matching included facies, porosity, lateral and vertical permeabilities of reservoir rock, cross-fault transmissibility based on fault orientation, and well connection transmissibility factors of CCS1 and CCS2. The iterative process of modeling and simulation has successfully incorporated and integrated new observed data to refine, improve, and honor the complex geologic features at the site. History matching to multiwell and multilevel downhole pressure data showed a good match except for the CCS1 response to CCS2 injection. Although history matching to periodic data (time-lapse saturation logs, spinner survey, and time-lapse seismic data) are not in strong agreement, history matching efforts with each of the dynamic data types provided valuable insights as to the complex architecture of the reservoir and confining units which could not be resolved with the well and seismic data. Additional data after CCS2 injection showed the significant effect of geologic heterogeneity (preferential pathway/channel and/or low-permeability baffles) between wells. Simulation results also show that injected CO_2 is confined within the Mt. Simon injection zones and there exists no leakage (pathway) of CO_2.

7 Lessons Learned

Schlumberger and the ISGS have been collaborating on the IBDP project for approximately 15 years. In April 2021, the IBDP project came to formal closure. With the completion of any significant project, it is useful to look back and identify the lessons learned so future projects like this can benefit. Schlumberger and the ISGS recently had a brainstorming session to identify some of the key lessons learned; these are outlined below:

7.1 Teamwork

A multidisciplinary team is required for a project of this scale to be successful. The IBDP project was successful because the ISGS provided a wealth of Illinois Basin geological knowledge while Schlumberger provided technology and operational expertise. Effective collaboration between these organizations and within these organizations helped drive IBDP project success. This does not mean that it was always easy to accomplish, there were periods where collaboration was strong and weak. When teamwork was strong, a free flow of information and ideas led to a robust model. Periods of weak teamwork were often caused by changing personal and lack of sufficient hand over. Changing personnel should be anticipated a long project like this. Below is a recommended approach to improve teamwork:

- Succession planning should be implemented to mitigate the inevitable changes in personnel.
- A form of succession planning could come in the form of annual reporting. It is hard for new staff to understand what was completed in 2009 or why something was not completed in 2009.
- It is critically important to ensure communication between teams, within and across organizations.
- It is necessary to conduct frequent technical reviews at key milestones. A fresh perspective during these reviews often highlighted important technical details that may have been otherwise overlooked.
- The project and modeling/simulation efforts experienced strong development when the Schlumberger and ISGS technical teams had well defined technical review pathways. Ensuring that these pathways are always clearly defined will helped to ensure that technical ideas are brought to fruition.

7.2 Environmental Protection Agency (EPA)

Developing a commercial scale CCS project with the EPA was a pioneering endeavor for both IBDP/ICCS and the EPA. Even now in 2021, this process is not straight forward. Below is a recommended approach to improve engagement with the EPA:

- Presenting regulators concise modeling and simulation results and eliminating extraneous information is recommended.
- It is important to work together with the EPA as the project evolves.

7.3 Software

During the project, Schlumberger would always use Schlumberger software (Petrel and Eclipse) and the ISGS would use Schlumberger software and sometime use other software (VIP/NEXUS and Petroleum Experts MOVE). While generally this was not problematic, there were times when the ISGS and Schlumberger found it difficult to share ideas because different software was being used. It is important to identify early on what software platforms will be used and make sure that data can be shared between software packages if the same software cannot be used.

7.4 Data

This long project resulted in an enormous amount of data. Some of the data collected was extremely useful for the model building, some was moderately useful, and some data was not useful and therefore not incorporated into the model. Below is a recommended approach to help manage data issues:

- Documentation of meta data and the reason why it was collected is necessary. The level of effort to accomplish this should not be underestimated. It is further important to recognize that the variety of data is large and cannot simply be managed by a database manager. The variety of data requires that the data generators, data users, and database manager are communicating and checking.
- Open ended questions about new data sets are very helpful. Often commercial vendors do not always deliver full datasets as a matter of course.
- If data collection was considered but ultimately not collected, the reasoning for this needs to be documented.
- Data versioning was very challenging; therefore, detailed metadata needs to be completed.
- Because IBDP was a first of its kind project, much data was collected for research purposes and some for operational purposes. At the time, the distinction between the two was not always clear. An annual cost benefit analysis of these data would be helpful for future projects to understand what the data collection value is.
- The value and purpose of data may change as project evolves and may change the way the data are used (i.e. the reprocessing of the seismic data used for this 2020 update).

7.5 Mindset

Over a long project like this it is easy for a team to get attached to a conclusion, way of thinking, or to a plan for the future. This mental anchoring can be a danger to the project because new data that challenges previous conclusions may be ignored to protect these previous conclusions. Below is a recommended approach to manage mindset issues:

- The team needs to be open to contrary opinions to generate fresh perspectives. This should be done at least annually or when a new team member is onboarded to get back to basics to see what the team missed.
- With any type of model or reservoir characterization the project staff constantly want to make their models as accurate as they can. This is a good quality that makes them professionals. The danger with this is that there is no natural end point to this work. Without an end point the work will go on and on with scope creep. The modeler will often feel like they abandoned their model; however, it is necessary to complete the model and document the work so it can be continued when additional information justifies it.
- As the project progressed, foundational understandings of geologic environment evolved (baffles, faults). The modeling and simulation workflows need to expect this and be ready to pivot.
- Conceptual characterization of assumed features that are identified in boreholes and interpolated stochastically between wells (baffles and faults) may introduce a high level of uncertainty that may be reduced through operational observations; however, the higher complexity the model, the higher the challenge of closely simulating reservoir behavior.

7.6 Summary of Lessons Learned

The IBDP project is unique because it was one of the first onshore saline CO_2 storage projects in the United States and the world. It is also unique in that it has moved through the Pre-Injection Phase through the Injection Phase and to the Post-Injection Phase (Figure 109). This figure is a Schlumberger designed project workflow that illustrates a CCS project lifecycle that every project will go through. The phases are described below:

- Pre-Selection: Initial site selection
- Appraisal / Characterization: Initial geological review and development plans
- Development: The development of the site in term of wells and seismic etc.
- Commissioning: Setting up the project and getting it ready to inject CO_2.
- Closure: The end of injection
- Post Closure and Liability Transfer: Once the CO_2 plume has been demonstrated to be stable safe, the liability of the plume will transfer to the state.
- Monitoring: During most of the project, monitoring of the plume is necessary to demonstrate the CO_2 has been injected safely and that there is no negative impact to the environment.

It has been 17 years since the beginning of the project and there have been many people and organizations involved in the project; therefore, there are many lessons learned to make CCS project successful. Because of the complexity of the project, teamwork collaboration within and between organizations is essential. Because of the long lifespan of these projects, documentation and succession planning is necessary to ensure knowledge is properly transferred. Effective collaboration with the EPA is essential to facilitate timely permit review. The management of the large volumes of data and the use of software is a challenge over the long lifespan of a project. Data archival and documentation is essential to avoid important to avoid lost knowledge. With a long project like this, a team can easily get attached to a conclusion, way of thinking, or plan. This is a risk to the project because new data that challenges previous conclusions may be ignored to protect these previous conclusions. Regular peer reviews and new staff will bring fresh ideas that will challenge previously made conclusions.

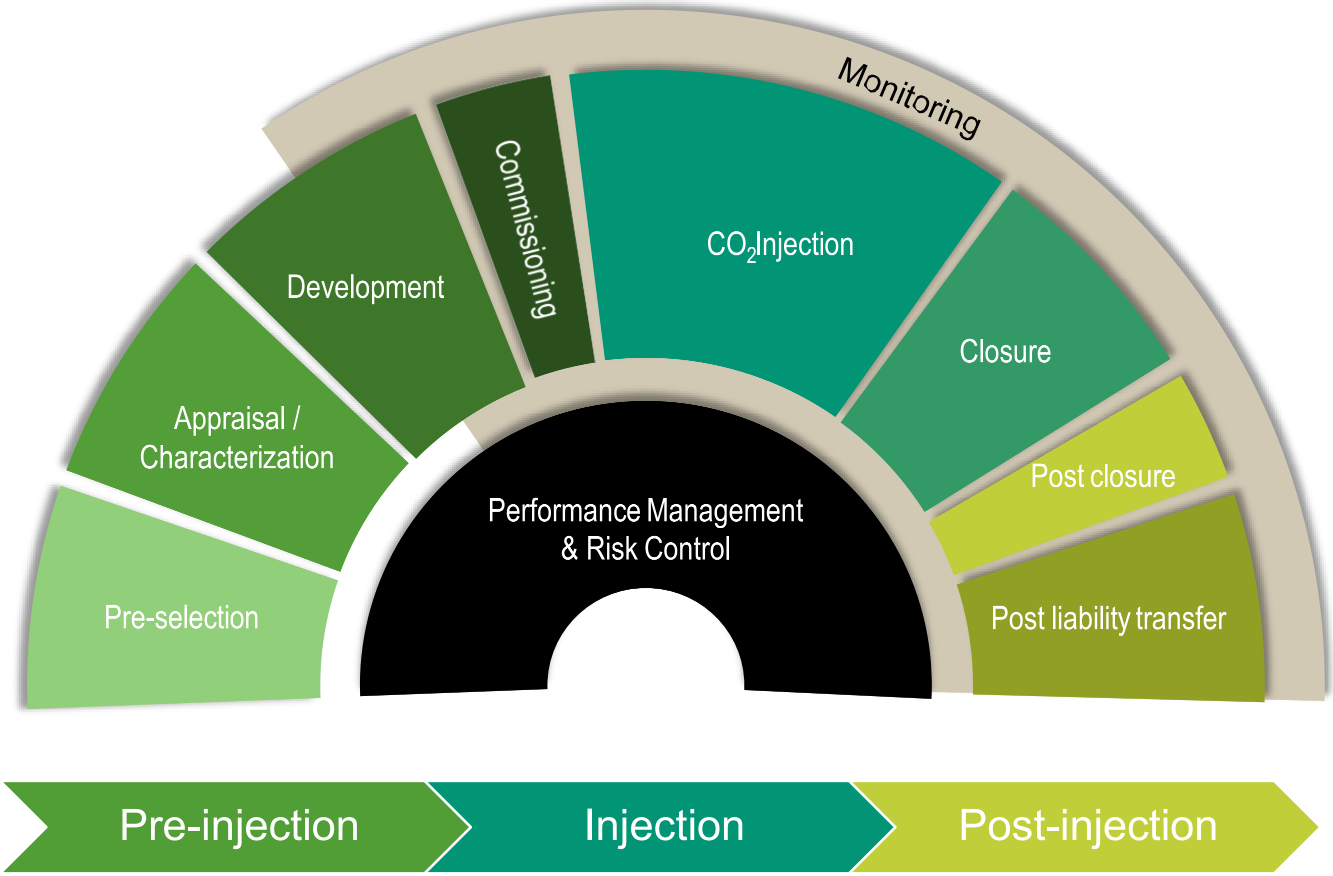

Figure 109. Schlumberger Carbon Services CCS Project Life Span

8 Acknowledgement

This work was funded by the U.S. Department of Energy's (DOE) National Energy Technology Laboratory (NETL) through the ISGS under contract number DE-FC26-05NT42588. The authors gratefully acknowledge all the valuable previous work and discussion with the below valuable contributors.

Ahsan Alvi
Alan Brown
Bob Bauer
Bob Will
Carl Carman
Charles Monson
Damon Garner
Dan Byers
Dwight Peters
Ed Mehnert
George El-Kaseeh
Graham Payne
Hannes Leetaru
James Damico
Jared Freiburg
Jim Kirksey
John McBride
John Medler
Lee Swager
Mansour Khosravi
Zoreh Askari
Marcia Coueslan
Michael Carney
Nick Malkewicz
Ola Babarinde
Ozgur Senel
Paul Jacques
Randy Locke
Rob Finley
Sallie Greenberg
Scott Frailey
Scott Marsteller
Sherilyn Williams-Stroud
Steve Whittaker
Valerie Smith
Wayne Rowe

9 Signature Page

Report Prepared By:

WADE ZALUSKI

Leesiyong

July 18, 2021

Wade Zaluski. P.Geo.
Senior Geologist
Schlumberger
Calgary, Alberta, Canada

Si-Yong Lee, Ph.D.
Reservoir Engineer
Schlumberger
Denver, Colorado, United States

The Association of Professional Engineers, Geologists
and Geophysicists of Alberta
Permit to Practice Number: P3551 (Schlumberger Canada)
Member Number: 80906

References

Brown, A. (2008). *IBDP Update on Petrel Models.* Schlumberger.

Brown, A. (2010). *ADM-Update of Base Case Modeling Decatur Project.* Schlumberger Carbon Services.

Freiburg, J. T. (2014). A Depositional and Diagenetic Characterization of the Mt . Simon Sandstone at the Illinois Basin - Decatur Project Carbon Capture and Storage Site , Decatur , Illinois , USA, 73.

Freiburg, J. T. (2016, 05 17). *Current Research on the Mt. Simon Geology; Refining the Lower Mt. Simon Depositional Interpretation.* Retrieved from http://www.sequestration.org/resources/PAGMay2016Presentations/04-Freiburg_IBDP_PAG_2016_Mt-Simon.pdf: http://www.sequestration.org/resources/PAGMay2016Presentations/04-Freiburg_IBDP_PAG_2016_Mt-Simon.pdf

ISGS. (2011). *Stratigraphic Column for the Illinois Basin .*

Smith, V. (2012). *IBDP Geomodeling Review.* Schlumberger Carbon Services.

Smith, V. (2013). *IBDP 2013_07_24_Model_IBDP-ICCS Geomodeling Overview.* Schlumberger.

Williams-Stroud, S. (2020). *IBDP Precambrian Discreet Fracture Model.*

Zaluski, W. (2016). *IDBP Static Geological Model Development.* Schlumberger Carbon Services.

Zaluski, W., & Lee, S.-Y. (2019). *2018 IBDP/ICCS Static Geological Model Development and Dynamic Modelling Updates.*